MARTIN MARIETTA ENERGY SYSTEMS LIBRARIES
3 4456 0250980 9

CENTRAL RESEARCH LIBRARY
DOCUMENT COLLECTION

ANP

[redacted]

AEC RESEARCH AND DEVELOPMENT REPORT

ORNL-2115
Vol. I
C-85—Propulsion Systems

4A

FIRST SEMIANNUAL ANP SHIELDING INFORMATION MEETING

MAY 7-8, 1956

VOLUME I

ENTRAL RESEARCH LIBRARY
DOCUMENT COLLECTION
BRARY LOAN COPY
T TRANSFER TO ANOTHER PERSON
wish someone else to see this document,
name with document and the library will
a loan.

DECLASSIFIED
CLASSIFICATION CHANGED
BY AUTHORITY OF: AEC 11-19-65
BY: C. Wells 6/17/66

[redacted]

OAK RIDGE NATIONAL LABORATORY
OPERATED BY
UNION CARBIDE NUCLEAR COMPANY
A Division of Union Carbide and Carbon Corporation
UCC
POST OFFICE BOX P · OAK RIDGE, TENNESSEE

[redacted]

[redacted]

LEGAL NOTICE

This report was prepared as an account of Government sponsored work. Neither the United States, nor the Commission, nor any person acting on behalf of the Commission:

A. Makes any warranty or representation, express or implied, with respect to the accuracy, completeness, or usefulness of the information contained in this report, or that the use of any information, apparatus, method, or process disclosed in this report may not infringe privately owned rights; or

B. Assumes any liabilities with respect to the use of, or for damages resulting from the use of any information, apparatus, method, or process disclosed in this report.

As used in the above, "person acting on behalf of the Commission" includes any employee or contractor of the Commission to the extent that such employee or contractor prepares, handles or distributes, or provides access to, any information pursuant to his employment or contract with the Commission.

[redacted]

C-85, Propulsion Systems

ORNL-2115 - Vol. I

This document consists of 187 pages. Copy 4 of 150 copies. Series A.

Papers Presented at the

FIRST SEMIANNUAL ANP SHIELDING INFORMATION MEETING, May 7-8, 1956,

VOLUME I

Date Issued

JUL 2 1956

Sponsored by
AIRCRAFT REACTORS BRANCH
Division of Reactor Development, USAEC

at

OAK RIDGE NATIONAL LABORATORY
Operated by
UNION CARBIDE NUCLEAR COMPANY
A Division of Union Carbide and Carbon Corporation
Post Office Box P
Oak Ridge, Tennessee

[redacted]

[redacted]

MARTIN MARIETTA ENERGY SYSTEMS LIBRARIES

3 4456 0250980 9

ORNL-2115
Reactors-Aircraft Nuclear
Propulsion Systems
M-3679 (18th ed.)

INTERNAL DISTRIBUTION

1. C. E. Center
2. Biology Library
3. Health Physics Library
4-5. Central Research Library
6. Reactor Experimental Engineering Library
7-31. Laboratory Records Department
32. Laboratory Records, ORNL R.C.
33. A. M. Weinberg
34. L. B. Emlet (K-25)
35. J. P. Murray (Y-12)
36. J. A. Swartout
37. E. H. Taylor
38. E. D. Shipley
39. A. H. Snell
40. M. L. Nelson
41. W. H. Jordan
42. S. J. Cromer
43. G. E. Boyd
44. R. A. Charpie
45. S. I. Lind
46. F. L. Culler
47. A. Hollaender
48. K. Z. Morgan
49. J. E. Winters
50. D. S. Billington
51. A. J. Miller
52. E. P. Blizard
53. D. D. Cowen
54. W. M. Breazeale (consultant)
55. M. J. Skinner
56. R. R. Dickison
57. A. Simon
58. F. C. Maienschein
59. A. D. Callihan
60. C. E. Clifford
61. F. L. Keller
62. R. W. Peelle
63-64. ORNL - Y-12 Technical Library, Document Reference Section

EXTERNAL DISTRIBUTION

65. AF Plant Representative, Baltimore
66-67. AF Plant Representative, Burbank
68. AF Plant Representative, Marietta
69-71. AF Plant Representative, Santa Monica
72-73. AF Plant Representative, Seattle
74. AF Plant Representative, Wood-Ridge
75. Air Research and Development Command (RDGN)
76. Air Research and Development Command (RDZPA)
77. Air Technical Intelligence Center
78. Air University Library
79-81. ANP Project Office, Fort Worth
82. Argonne National Laboratory
83. Armed Forces Special Weapons Project, Sandia
84. Armed Forces Special Weapons Project, Washington
85. Assistant Secretary of the Air Force, R&D
86-91. Atomic Energy Commission, Washington
92. Bureau of Aeronautics
93. Bureau of Aeronautics General Representative
94. Chicago Operations Office
95. Chicago Patent Group

96. Chief of Naval Research
97. Convair-General Dynamics Corporation
98-101. General Electric Company (ANPD)
102. Hartford Area Office
103. Headquarters, Air Force Special Weapons Center
104. Lockland Area Office
105. Los Alamos Scientific Laboratory
106. National Advisory Committee for Aeronautics, Cleveland
107. National Advisory Committee for Aeronautics, Washington
108. Naval Air Development and Material Center
109. Naval Research Laboratory
110. North American Aviation, Inc. (Aerophysics Division)
111. Nuclear Development Corporation of America
112. Office of the Chief of Naval Operations (OP-361)
113. Patent Branch, Washington
114-117. Pratt & Whitney Aircraft Division (Fox Project)
118. Sandia Corporation
119. School of Aviation Medicine
120. USAF Project Rand
121. University of California Radiation Laboratory, Livermore
122-139. Wright Air Development Center (WCOSI-3)
140-149. Technical Information Service Extension, Oak Ridge
150. Division of Research and Development, AEC, ORO

[redacted]

PREFACE

The papers presented at the First Semiannual ANP Shielding Information Meeting are published in three volumes. Volumes II and III are also identified as ORNL-2115.

[redacted]

[redacted]

TABLE OF CONTENTS

Volume I

	Paper No.
GE Shielding Experiments at NARF ..... R. L. French, Convair, Ft. Worth	I-A
ASTR Crew Shield and Mapping Experiments ..... C. F. Malone, Convair, Ft. Worth	I-B
ASTR Mapping Predictions ..... C. E. Humphries, Convair, Ft. Worth	I-C
Recent Results in the Airborne Shielding Program ..... C. F. Cook, Convair, Ft. Worth	I-D
Preliminary Gamma-Ray Differential Shielding Experiments at the Tower Shielding Facility ..... F. N. Watson, Oak Ridge National Laboratory	I-E
Tower Shielding Facility Gamma Ray Spectra (Preliminary Results) ..... G. J. Rausa, Martin, at Oak Ridge National Laboratory	I-F
Measurements of the LTSF Source Plate Power ..... W. J. McCool, Pratt and Whitney, at Oak Ridge National Laboratory	I-G
Analysis of LTSF Source Plate Calibration Data ..... D. R. Otis, Convair, San Diego, at Oak Ridge National Laboratory	I-H
Analysis of the Dynamic Source Tests on Mockups of the Reflector-Moderated Reactor and Shield ..... H. C. Woodsum, Pratt and Whitney, at Oak Ridge National Laboratory	I-I
Application of the KAPL "Mug 2" Reactor Code to the Analysis of RMR Lid Tank Shielding Experiments ..... L. Joseph, P. S. Mittelman, M. S. Silberstein, Nuclear Development Corporation of America	I-J
Time Dependence of Fission Product Gamma Radiation ..... W. Zobel, T. A. Love, Oak Ridge National Laboratory	I-K
The Gross Fission Product Photon Energy Spectrum ..... R. W. Peelle, T. A. Love, W. Zobel, Oak Ridge National Laboratory	I-L

[redacted]

[redacted]

Paper I-A

GE SHIELDING EXPERIMENTS AT NARF*

R. L. French
Convair, Ft. Worth

*Published at Convair, Ft. Worth, as Report No. FZM-438.

[redacted]

[redacted]

GE SHIELD EXPERIMENT AT NARF
(Title Unclassified)

by

R. L. French

Convair, A Division of General Dynamics
Corporation, Fort Worth, Texas

Present Convair-General Electric design concepts for direct cycle reactor shield systems require that the shield be penetrated by ducts capable of carrying large volumes of air. Hence, it is desirable to understand the leakage of radiation from ducted shields. A mock-up experiment was recently performed with the Ground Test Reactor in the Convair swimming pool to provide data useful in analyzing the scattering effect of annular ducts on reactor radiation and to check the adequacy of using rectangular sections for simulating annular ducts. This paper presents a brief description of the experiment, the methods of analysis, preliminary results, and tentative conclusions. An albedo method is shown to be promising for calculating the scattering of fast neutrons in annular ducts. The radiation pattern in the horizontal midplane of a rectangular duct is found to be similar to that of an annular duct of corresponding dimensions.

THE EXPERIMENT

Figure 1A shows the position of the annular duct mock-up relative to the Ground Test Reactor. A simplified design was chosen for the mock-up to facilitate a detailed theoretical analysis. The dimensions, however, are considered to be representative of outlet air duct designs. The transition section consists of an array of air-filled stainless steel tubes between two rectangular end plates. The plenum chamber is made of 3/8-inch stainless steel.

AEC-3312-CVAC

[redacted]

[redacted] 1954

[redacted]

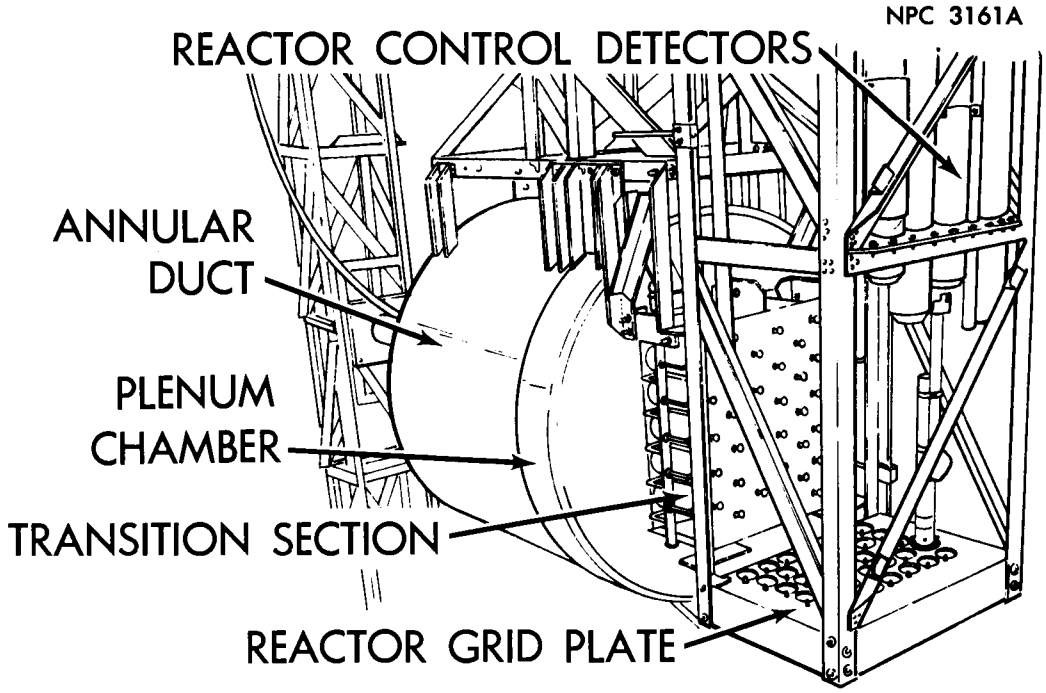

Figure 1A. Annular Duct Mock-up

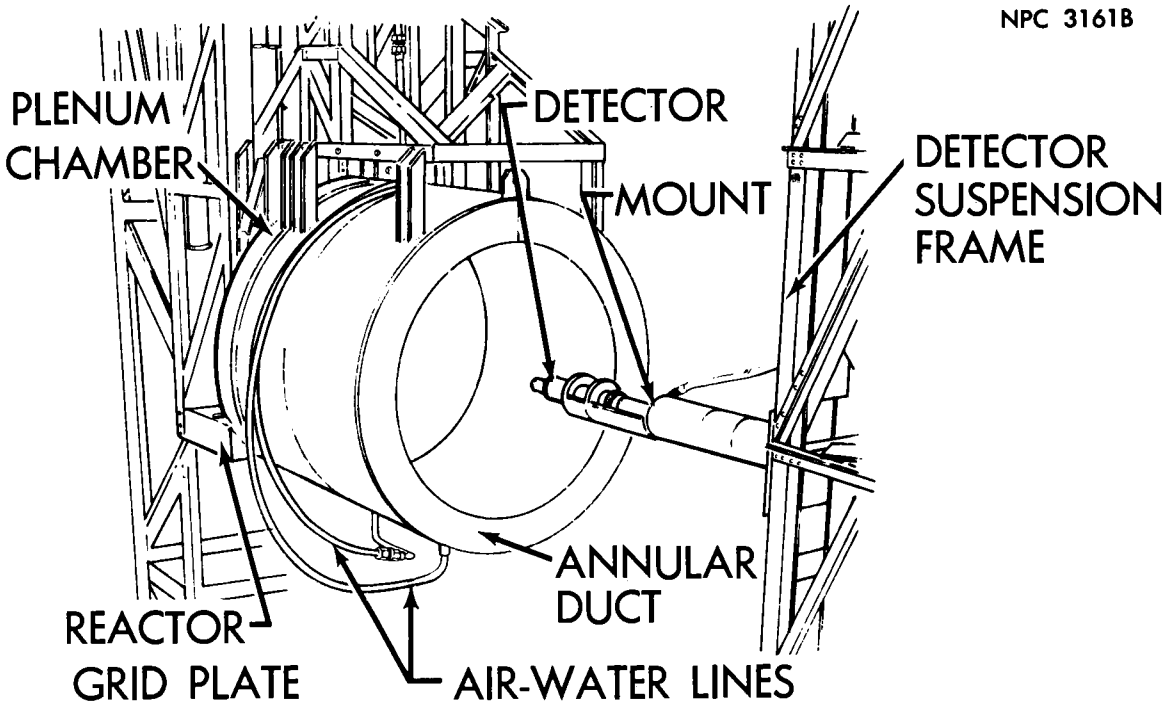

Figure 1B. Annular Duct Mock-up

[redacted]

[redacted] 1954

[redacted]

A different view of the annular duct is shown in Figure 1B. The annular section is constructed of 1/4-inch stainless steel. The plenum chamber and annular duct may, independently of one another, be filled with either water, or air. Gamma dose rates, fast neutron dose rates, and thermal neutron fluxes were measured along several traverses both inside and outside the annular duct for each of the four possible air-water configurations. With the exception of a few symmetry checks, all measurements were made in the horizontal midplane. In Figure 1B a Hurst-type fast neutron dosimeter may be seen positioned near the end of the annular duct.

A knowledge of the correlation between annular ducts and simulated annular ducts will enhance the usefulness of previous duct experiments(1,2) performed at Oak Ridge National Laboratory. Figure 2 shows the L-shaped duct made up of rectangular sections to simulate the annular duct. The dimensions of the L-shaped duct correspond to those of the annular duct with the exception of the effective radius which is variable. Midplane measurements were made with its radius set to three different values; one less than, one equal to, and one greater than that of the annular duct. The L-shaped duct was filled with air during all measurements.

THEORETICAL METHODS

Two independent preanalyses were performed prior to the experiment. One, performed by General Electric(3), used the modified Albert-Welton Point Kernel(4), and the other, performed by Convair(5), used the moments method(6). A comparison of some of the features of each is given in Table I.

Each method assumed that only interactions in the materials along the line-of-sight between a source point and a detector point would affect the results at the detector. Build-up was included. Hence the preanalysis calculations gave only the direct beam dose rates. Calculations were performed for approximately 25 detector points for three different air-water configurations.

To date, post-analysis of the experiment has been directed toward the development of a unified theoretical method for calculating the scattering of radiation in annular ducts. An albedo approach has yielded favorable results for the scattering of fast neutrons from the outer wall of the air-filled annular duct. The calculations have been based on the assumptions listed in Table II.

[redacted]

[redacted]
ATOMIC ENERGY ACT - 1954

[redacted]

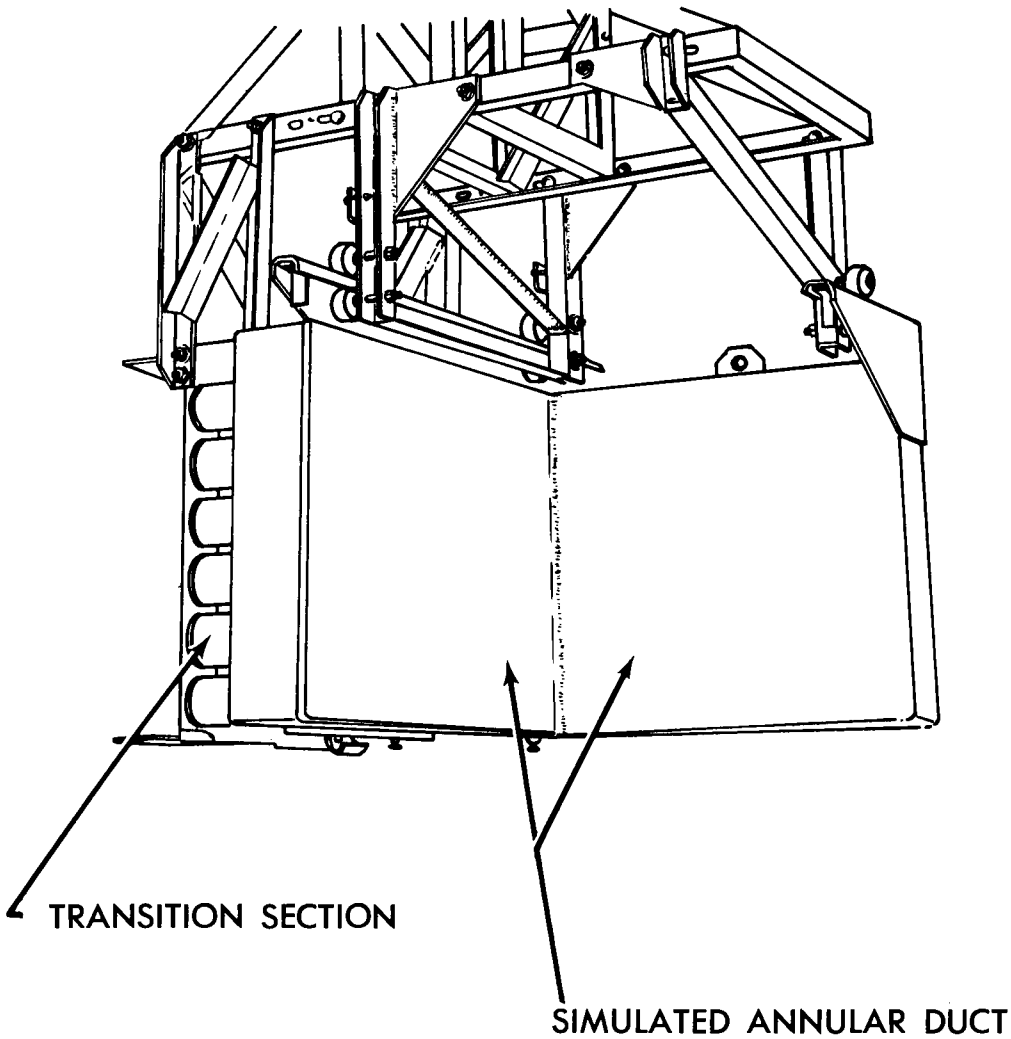

Figure 2. Simulated Annular Duct

AEC-3312-CVAC
[redacted]
ATOMIC ENERGY ACT--1954

[redacted]

TABLE I

Preanalysis of Annular Duct Experiment

	Modified Albert Welton Point Kernel	Moments Method
Source Representation	Cylindrical array of 250 point sources	Rectangular array of 44 point sources
Source Terms	Flat power distribution	Based on experimental mapping and theoretical calculations
Treatment of Geometry	Homogeneous Cylindrical Regions	Exact plus Homogeneous
Yield	Gamma and fast neutron dose rates	Gamma dose rates and spectra, fast neutron dose rates
Normalization	Gamma results must be normalized to experiment	None

TABLE II

Assumptions for Scattering of Fast Neutrons

1. A constant fraction (the albedo) of the fast neutron flux incident upon the duct walls are scattered or reradiated.

2. The reradiated flux has a cosine distribution about the normal to the scattering surface.

3. The neutrons undergo no change in energy upon reradiation.

AEC-3312-CVAC

[redacted]

ATOMIC ENERGY ACT - 1954

[redacted]

The geometry and basic equation of the problem are given in Figure 3. The scattered radiation at a point P_1 is given by the equation. The exponential term attenuates for the portion of the scattered neutron path which is in water. The scattered radiation at a point P_2 on the surface of the inner wall may be obtained if the exponential term is dropped and R_o set equal to R_1. If R_o is set equal to R_2, the scattered radiation at a point P_3 on the outer wall may be obtained.

The limits of the double integral are set to exclude any part of the scattering surface which is hidden by water or steel from the detector unless, of course, the detector is located in water.

RESULTS

1. Gamma

Comparison of experimental results and the results of preanalysis direct beam calculations shows no appreciable envidence of gamma scattering. Figure 4 shows experimental and theoretical data for traverses across the end of the annular duct. Figure 4A is for configuration 2 - air in the plenum chamber and water in the annular duct. The solid curve is from the moments method preanalysis and the dashed curve is from the point kernel preanalysis.

Figure 4B is for configuration 3 - air in both the plenum chamber and annular duct. The dip in the moments method curve does not appear in the experimental results. This may result from a number of causes: First of all, the detector was a 50 cc ionization chamber rather than the point detector assumed in the calculations. The dip could be overshadowed by local capture gammas or a small amount of scattering.

The moments method gamma results are generally low by an amount typical of that seen in Figure 4. It is thought that this discrepancy results from the omission of fission product decay gammas and capture gammas originating outside the reactor core. New calculations, including the decay gammas, have been made for several points. They are all well within 20% of the experimental values. It is planned to continue these calculations and to calculate separately the capture gamma component at each point.

[redacted]

ATOMIC ENERGY ACT - 1954

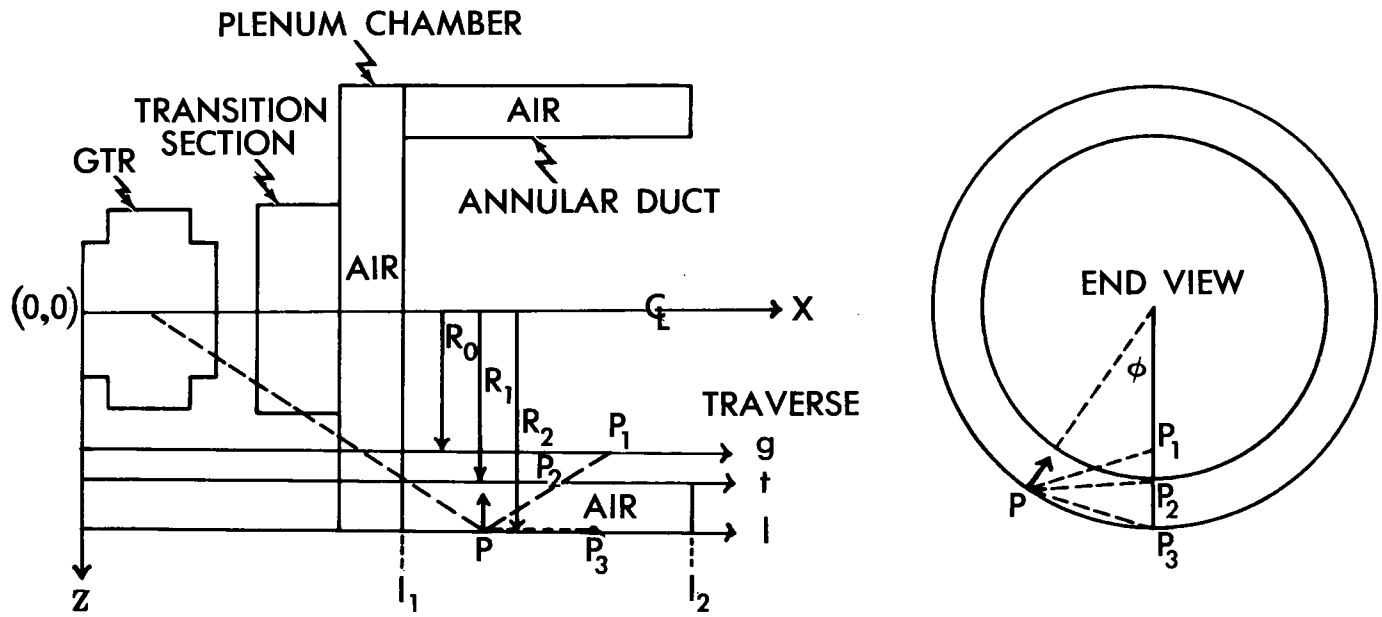

$$D_s(g) = \frac{\alpha R_2}{\pi} \int_{\phi_1}^{\phi_2} \int_{l_1}^{l_2} \frac{D_D(l)\,(R - R_2 \cos\phi)\,e^u}{[R_0^2 + R_2^2 - 2R_0R_2\cos\phi + (g-l)^2]^{3/2}}\, dl\, d\phi$$

Where:

$$u = -\frac{1}{\lambda}\left[\frac{R - R_0R_2\cos\phi}{R_0^2+R_2^2-2R_0R_2\cos\phi} + \sqrt{\left(\frac{R^2 - R_0R_2\cos\phi}{R_0^2+R_2^2-2R_0R_2\cos\phi}\right)^2 - \frac{R_0^2 - R_1^2}{R_0^2+R_2^2-2R_0R_2\cos\phi}}\right]\sqrt{R_0^2+R_2^2-2R_0R_2\cos\phi+(g-l)^2}$$

α = THE ALBEDO

$D_D(l)$ = DIRECT DOSE RATE ON SCATTERING SURFACE

Figure 3. Annular Duct Scattering Geometry and Basic Equation for Scattering Calculations

AEC-3312-CVAC
[redacted] ATOMIC ENERGY ACT--1954
NPC-3159

[redacted]

NPC 3169

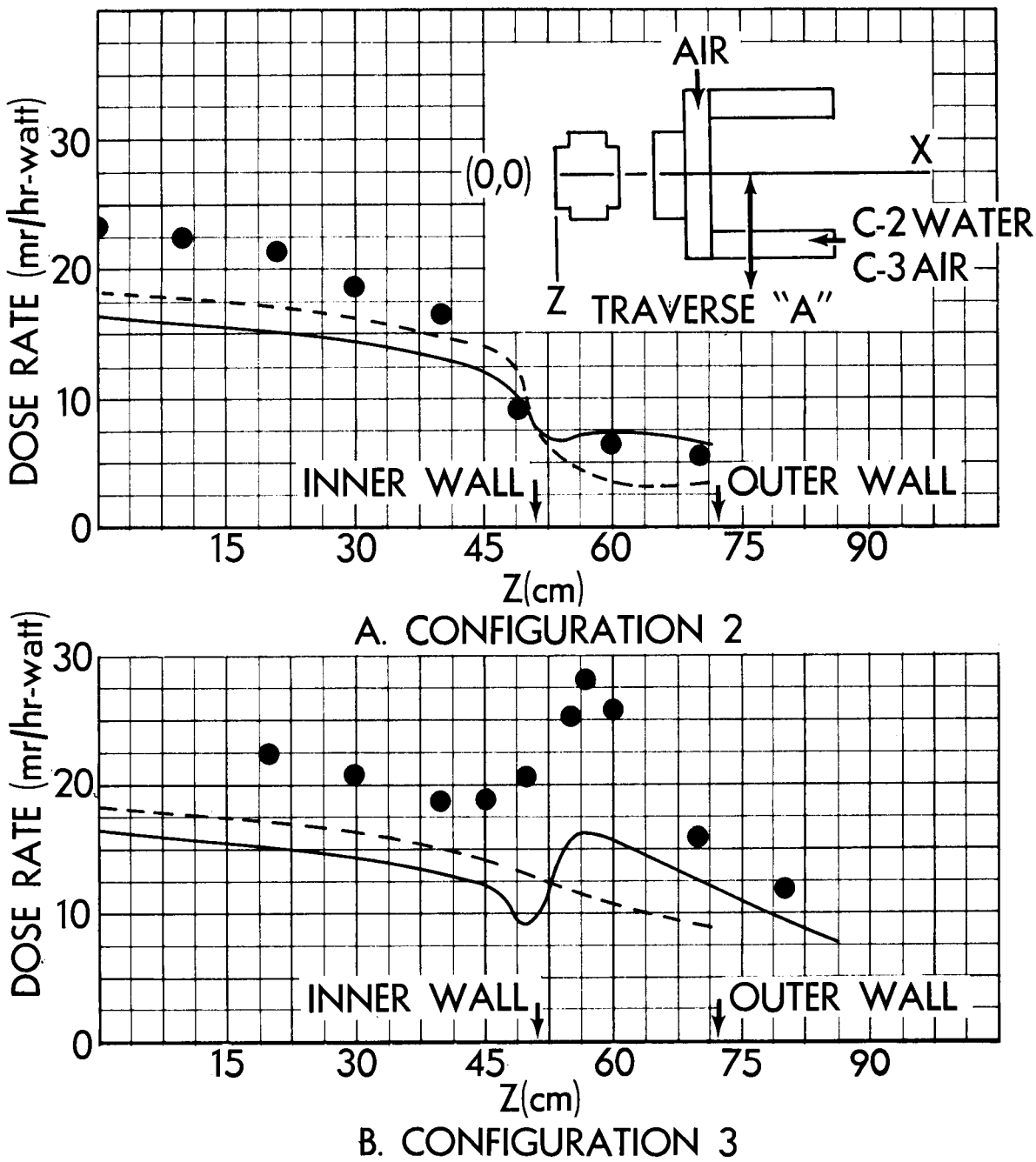

● EXPERIMENTAL RESULTS
— MOMENTS METHOD PREDICTION
-- POINT KERNEL PREDICTION

Figure 4. Experimental and Theoretical Gamma Dose Rates on Traverse "A" of Annular Duct

AEC-3312-CVAC

[redacted]

ATOMIC ENERGY ACT - 1954

[redacted]

2. Fast Neutron

The experimental results show evidence of a marked scattering effect on fast neutrons. Figure 5 is a topographical drawing showing the fast neutron dose rate in the shaded plane for two different air-water configurations. The position of a point is given by the X and Z scales. The dose rate is given by the elevation on the logarithmic vertical scale.

Surface ABED gives the dose rate for configuration 3 - both the plenum chamber and annular duct filled with air. When the annular duct is filled with water (configuration 2) the dose rate is given by surface ABCD. Since the direct beam path is the same for both configurations, the difference between the two surfaces represents the scattered component from the annular duct.

Before making comparisons between experimental and theoretical fast neutron data it should be pointed out that power corrections have not been applied to the experimental data. Upon completion of the gamma measurements the Ground Test Reactor was loaded with new fuel elements. Although final power correction factors for the new core are not yet available, there is evidence that they may be as great as 1.7 for low power levels.

Figure 6 gives the experimental and theoretical scattered component of the fast neutron dose rate along a traverse 7 cm from the inside wall of the annular duct. The experimental points were obtained by subtracting configuration 2 dose rates from configuration 3 dose rates. An albedo of 0.25 was used in the calculations. By making cross-plots and extrapolating, experimental dose rates may be obtained for the walls of the annular duct. Figures 7 and 8 show experimental and theoretical scattered dose rates for the inner and outer walls, respectively, of the annular duct.

The discrepancy between the experimental and theoretical results near the plenum chamber is greatest for the outer wall. This supports the assumption that the discrepancy is due to scattering from the plenum chamber. Calculations are now being made to check this assumption.

[redacted]

ATOMIC ENERGY ACT - 1954

[redacted]

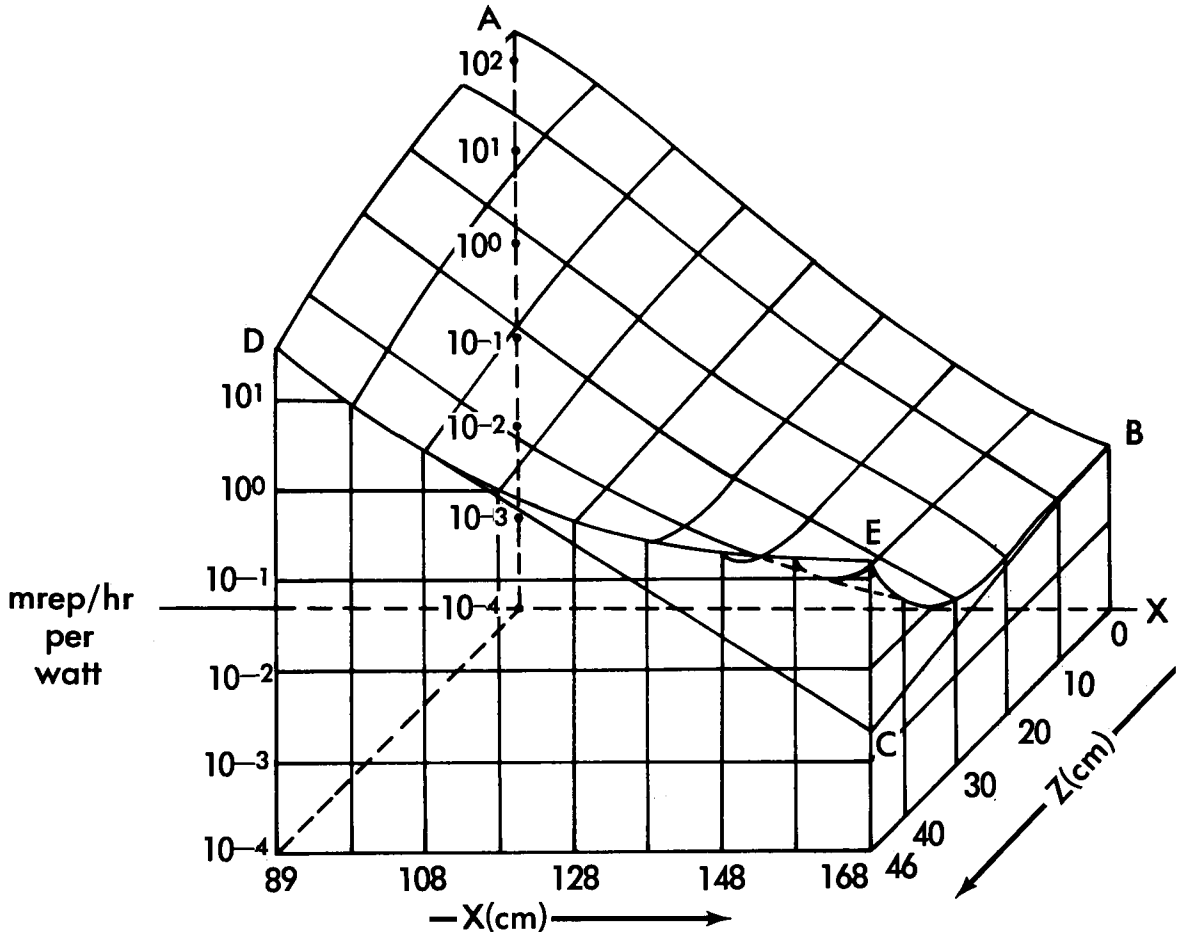

FIGURE 5A. Fast Neutron Dose Rate in Shaded Area of Fig. 5B.

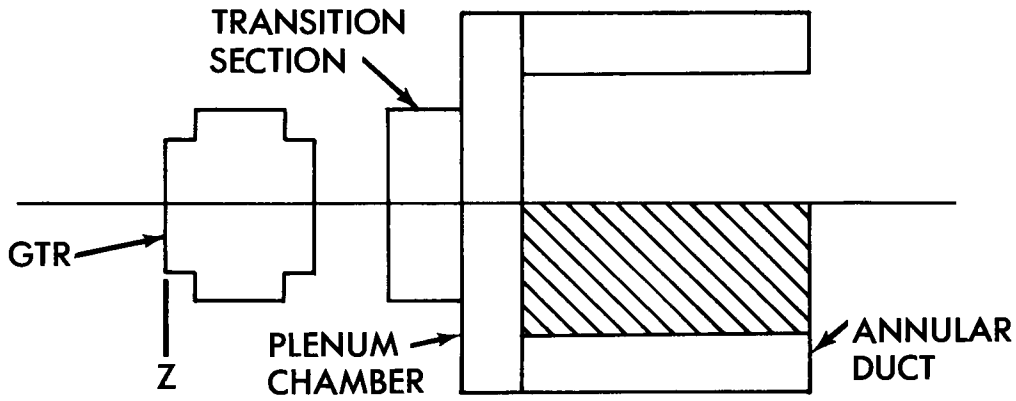

Figure 5B. Arrangment of Annular Duct Experiment

[redacted]

AEC-3312-CVAC
[redacted]
ATOMIC ENERGY ACT--1954

[redacted]

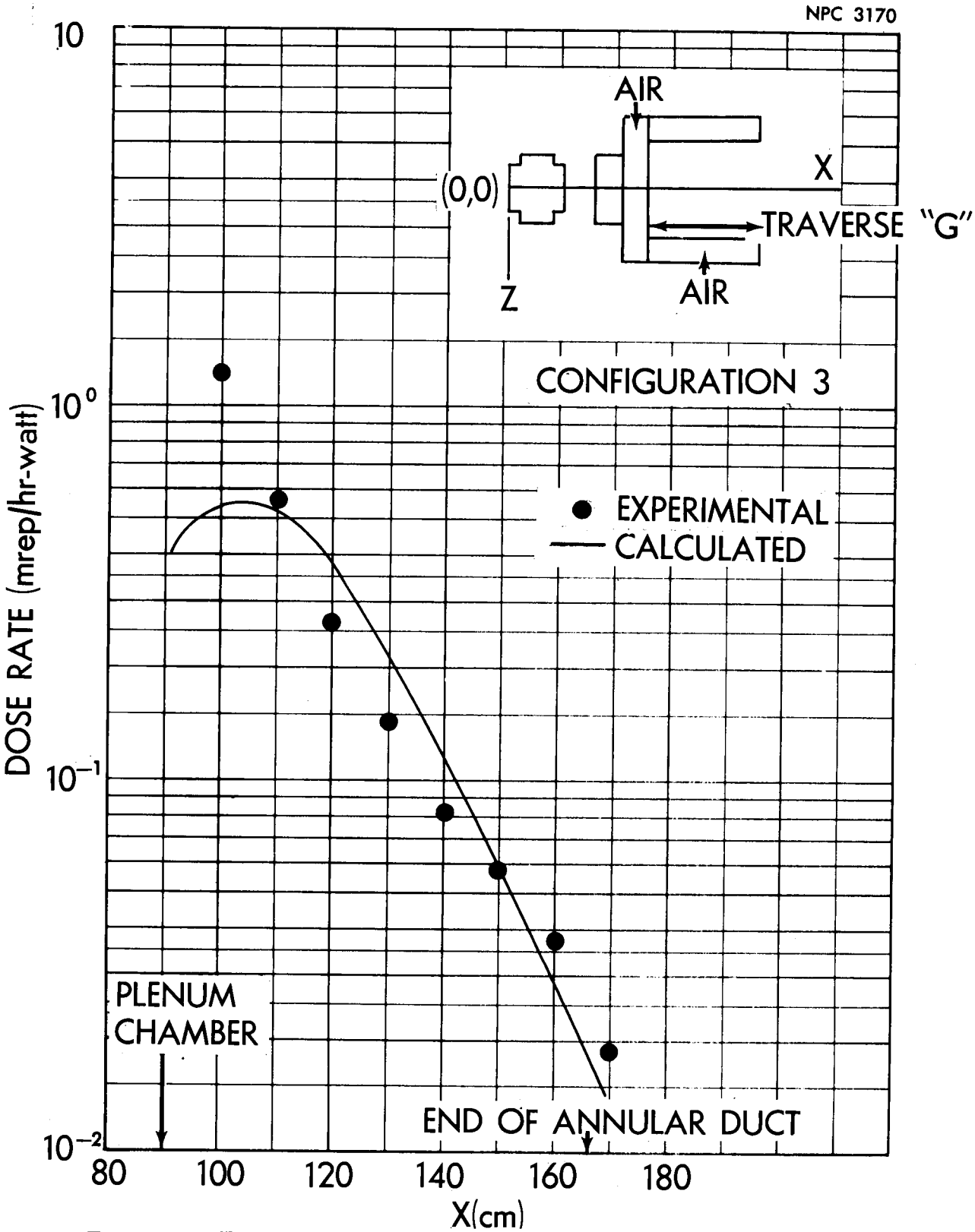

Figure 6. Experimental and Theoretical Scattered Components of Fast Neutron Dose Rate on Traverse "G" of Annular Duct (Configuration 3)

[redacted]

AEC-3312-CVAC
[redacted]
ATOMIC ENERGY ACT - 1954

[redacted]

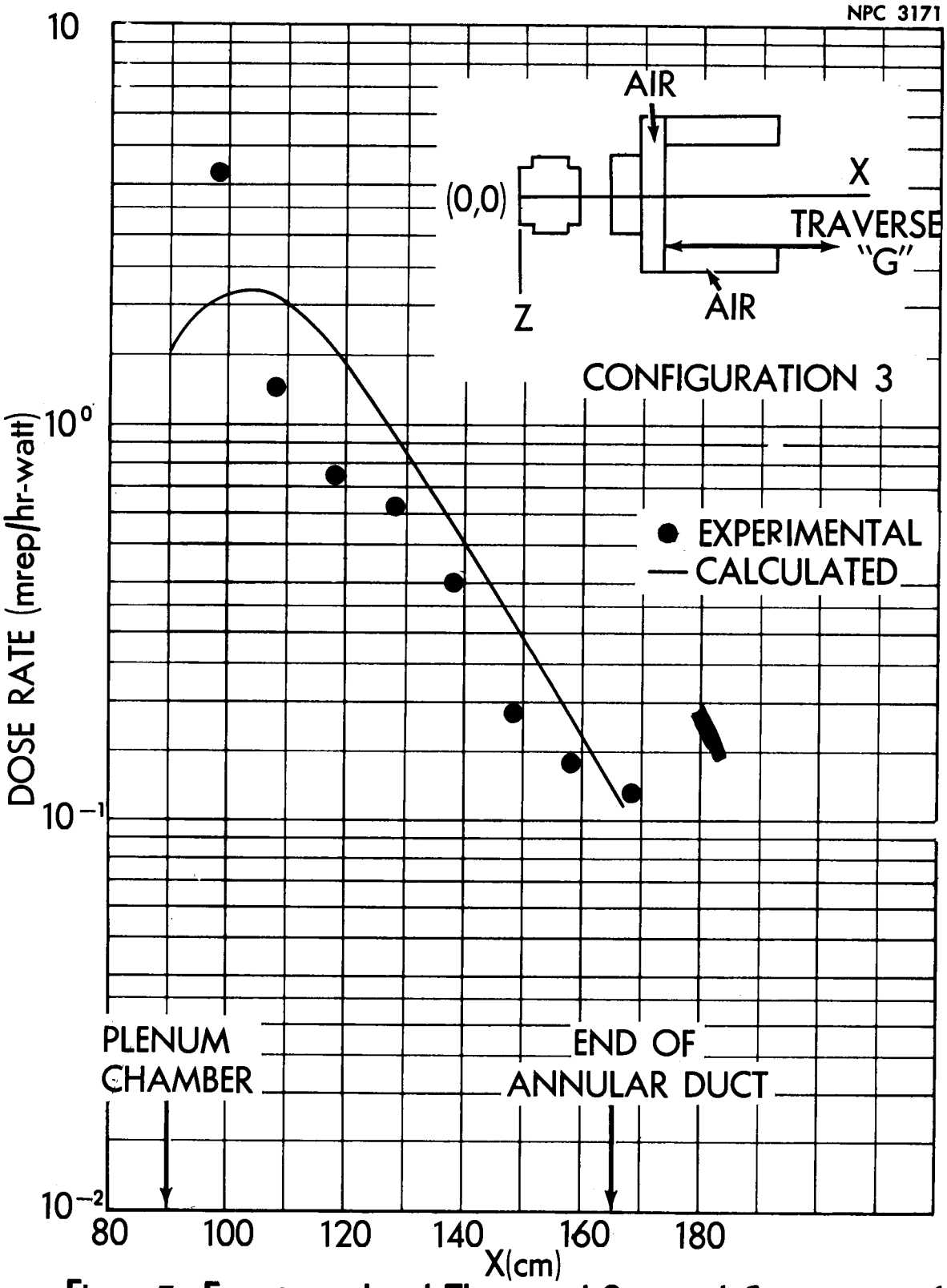

Figure 7. Experimental and Theoretical Scattered Components of Fast Neutron Dose Rate on Traverse "G" of Annular Duct (Configuration 3)

[redacted]

AEC-3312-CVAC
[redacted]
ATOMIC ENERGY ACT - - 1954

[redacted]

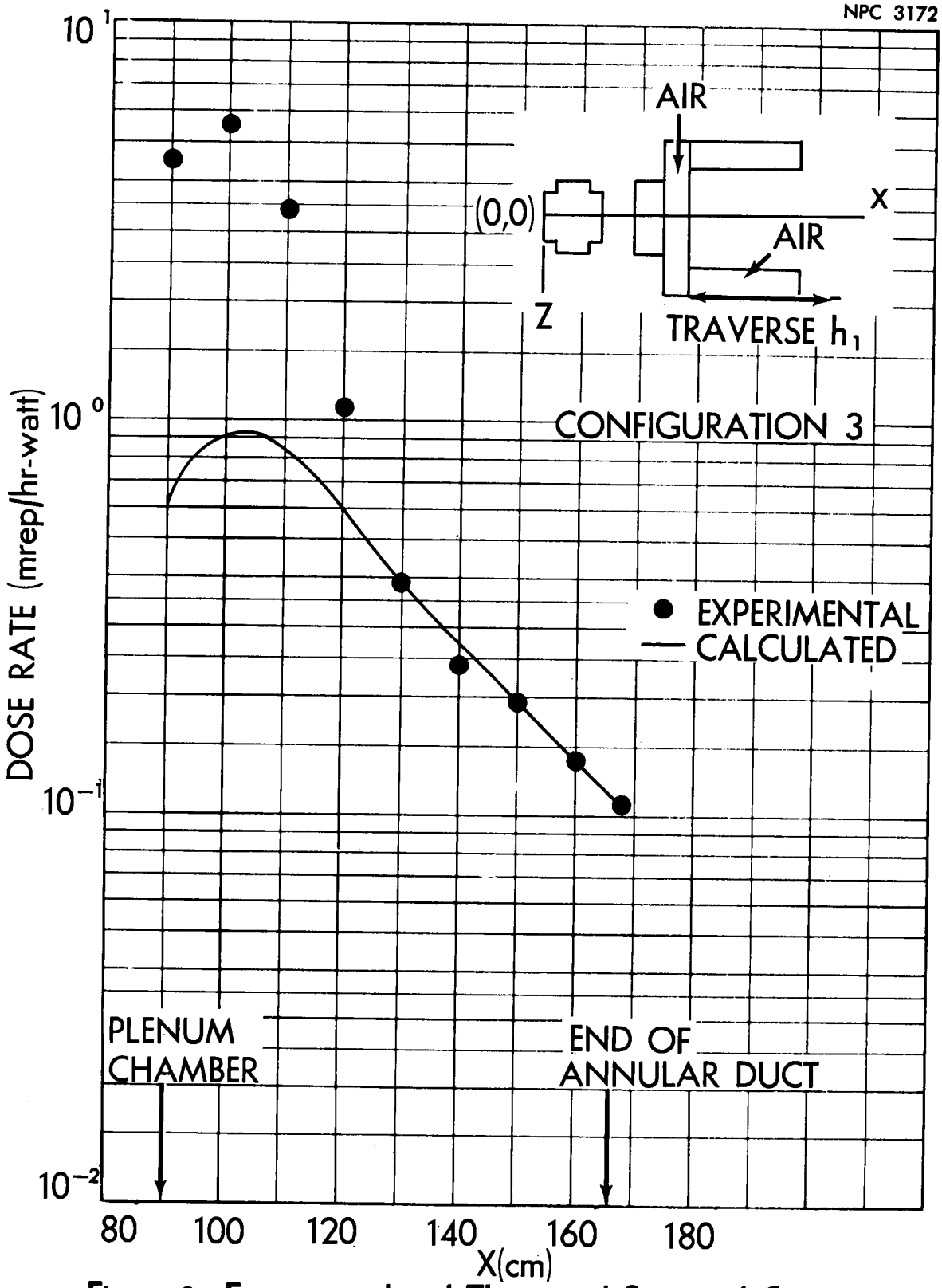

Figure 8. Experimental and Theoretical Scattered Components of Fast Neutron Dose Rate on Traverse "H" of Annular Duct (Configuration 3)

AEC-3312-CVAC

[redacted]

ATOMIC ENERGY ACT - 1954

[redacted]

3. Thermal Neutron

The scattering effect is more pronounced for thermal neutrons than for fast neutrons. Figure 9 shows a comparison of thermal neutron isoflux and fast neutron isodose curves for configuation 3. The dashed curves are for thermal neutrons and the solid curves are for fast neutrons.

4. L-Shaped Duct

Some idea of the effectiveness of using rectangular sections to simulate annular ducts may be gained from Figure 10. Here the radius of the L-shaped duct is set equal to that of the annular duct so that in a section taken through the horizontal midplane they appear identical.

The dashed curves are fast neutron isodoses for the L-shaped duct. The solid curves are fast neutron isodoses for the annular duct. It is planned to make scattering calculations for the L-shaped duct similar to those being made for the annular duct.

CONCLUSIONS

Several tentative conclusions have been drawn:

1. There appears to be no significant scattering of gammas in the annular duct.
2. Scattering causes a great increase in the fast neutron dose rate near the ends of the annular duct.
3. The albedo method appears promising for calculating the scattered component of the fast neutron dose rate.
4. The radiation pattern in the horizontal midplane of the L-shaped duct is similar to that of the annular duct of the same radius.

AEC-3312-CVAC

[redacted]

[redacted] ATOMIC ENERGY ACT - 1954

[redacted]

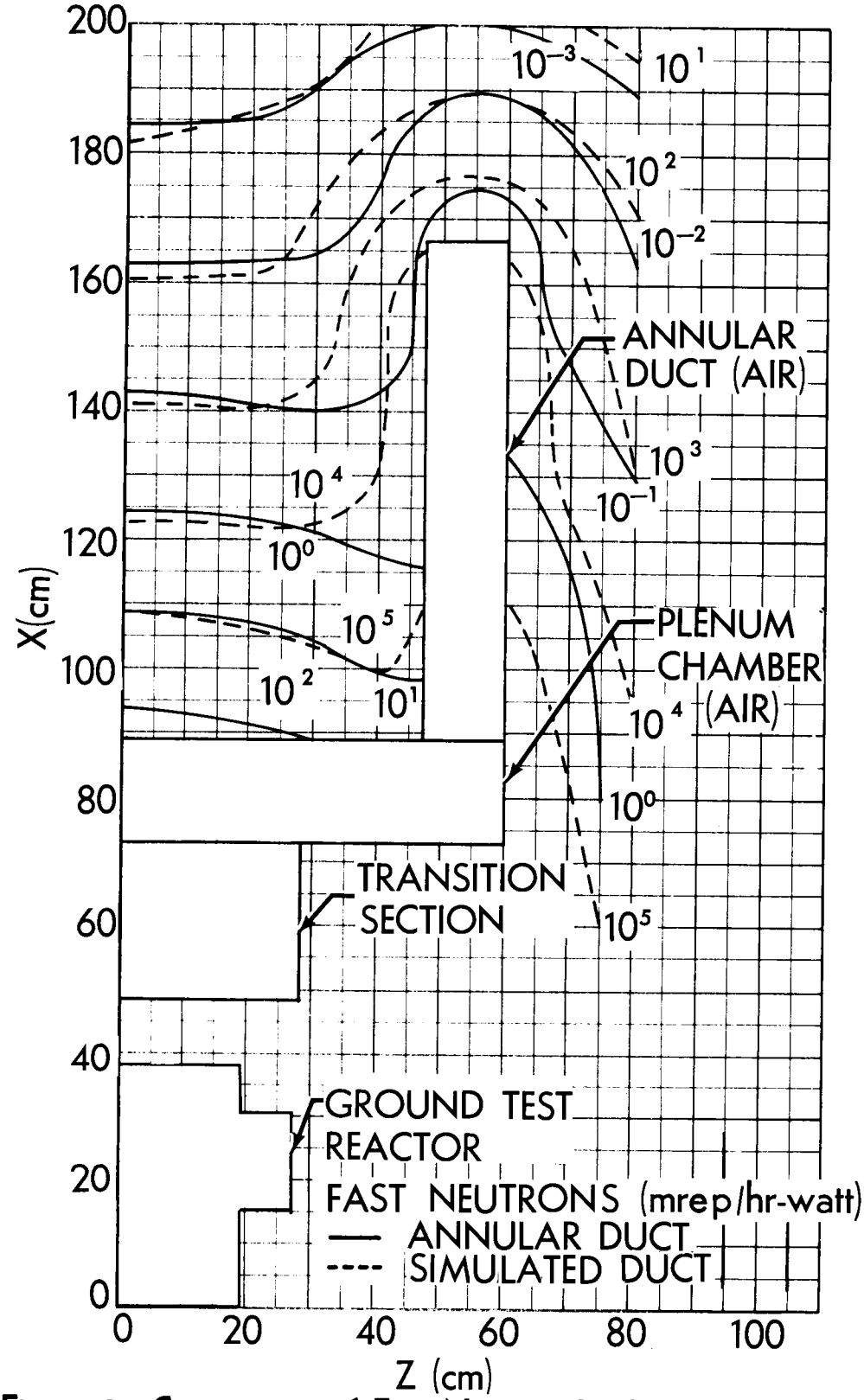

Figure 9. Comparison of Fast Neutron Isodose and Thermal Neutron Isoflux Curves for Annular Duct (Configuration 3)

AEC-3312-CVAC

[redacted]

ATOMIC ENERGY ACT - 1954

[redacted]

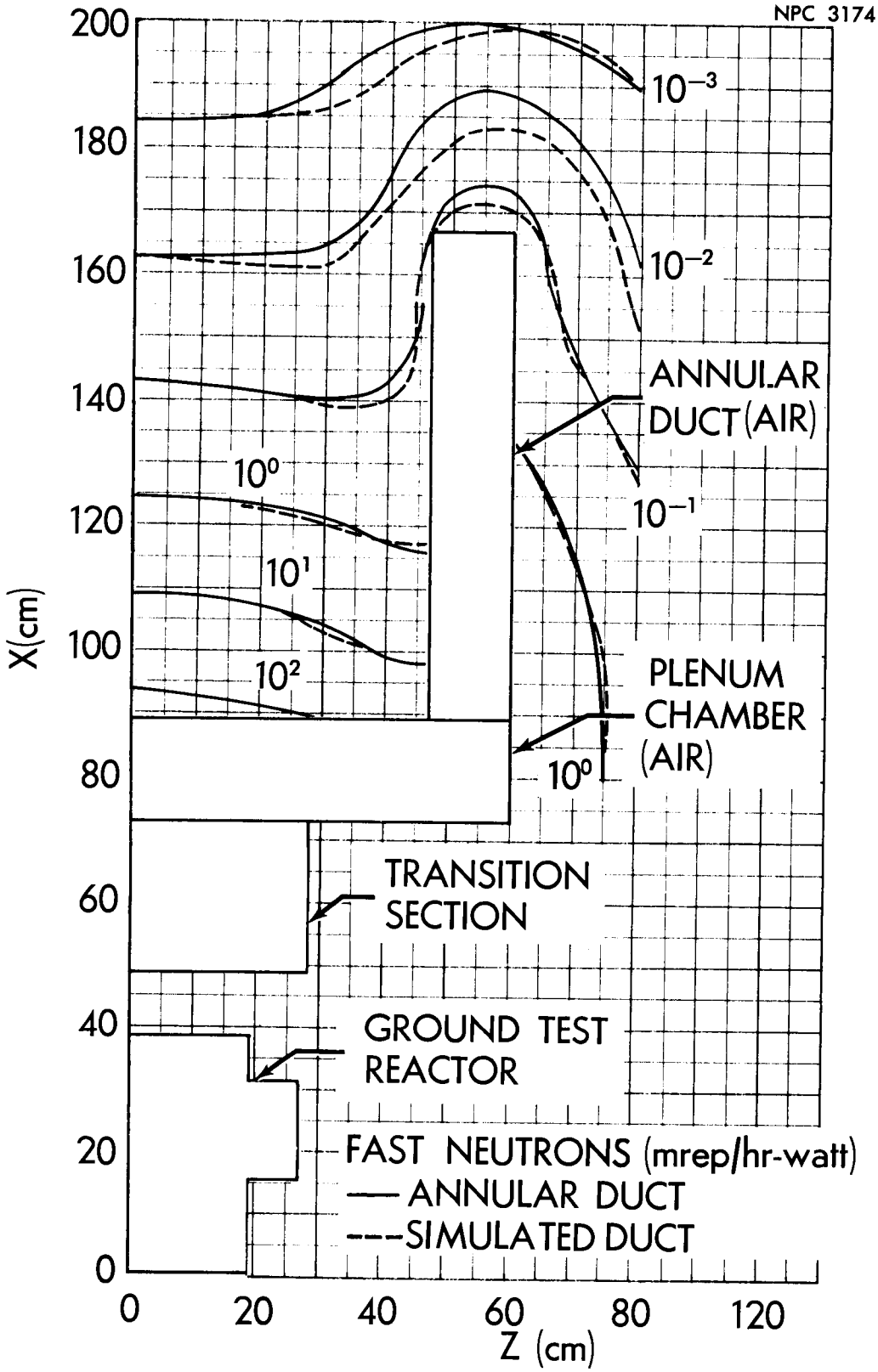

Figure 10. Comparison of Annular Duct and L-Shaped Duct Fast Neutron Isodose Curves (Configuration 3)

[redacted]

AEC-3312-CVAC
[redacted]
ATOMIC ENERGY ACT - 1954

[redacted]

REFERENCES

1. C. E. Clifford and C. L. Storrs, Jr., Neutron and Gamma Dose Distribution in Water Surrounding the GE Outlet Air Duct, Oak Ridge National Laboratory Report CF-52-6-158 (June 26, 1952).

2. J. W. Haffner, Analysis of the Mock-up Experiments Conducted at the BSF During February and March 1955, General Electric ANPD, Report XDC 55-7-103, Cincinnati (July 26, 1955).

3. F. A. Aschenbrenner and R. J. Klotz, Description and Preanalysis of Mock-up Experiments to be performed in Convair NARF Swimming Pool, General Electric ANPD Report DC 55-10-104, Cincinnati (October 25, 1955).

4. J. G. Carver, et. al., GE-ANPD Methods of Shield Design, General Electric ANPD, Report APEX 230, Cincinnati (December 30, 1955).

5. GTR - GE Annular Duct Experiment, p. 43, 48-52, Convair-Fort Worth, MX-1589 Quarterly Progress Report, 1 October-31 December 1955, NARF-55-94R.

6. H. Goldstein and J. E. Wilkins, Jr., Calculations of the Penetration of Gamma Rays, Nuclear Development Associates, Report NYO-3075, NDA-15C-4, White Plains, N.Y., (June 1954).

[redacted]

ATOMIC ENERGY ACT - 1954

[redacted]

Paper I-B

ASTR CREW SHIELD AND MAPPING EXPERIMENTS*

C. F. Malone
Convair, Ft. Worth

*Published at Convair, Ft. Worth, as Report No. FZM-437.

[redacted]

[redacted]

ASTR CREW SHIELD AND MAPPING EXPERIMENTS
(Title Unclassified)

by

C. F. Malone

Convair, A Division of General Dynamics Corporation, Fort Worth, Texas

A series of ground experiments were carried out to determine the total and scattered fast neutron and gamma dose rates from the ASTR. Measurements were made for several ASTR configurations inside the shielded crew compartment, along the ASTR centerline in air, and at a constant radial distance of 33 feet from the ASTR core. Experimental data are presented for a portion of the measurements made. Comparison of data for the various ASTR configurations indicates that the side shielding rather than the front and rear shielding control the fast neutron and gamma dose rates in the engineered crew compartment. Similarly, it was found that the dose rates in air along the forward centerline of the ASTR are primarily dependent on the side shielding of the ASTR.

Measurements of the total and scattered fast neutron and gamma dose rates from the Aircraft Shield Test Reactor (ASTR) have been completed. When integrated into the balance of the airborne program, these experiments give information concerning air, ground, and structure components of scattered radiation. Comparison of these results with those obtained by theoretical predictions allow an evaluation of the current theoretical methods.

The experiments under consideration are as follows:

1. Measurements inside the Shielded Crew Compartment

2. ASTR Centerline Measurements in Air

AEC-3311-CVAC

[redacted]

ATOMIC ENERGY ACT - 1954

[redacted]

3. Radial Mapping Measurements - Source Anisotropy

The shielding on the reactor was varied for each of the above experiments. Reactor shield configurations that yield over-all effects of the front, side, and rear shields were of prime importance and were consequently repeated in each experiment. A portion of the results obtained during these experiments is presented in this paper.

EXPERIMENTAL SET-UP

Shielded Crew Compartment

The shielded crew compartment and the ASTR were removed from the Nuclear Test Airplane (NTA) for this experiment. The separation distance of the crew compartment and the ASTR was identical to that when both are in the airplane. Fast neutron and gamma dose rates were measured along the centerline of the crew compartment. Other fixed detector locations inside the compartment were established to obtain correlation of data taken on the ground with data taken at various altitudes.

ASTR Centerline Measurements in Air

With the ASTR located on a stand, the scattered and total dose rates for gammas and fast neutrons were measured as functions of distance along the forward centerline of the ASTR. The distances covered were from 33 to 100 feet. Figure 1 is a plan view of the experimental arrangement. The lead shadow shield is removable; dose rates have been measured both with and without the shadow shield in place. The entire unit, containing the two detectors and the direct beam shield, was positioned by remote control.

Radial Mapping

Figure 2 shows the plan view of the experimental setup for radial mapping. Scattered and total dose rates for fast neutrons and gammas were measured at a distance of 33 feet from the center of the ASTR core.

ASTR Configurations

The ASTR shield configurations discussed in this report are shown in Figure 3.

[redacted]

[redacted]

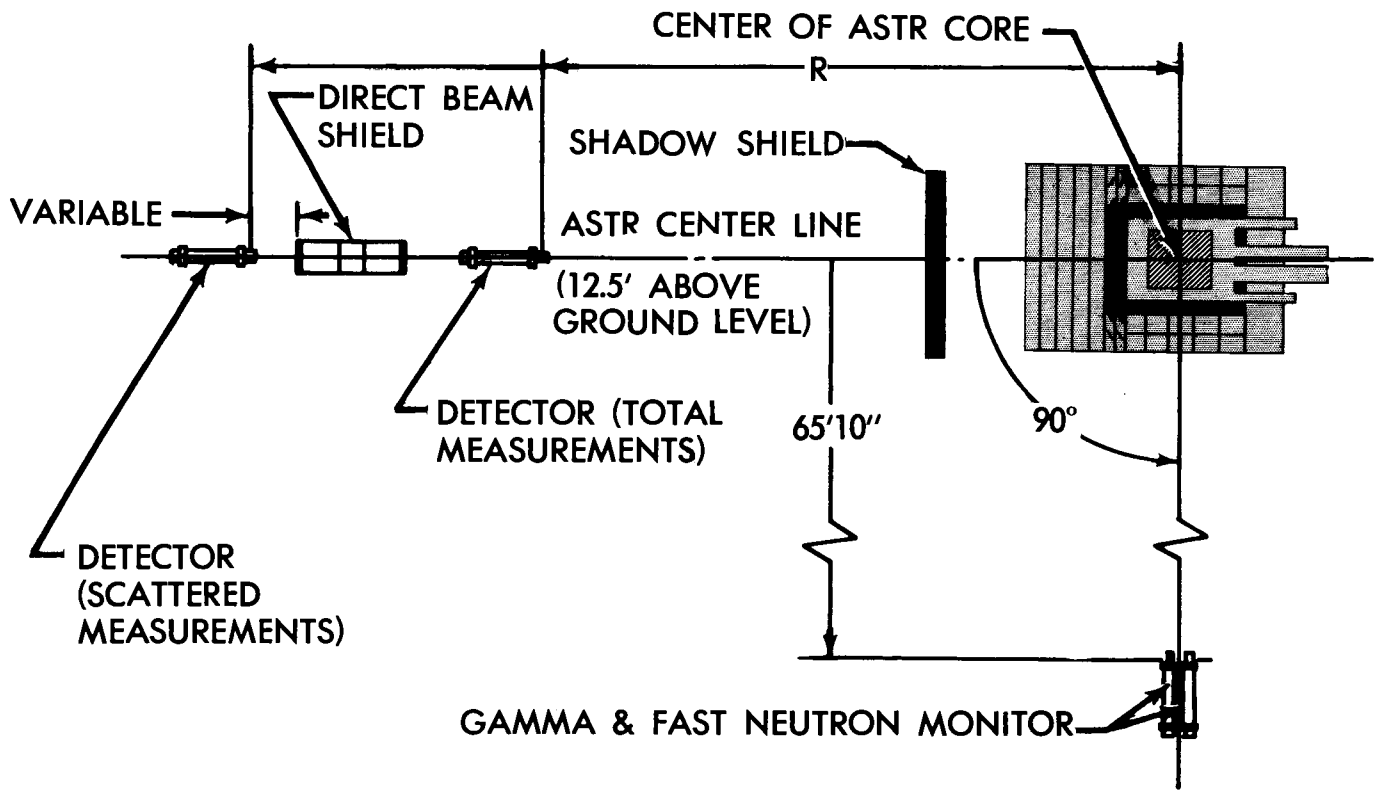

Figure 1. Centerline Measurements In Air

[redacted]

[redacted]

NPC 3203

AEC-3311-CWAC
ATOMIC ENERGY ACT - 1954

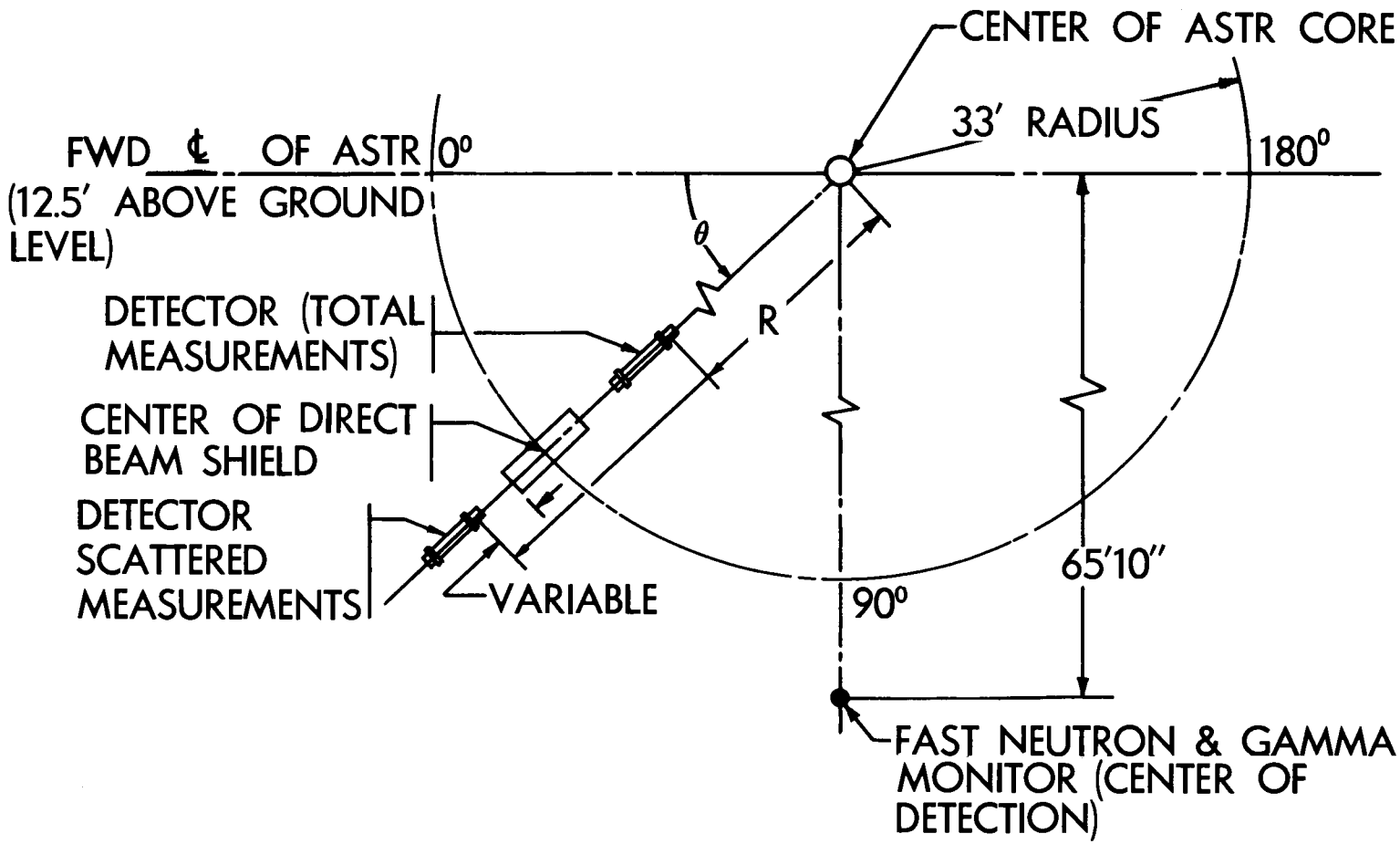

Figure 2. Radial Mapping

AEC-2311-CWAC
ATOMIC ENERGY ACT - 1954

NPC 3204

[redacted]

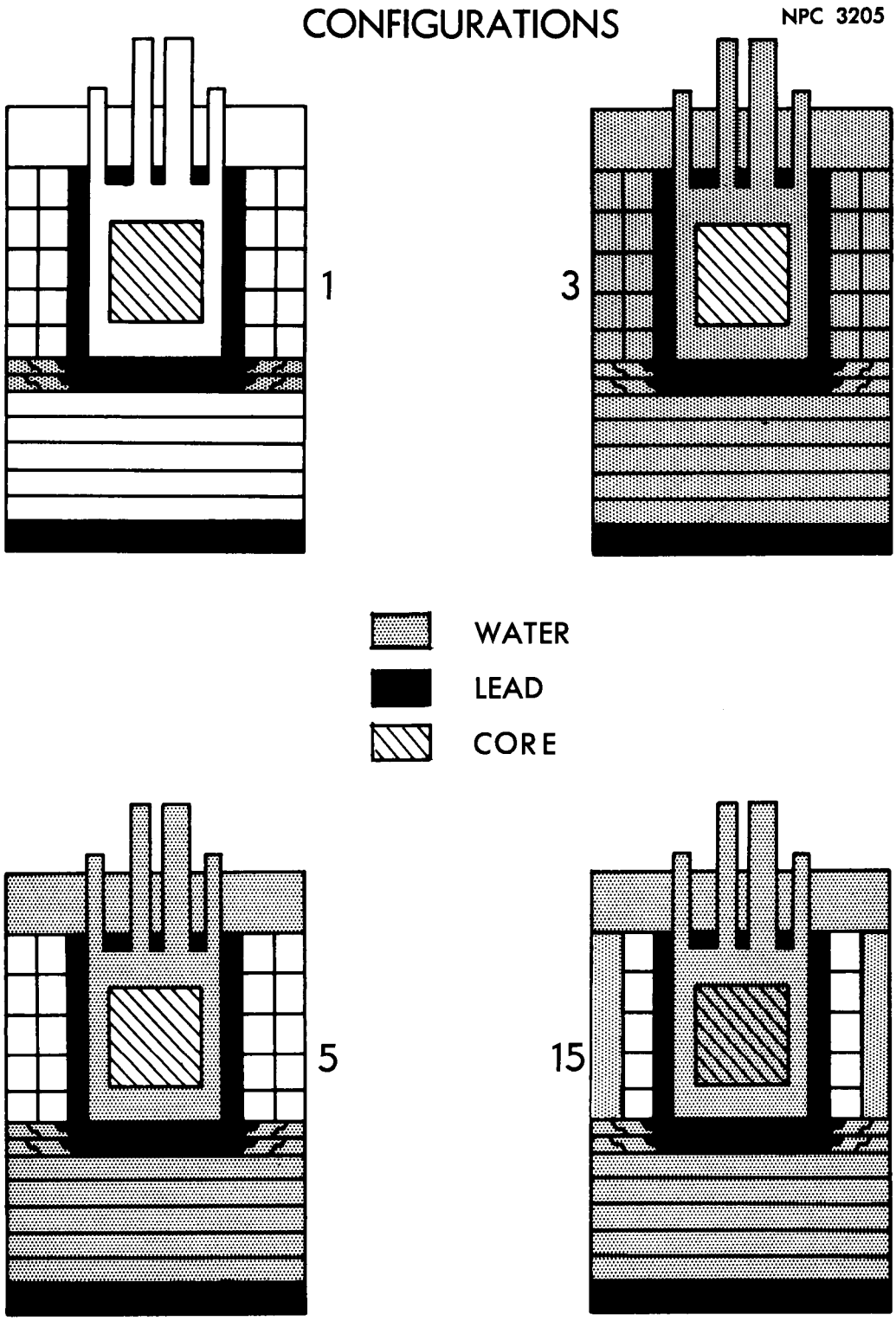

Figure 3. ASTR Configuration

[redacted]

AEC-3311-CVAC
[redacted]
ATOMIC ENERGY ACT - 1954

[redacted]

RESULTS

Shielded Crew Compartment

Figure 4 gives the total fast neutron and gamma dose rates as measured along the centerline of the crew compartment as a function of distance from the aft wall.

Comparison of data obtained with ASTR Configurations 3, 15, and 5 will yield information on the shielding properties of the side tanks of the ASTR. Removing 7 inches of water from the sides (Configurations 3 and 15) results in an increase in the fast neutron dose rate in the crew compartment of about a factor of 5. A further reduction of 7 inches of water on the sides of the ASTR (Configurations 15 and 5) results in an additional increase in fast neutron dose rate of a factor of 7. Thus, the over-all increase in fast neutron dose rate in the crew compartment by removal of the side shielding is a factor of 35.

Similarly, the removal of 7 inches of water from the sides results in an increase in gamma dose rates in the crew compartment by a factor of 7. A further reduction of 7 inches of water on the sides of the reactor results in an additional increase in the gamma dose rate of about a factor of 11. Thus, the over-all increase in gamma dose rate in the crew compartment by removal of the side shielding is a factor of 77. These large increases are due solely to the scattered dose rate increases.

A comparison of the fast neutron dose rates for ASTR Configurations 1, 5, and 3 shows that removal of the side shielding increases the fast neutron dose rate by a factor of 35, while removing the front and rear shielding increases the fast neutron dose rate by only an additional 30%. Thus, the side shielding of the ASTR controls the fast neutron dose rate in the engineered crew compartment.

A similar comparison of the gamma dose rate for ASTR Configurations 1, 5, and 3 shows that removal of the side shielding increases the gamma dose rate in the crew compartment by a factor of 77, while the removal of the front and rear shielding increases the gamma dose rate by an additional 25%. This result points out the large effect of the side shielding of the ASTR on gamma dose rates in the engineered crew compartment.

[redacted]

[redacted]
ATOMIC ENERGY ACT--1954

[redacted]

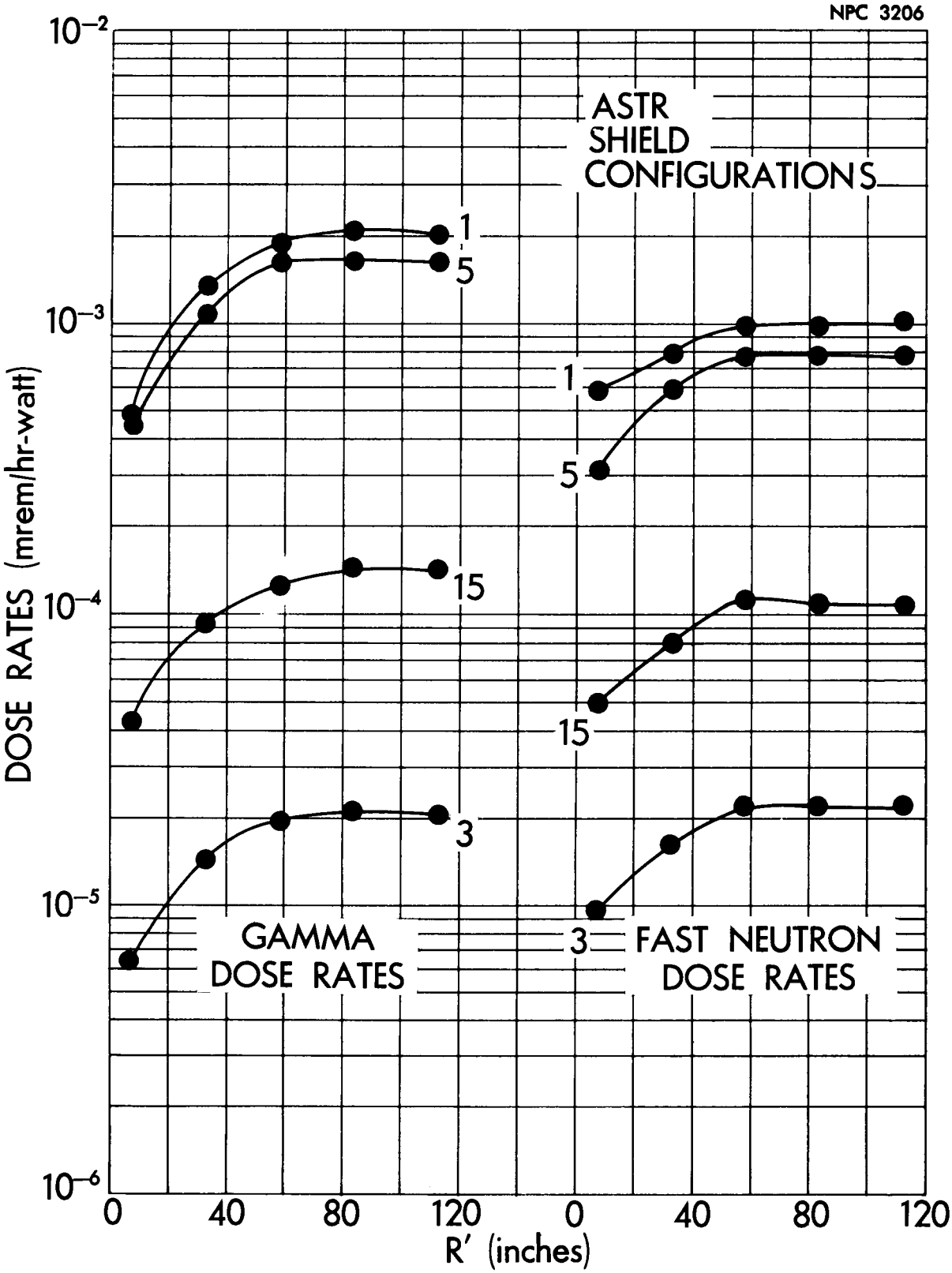

Figure 4. Centerline Measurements In The Shielded Crew Compartment

[redacted]

AEC-3311-CVAC
[redacted]
ATOMIC ENERGY ACT - 1954

[redacted]

ASTR Centerline Measurements in Air

Figure 5 gives the total and scattered fast neutron dose rates in air measured as a function of distance from the center of the ASTR core. Figure 6 gives the same data for gamma dose rates.

Comparisons of ASTR Configurations 1, 5, 3, and 15 may be made similar to the comparisons made for dose rates inside the crew compartment. A generalized conclusion may be drawn here, as before, that dose rates along the forward centerline of the ASTR in air are primarily dependent on the side shield tanks of the ASTR.

The curves of dose rate vs distance from the ASTR vary in slope for the various shield configurations. The typical slope for all the curves might be considered to be approximately 1.4.

All gamma dose rates were measured with an anthracene scintillation dosimeter which has some response to neutrons. A correction factor has been applied to the gamma data to compensate for the neutron sensitivity of anthracene according to the analysis made by K. R. Spearman(1).

Radial Mapping Source Anisotropy

Figure 7 gives the total and scattered fast neutron dose rates as measured in the horizontal plane containing the centerline of the ASTR. Figures 8 and 9 present similar data for gamma dose rates. A comparison of the theoretical and experimental mapping terms is being made by Mr. C. E. Humphries in his paper(2).

[redacted]

ATOMIC ENERGY ACT - 1954

[redacted]

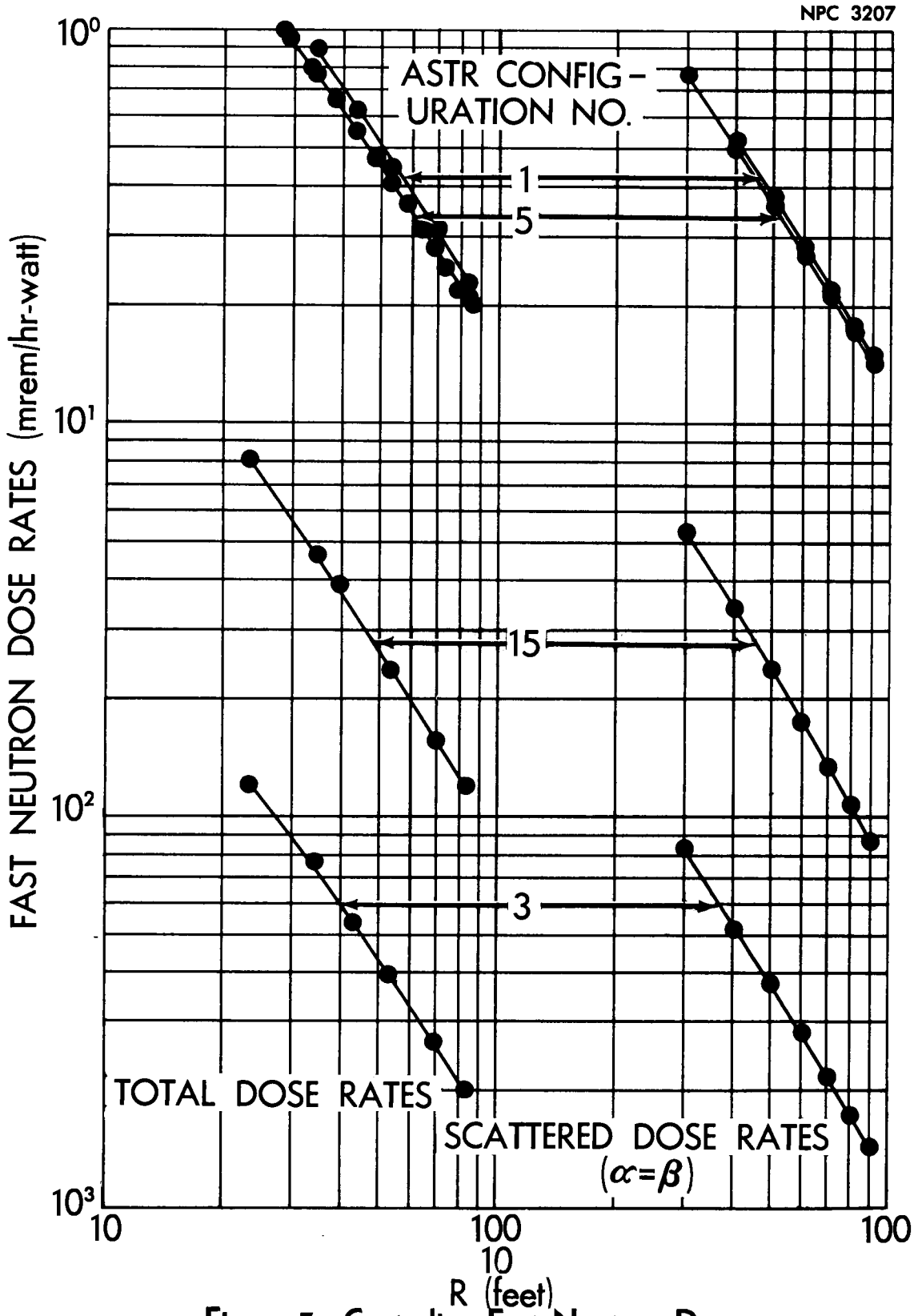

Figure 5. Centerline Fast Neutron Dose Rate Measurements In Air

[redacted]

AEC-3311-CVAC
[redacted]
ATOMIC ENERGY ACT - 1954

[redacted]

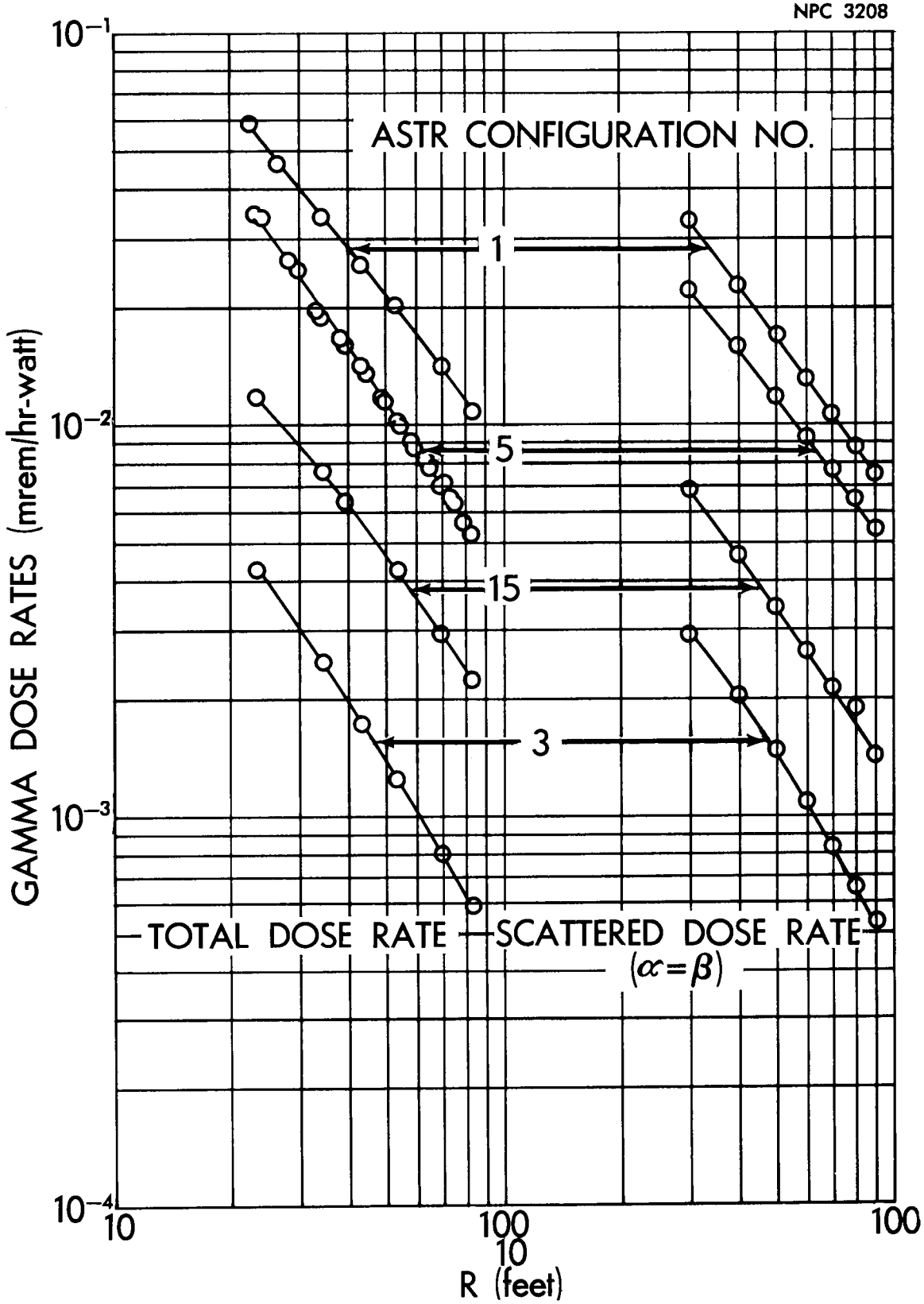

Figure 6. Centerline Gamma Dose Rate Measurements In Air

AEC-3311-CVAC

[redacted]

ATOMIC ENERGY ACT - 1954

[redacted]

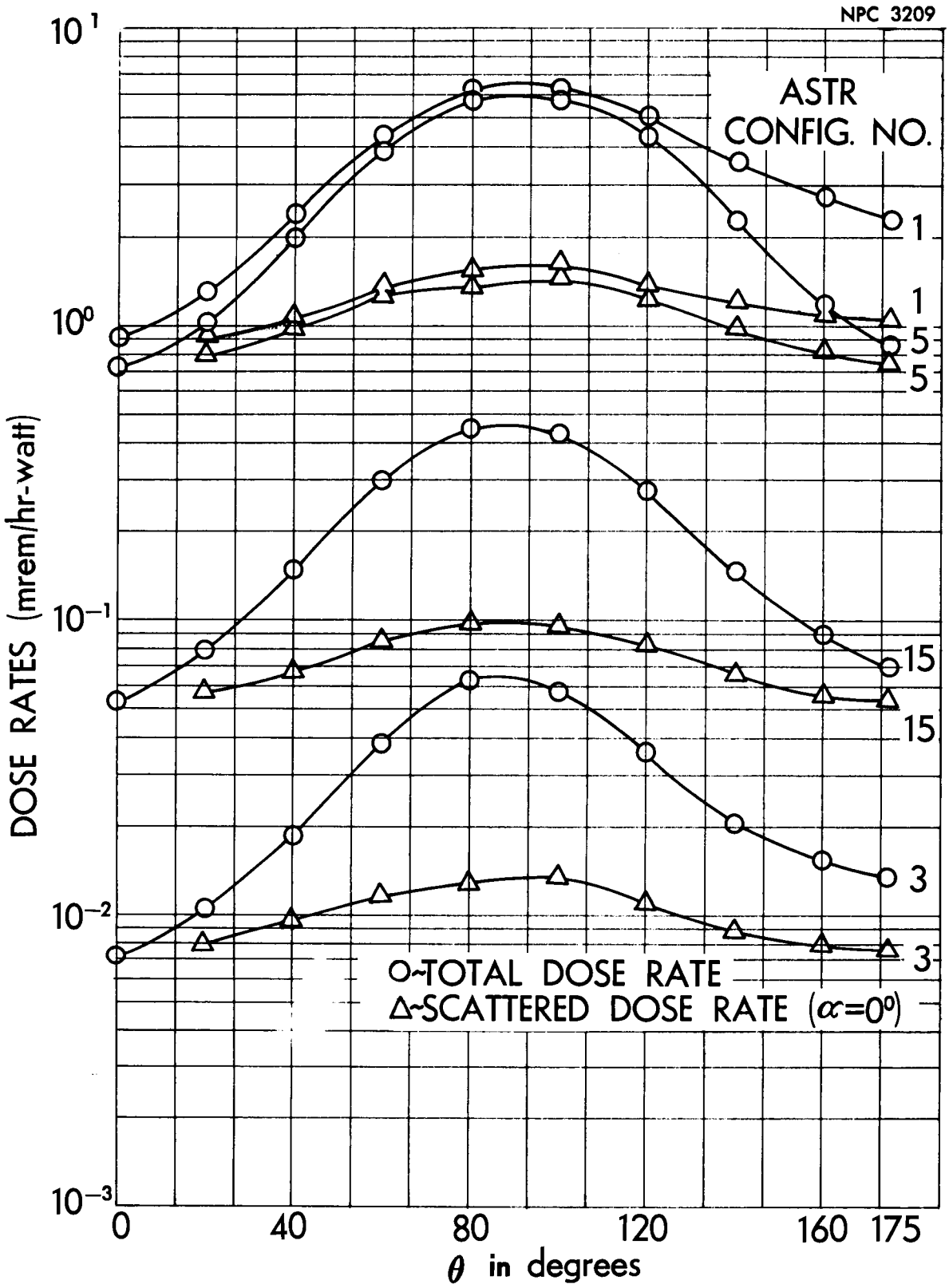

Figure 7. Radial Mapping Total And Scattered Gamma Fast Neutron Dose Rates vs. Azimuthal Angle

AEC-3311-CVAC

[redacted]

ATOMIC ENERGY ACT - 1954

[redacted]

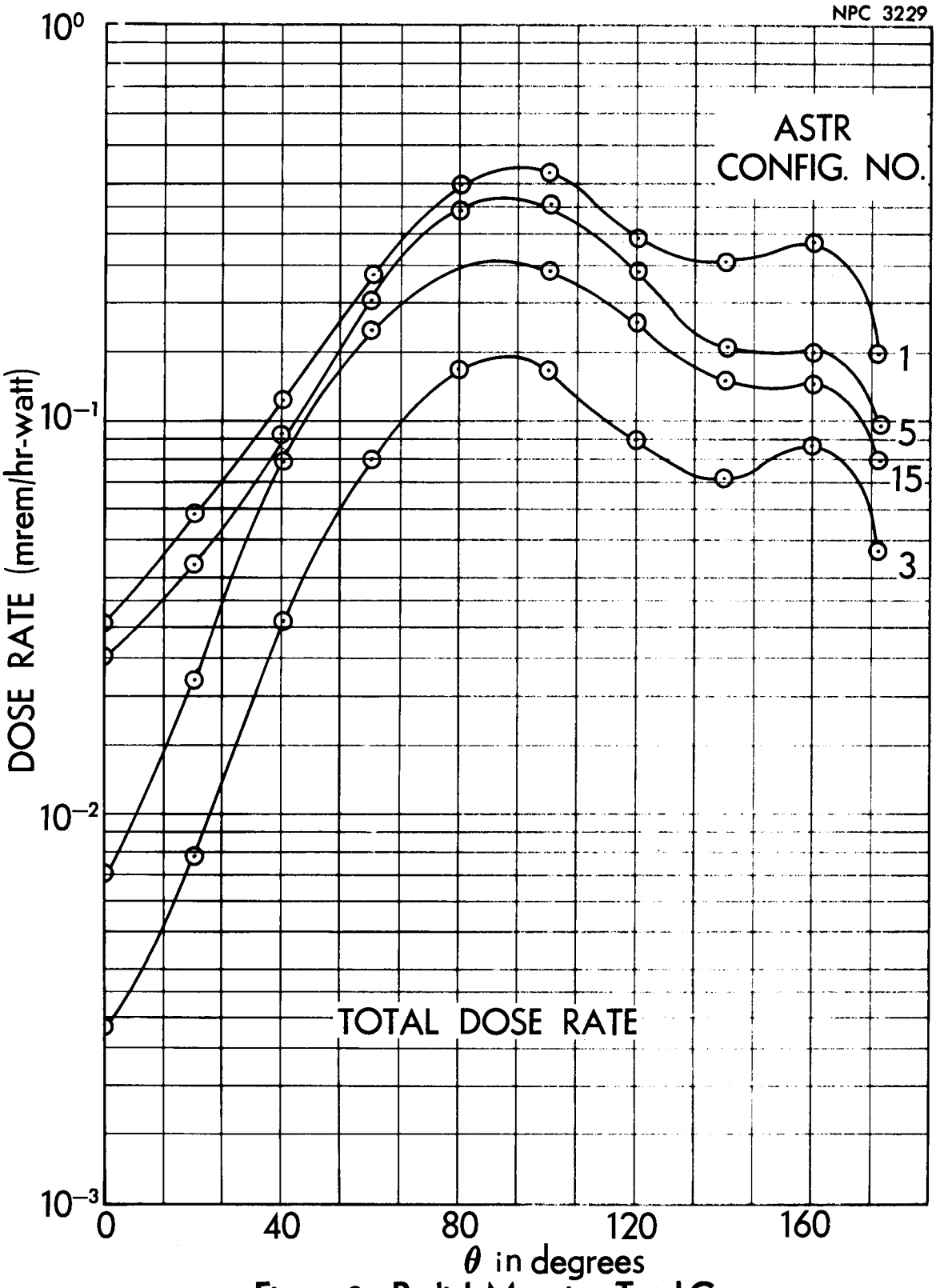

Figure 8. Radial Mapping Total Gamma Dose Rates vs. Azimuthal Angle

[redacted]

AEC-3311-CVAC
[redacted]
ATOMIC ENERGY ACT - 1954

[redacted]

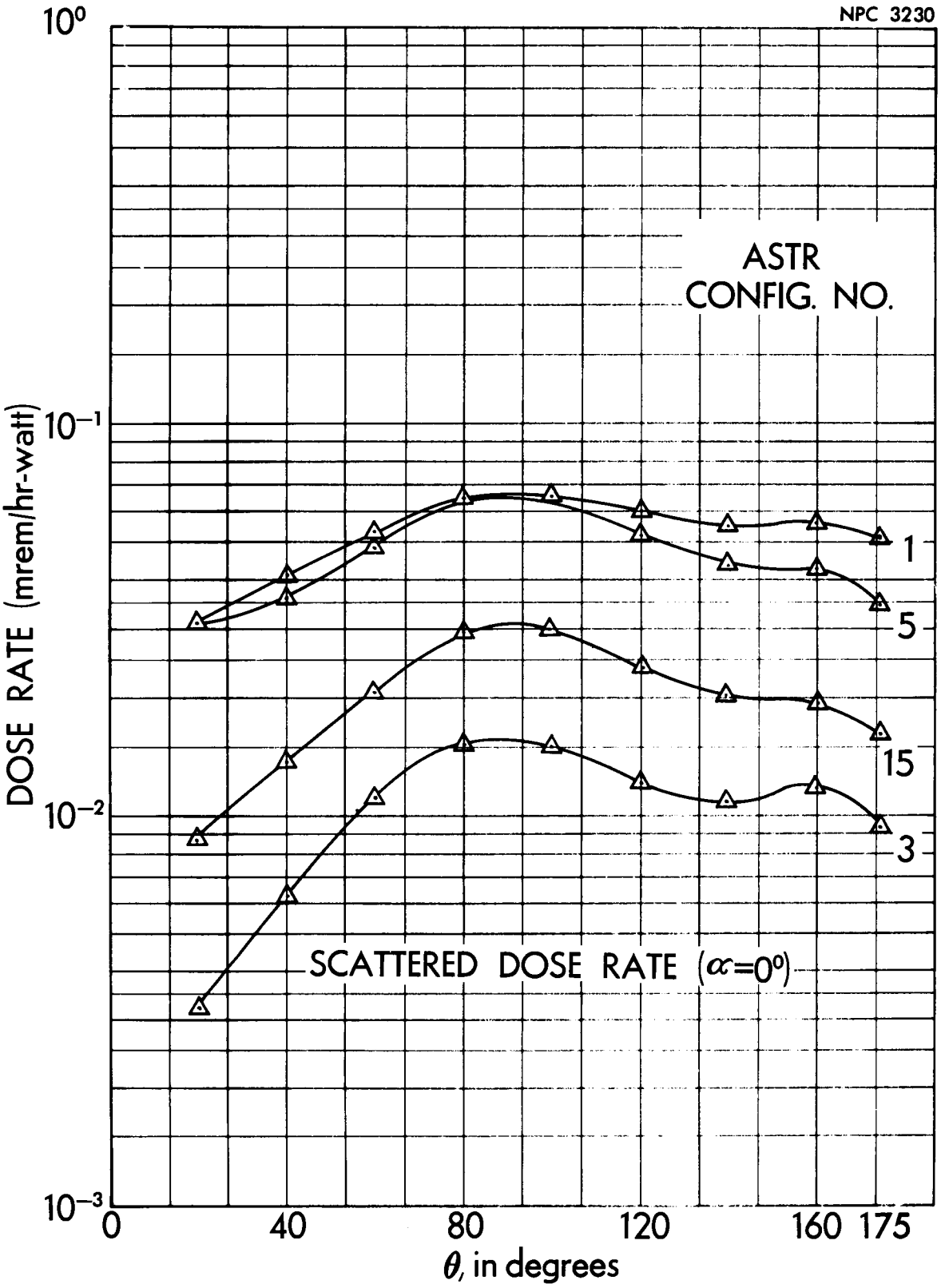

Figure 9 Radial Mapping Scattered Gamma Dose Rates vs. Azimuthal Angle

[redacted]

AEC-3311-CVAC
[redacted]
ATOMIC ENERGY ACT - 1954

[redacted]

REFERENCES

1. K. R. Spearman, Neutron Sensitivity of Anthracene Dosimeters, Convair-Fort Worth Report MR-N-100, NARF-55-67T, (18 October 1955).

2. C. E. Humphries, ASTR Radiation Mapping Calculations, Talk presented at ANP Shielding Meeting, Oak Ridge, Tennessee, (7-8 May 1956).

[redacted]

[redacted]

ATOMIC ENERGY ACT - 1954

SECRET

Paper I-C

ASTR MAPPING PREDICTIONS*

C. E. Humphries
Convair, Ft. Worth

*Published at Convair, Ft. Worth, as Report No. FZM-436.

SECRET

[redacted]

ASTR MAPPING PREDICTIONS
(Title Unclassified)

by

C. E. Humphries

Convair, A Division of General Dynamics
Corporation, Fort Worth, Texas

A comparison of measured and predicted dose rates emitted from the Airborne Shield Test Reactor (ASTR) is made. These comparisons are performed for various reactor shield configurations. Agreement between measured and predicted dose rates appears to be good except when a duct or a material that acts as a duct is present. The results indicate the importance, barring adequate angular distribution data, for predicting the effectiveness of reactor shields.

The Airborne Shield Test Reactor (ASTR) operated by Convair-Fort Worth is a water moderator type reactor similar to the Bulk Shield Reactor (BSR). The variable reactor shield, which consists of 9 water tanks, a lead disc, and 4 lead or water rings, allows various shielding configurations around the ASTR. Figure 1 shows the arrangement of the tanks, discs, and rings. Table I shows the shielding configurations giving the condition of tanks, discs, and rings.

Measurements were made at various angles with respect to the reactor centerline with detector and reactor located 12.5 feet above the ground. These scattered and total measurements for gammas and neutrons were corrected to a 32-foot separation distance between the center of the ASTR core and the detector. Predictions of dose rates were performed only for the direct beam radiation since the scattered predictions are difficult to obtain when the detector is placed off the centerline of the reactor.

The predictions were accomplished with several simplifying assumptions. They are:

AEC-3310-CVAC

[redacted]

[redacted]

[redacted]

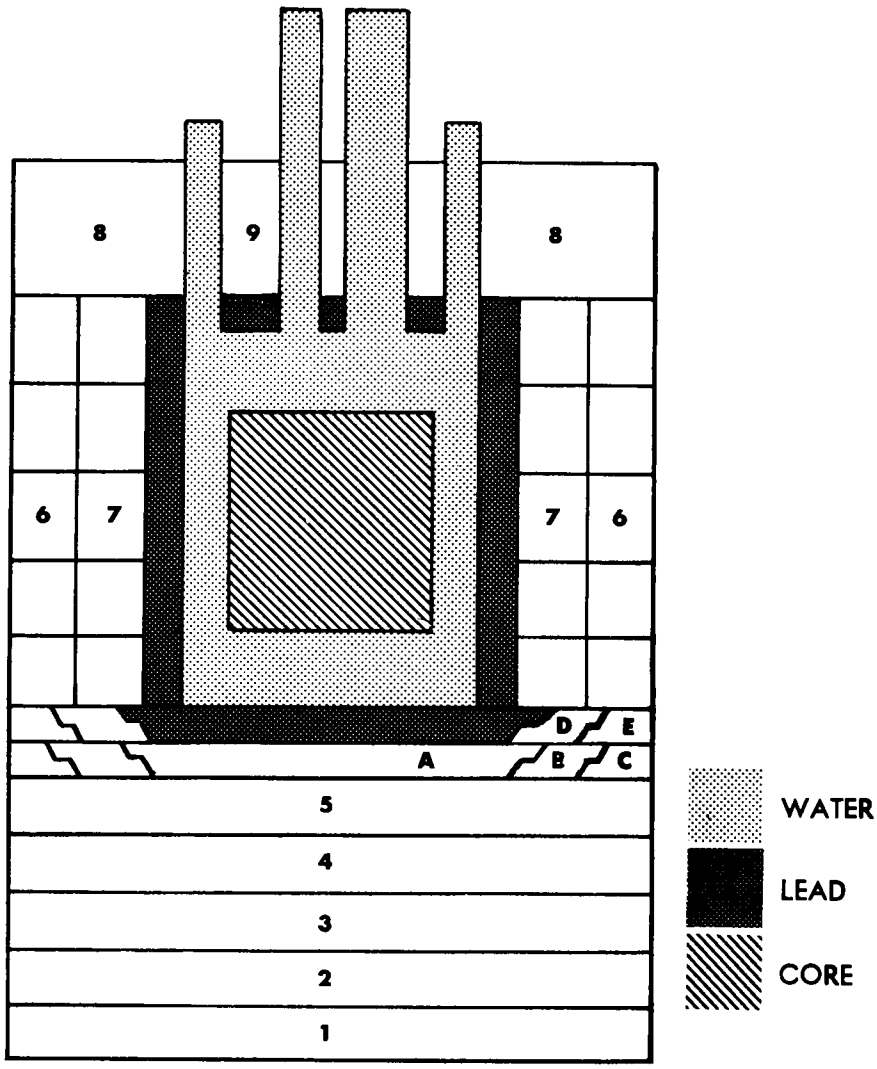

[redacted]

Figure 1. ASTR with various Shield Tanks, Rings and Disks.

[redacted]

[redacted]

TABLE I

ASTR SHIELD CONFIGURATIONS

Config. No.	Inner Rings B and D	Outer Rings C and E	Disc A	Front Tanks Filled					Side Tanks Filled		Rear Tanks Filled	
				1	2	3	4	5	6	7	8	9
1	Water	Water	Lead									
3	Water	Water	Lead	x	x	x	x	x	x	x	x	x
5	Water	Water	Lead	x	x	x	x	x			x	x
11	Lead	Lead	Lead	x	x	x	x	x	x	x	x	x

AEC-3310-CVAC
ATOMIC ENERGY ACT - 1954

[redacted]

1. For gamma radiation, the ASTR bare core fission spectrum per watt is that reported by Maienschein for the BSR(1).

2. For neutron radiation, the ASTR bare core fission spectrum per watt is that reported by Cochran and Henry for the BSR(2). This spectrum was normalized to the centerline dose rate measurements for neutrons from the BSR(3).

3. The flux, to account for the anisotropic core, was assigned a cosine distribution as shown in Figure 2, where $f(\alpha)$ is the ratio of the flux emitted from the ASTR as a function of the source angle to the flux emitted from the BSR centerline.

4. This flux is emitted radially from the core center.

5. The flux at the surface of the reactor shield can be calculated using the differential energy spectra data (moments method tabulated by NDA(4). The method is outlined in MR-N-84(5).

6. Except for the 2.2-Mev gamma production due to the capture of thermal neutrons by hydrogen in the water, gamma production within the shielding will be unimportant.

7. As moments method data was not available for neutrons in lead or aluminum, straight exponential attenuation was used when the lead and aluminum were not backed by water. Relaxation lengths of 9.5 cm for lead and 26.2 cm for aluminum were used.

8. The angular distribution of the gamma radiation emitted from the shield is shown in Figure 3. This distribution was obtained from normalized ORNL data(7). The neutron angular distribution is shown in Figure 4 along with a comparison to that measured by ORNL(8). Calculations were performed before the ORNL data became available.

9. The shape of the angular distribution of the radiation emitted from the reactor is the same at all points on the shield surface as that shown. However, the magnitude of the distribution function will be that which was calculated by the moments method with its maximum in a radial direction with respect to the center of the core.

Figures 5 through 12 show comparison of measured data to predicted values. The measured values are the averaged total minus the averaged scattered values. The measured values seem to have a probable error of 5 percent, but since few points were measured more than once, no error analysis was made.

[redacted]

ATOMIC ENERGY ACT--1954

[redacted]

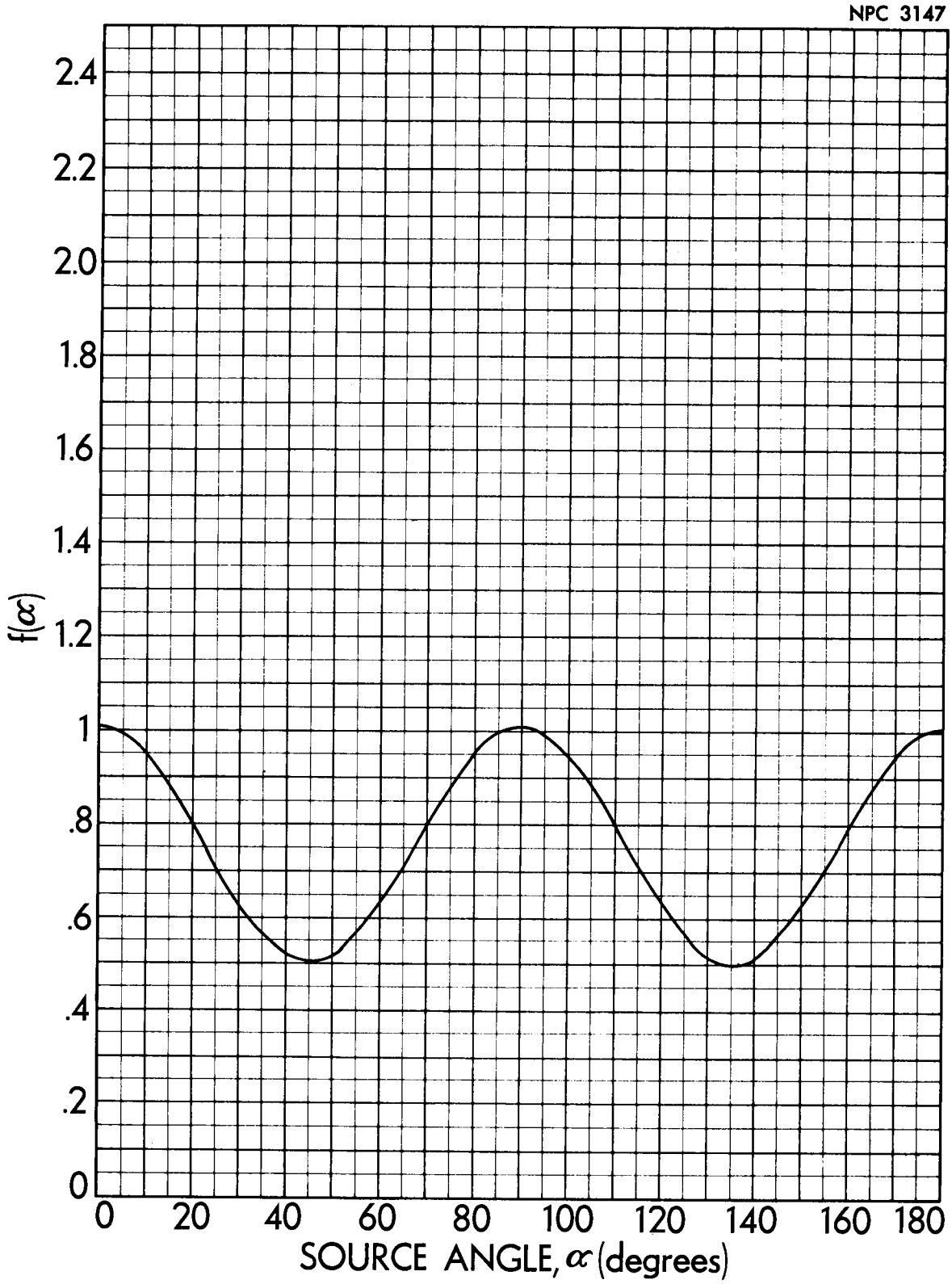

Figure 2. Flux Distribution at Reactor Core as a Function of Source Angle.

AEC-3310-CVAC

[redacted]

[redacted]

ATOMIC ENERGY ACT - - 1954

[redacted]

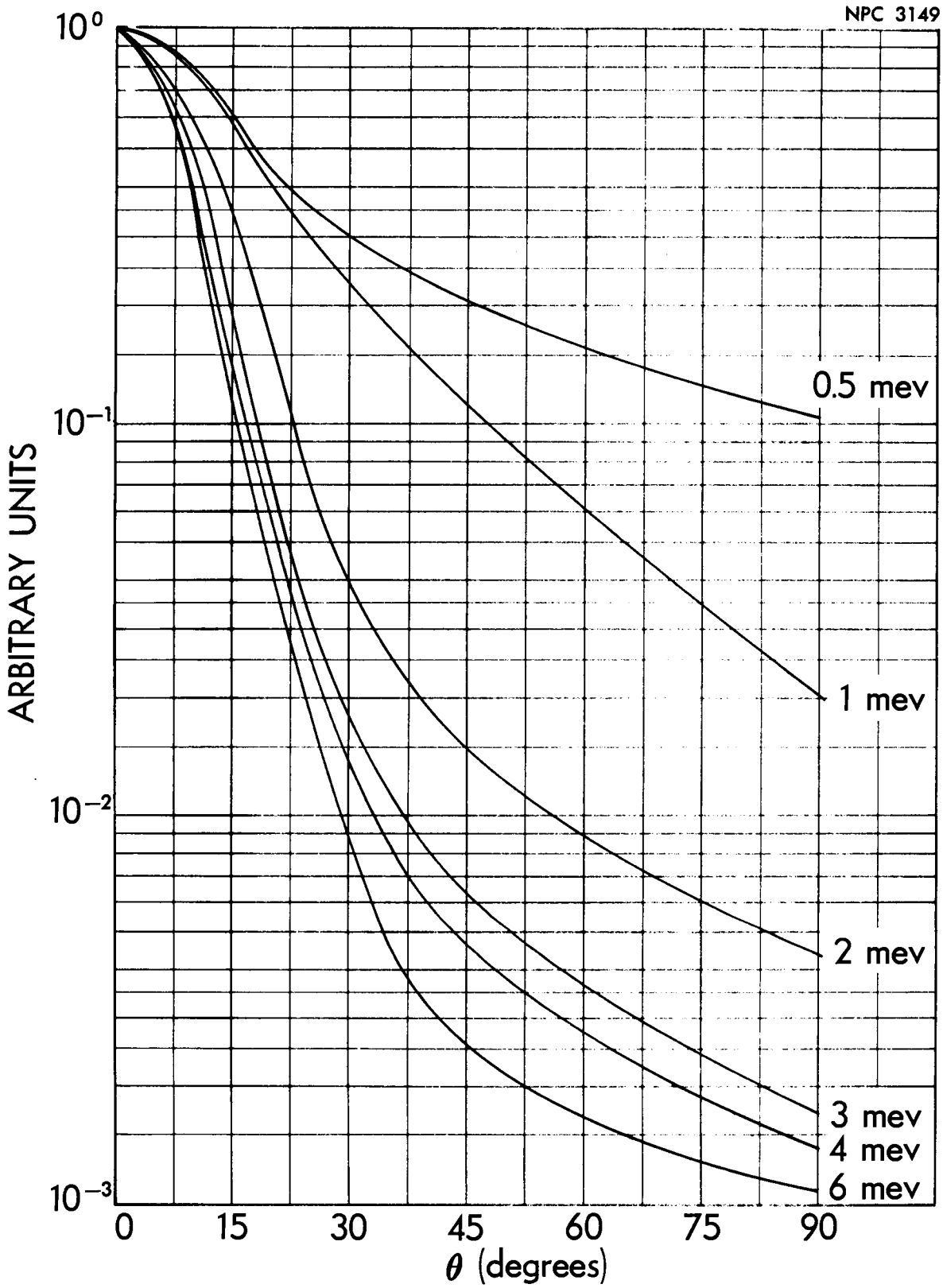

Figure 3. Angular Distribution of Gammas at Shield Surface.

AEC-3310-CVAC

[redacted]

[redacted]

[redacted]

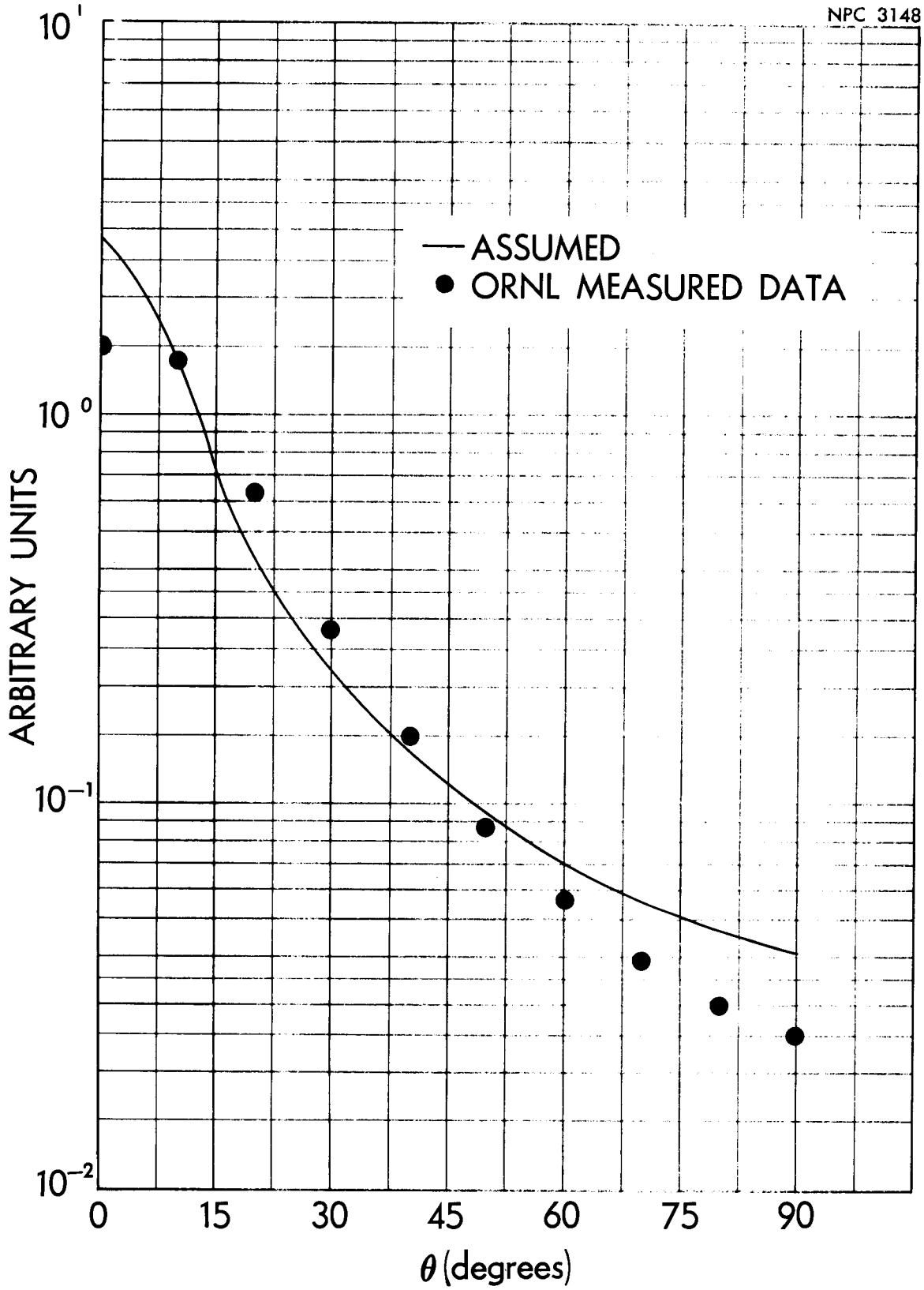

Figure 4. Angular Distribution of Neutrons at Shield Surface.

AEC-3310-CVAC

[redacted]

[redacted]

[redacted]

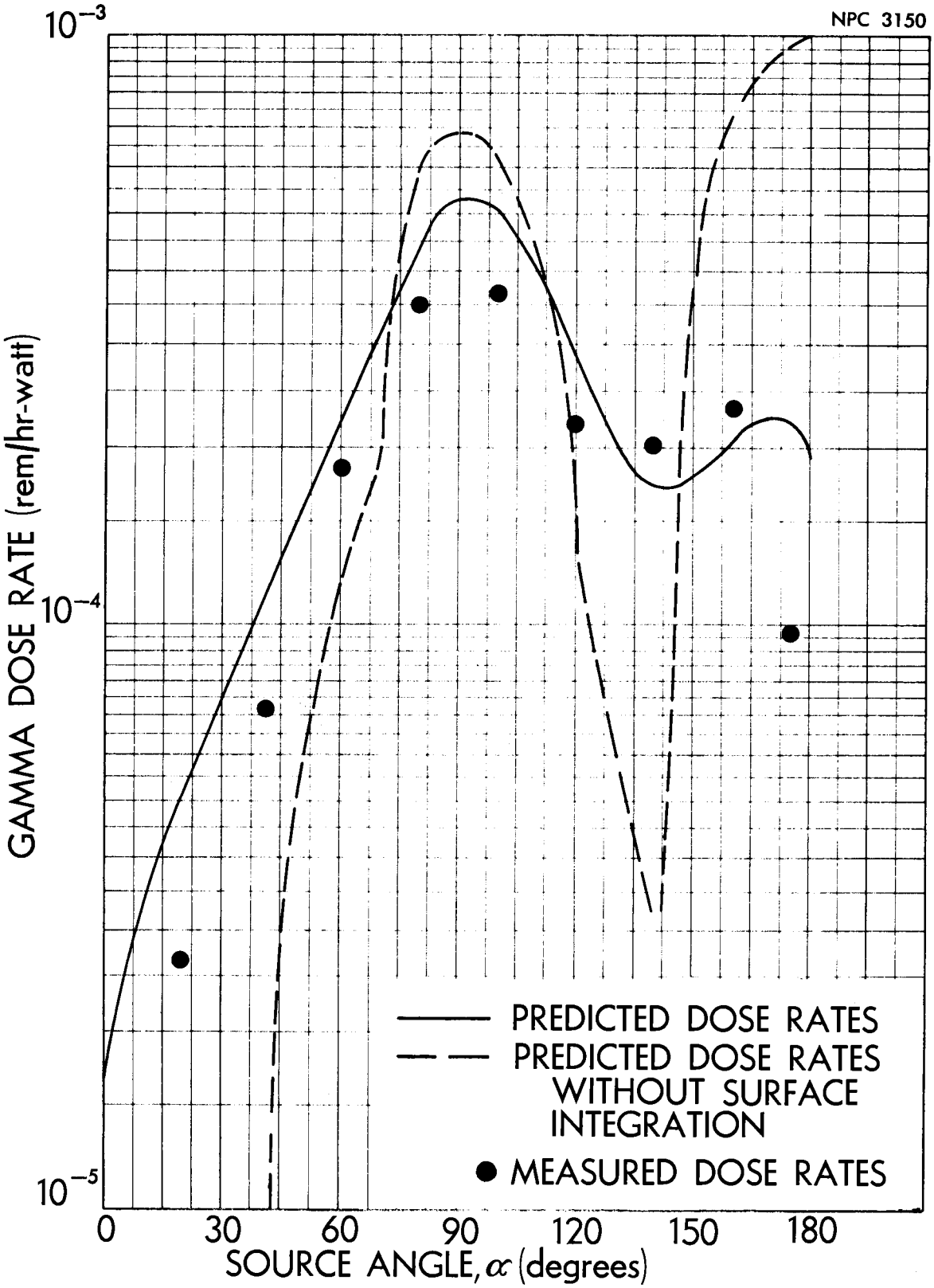

Figure 5. Comparison of Predicted to Measured Gamma Dose Rates for Configuration 1.

[redacted]

[redacted]

ATOMIC ENERGY ACT - 1954

[redacted]

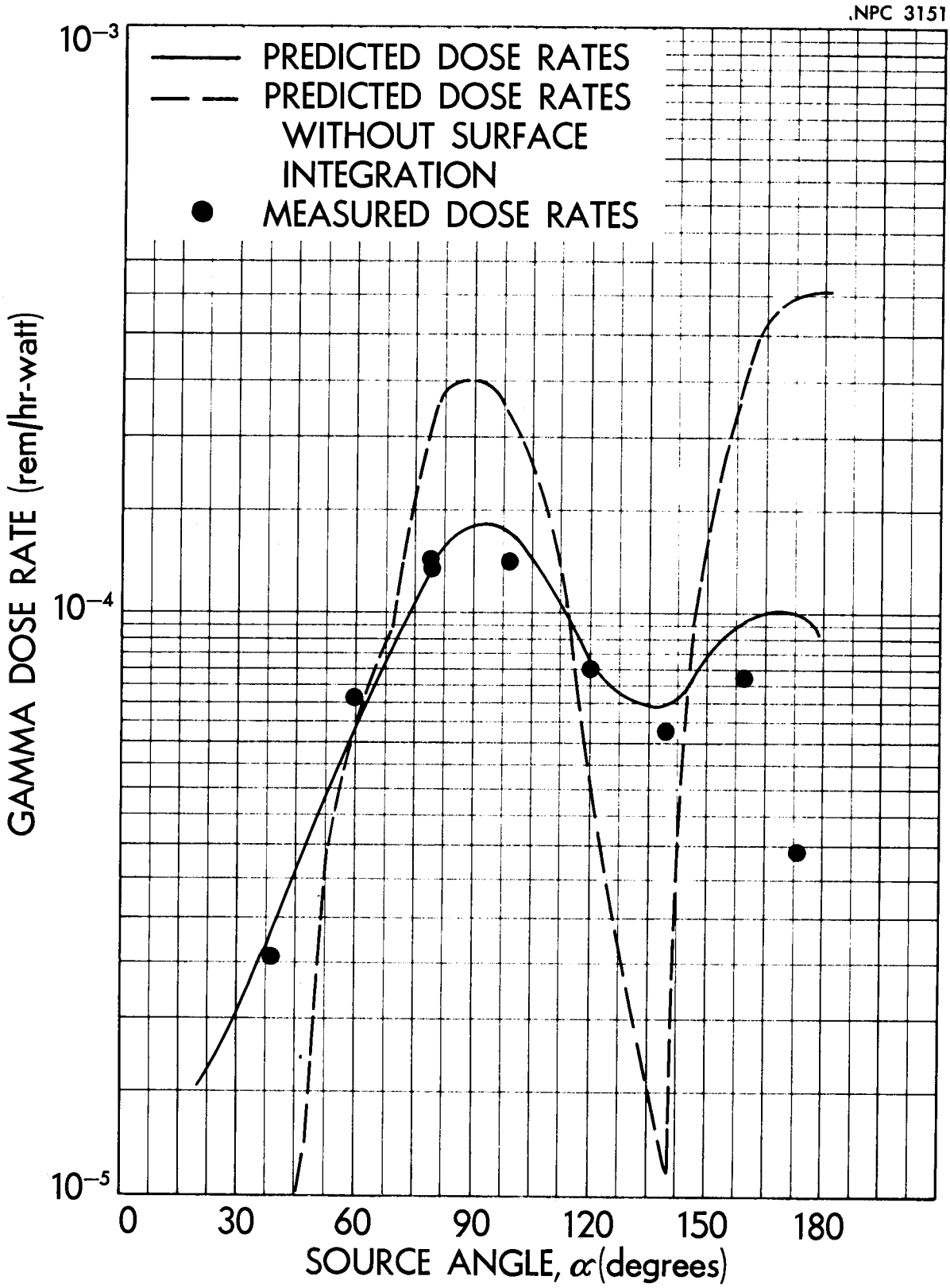

Figure 6. Comparison of Predicted to Measured Gamma Dose Rates for Configuration 3.

[redacted]

[redacted]

ATOMIC ENERGY ACT - 1954

[redacted]

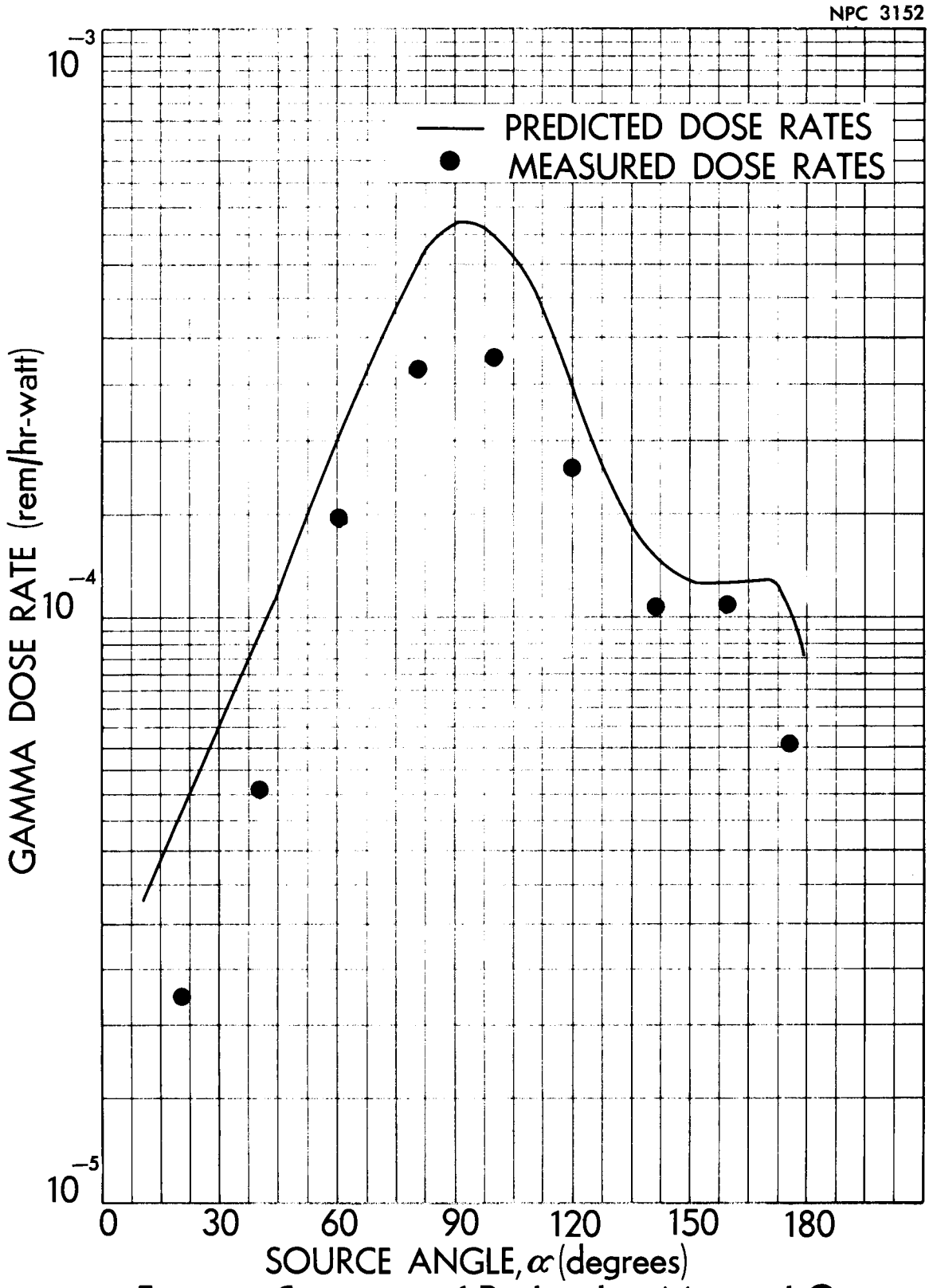

Figure 7. Comparison of Predicted to Measured Gamma Dose Rates for Configuration 5.

[redacted]

[redacted]
ATOMIC ENERGY ACT - 1954

[redacted]

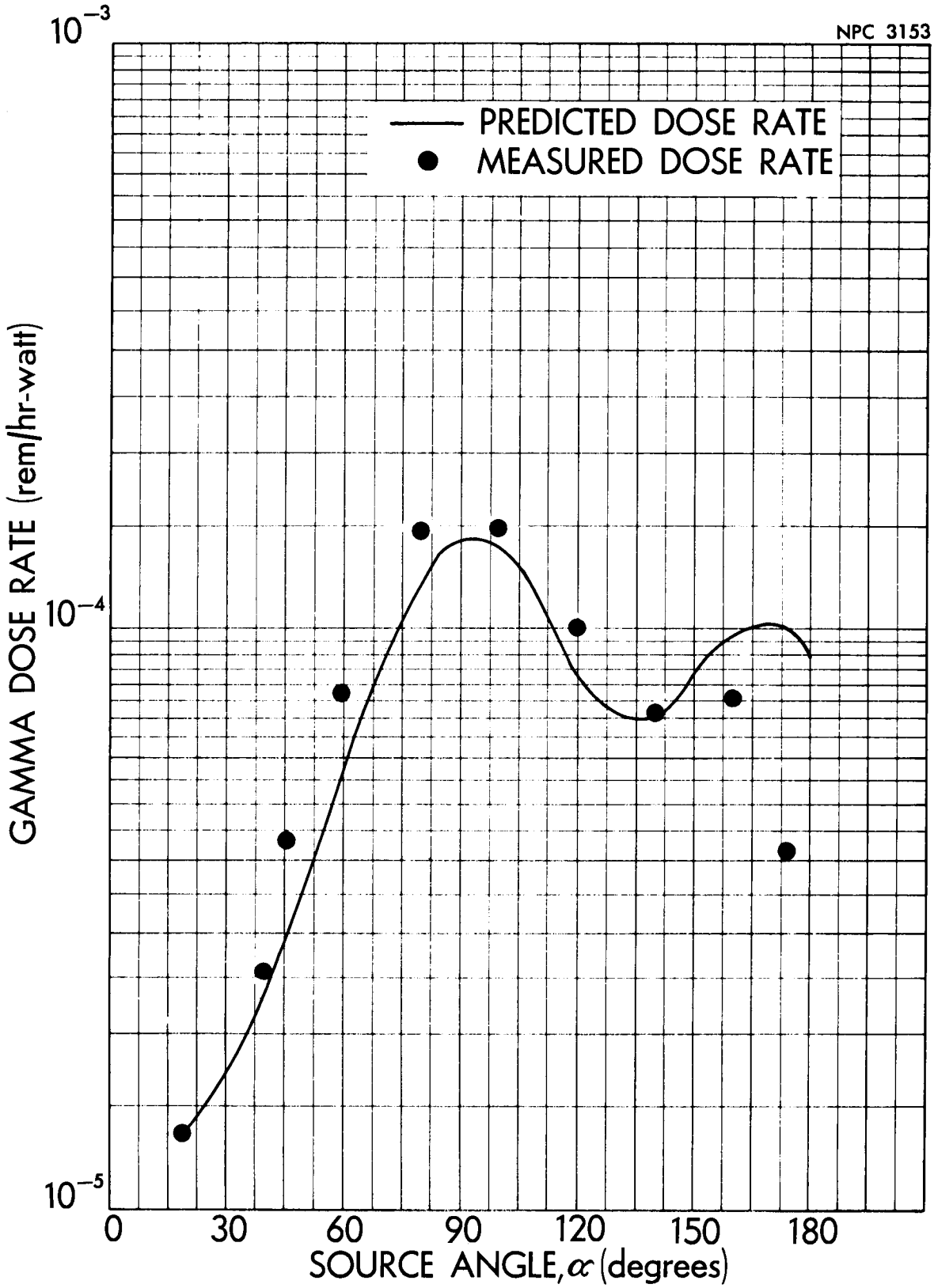

Figure 8. Comparison of Predicted to Measured Gamma Dose Rates for Configuration 11.

[redacted]

[redacted]

ATOMIC ENERGY ACT - 1954

[redacted]

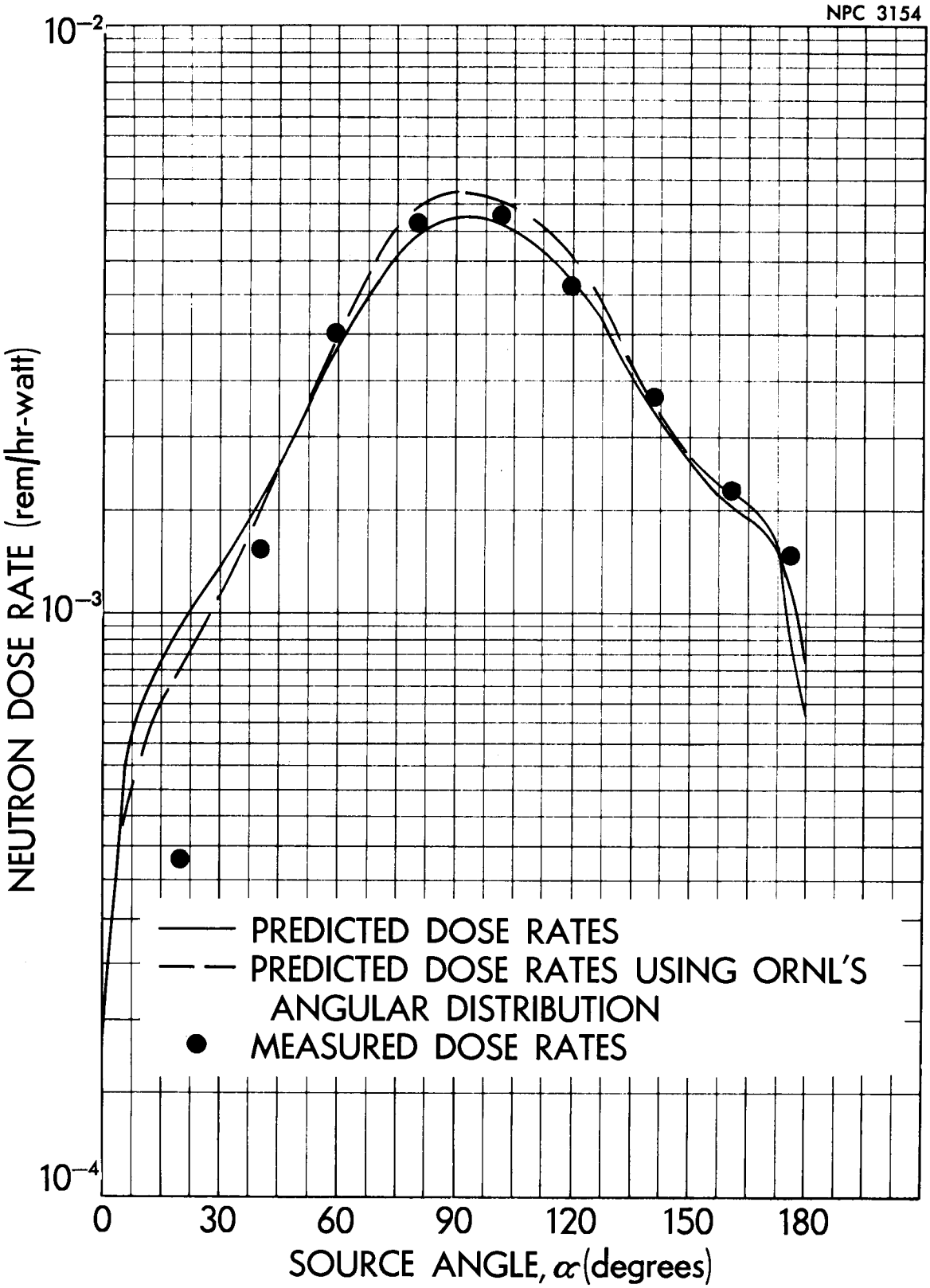

Figure 9. Comparison of Predicted to Measured Neutron Dose Rates for Configuration 1.

[redacted]

[redacted]

ATOMIC ENERGY ACT - 1954

[redacted]

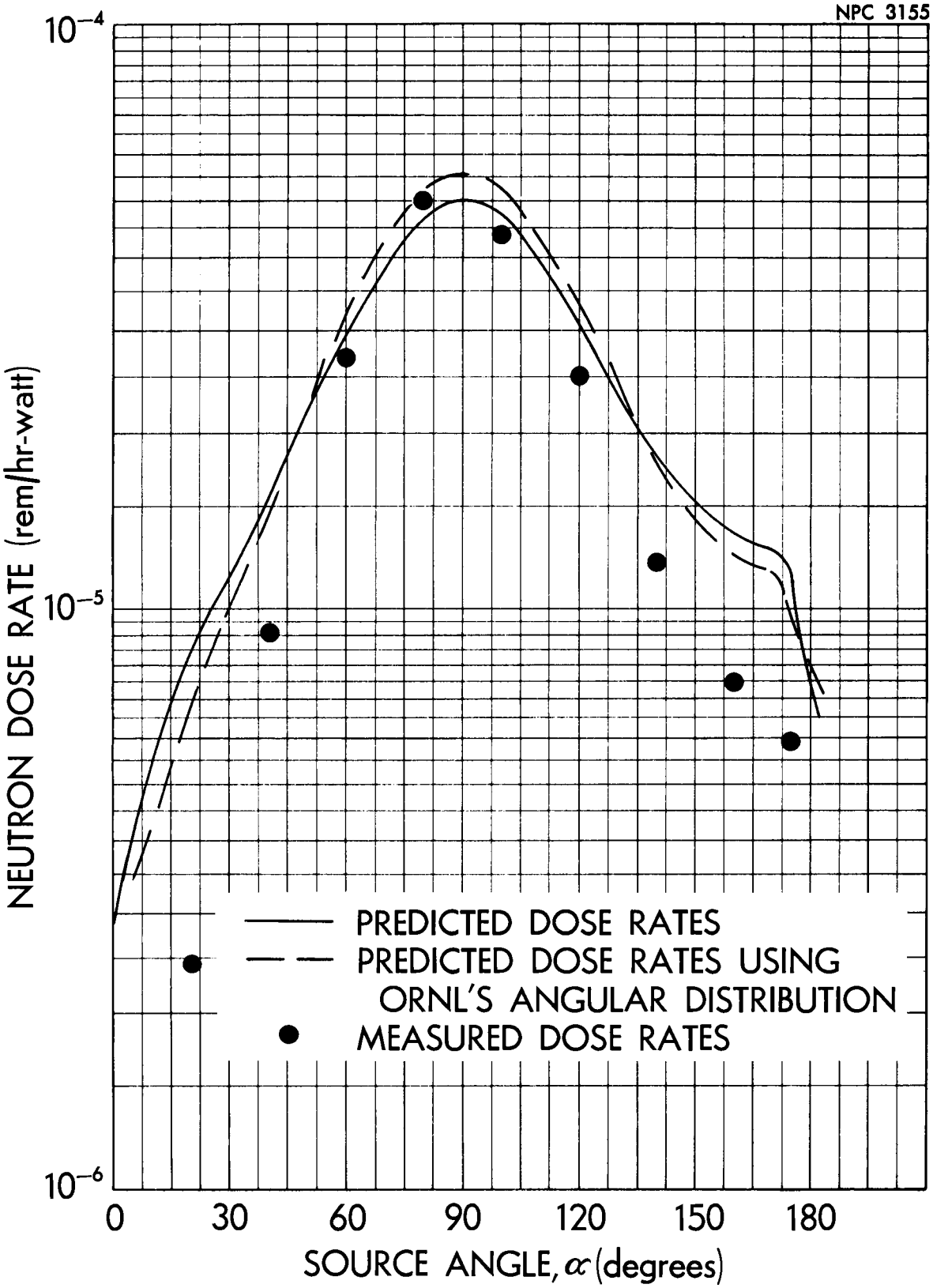

Figure 10. Comparison of Predicted to Measured Neutron Dose Rates for Configuration 3.

[redacted]

ATOMIC ENERGY ACT - 1954

[redacted]

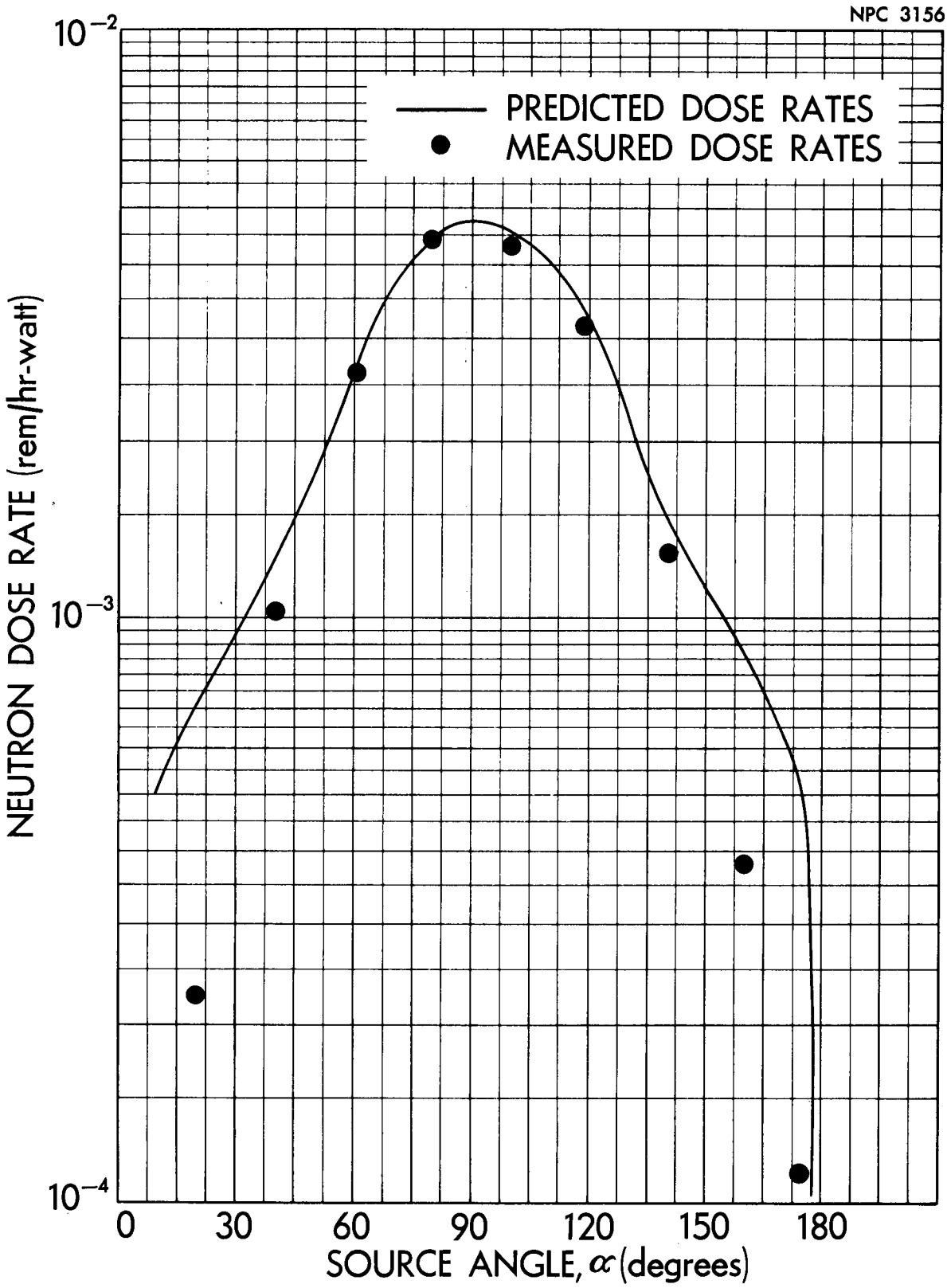

Figure 11. Comparison of Predicted to Measured Neutron Dose Rates for Configuration 5.

[redacted] [redacted]

ATOMIC ENERGY ACT - 1954

[redacted]

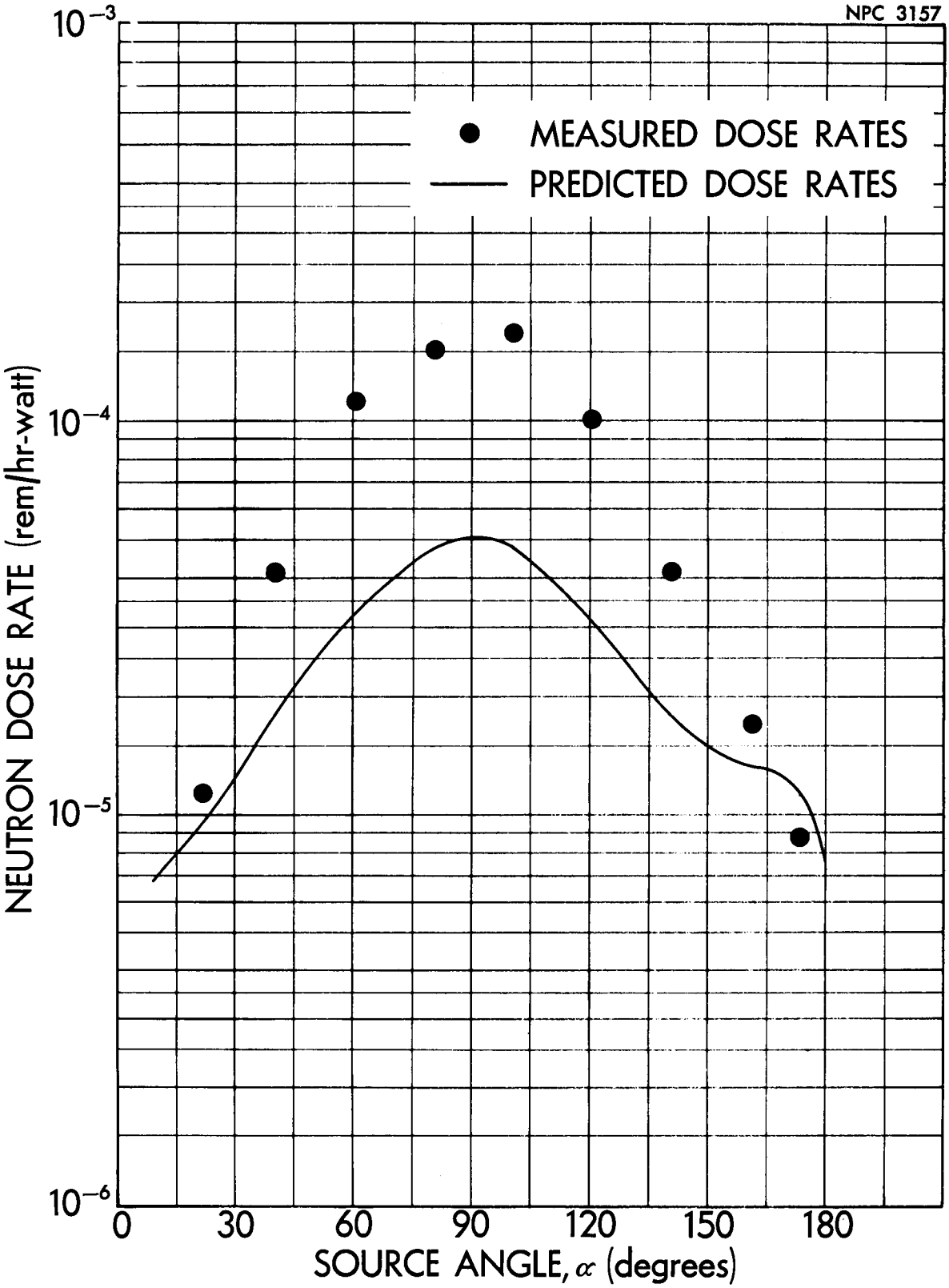

Figure 12. Comparison of Predicted to Measured Neutron Dose Rates for Configuration 11.

[redacted]

[redacted]

ATOMIC ENERGY ACT - 1954

[redacted]

Figures 9 and 10 show a comparison of the results when the angular distribution of neutrons is changed from that used in this report to that which was measured by ORNL.

Several conclusions may be drawn from these results. They are:

1. When the moments method is used in predicting the flux at the surface of the reactor shield, integration should be performed over the reactor shield to achieve a more realistic dose rate at some distance from the reactor. For example see Figures 5 and 6.

2. The method seems to hold for a range of material thicknesses of several mean free paths. When these were varied, agreement did not change noticeably.

3. As is seen from Figure 12 for configuration 11 the lead acts as a duct for the neutrons. Therefore, when a duct, or a material that acts as a duct to neutrons, is present, predictions by this method are not feasible due to the streaming of neutrons.

[redacted]

AEC-3310-CVAC
[redacted]
ATOMIC ENERGY ACT--1954

[redacted]

REFERENCES

1. F. C. Maienschein and T. A. Love, Spectrum of Gamma Rays Emitted by the Bulk Shielding Reactor, Oak Ridge National Lab Report CF-53-10-16 (October 1953).

2. R. G. Cochran and K. M. Henery, Fast-Neutron Spectra of the BSF Reactor, Oak Ridge National Laboratory Report CF-53-5-105, p. 11, (May 1953).

3. H. E. Hungerford, Bulk Shielding Facility Water Data Work Sheet, Oak Ridge National Laboratory Report CF-52-2-37, p. 1, (February 1952).

4. H. Goldstein and J. E. Wilkins, Jr., Calculations of the Penetration of Gamma Rays, Nuclear Development Associates Report NYO-3075, NDA-15C-41, White Plains, N.Y. (June 1954).

5. R. Aronson, J. Certaine, and H. Goldstein, Penetration of Neutrons from Point Isotropic Monoenergetic Sources in Water, Nuclear Development Associates Report NYO-6269, NDA-151-60, White Plains, N.Y. (December 1954).

6. B. J. Workman, C. E. Humphries, A Comparison Between BSR Centerline Dose Rates and Dose Rates Calculated By the Moments Method, Convair-Fort Worth Report MR-N-84, AEC-3375-CVAC (March 1956).

7. F. C. Maienschein, Gamma Ray Spectral Measurements With the Divided Shield Mock-up Part III, Oak Ridge National Laboratory Report CF-52-8-38 (August 1952).

8. ANPP Quarterly Progress Report for Period Ending September 10, 1955, Oak Ridge National Laboratory Report ORNL 1974.

[redacted]

[redacted]
ATOMIC ENERGY ACT - 1954

[redacted]

Paper I-D

RECENT RESULTS IN THE AIRBORNE SHIELDING PROGRAM*

C. F. Cook
Convair, Ft. Worth

*Published at Convair, Ft. Worth, as Report No. FZM-435.

[redacted]

[redacted]

RECENT RESULTS IN THE AIRBORNE SHIELDING PROGRAM
(Title Unclassified)

by

C. F. Cook

Convair, A Division of General Dynamics
Corporation, Fort Worth, Texas

Experimental data are being obtained both in the Nuclear Test Airplane (NTA) and the B-50 escort airplane from flights with the ASTR. Some of these data are presented and comparisons are made with theoretical predictions. These comparisons, which are preliminary in nature, indicate that the build-up and attenuation factors used for the theoretical neutron dose rate calculations should be revised to obtain agreement with experiment. The fast neutron dose rates measured in the B-50 escort airplane agree fairly well with theoretical predictions. The gamma predictions, however, are low by almost a factor of two.

INTRODUCTION

The Convair Airborne Shielding Program is designed to obtain the first experimental data for an engineered shield system under environmental conditions approximating those to be expected tactically. In addition, this program is so designed as to allow separation of air, ground, and structure effects on scattered fast neutron and gamma radiation. Obvious results obtained from such a program are the experimental determination of scattered fast neutron and gamma dose rates as a function of air density, and the variation in fast neutron and gamma dose rates with large distances from the source. This information is being used to determine the reliability of current theoretical methods of analysis for scattered dose rate calculations. In particular, this paper presents a comparison of theoretical predictions with shielding data obtained in flight using the Nuclear Test Airplane (NTA). Since the initial flight of the NTA on

AEC-3309-CVAC

[redacted]

ATOMIC ENERGY ACT - 1954

[redacted]

20 July 1955, there have been a total of 18 flights of this airplane. The majority of these flights have been airplane shakedown and checkout of nuclear systems. There have been limitations on ASTR power in flight due to heat exchanger difficulties. Data have been obtained on three of the 18 flights. The results included in this paper are preliminary in nature and caution should be exercised in applying these results.

THEORETICAL METHOD

The theoretical method used in the calculations presented is referred to as the hemisphere-slab method. This method represents a single scattering calculation. For neutrons multiple scattering effects were estimated to be 40% of the single scattered dose rates. No multiple scattering of gamma rays was taken into account. The calculation assumes an upper hemisphere of air and a slab of air between the ground and the horizontal plane containing the source and detector centerline. At large heights above the ground, this calculation reduces to a "sphere" of air. The dose rate is calculated using attenuation on the outgoing, as well as the incoming, leg of the path of the particle under consideration. The differential scattering cross section was calculated using the cloudy crystal ball model for neutrons and Klein-Nishina cross sections for gammas. The source terms used in these calculations were those measured during a previous experiment(1). Buildup and attenuation factors were used for aircraft structure and/or shielded crew compartment. Integration over the emergent and incident angles was performed. For gammas, the energy region was divided into $\frac{1}{2}$, 1, 2, 3, 4, 5 Mev blocks while for neutrons an average neutron energy of 3.25 Mev was used. Numerical calculations were carried out using the IBM-701 computer at Convair-Fort Worth.

The fast neutron and gamma dose rates as measured at large distances from the source in flight were assumed to be primarily due to the direct beam. The source terms used were again those measured in a previous experiment(1). An inverse square with an exponential attenuation and buildup factor was used for gamma rays. In addition, the N^{14} (n,γ) N^{15} capture gamma radiation was calculated using attenuation on both legs. The fast neutron dose rate was calculated with an inverse square and an exponential attenuation factor.

[redacted]

[redacted]

[redacted]

EXPERIMENTAL SET-UP

The experimental shielding data presented in this paper were obtained on two separate flights. The airplane configuration was identical for both flights, that is the same Aircraft Shield Test Reactor (ASTR) shielding and the same cylindrical crew shield were used. The ASTR shield was Configuration No. 1 which has all water shield tanks empty (no neutron shielding beyond the water moderator). The cylindrical crew shield has a side and forward end thickness of 5 inches of borated rubber. There is an inner cylinder of 0.093 inches of lead.

One overlapping altitude was flown so that reproducibility of the data could be checked. During the first flight data were recorded at 10,000 and 17,000 feet, while during the second flight data were recorded at 17,000, 26,000 and 34,500 feet. The range of reactor power was 30 kw to 100 kw for these flights.

Fast neutron and gamma dose rates were measured at various stations located throughout the NTA. These locations (Figures 1 and 2) are fore and aft of the ASTR, inside the cylindrical crew compartment, and inside the shielded crew compartment. All detector stations outside the shielded crew compartment are temperature controlled to $80^{\circ} \pm 5^{\circ}F$.

In addition to the nuclear information recorded on the NTA, data were obtained on a B-50 escort airplane equipped with nuclear instruments. From the escort airplane, fast neutron and gamma dose rates were obtained around the NTA as was the dependence of these dose rates on the separation distance of the two aircraft.

The fast neutron dose rate is measured using a Hurst type fast neutron dosimeter (FND). The gamma dose rate is measured using an anthracene scintillation dosimeter (ASD). The neutron sensitivity of anthracene has been measured, and the gamma data presented here have been corrected for the neutron response of anthracene.(2)

The nuclear information obtained aboard the NTA during a reactor power run at altitude is recorded on an analog and digital automatic recorder. The information is permanently recorded on a magnetic tape in flight. Initiation of a recording cycle is accomplished from the shielded crew compartment of the NTA by a nuclear engineer. Upon completion of a flight, the magnetic tape is removed from the recorder

[redacted]

AEC-3309-CVAC
[redacted]
ATOMIC ENERGY ACT - 1954

[redacted]

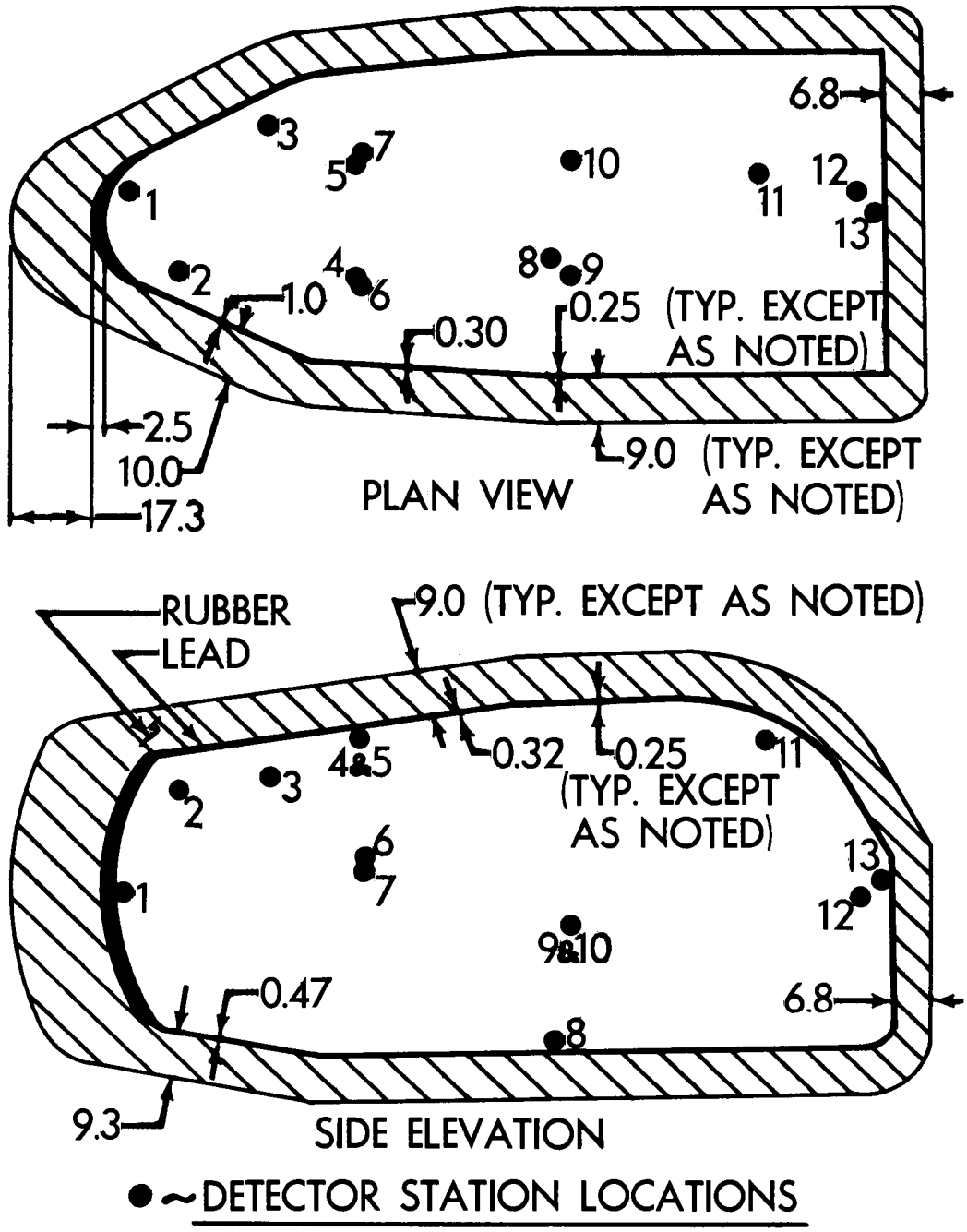

Figure 1. Detector Stations Inside Engineered Crew Compartment

[redacted]

[redacted]

ATOMIC ENERGY ACT - 1954

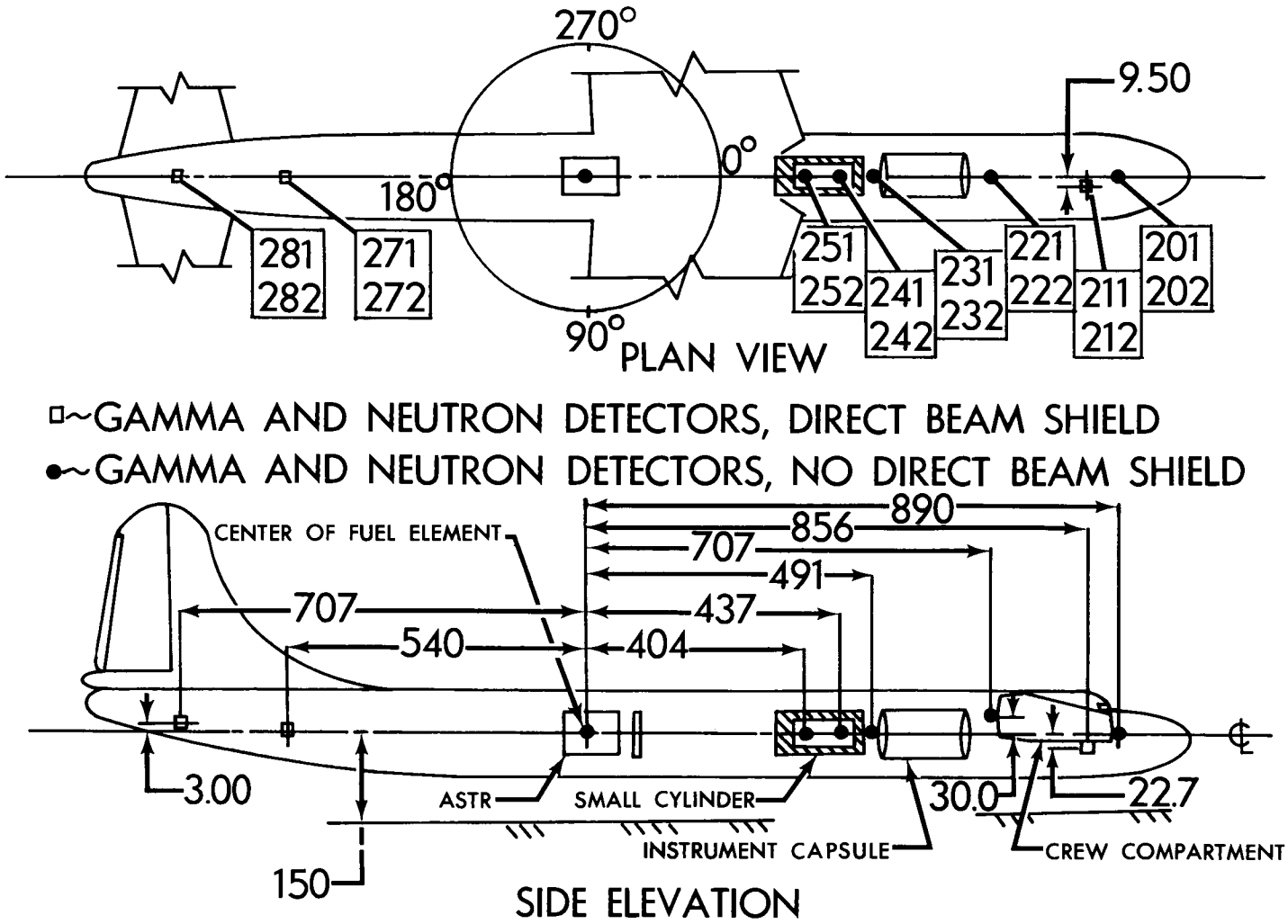

Figure 2. Detector Positions Outside Engineered Crew Compartment

AEC-3309-CVAC
ATOMIC ENERGY ACT--1954

NPC 3190

[redacted]

and placed in a translator. Here, the information is placed on IBM cards in a form such that the 701 computer may produce the dose rate in a tabulated form. Conversion and correction factors are put on the IBM cards prior to supplying them to the 701.

During the recording of information in flight, a manual back-up data-monitoring system is used to spot check the automatic recorder. This manual data is reduced by hand and is used as an over-all check on the automatic data recording and reduction system. All data on the escort aircraft are recorded manually.

RESULTS AND DISCUSSION

The dose rates recorded on the NTA and the escort airplane are given in Tables I and III. The corresponding theoretical predictions are given in Tables II and IV.

Examination of the fast neutron dose rates inside the shielded crew compartment (stations 7 and 9) shows that the theoretical values are approximately a factor of 10 higher than the experimental values. On the other hand, if a similar comparison is made for station 221 located just aft of the engineered crew compartment, the agreement is quite good.

These results indicate that the buildup and attenuation factors used for the theoretical neutron dose rate calculations inside the cylindrical crew compartment are probably incorrect. Further work on these calculations is now in progress.

Similar conclusions concerning the buildup and attenuation factors are reached when the theoretical and experimental fast neutron data inside the cylindrical crew shield are compared.

Calculations of the theoretical predictions of the gamma dose rates for stations on the NTA are now in progress, but the results are not yet complete. It should be mentioned again that the results reported here are preliminary in nature and caution should be exercised in applying them.

AEC-3309-CVAC

[redacted]

ATOMIC ENERGY ACT - 1954

[redacted]

TABLE I

GAMMA AND NEUTRON DOSE RATE MEASUREMENTS IN NTA
(Dose Rates in 10^{-3} MRem/Hr-Watt)

Station	Flight	Altitude (feet)			
		Gamma (feet)			
		10,000	17,000	26,000	34,500
202	10	2.77	2.26		
212	10	1.44	2.75		
	12		2.41	1.85	1.32
222	10	5.91	5.31		
	12		4.91	4.23	3.74
242	10	3.26	2.96		
	12		2.51	2.16	1.92
252	10	1.51	1.26		
	12		1.35	1.17	1.01
272	10	9.90	9.02		
	12		8.33	8.22	8.09
282	10	4.05	3.25		
	12		3.05	2.39	2.13
6	10	.417	.343		
	12		.316	.255	.200
10	10	.4[illegible]4	.389		
	12		.381	.305	.259
		Fast Neutron			
7	10	.504	.507		
	12		.381	.320	.288
9	10	.345	.321		
	12		.267	.213	.182
11	10	.545			
	12		.357	.297	.242
201	10	57.0	47.7		
211	10	55.6	48.8		
	12		44.8	37.6	31.9
221	10	120	105		
	12		80.9	69.0	58.4
241	10	11.6	10.0		
	12		8.14	7.19	6.35
251	10	8.77	7.70		
	12		7.65	6.73	5.86
271	10	339	299		
	12		204	171	145
281	10	197	173		
	12		172	144	121

AEC-3309-CVAC

[redacted]

[redacted]
ATOMIC ENERGY ACT - 1954

[redacted]

TABLE II

THEORETICAL PREDICTIONS
NEUTRON DOSE RATE MEASUREMENTS IN NTA
(Dose Rates in 10^{-3} MRem/Hr-Watt)

Station	Altitude (Feet)			
	10,000	17,000	26,000	34,500
7	3.4	3.0	2.5	2.0
9	3.2	2.9	2.4	1.9
211	60	53	44	35
221	152	126	91	75
251	32	27	24	17
271	240	200	160	130
281	201	174	138	102

[redacted]

ATOMIC ENERGY ACT - 1954

[redacted]

TABLE III

GAMMA AND NEUTRON DOSE RATE MEASUREMENTS
IN ESCORT AIRCRAFT

Density Altitude (ft)	θ (Degrees)	R (Yds)	Fast Neutron MRem/Hr-Watt / 1	Gamma MRem/Hr-Watt / 1
10,000'	90°	500	1.41 (-3)	1.26 (-4)
	105°	500	1.17 (-3)	7.6 (-5)
	137.5°	500	9.5 (-4)	7.3 (-5)
	158°	500	8.4 (-4)	5.6 (-5)
	180°	500	6.7 (-4)	5.5 (-5)

TABLE IV

THEORETICAL PREDICTIONS
GAMMA AND NEUTRON DOSE RATE MEASUREMENTS IN
ESCORT AIRCRAFT

Density Altitude (ft)	θ (Degrees)	R (Yds)	Fast Neutron MRem/Hr-Watt / 1	Gamma MRem/Hr-Watt / 1
10,000'	90°	500	1.335 (-3)	8.515 (-5)
	120°	500	1.152 (-3)	4.808 (-5)
	150°	500	9.440 (-4)	4.374 (-5)
	175°	500	7.579 (-4)	3.176 (-5)

[redacted]

[redacted]
ATOMIC ENERGY ACT - 1954

[redacted]

The theoretical neutron dose rates around the NTA (measured in the B-50 escort airplane) agree fairly well with the experimental values. The gamma predictions are low by almost a factor of two.

Current plans are to continue examination of the theoretical methods of analysis to eliminate the discrepancies discussed above. Concurrent with these theoretical efforts, additional experimental data will be taken for other reactor shield configurations. These experiments will not only provide shielding handbook data, but will also provide more data for comparison with the theoretical predictions.

[redacted]

[redacted]

[redacted]

REFERENCES

1. C. F. Malone, ASTR Crew Shield and Mapping Experiments, Talk presented at ANP Shielding Meeting, Oak Ridge, Tennessee, (7-8 May 1956).

2. K. R. Spearman, Neutron Sensitivity of Anthracene Dosimeters, Convair-Fort Worth Report MR-N-100, NARF-55-67T (18 October 1955).

[redacted]

[redacted]
ATOMIC ENERGY ACT - 1954

SECRET

Paper I-E

PRELIMINARY GAMMA-RAY DIFFERENTIAL SHIELDING EXPERIMENTS AT THE TOWER SHIELDING FACILITY

F. N. Watson
Oak Ridge National Laboratory

SECRET

[redacted]

PRELIMINARY GAMMA-RAY DIFFERENTIAL SHIELDING EXPERIMENTS AT THE TOWER SHIELDING FACILITY

by

F. N. Watson
Oak Ridge National Laboratory

Some preliminary gamma-ray differential shielding measurements are presented which are useful both in understanding the phenomena involved and in calculating optimum gamma-ray shields. Included in these measurements are gamma-ray dose rate measurements inside and outside of a crew compartment mockup and thermal neutron measurements in space around a reactor shield.

INTRODUCTION

The Tower Shielding Facility group has to date been concerned primarily with the problems of optimum placing and shaping of shielding in a nuclear-powered aircraft. These problems have been approached through the use of differential type shielding experiments and partial differential equations.

The data which is reported in this paper was taken to supply experimental information needed in the gamma-ray shield optimization. It is of a preliminary nature, however, and serves primarily as an aid to understanding the phenomena involved and to give direction to future experiments.

EXPERIMENTAL RESULTS AND PARTIAL ANALYSIS

Experimental Arrangement

In examining the data the following salient features of the experimental arrangements should be kept in mind. The source of radiation was the Tower Shielding Reactor with a standard 5 x 6 fuel element loading. The standard TSF geometry and coordinate system (Fig. 1) was maintained wherever applicable. A crew compartment mockup (Fig. 2) was substituted in lieu of the detector tank shown at the right of Fig. 1. The coordinate system remained unchanged, the separation distance "d" being measured from the outside rear of the mockup. (The crew compartment mockup is always identified as the GE crew compartment mockup since it was first used in an experiment for GE.)

[redacted]

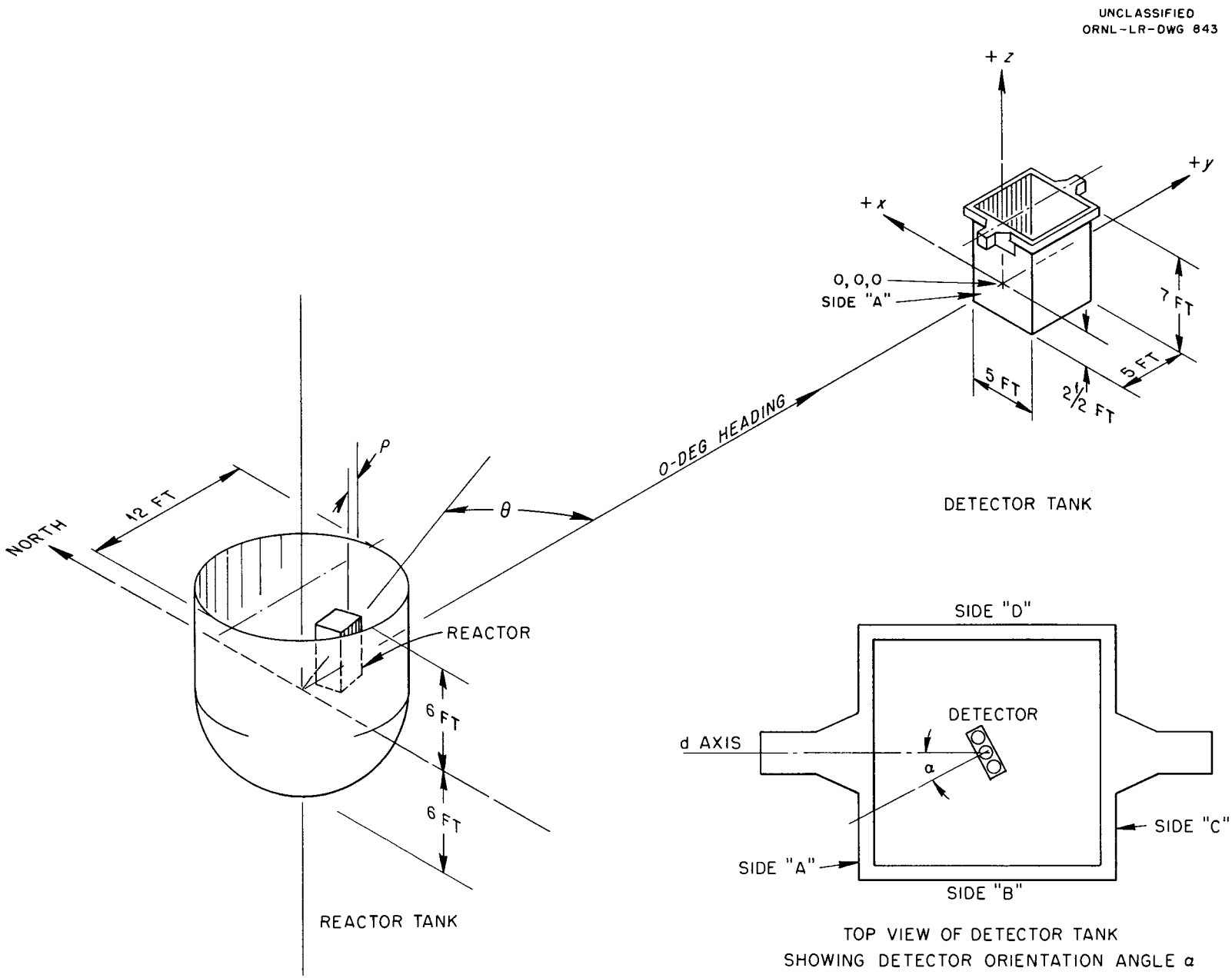

Fig. 1

Coordinate System for Reactor and Detector Positions within Their Respective Tanks — Tower Shielding Facility.

[redacted]

2-01-056-3-T24-81

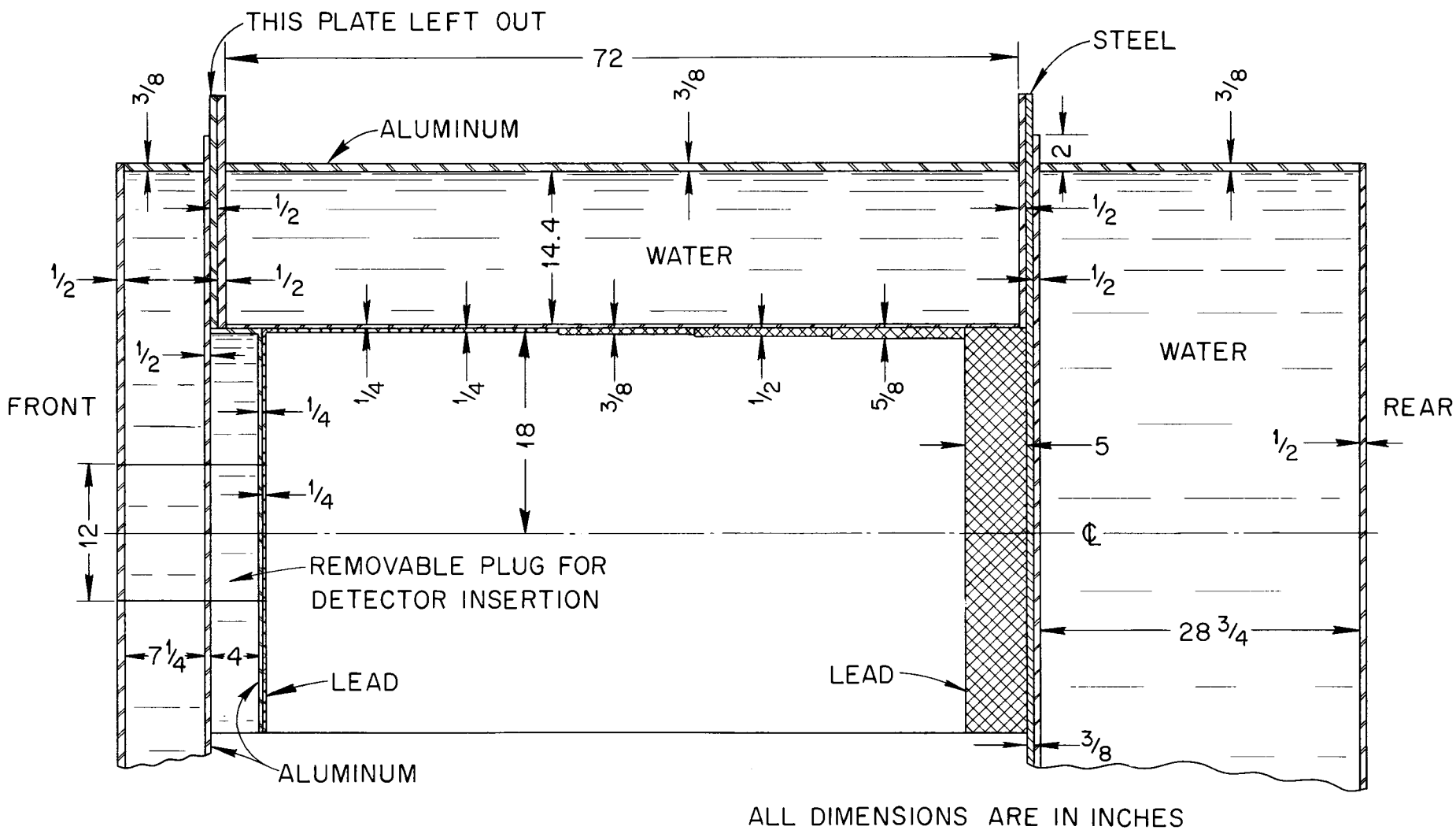

Fig. 2. Schematic Diagram of GE-ANP Crew Compartment.

[redacted]

In the standard configuration 1/4 in. of lead was added to the side wall liner of the crew compartment making it 1/2-in.-thick at the front and 7/8-in.-thick at the rear. Variations in the standard configuration included (1) removal of all the lead at the sides, (2) removal of the lead and borated water at the sides, and (3) removal of the lead and borated water at the sides and the entire rear section of the shield.

Measurements of Beam Shape

One of the first essentials in differential shielding experiments is to have a collimated source of radiation and to know the degree of collimation. The data (Fig. 3) shows that a collimated source of gamma rays is obtained simply by moving the TSR away from the center of the reactor tank. This data was taken with a detector placed at the rear of the GE crew compartment, 64 ft away from the reactor tank center. The thickness of water over the most exposed face of the reactor was held constant as the reactor was moved through the angle θ.

Of course the degree of collimation can not be measured experimentally since there are scattering centers present but certainly the gamma-ray beam is not less collimated than this data indicates. The dose rate (D) for ρ = 45 cm (see Fig. 4) can be approximated by the relation $D = D_0 \cos^2\theta$ out to θ = 70 deg, where D_0 is the dose rate for θ = 0 deg.

In the measurements for ρ = 30 to 156 cm, the decay gamma-ray level relative to the fission gamma-ray level was low, so it need not be considered as a background. When the reactor reaches the center of the tank (ρ = 156 cm) the tank with the reactor becomes an isotropic source in the horizontal plane.

In order to look at the shape of the beam in the vertical plane, data was taken (see Figs. 5, 6 and 7) with a detector attached to the outside rear of the crew compartment mockup stationed at an altitude of 100 ft while the reactor was elevated from zero altitude to 200 ft. The beam is symmetrical for small values of ρ, but as ρ increases an asymmetry results from the asymmetrical shape of the tank in the vertical plane.

A comparison of the beam in the vertical plane to that in the horizontal plane (Fig. 8) reveals that the intensity falls off a little more rapidly with α in the vertical plane than with θ in the horizontal plane. This probably is due to the bottom face of the reactor being considerably smaller than the side face, i. e., 15 x 18 in. compared to 18 x 24 in.

So far, this report has considered these curves only in the light that they indicate the beam shape. Before passing to another set of data, it should be pointed out that, with some adjustments, these curves will become probability curves used in determining the shield shape. That is, they

[redacted]

[redacted]

1-01-056-11-24-(-1)253

Fig. 3 Gamma-Ray Dose Rate Outside Rear of GE Crew Compartment as a Function of Reactor Orientation Angle, ρ = 16 cm.

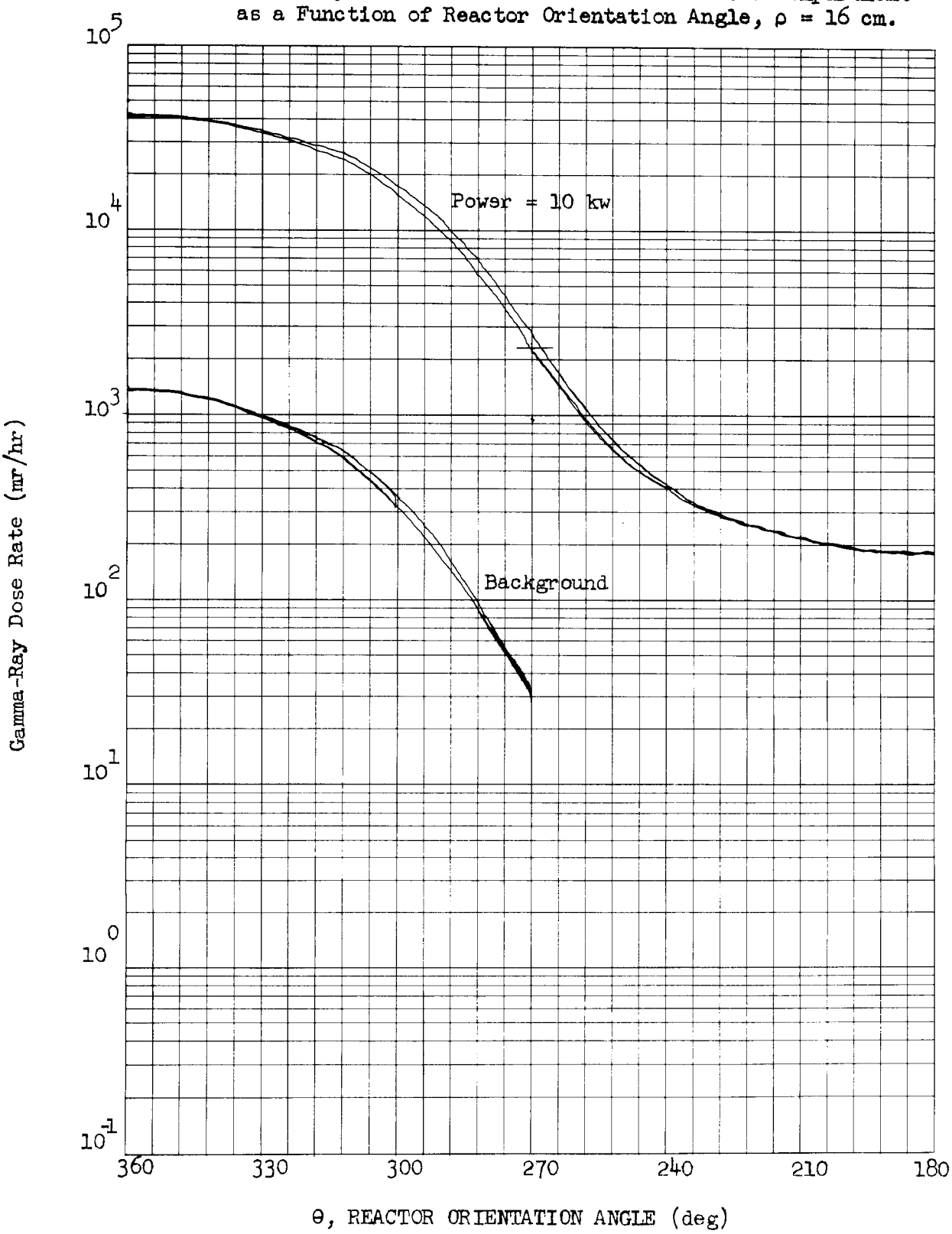

h = 195 ft
d = 64 ft

ρ = 16 cm
Detector outside rear of GE crew Compartment

Fig. 4 Gamma-Ray Dose Rate Outside Rear of GE Crew Compartment as a Function of Reactor Orientation Angle for Several Values of ρ

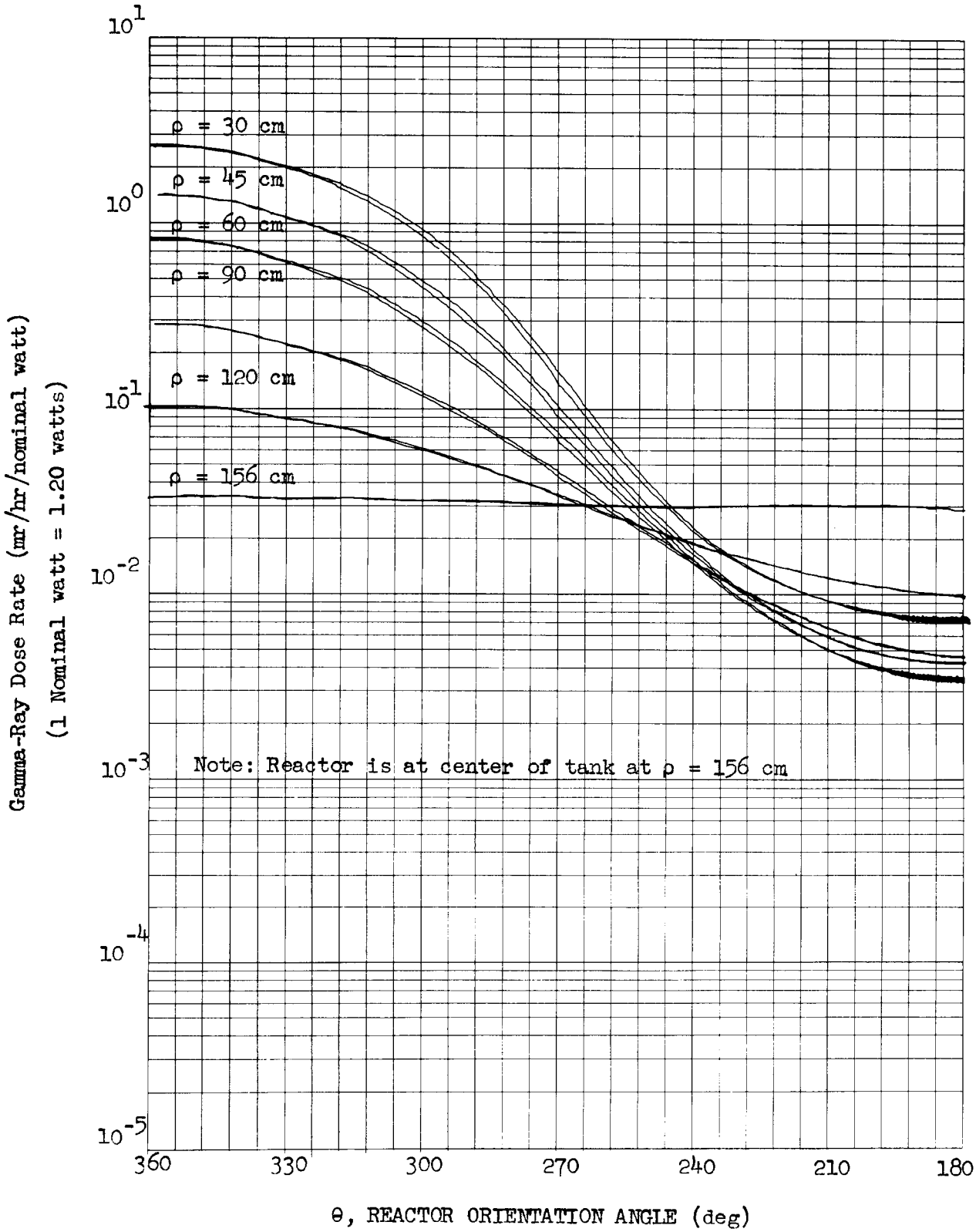

h = 195 ft

d = 64 ft

Detector outside rear of GE Crew Compartment

[redacted]

1-01-056-11-37-(-1)-255

Fig. 5 Gamma-Ray Dose Rate Outside Rear of GE Crew Compartment as a Function of Reactor Altitude, ρ = 16 cm.

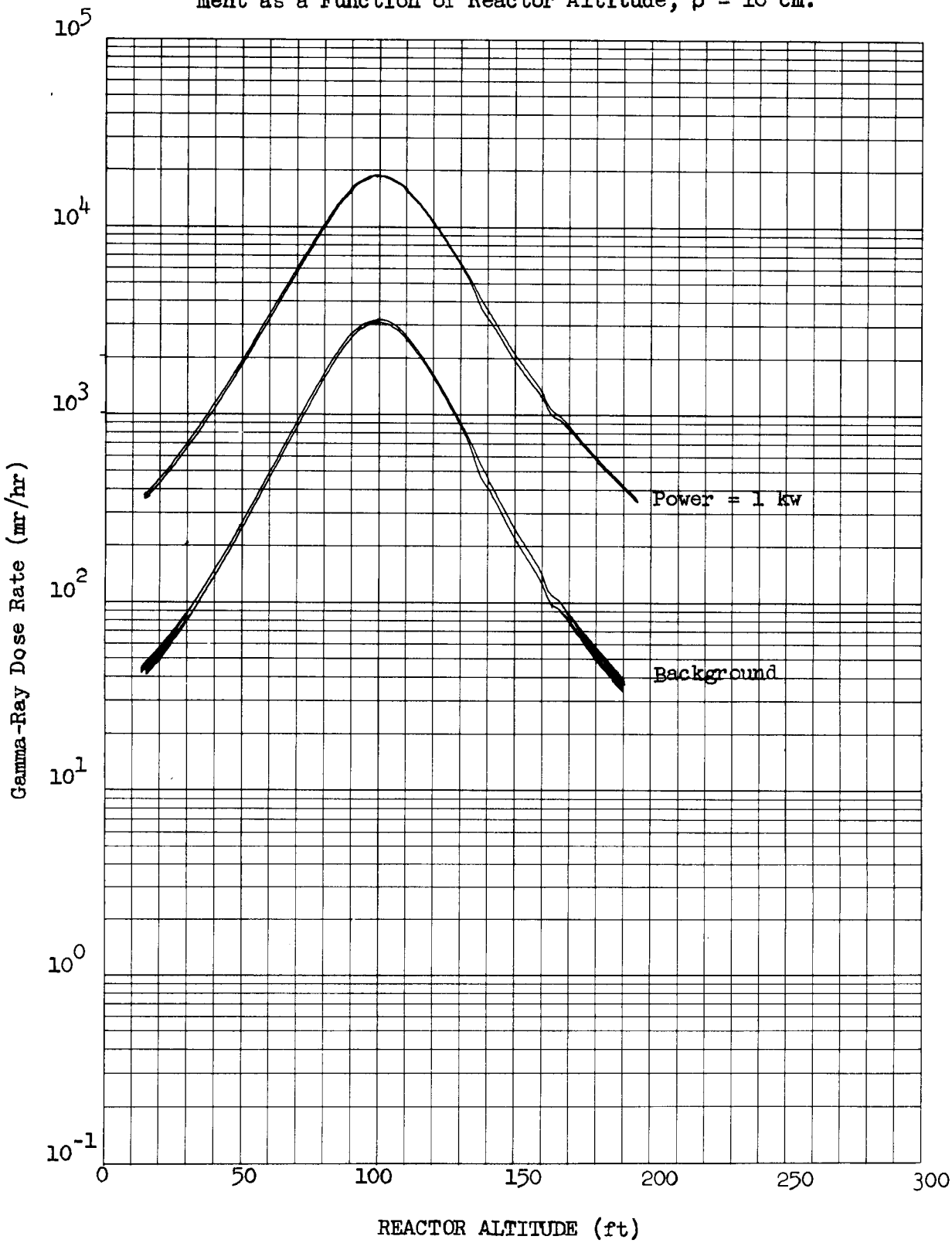

Detector outside rear of GE crew compartment d = 38 ft
Detector altitude = 100 ft θ = 0 deg

[redacted]

1-01-056-11-39-(-1)-256

Fig. 6 Gamma-Ray Dose Rate Outside Rear of GE Crew Compartment as a Function of Reactor Altitude, $\rho = 45$ cm.

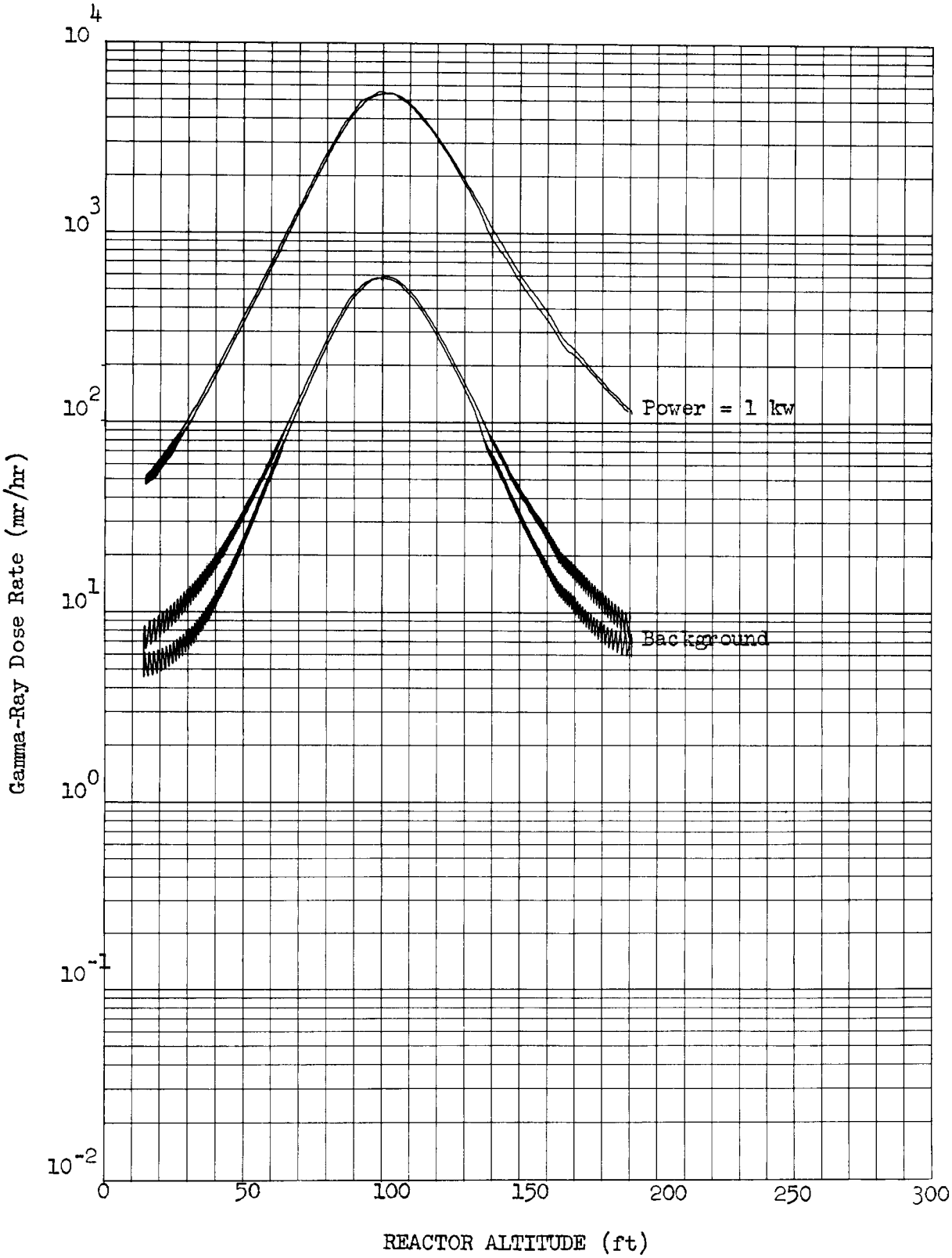

Detector outside rear of GE crew compartment $d = 38$ ft

Detector altitude = 100 ft $\theta = 0$ deg, $\rho = 45$ cm

Fig. 7 Gamma-Ray Dose Rate at Outside Rear of GE Crew Compartment as a Function of Reactor Altitude, ρ = 90 and 156 cm.

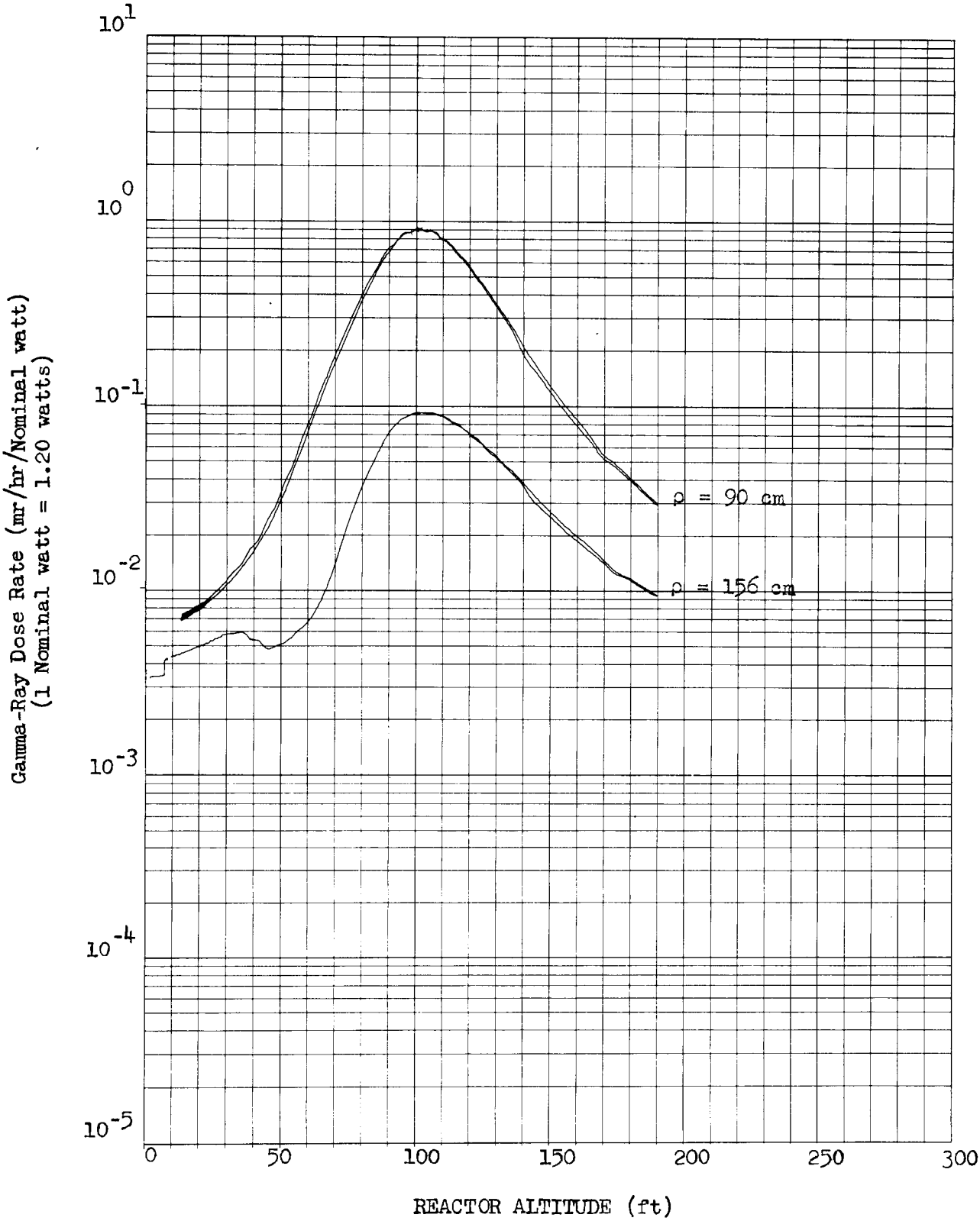

Detector outside rear of GE crew compartment
Detector altitude = 100 ft
d = 38 ft θ = 0 deg

[redacted]

2-01-056-11-24 AND 37-291

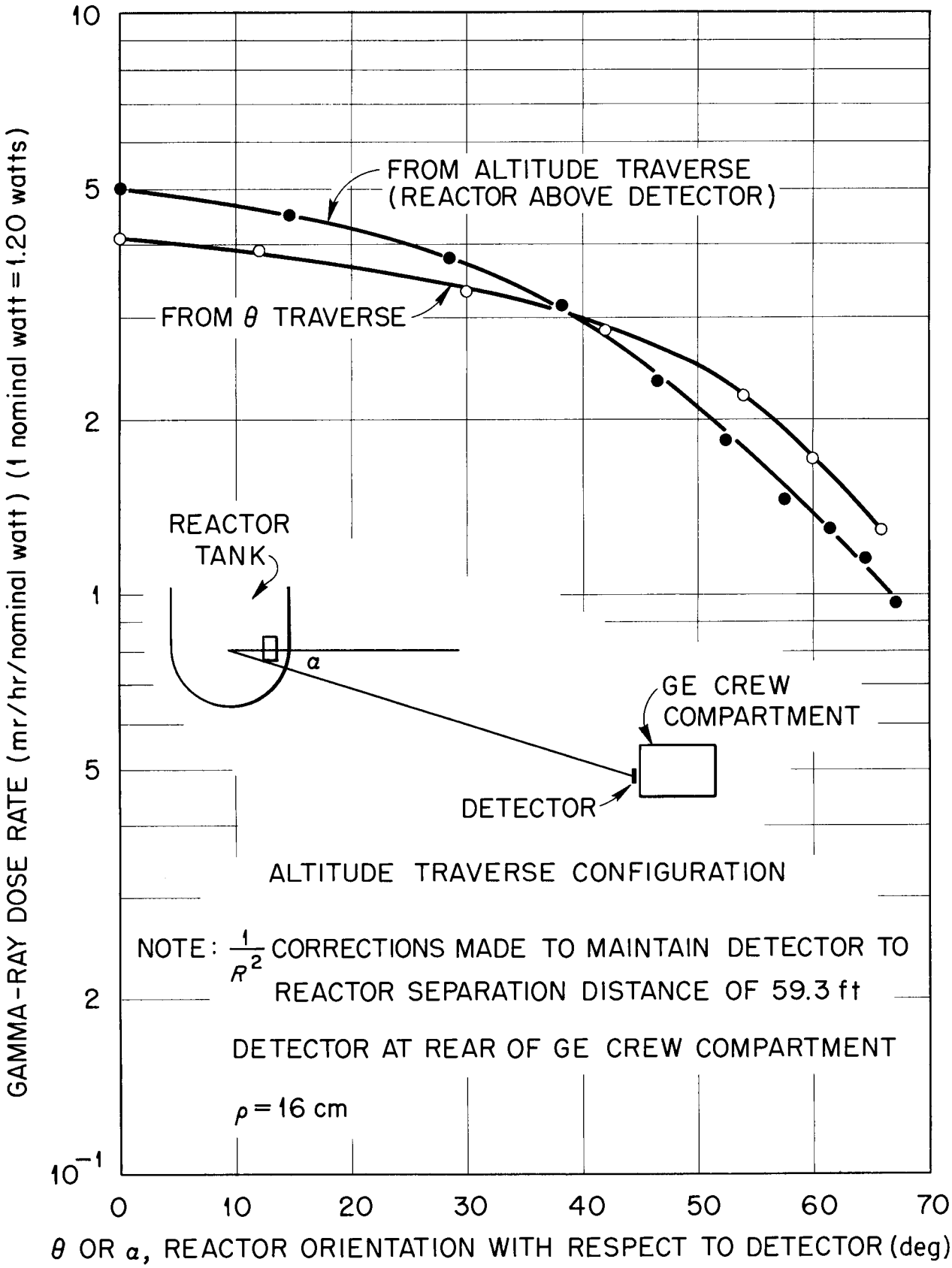

Fig. 8. Comparison of Beam Shape in Horizontal and Vertical Planes.

indicate the probability of a gamma ray arriving at the rear of the crew compartment as a function of the angle of emission from the reactor shield.

Standard Configuration Results

The standard configuration results can be typified by four curves plotted as a function of the coordinate ρ (see Fig. 9). The first of these curves is the one giving the thermal-neutron flux as a function of reactor position (ρ) within the reactor tank. The portion of the curve to the left was taken with the reactor front face looking toward the detector and crew compartment mockup and the portion to the right was taken with the front face turned in the opposite direction. The graph is the same width as the reactor tank. The curves do not meet in the center due to the finite width of the reactor. ρ is not measured from the same side of the tank in both cases but is measured from the front face of the reactor to the nearest point on the reactor tank wall. This results in a more precise measurement for calculational purposes. The tank is not perfectly round and changes shape slightly with changes in weight distribution. On the left, the curve falls off with water thickness in the normal manner. On the right-hand side, it can be seen that a point is reached where the contribution from scattered neutrons is first equal to and then far exceeds the direct beam contribution.

In the next curve the gamma-ray dose rate measured at essentially the same point is also plotted as a function of ρ. As the reactor moves across the tank, the dose rate changes in much the same fashion as did the thermal-neutron flux, the relaxation lengths being somewhat longer as is to be expected with gamma rays. Possibly the right-hand end of the curve rises a little more sharply than might be expected.

In the bottom curve some unusual phenomena are exhibited. This data was taken with a detector placed inside and near the center of the crew compartment. First the portion of the curve to the left shows a significant change in relaxation length as the reactor approaches the outside of the tank. It might first be supposed that as the reactor nears the outside, the beam becomes less collimated and the wide angle rays having a more favorable chance to get around the shadow shield might cause this change in relaxation length. A check of Figs. 3 and 4 shows, however, that there was hardly any change in beam shape between $\rho = 16$ and 45 cm. From the right-hand portion of the gamma-ray dose rate curve it is evident that as the reactor nears the opposite side of the tank, the dose rate inside the crew compartment increases at an extremely rapid rate. In fact, the relaxation length measured at $\rho = 20$ cm and $\theta = 180$ deg is 6.7 cm for the gamma rays. For the thermal neutrons it is 5.4 cm. This marked similarity in gamma-ray and neutron relaxation lengths indicates that for these values of ρ neutron captures in air probably contribute more to the gamma-ray dose rate than do air-scattered gamma rays.

[redacted]

2-01-056-11-1 to 10-285

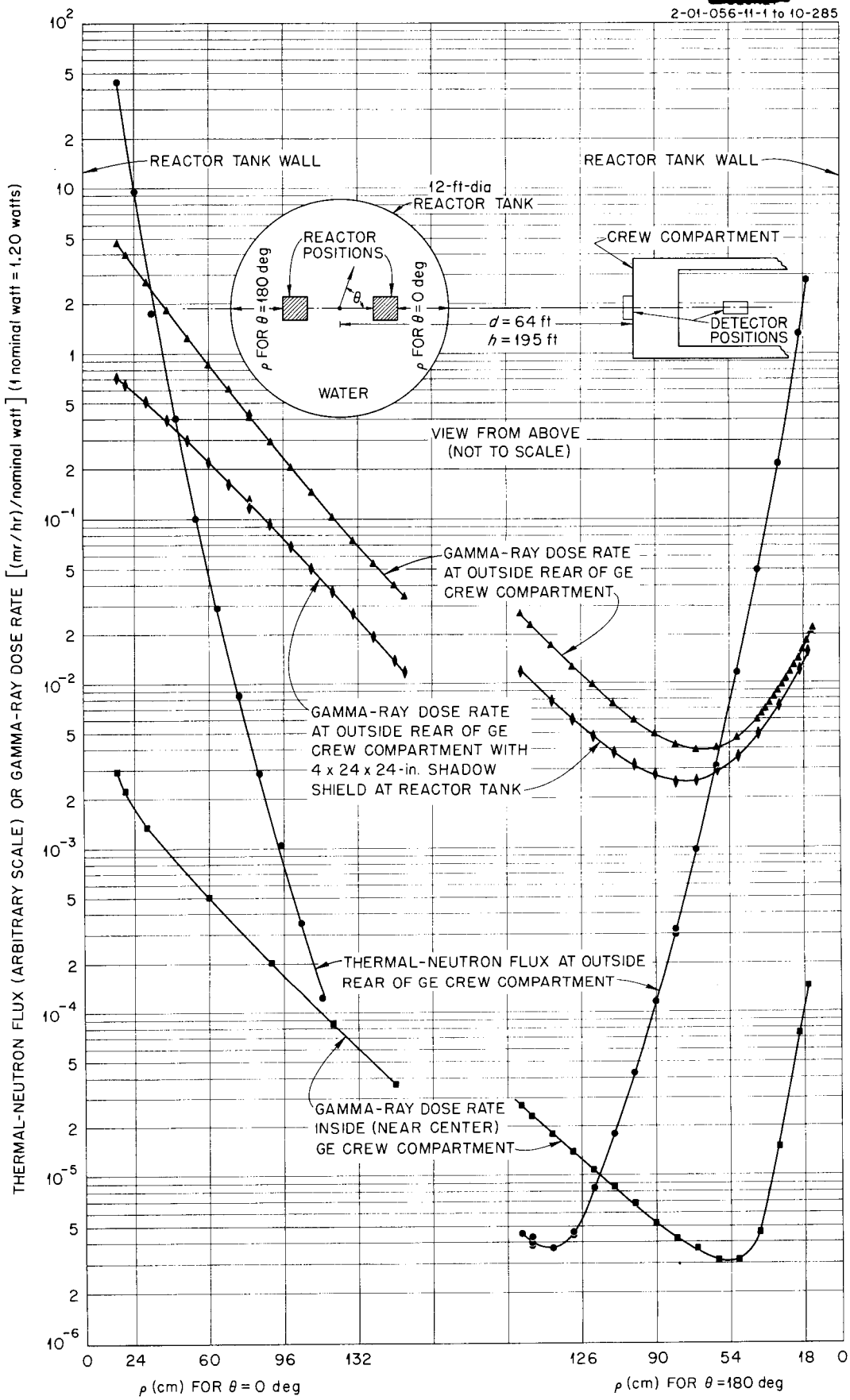

Fig. 9. Thermal-Neutron Flux and Gamma-Ray Dose Rate Inside and Outside GE Crew Compartment as a Function of Reactor Position Within Tank.

The fourth curve reveals the effect of placing a 4 x 24 x 24 in. lead shadow shield at the outside of the reactor tank and centered on $\theta = 0$ deg. The inverse curvature is due to the shadow shield covering a larger and larger portion of the solid angle from the reactor. At $\theta = 180$ deg, these two curves would be expected to be coincident. It has been assumed that this difference can be attributed to experimental error until further experiments are made. One explanation which may partially account for it is that the tank wall itself becomes activated when the reactor is at $\theta = 0$ deg and this activation may show up at $\theta = 180$ deg.

Adjusted Configuration Results

In the interest of finding the shielding value of the various components of the crew compartment shield, data was taken with certain portions removed (see Fig. 10). In taking the data shown in this figure, the gamma-ray detector was placed inside the crew compartment mockup. ρ traverses were made with various parts of the crew compartment shielding removed.

The bottom curve in Fig. 10 is the same data as was shown in Fig. 9 and is given here for comparison only.

The next curve was taken after removing the lead liner from the crew compartment. The change in dose rate indicated that the gamma rays had a relaxation length of approximately 1 cm in passing through this lead. This is quite good and not unreasonable as these gamma rays are both degraded in energy from scattering and generally follow a slant path through the lead.

Next, the borated water was removed from the side of the tank but not from the front or rear. The resulting change in dose rate indicated that the gamma rays had a relaxation length of approximately 30 cm. This is quite poor and was very surprising since the lead had been so effective. It can be pointed out, however, that a significant number of gamma rays were scattered by the water from a path which would miss the detector into a path which passed through it. When the water was removed, these scattering centers no longer existed. It is evident that the lead on the rear of the crew compartment should extend sufficiently far in radius so that scattering in the hydrogenous side material does not contribute excessively to the dose rate.

As indicated above, Fig. 9 showed the effect that a 4 x 24 x 24 in. lead shadow shield placed on the reactor axis just outside the reactor shield tank has on the gamma-ray dose rate just outside the rear of the crew compartment. Figure 10 shows the same information for the dose rate inside the crew compartment. The dose rate measurements inside the crew compartment with the shadow shield in place show a reduction in dose rate of approximately a factor of 2 at ρ thicknesses as great as 80 cm. This indicates that at least half of the dose rate measured inside the crew compartment for these values of ρ without the shadow shield must result from gamma rays which passed through the area later covered by the shadow shield.

The upper curve in Fig. 10 results from measurements taken with the complete rear shield removed. This data may be compared with the data taken outside the shield. The measurements inside the compartment with the rear

[redacted]

2-01-056-11-IN-293

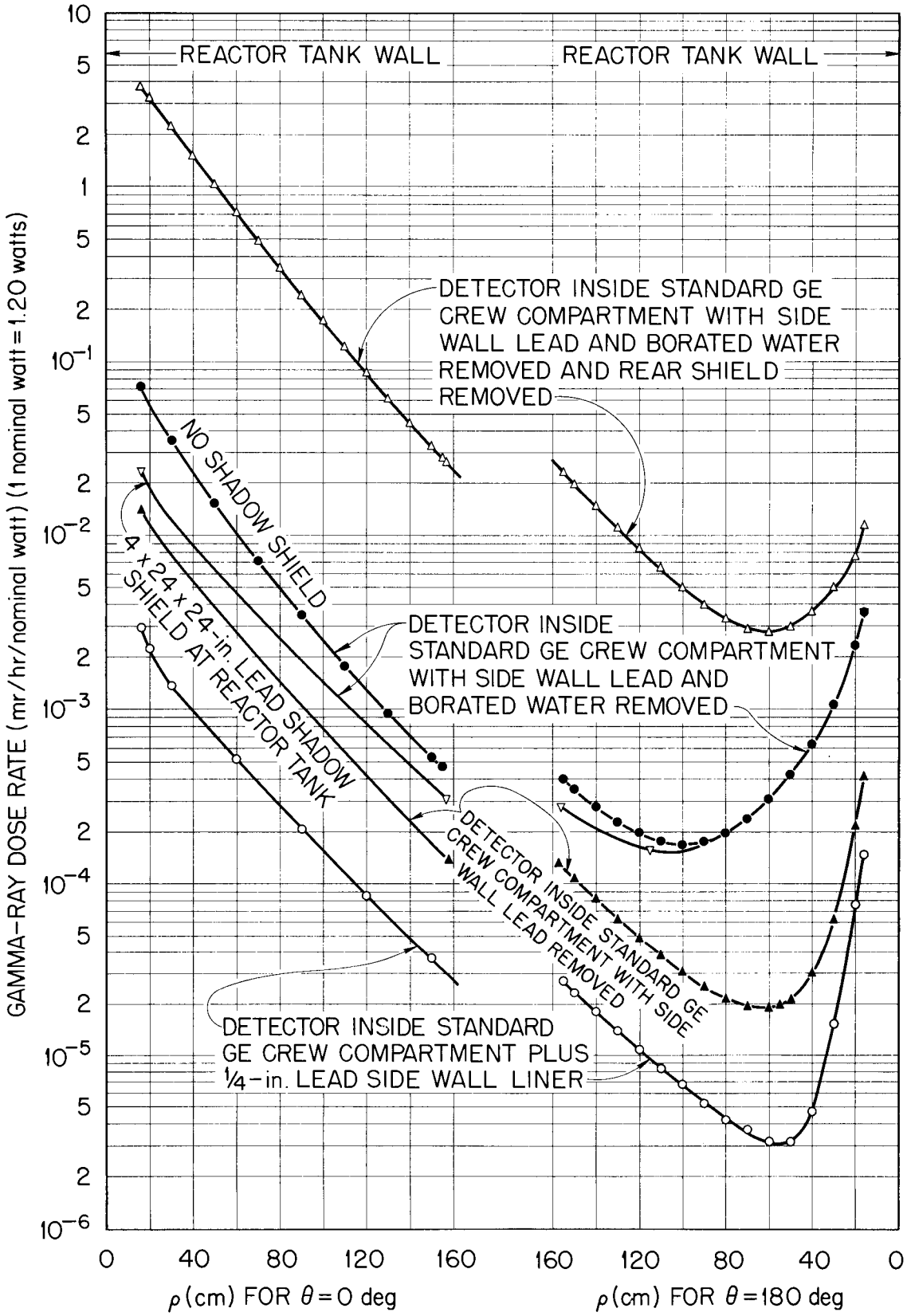

Fig. 10. Gamma-Ray Dose Rates Inside the GE Crew Compartment as a Function of Reactor Position Within Reactor Tank for Several Configurations.

[redacted]

shield removed are lower, showing that there is a contribution to the measurements outside due to boron and aluminum capture gamma rays. A calculation of thermal-neutron induced capture gamma rays from the boron confirmed this as a reality.

Thermal-Neutron Flux as a Function of Reactor-Detector Separation

A machine calculation of the capture gamma rays from neutron captures in air arriving inside the crew compartment is now underway at ORNL. One piece of experimental data needed in this calculation is the thermal-neutron distribution in space around the reactor. Six figures (Figs. 11 through 16) are included to show the results of these space distribution measurements. The first of these figures (Fig. 11) shows how the flux decreases with distance R between the reactor tank and the detector. In taking this data the reactor was positioned within the tank such that the beam emerged in the direction of the detector. This curve can be fitted approximately by the relationship

$$nv_{th} = \frac{C_1}{R^2} e^{-R/C_2}$$

where C_1 and C_2 are constants. The next figure (Fig. 12) shows the flux as a function of distance with the source beam at 90 deg to the source-detector axis. This curve shape follows a combination of $1/R^2$ and $1/R$ plus air attenuation. However, an entirely satisfactory fit has not been found at this time. Figure 13 shows the flux as a function of distance with the neutron beam emerging from the reactor tank in the opposite direction from the detector. This curve can be approximated by the relationship

$$nv_{th} = \frac{C_3}{R} e^{-R/C_4}$$

Thermal-Neutron Flux as a Function of Reactor Orientation Angle

In addition to the measurements taken as a function of distance at three discrete values of θ, the thermal-neutron flux was measured at a discrete separation distance as a function of the angle θ. This measurement was made using first a bare BF_3 chamber (see Fig. 14) and then using a cadmium-covered BF_3 chamber (see Fig. 15). At least one interesting observation can be made concerning these two curves. If a ratio is made between the 180 deg and the 0 deg values, a factor of 7.4 is observed for the bare chamber and 5.3 for the cadmium-covered chamber data. This shows that epicadmium neutrons have a better chance of scattering 180 deg than the thermal neutrons. This probably results from the fact that thermal

[redacted]

1-01-056-11-57-(-1)-264

Fig. 11 Thermal Neutron Flux at a Point in Space as a Function of Distance between Reactor Tank and the Point, θ = 92 deg

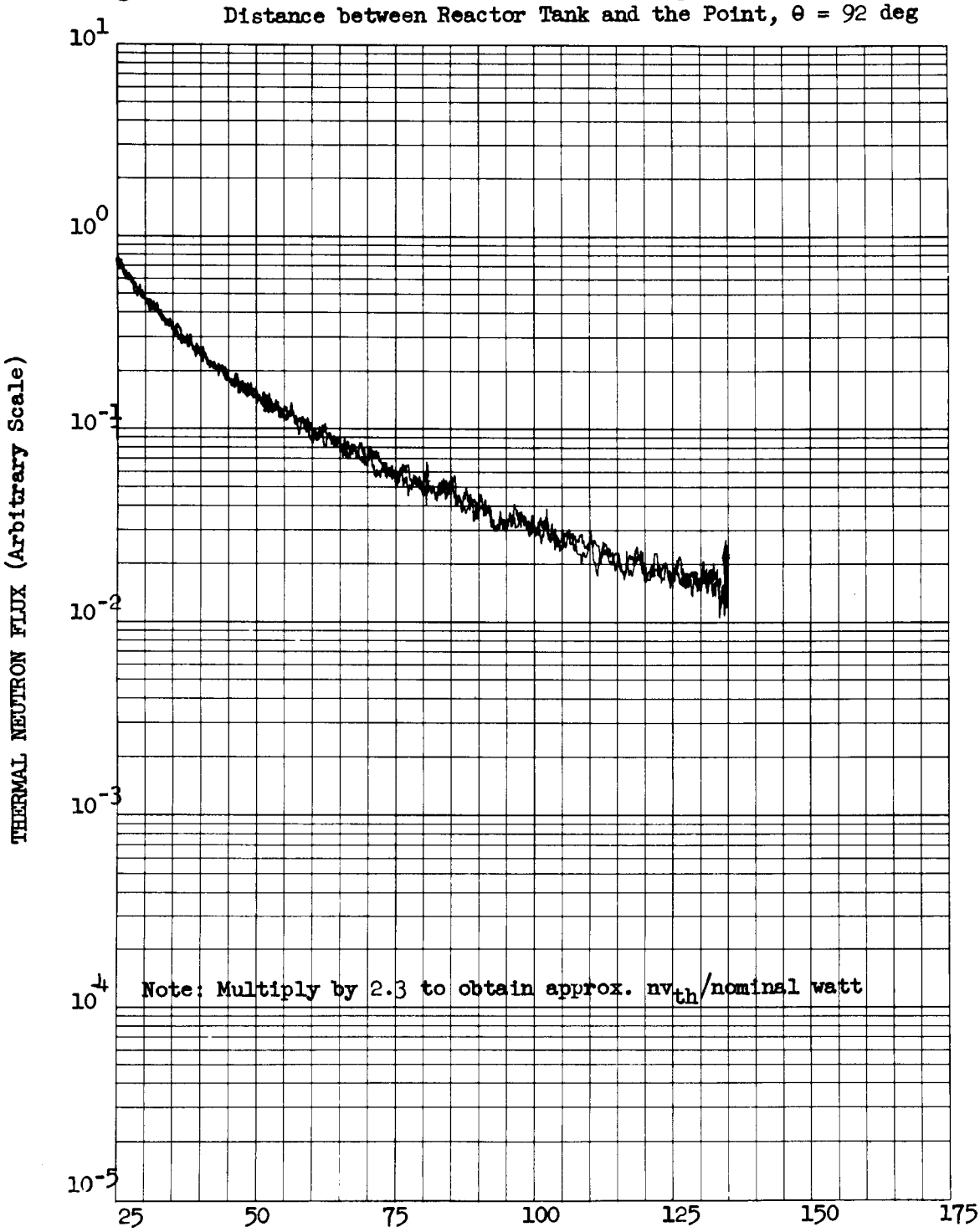

s, DISTANCE FROM REACTOR TANK CENTER TO DETECTOR (ft)

h = 140 ft
ρ = 45 cm

$\theta = 92^\circ$
Detector on Tower Leg I

[redacted]

1-01-056-11-54-(-3)-262

Fig. 12 Thermal Neutron Flux at a Point in Space as a Function of Distance between Reactor Tank and the Point, θ = 0 deg.

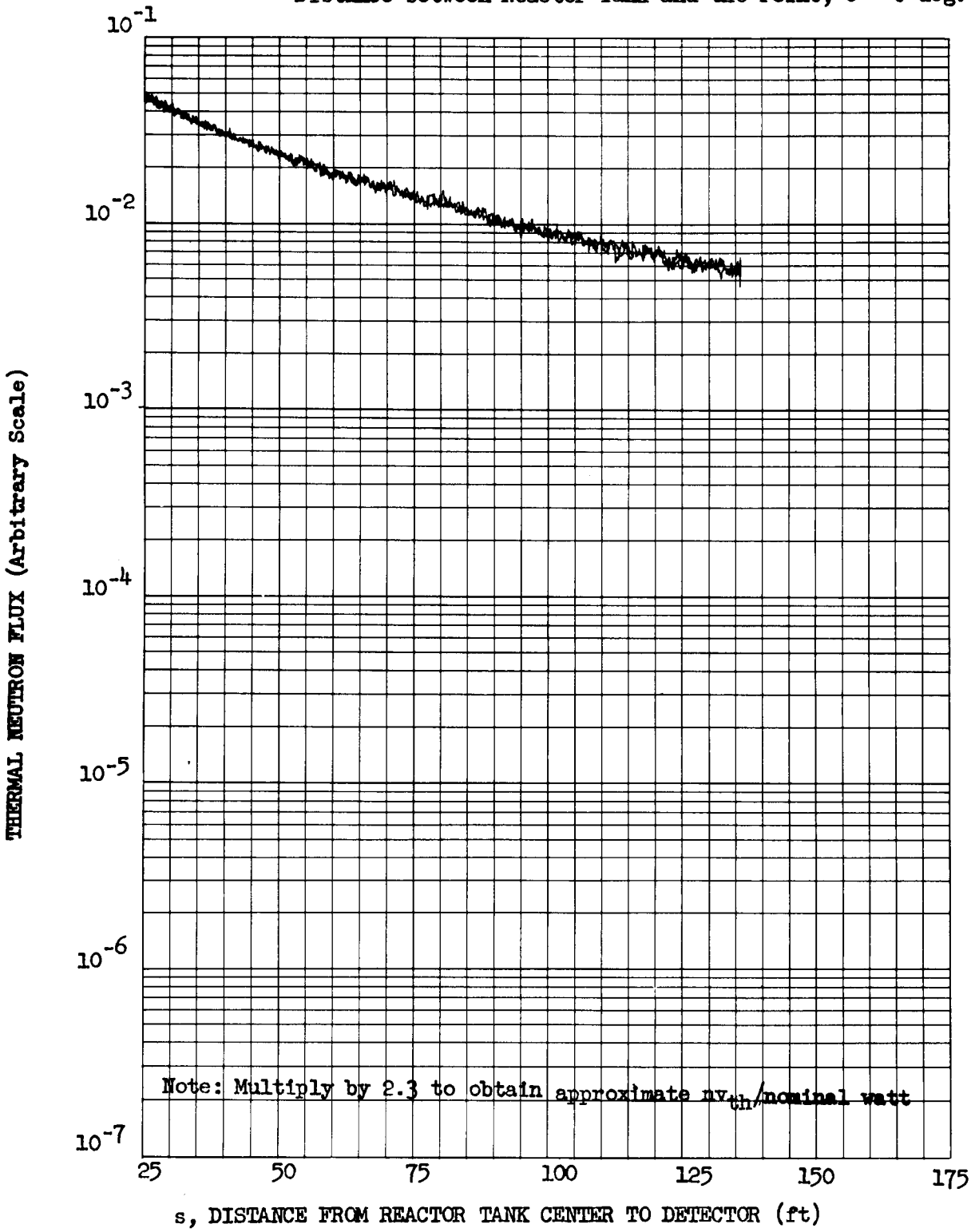

h = 140 ft
ρ = 45 cm

θ = 0 deg
Detector on Tower Leg I

[redacted]

1-01-056-11-55-(-3)-263

Fig. 13 Thermal Neutron Flux at a Point in Space as a Function of Distance between Reactor Tank and the Point, θ = 270 deg.

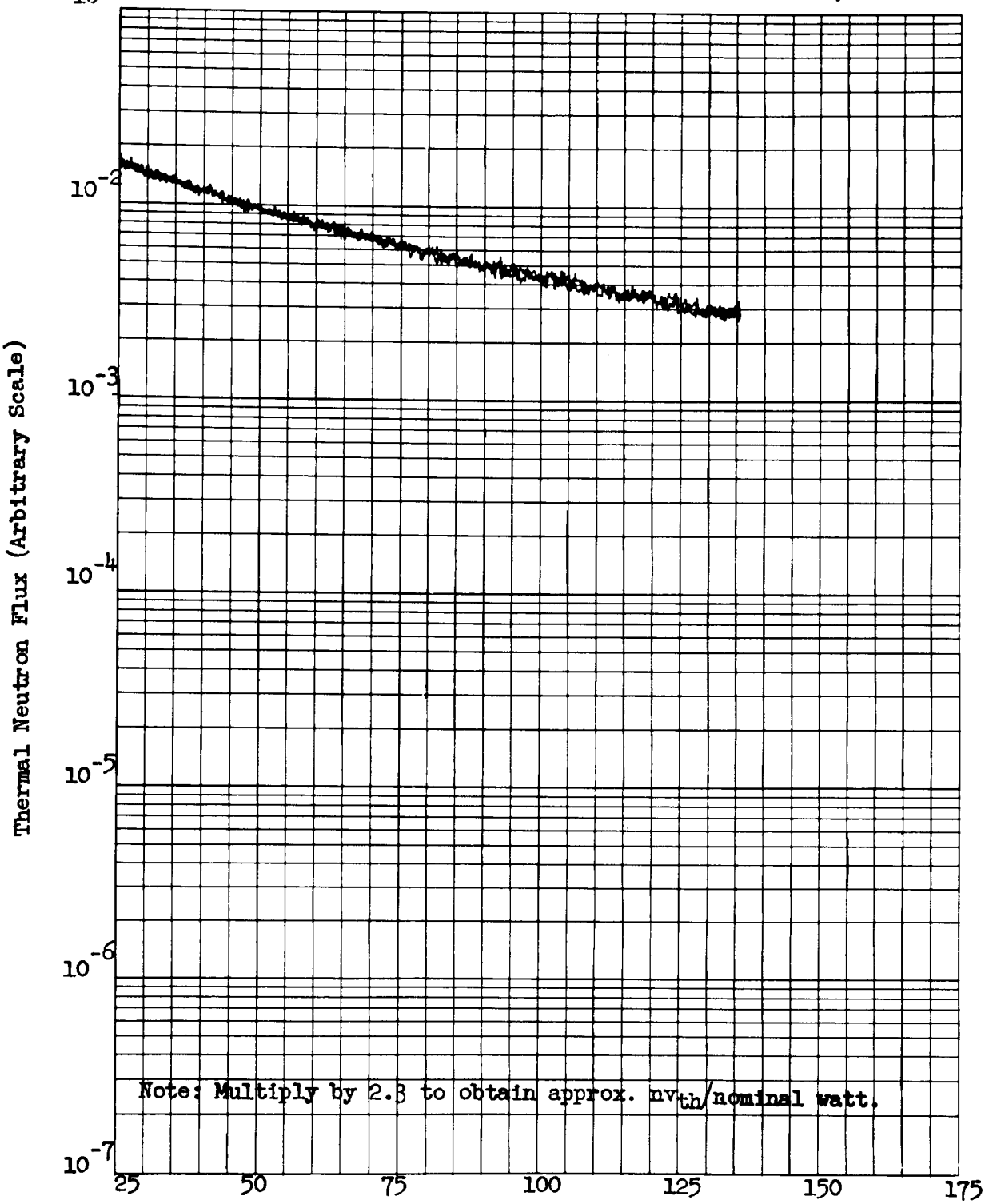

s, DISTANCE FROM REACTOR TANK CENTER TO DETECTOR (ft)

h = 140 ft
ρ = 45 cm

θ = 270 deg
Detector on Tower Leg I

[redacted]
1-01-056-11-63-(-2)-270

Fig 14 Thermal Neutron Flux at a Point in Space as a Function of Reactor Orientation Angle, ρ = 45 cm.

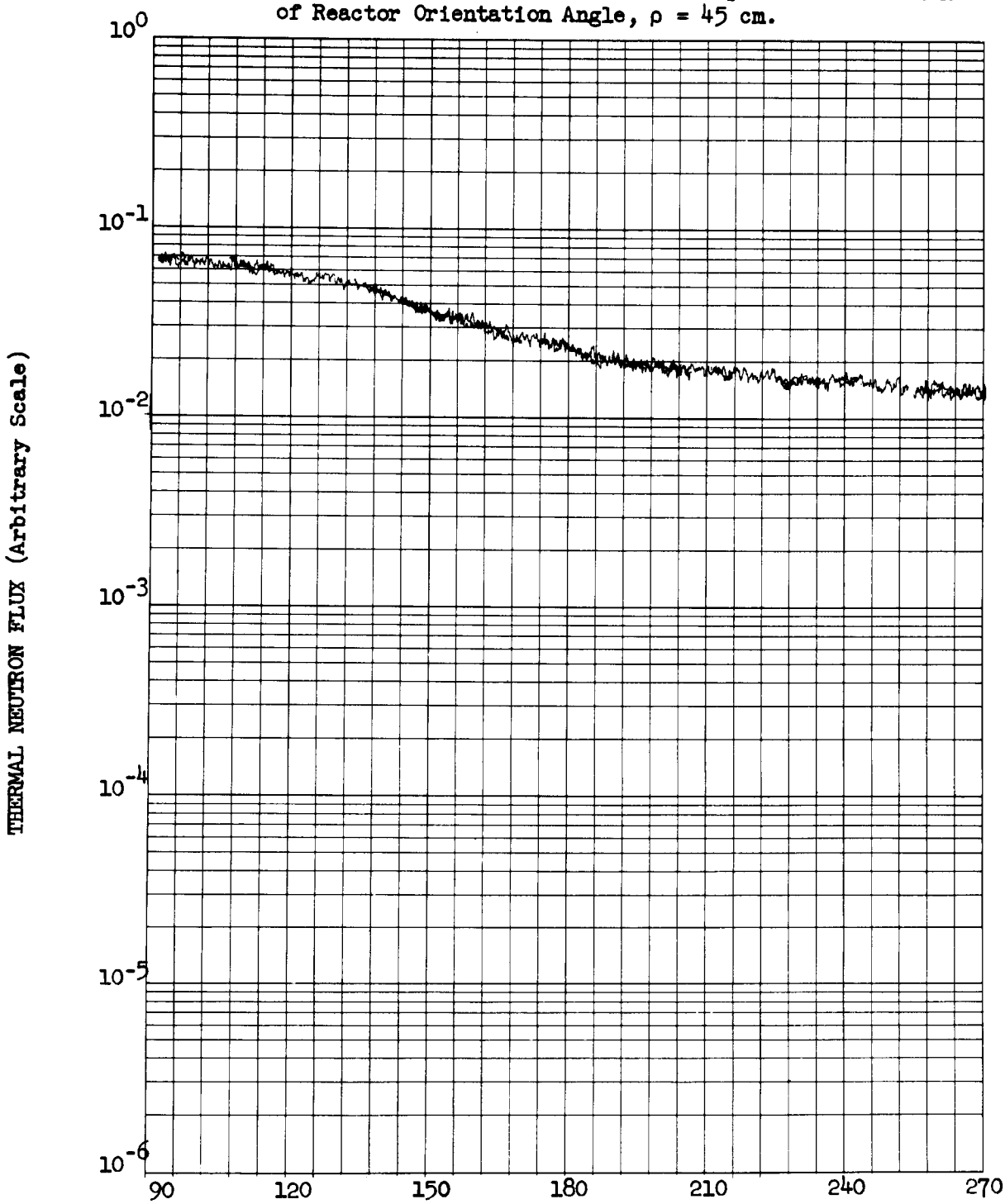

θ, REACTOR ORIENTATION ANGLE, deg

Bare BF_3 chamber mounted on Tower Leg I

h = 140 ft
ρ = 45 cm

Reactor Tank Center to Detector Center = 100 ft.

[redacted]
1-01-056-11-65-(-3)-271

Fig 15

Epithermal Neutron Flux at a Point in Space as a Function of Reactor Orientation Angle, ρ = 45 cm

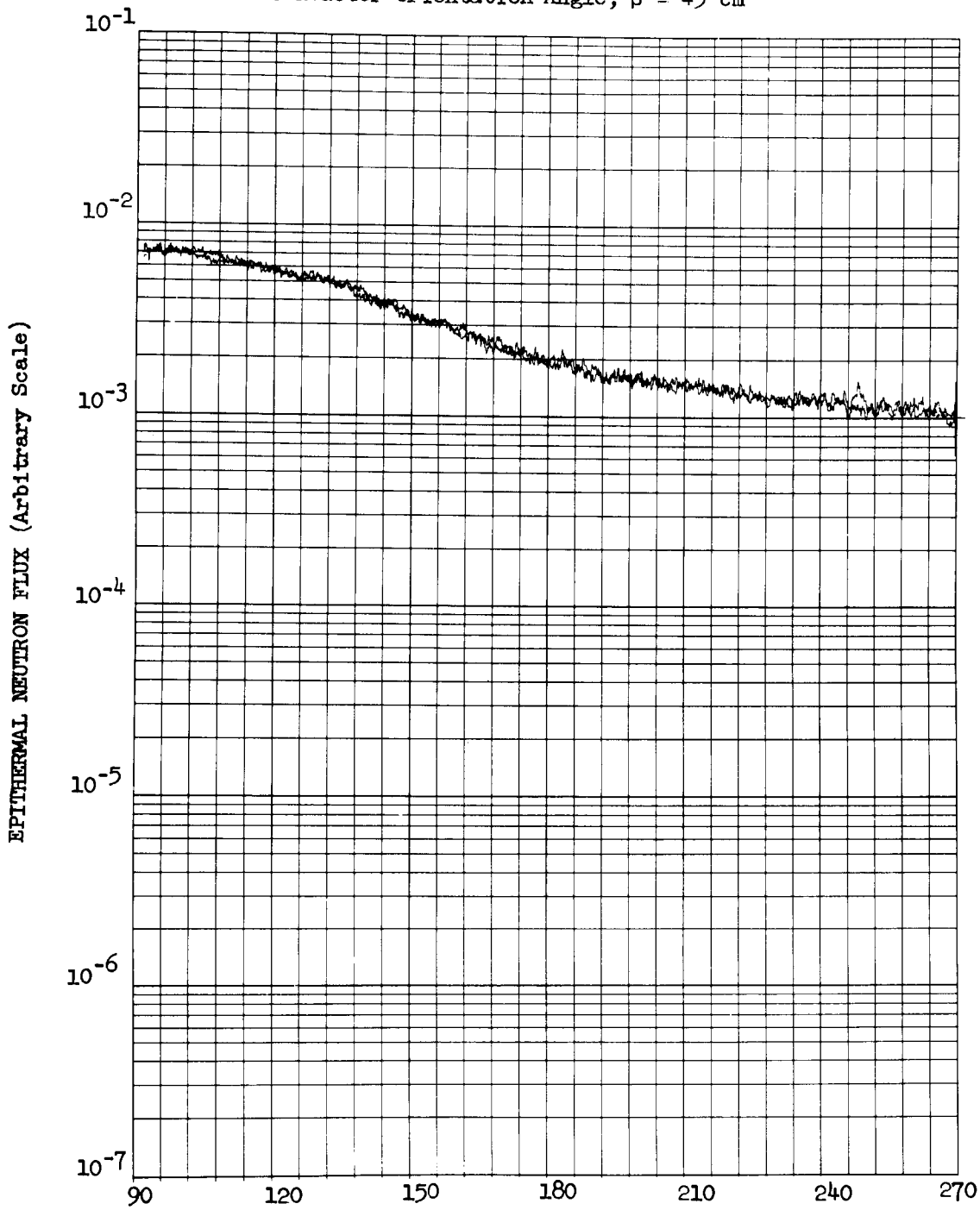

θ, REACTOR ORIENTATION ANGLE, deg

Cadmium Covered BF_3 Chamber Mounted on Tower Leg I

h = 140 ft
ρ = 45 cm

Reactor Tank Center to Detector Center = 100 ft

[redacted]

1-01-056-11-11,14,17-( )-301

Fig. 16 Thermal Neutron Flux at the Rear of the GE Crew Compartment as a Function of Reactor Orientation Angle

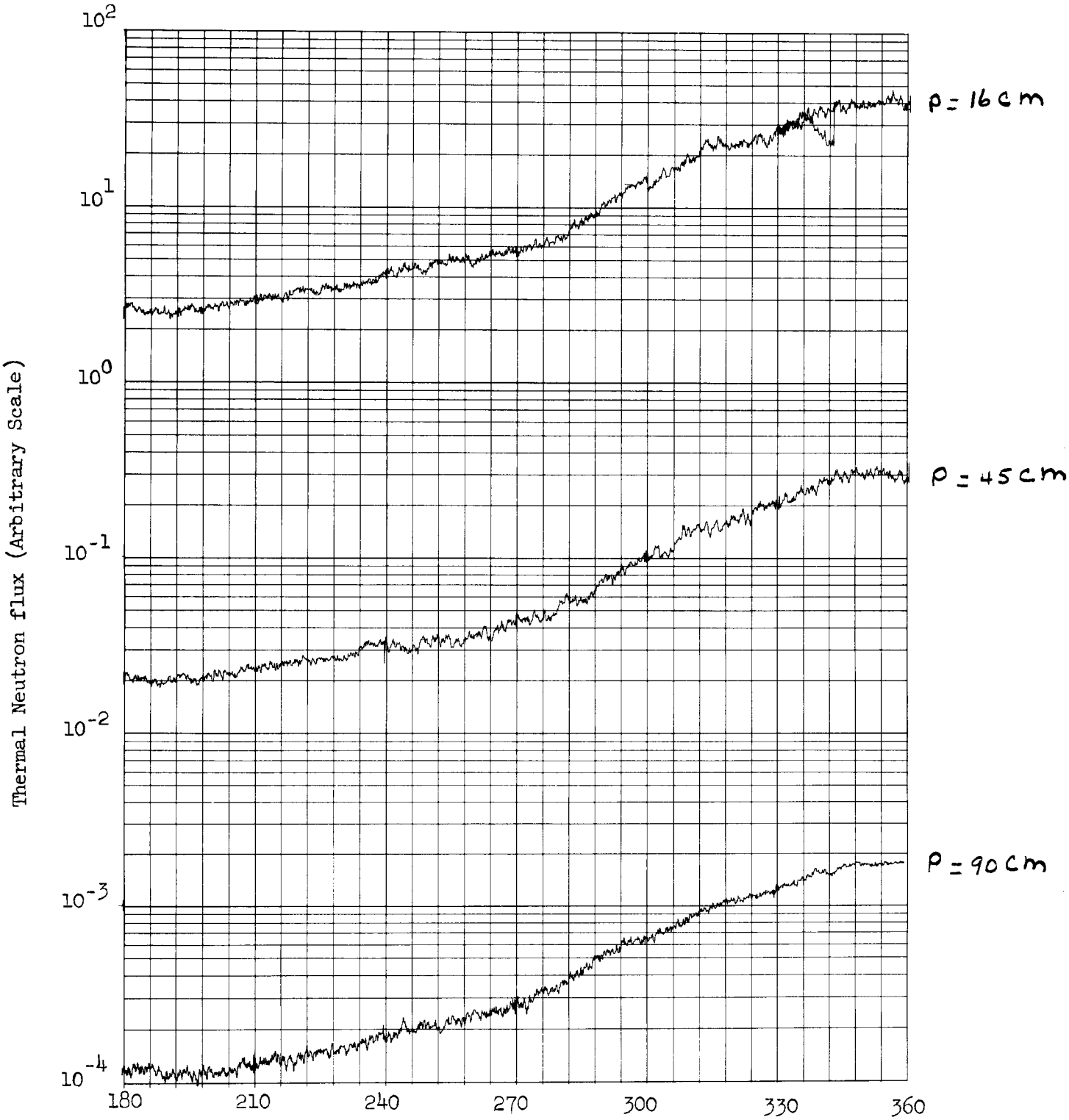

θ, Reactor Orientation Angle, deg
Detector Outside Rear of GE Crew Compartment
h = 195 f+ d = 64 f+

[redacted]

neutrons have a much higher absorption cross section and only a slightly higher scattering cross section than the epithermal neutrons.

Figure 16 shows the results of measurements of the thermal-neutron flux at the rear of the GE crew compartment as a function of θ for three values of ρ. The shapes of these curves change very little with ρ. The ratios from 0 to 180 deg are considerably higher here at d = 64 ft than on the tower leg at 100 ft. This is reasonable, however, as the $1/R^2$ effect would be less noticeable at 100 ft and also a 1/R correction has to be applied to the 180-deg radiation. Applying these corrections, it is found that the ratios at 64 ft are about 25% higher than those at 100 ft. This discrepancy is probably due to the inadequacy of the 1/R theory for this problem of diffusion.

CONCLUSIONS

The data which are reported herein are useful both in understanding the mechanism through which gamma rays are able to get inside a crew compartment and in indicating the direction in which future experiments should proceed. Strong experimental evidence is given that air capture gamma rays are important contributors in certain configurations.

In future experiments every effort should be made to separate the sources of radiations which arrive in the crew compartment. That is, gamma rays from the reactor should be shielded out while allowing a strong neutron beam to escape, thus separating capture gamma rays from direct and scattered gamma rays. Conversely, a heavy shield with little gamma-ray shielding in the beam direction should help to separate the direct and scattered components.

[redacted]

[redacted]

Paper I-F

TOWER SHIELDING FACILITY GAMMA RAY SPECTRA
(Preliminary Results)

G. J. Rausa*
Oak Ridge National Laboratory

* Loan employee from The Martin Company

[redacted]

[redacted]

TOWER SHIELDING FACILITY GAMMA RAY SPECTRA
(Preliminary Results)

by

G. J. Rausa*

In order to interpret the results of the shielding measurements at the Tower Shielding Facility, it has become apparent that the spectra of gamma rays from the reactor, the reactor shield and in the vicinity of the detector tank (or crew compartment) must be known. A program has been initiated which will attempt to determine these spectra.

The results of pilot experiments have indicated that the radiation normally labeled scattered probably includes high energy, neutron-induced gamma radiation. It also appears that the assumption of 3 Mev gamma radiation leaving the reactor shield, for calculating the scattered dose, is not valid for the TSF reactor and shield.

INTRODUCTION

In order to interpret the results of many shielding experiments, knowledge must be obtained concerning the energy spectrum of the source and the change in energy spectrum as a function of shield thickness. The effectiveness of the shield is dependent upon the spectrum because of the change in the absorption coefficients as a function of energy. The dose rate at a point due to scattered radiation is dependent upon the energy spectrum leaving the shield as is seen from the cross sections for scattering. It is also necessary to determine the spectrum of the scattered radiation at the detector tank (crew compartment) in order to make more efficient use of the crew compartment shielding materials.

It is probable that the neutrons leaving a reactor shield will produce gamma radiation external to the shield, in air, ground, and structures, against which it is necessary to shield.

At the Tower Shielding Facility an investigation of the gamma ray spectra for the conditions listed above has been initiated. It should be emphasized that the data presented herein is preliminary. Future experiments are contemplated using more refined equipment.

* Loan employee from The Martin Company.

[redacted]

[redacted]

APPARATUS

The apparatus used for these measurements was a 3-in.-high by 3-in.-dia NaI(Tℓ) crystal and a portable, three-channel analyzer.[a] The unit was used as a total absorption spectrometer. Window widths of 1 Mev were used when covering the spectrum from 0 - 12 Mev, while widths of 0.2 Mev were used for the range from 0 - 2.4 Mev.

The crystal has a total intrinsic efficiency as shown in Fig. 1 for a parallel beam source. During its use, the instrument was calibrated in energy with Cs-Ba (0.66 Mev) and thorium. An attempt was made to calibrate with $O^{16}(n,p)N^{16}$(6.1 Mev) by circulating water from the reactor through a tube around the crystal. No conclusive results were obtained. The spectral response of this crystal to line spectra are published in numerous ORNL reports.[1]

EXPERIMENTAL PROCEDURE [b]

Data were obtained with a bare detector, a shadow-shielded detector and a detector having a collimator. The shadow shield was estimated to be a 2-deg[c] shadow shield at 1150 ft, and a 0.75-deg shadow shield at 195 ft, i. e., the radiation scattered less than the angle designated and measured by the detector was considered to be unscattered. Figure 2 shows the geometry for the data obtained with the bare detector and the shadow-shielded detector. Data at position 1 were obtained with the reactor in the center of its tank (water thickness, $\rho \cong 150$ cm) at an altitude of 195 ft. At position 2, data were obtained with a bare detector only for $\rho = 16$ and 60 cm with $\theta = 180$ and 0 deg respectively - the separation distance being 600 ft. The third position was approximately 1150 ft from the reactor. Here the shadow shield blocked an area 72 ft in diameter as compared to 5.4 ft for position 1. Data at position 3 were obtained for $\rho = 16$ and 25 cm with $\theta = 0$ deg. The detector was located approximately 3 ft above ground level at these positions.

The geometry for the experiment in which the collimator was used is shown in Fig. 3. The collimator is a 5 ft^2, 15-in.-thick, lead slab with a 1-in.-dia hole in the center. The crystal was housed in a 4-in.-thick lead, scatter shield at 5 ft beyond the collimator. From the geometry, it is estimated that the crystal saw an 8-ft-dia spot at the reactor tank. Measurements were made for water thicknesses of 25, 40, 60 and 100 cm with the reactor scrammed as well as operating, and with the collimator open and plugged.

---

a. The author wishes to express his appreciation to the Physical Electronics Group, Physics Division, for the loan of equipment and the helpful assistance and advice.

b. See preceding paper by F. N. Watson for description of TSF geometry.

c. Half angle.

[redacted]

UNCLASSIFIED
2-01-056-12-A-294

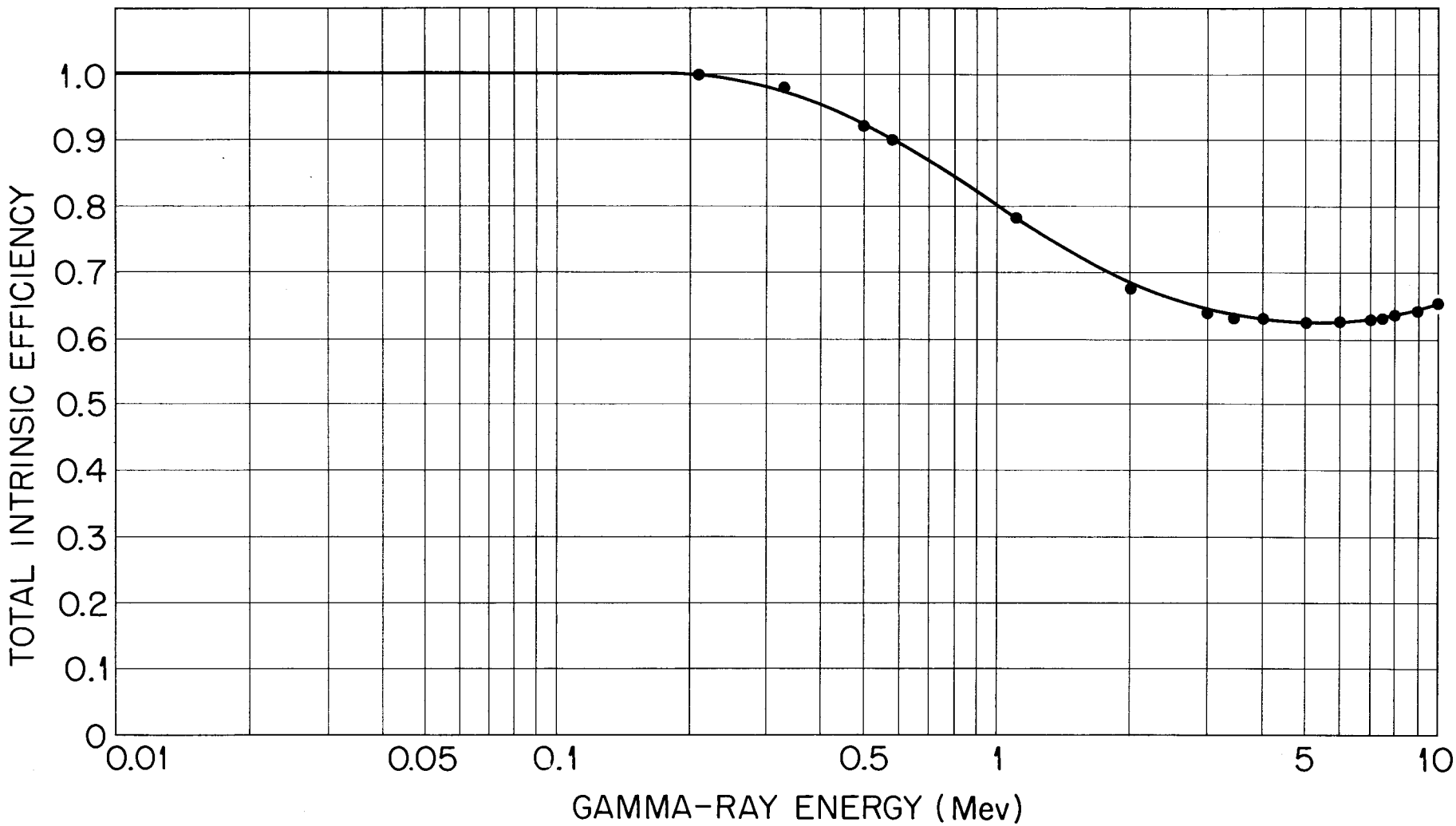

Fig. 1. Total Efficiency of NaI (3 x 3-in. dia Crystal) vs Gamma-Ray Energy.

UNCLASSIFIED
2-01-056-12-D-295

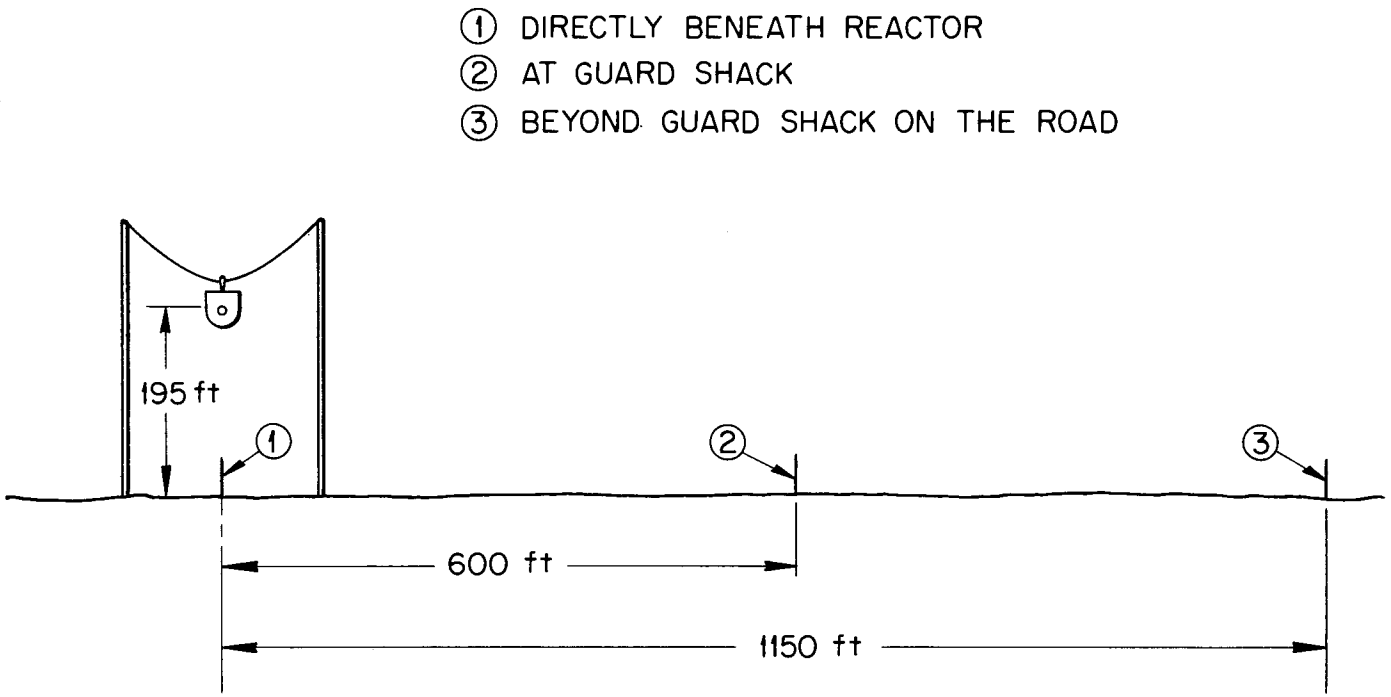

Fig. 2. Geometry for TSF Spectral Measurements Using Shadow Shield.

UNCLASSIFIED
2-01-056-12-D-296

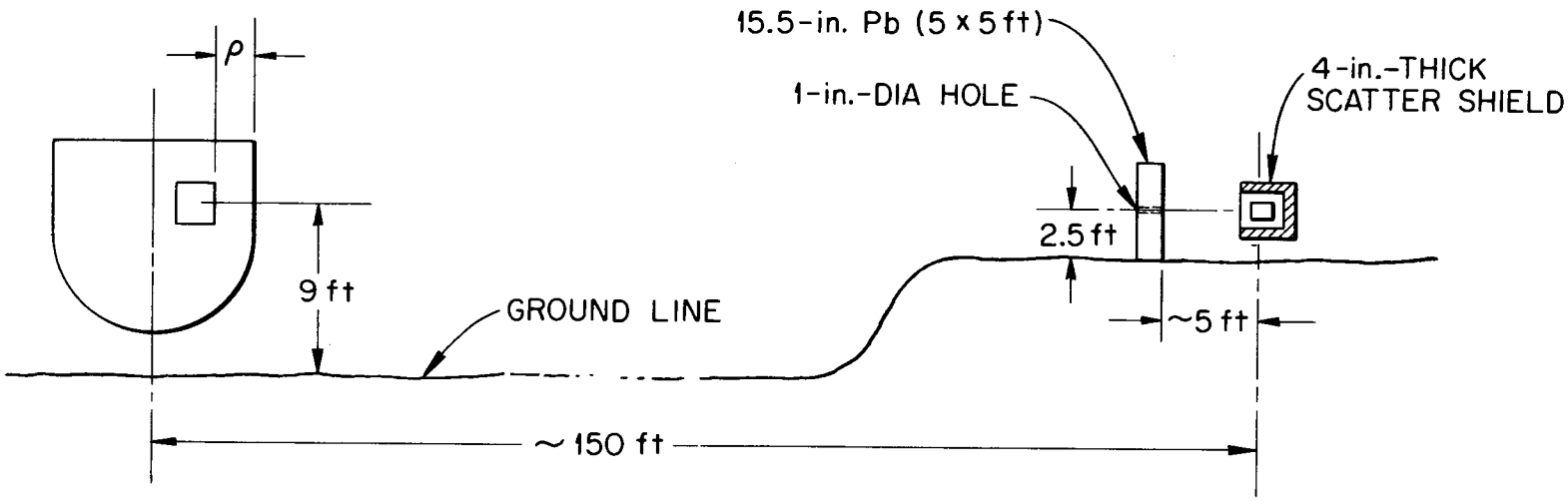

Fig. 3. Geometry for TSF Spectral Measurements with Collimator.

[redacted]

METHOD OF ANALYSIS

In order to convert the data obtained (counting rate/energy interval) into a spectrum, it is necessary to use an analysis which is a series of successive subtractions. Histograms are generated from the spectral response of the spectrometer to discrete energies up to the maximum under consideration. The histograms have energy widths equal to the window widths with which one is concerned. The portion of the histogram representing the photopeak for the highest energy under consideration is then matched to the counting rate in the highest energy interval. The Compton portion of the histogram is then subtracted from the lower energy intervals. The difference in the second highest energy interval is then considered to be the photopeak for that interval. The process is then repeated so that there are one subtraction in the second highest channel, two subtractions in the third highest channel, and so on. The errors are cumulative, of course, but as long as the spectrum drops fairly rapidly, the effect is small. The uncertainty becomes greater in the channel below a peak. The results of the subtraction are then corrected by the crystal efficiency and the ratio of gammas in the photopeak to the total spectrum for a given energy interval.

SUMMARY OF RESULTS

The results of the analysis of the collimator data are plotted in Fig. 4. The cumulative errors were estimated only for $\rho = 25$ cm. It will be noted that the error for the peak is approximately 5% while that in the valley is 25%. The peak occurs for the interval centered at 7 Mev and falls with a relaxation length of 31 cm. The theoretical relaxation length for this energy in water is 40 cm. The reason for the discrepancy has not been ascertained as yet. At any rate, the attenuation is most like gamma radiation, indicating that the source of this peak is in all probability the reactor itself. Neutron captures in aluminum give rise to a 7.72-Mev gamma ray and since there is aluminum in the fuel elements, it is most likely that this is the source of the peak in the spectrum. The effect of the energy dependence of the absorption coefficient is noted in the "hardening" effect that occurs with an increase in the thickness of shielding. There is some indication that the spectrum is beginning to peak or at least flatten in the vicinity of 2 to 3 Mev. A peak in this energy interval could be explained on the basis of the neutron captures occurring in hydrogen (2.2 Mev).

Figure 5 is a plot of the direct radiation spectrum at positions 1 and 3. The data from position 1 have been corrected to the same distance as position 3 by the inverse square law for easier comparison.

[redacted]

UNCLASSIFIED
2-01-056-12-A297

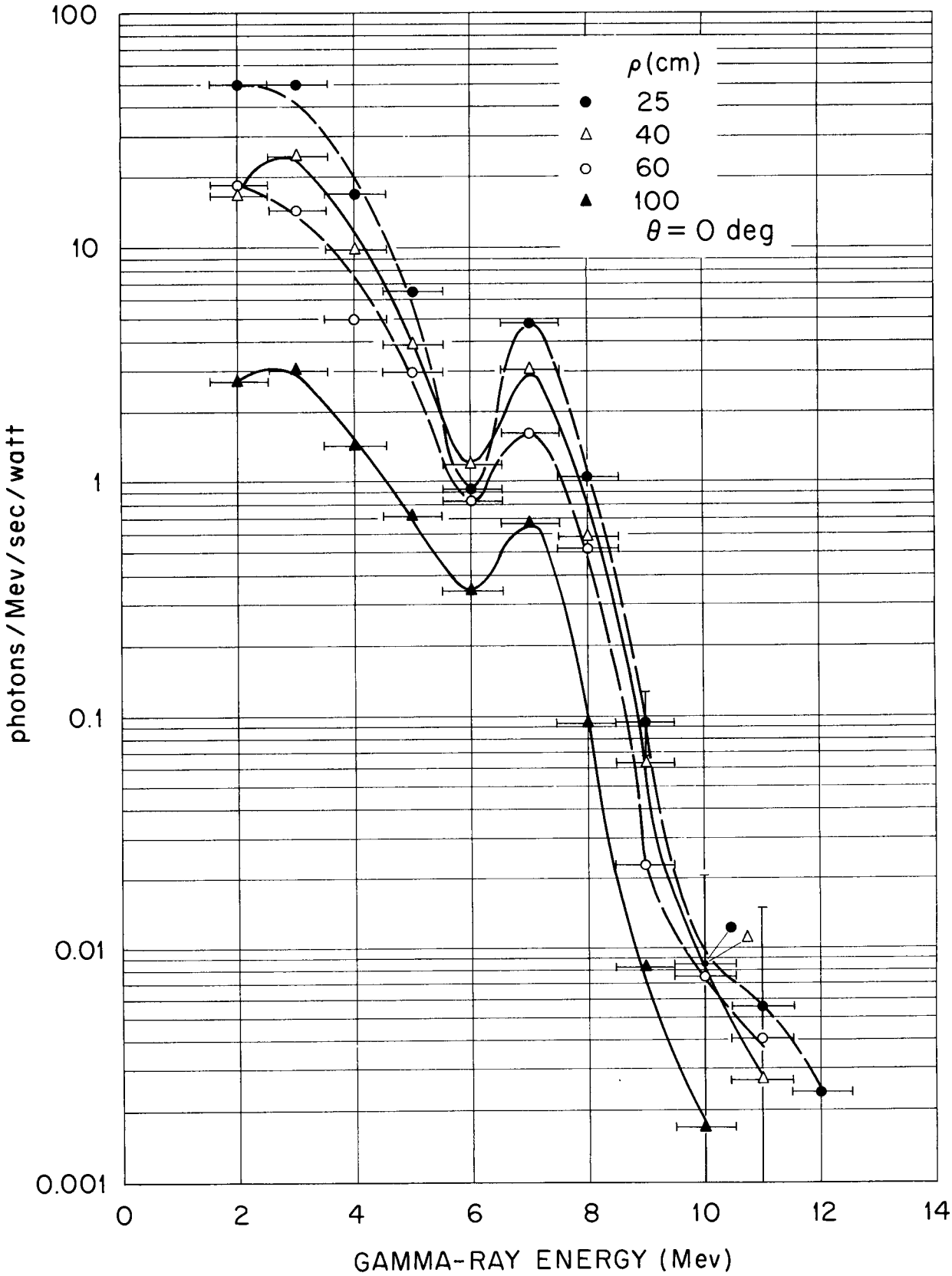

Fig. 4. TSF Gamma-Ray Spectra (Direct plus Collimator Scattered.)

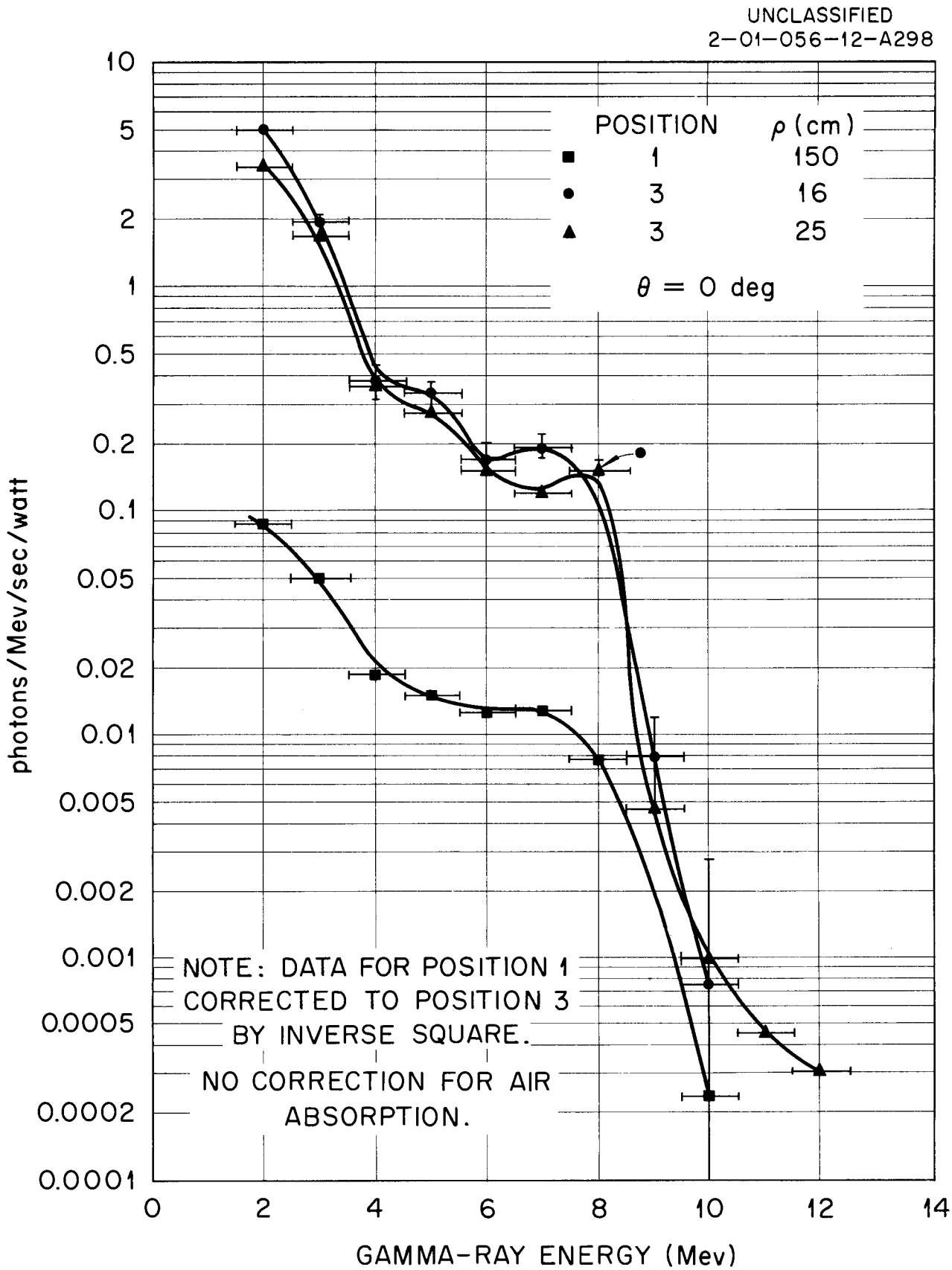

Fig. 5. TSF Spectra (Direct).

[redacted]

Air attenuation which should also modify the spectrum because of the energy dependence of the absorption coefficients and because of the degradation in energy associated with Compton scattering has not been taken into account. The errors are shown for one curve only (ρ = 16 cm in this case). As one might expect, there is a rapid decrease in the direct spectrum for E $>$7 Mev. It will be noted that the peak seems to occur at 8 Mev for ρ = 25 cm. In all probability, this was due to a shift in energy calibration. There is a suggestion of a peak in the vicinity of 5 Mev for ρ = 16 cm, which is not apparent for ρ = 25 cm. The same effect is noted to some extent in Fig. 6. It is difficult to make a concrete statement on the basis of these curves, but neutron captures in the tank wall at ρ = 16 cm could be decreased by as much as a factor of 5 in moving to ρ = 25 cm. The capture gamma rays from iron give rise to 24, 24 and 50 photons for energy intervals of 3 to 5, 5 to 7 and $>$7 Mev respectively per 100 neutron captures.[2] On the other hand, the errors are sufficiently large to eliminate these apparent peaks. Because of the large error in the data at 10, 11 and 12 Mev any comment would be difficult to justify.

The final plot, Fig. 7, is the result of the data taken at position 2 for ρ = 16 cm, θ = 180 deg. No shadow shield was used here, but on the basis of the data taken at position 1, an estimate was made of the direct spectrum at position 2 for ρ = 16 cm, θ = 180 deg. It is seen therefore that the spectrum is due primarily to scattered radiation or the result of neutron captures in the air, ground or structures. It will be noted that there are definite peaks at 6 and 10 Mev, the 10-Mev peak not having been seen in the direct radiation spectra. It must be concluded that the 10-Mev peak is due to neutron effects in air, ground and structures or to a sum peak occurring in the crystal which might not have been taken into account in the analysis. The probability of the second possibility is thought to be extremely small. It is also reasonable to assume that the 6-Mev peak is due to neutron effects external to the shield.

In future experiments the spectrum will be determined more accurately with the aid of a 20-channel analyzer. Experiments with a 4 x 4-in.-dia crystal have been carried out to determine the gain over a 3 x 3-in.-dia crystal for total absorption measurements. As yet no marked advantage is clear.

[redacted]

UNCLASSIFIED
2-01-056-12-A-299

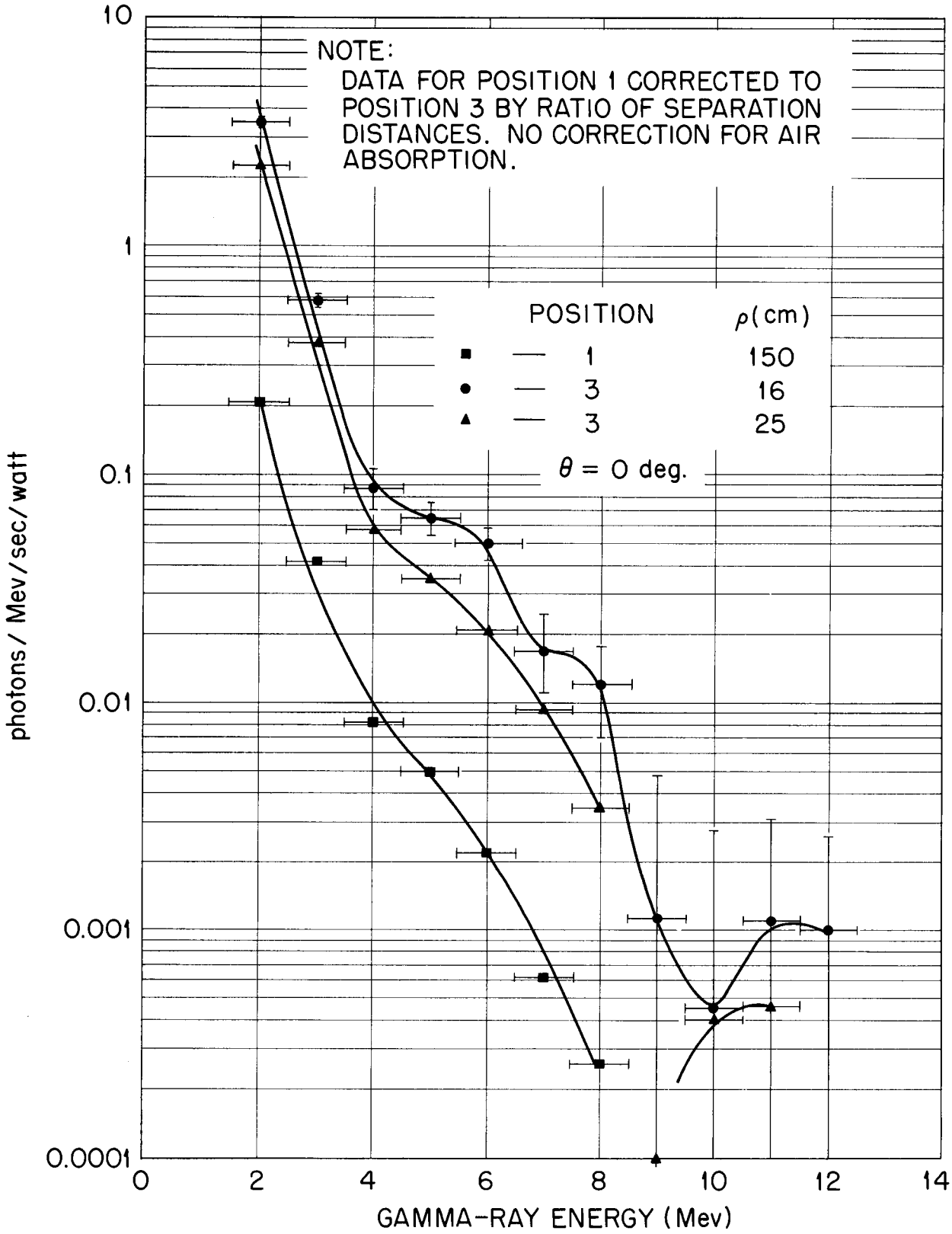

Fig. 6. TSF Gamma-Ray Spectra (Scattered).

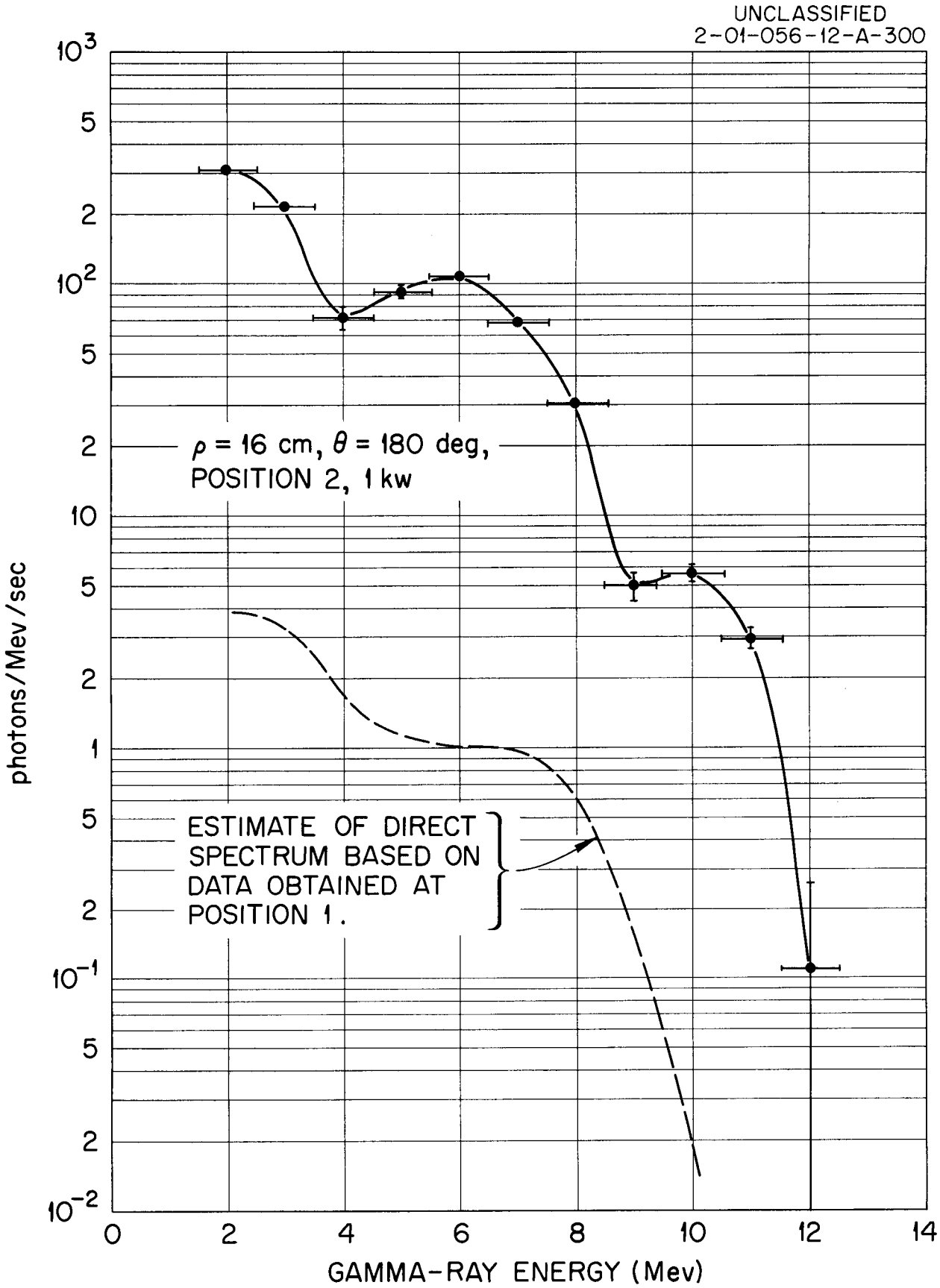

Fig. 7. TSF Gamma-Ray Spectra (Direct Plus Scattered).

[redacted]

REFERENCES

1. Spectrometry Handbook, Physics Division, Oak Ridge National Laboratory.

2. Mittleman, P. S. and Liedtke, R. A., "Gamma Rays from Thermal Neutron Capture," Nucleonics 13, No. 5, p. 51, (1955).

[redacted]

Paper I-G

MEASUREMENTS OF THE ITSF SOURCE PLATE POWER

W. J. McCool*

Oak Ridge National Laboratory
Oak Ridge, Tennessee

* Loan employee from Pratt and Whitney Aircraft Company, E. Hartford, Conn.

MEASUREMENTS OF THE LTSF SOURCE PLATE POWER

by

W. J. McCool*

Oak Ridge National Laboratory
Oak Ridge, Tennessee

A description of the Lid Tank Shielding Facility and the original converter plate is followed by a justification for and description of the new converter plate. Experimental methods for the power calibration of the new converter plate are described.

DESCRIPTION OF THE LID TANK SHIELDING FACILITY

The Lid Tank Shielding Facility may be described as a large tank of water (11' x 7' 5" x 7') covering a hole, approximately thirty inches square through the west face of the Oak Ridge National Laboratory Graphite Reactor Shield. Figure 1 shows a cutaway view of the facility. That portion of the tank wall directly over the hole in the reactor shield has been removed and replaced by a converter plate. The converter plate is made of a U^{235} containing material whose function is to convert thermal neutrons, from the Graphite Reactor, into a fission spectrum of both neutrons and gamma rays. Differentiations between radiations having their origin in the reactor and those originating in the converter plate are made by utilizing a boral shutter which may be interposed between the converter plate and the Graphite Reactor. If a detector is placed in the tank of water and the shutter opened, the detector responds to radiations originating both in the converter plate and in the Graphite Reactor. With the shutter closed the detector response is due almost entirely to pile radiations since the shutter absorbs essentially all of the thermal neutrons to which the converter plate is sensitive. Thus by taking the difference between the detector response with the shutter open and that with the shutter closed, one obtains that portion of the response due to radiation originating in the converter plate. All data are normalized to a constant pile power, since the converter plate is dependent upon the Graphite Reactor for thermal neutrons. Bulk shielding measurements are made with calibrated detectors, first with nothing but pure water in the Lid Tank, then with a slab of some proposed shielding material interposed between the detector and the converter plate. After making appropriate corrections, the difference between the two sets of data represents the effect of the shielding material on the radiation field. With enough data and patience one may obtain a gross shielding optimization of reactor components.

---

* Loan employee from Pratt and Whitney Aircraft Co., E. Hartford, Conn.

Unclassified

DWG. 15125

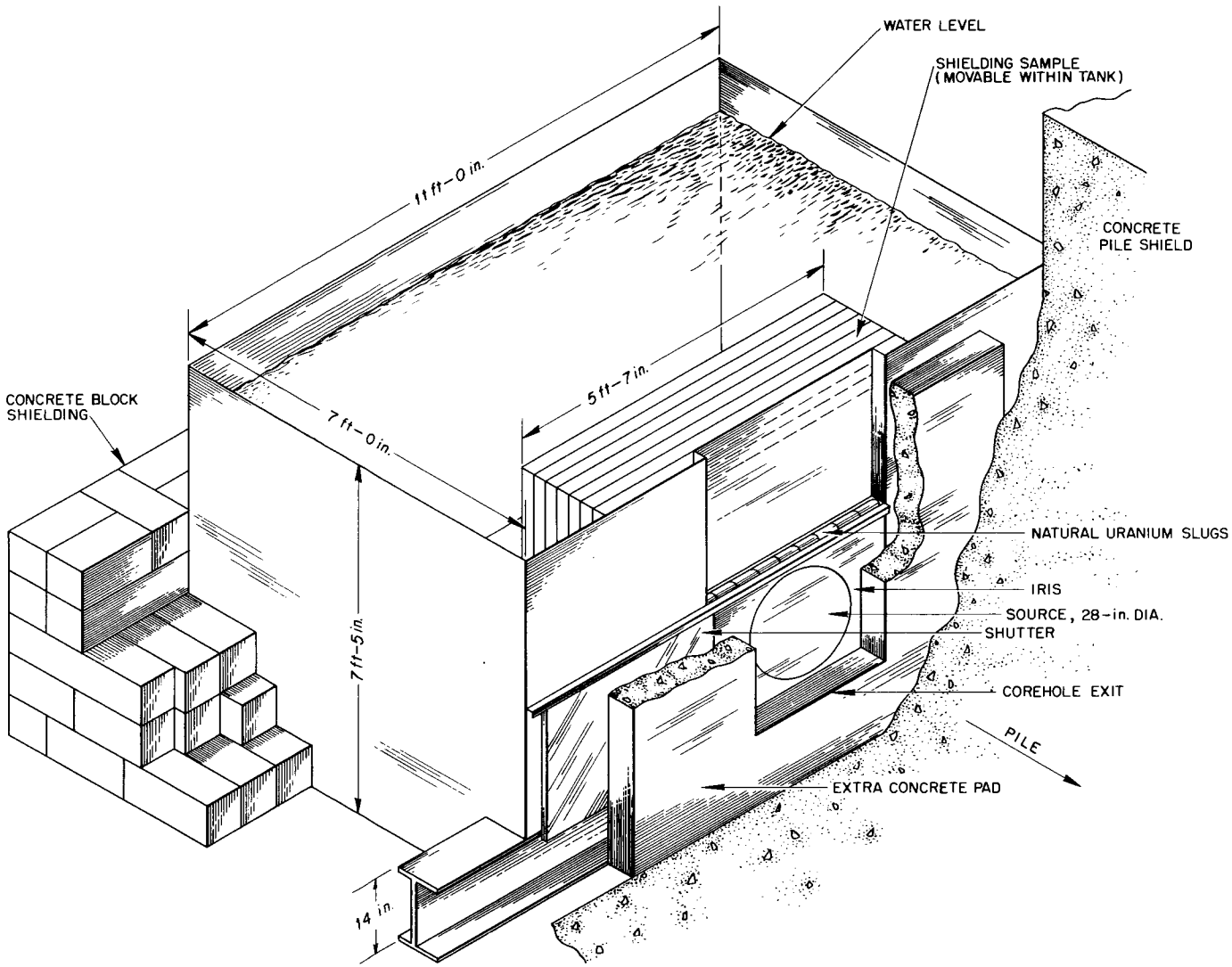

Fig. 1

DESCRIPTION OF ORIGINAL CONVERTER PLATE

Figure 2 is a cross sectional view of the original source or converter plate installed at the Lid Tank. It consisted of rows of natural uranium slugs stacked one row upon the other with the axis of the cylinders parallel with the west face of the Graphite Reactor. The thermal neutrons from the Graphite Reactor were collimated into a circular source by a boral iris placed between the converter plate and the reactor. The purpose of the boron curtain between the source plate and the Lid Tank was to prevent neutrons that were thermalized in the Lid Tank from diffusing back to the source plate.

JUSTIFICATION FOR NEW CONVERTER PLATE

The facility was put into service in 1949. With the advent of the aircraft program and more stringent shielding requirements, it became apparent that the original source plate left something to be desired. There were large discrepancies between bulk shielding measurements made at the Lid Tank Facility and the ORNL Bulk Shielding Facility (Swimming Pool Reactor). These discrepancies were sometimes attributed to the lack of a satisfactory power calibration of the Lid Tank source plate. Analytical methods of determining the thermal neutron flux utilization and the leakage from the source plate were only approximate because of the geometry and orientation of the uranium slugs. In addition, the fission spectrum of neutrons and gamma rays were altered on passing through the thick uranium slugs and structural materials.

SPECIFICATIONS OF THE NEW CONVERTER PLATE

The new converter plate is a thin circular disk of pure uranium enriched to 21% U^{235} for which the thermal utilization and leakage can be calculated rather accurately. The plate is twenty-eight inches in diameter and sixty mils thick, and the structural materials are as thin as possible in keeping with structural requirements. The assembly was installed in late 1955. An exploded view of the assembly is shown in Fig. 3. The new converter plate, as seen by a neutron from the Graphite Reactor, consists of a one-quarter inch aluminum pressure plate, a one-quarter inch void, a frame of one eighth-inch aluminum for holding the converter plate, the converter plate, one-eighth-inch boral, and a one-sixteenth inch aluminum cover plate. The void between the pressure plate and the source plate frame is pressurized with air to enable the thin source plate frame to withstand the water pressure from the Lid Tank. The converter plate rests in a slight recess in the aluminum frame such that the boral lays flush against the aluminum frame and converter plate. The aluminum cover plate covers the boral and converter plate and is welded to the aluminum frame, forming an air and water tight compartment for the converter plate and boral. A vacuum pump-out tube is used to maintain a vacuum on the chamber containing the source plate, at all

DECLASSIFIED BY E. J. Murphy
[redacted] 5-22-56

DWG. 15137

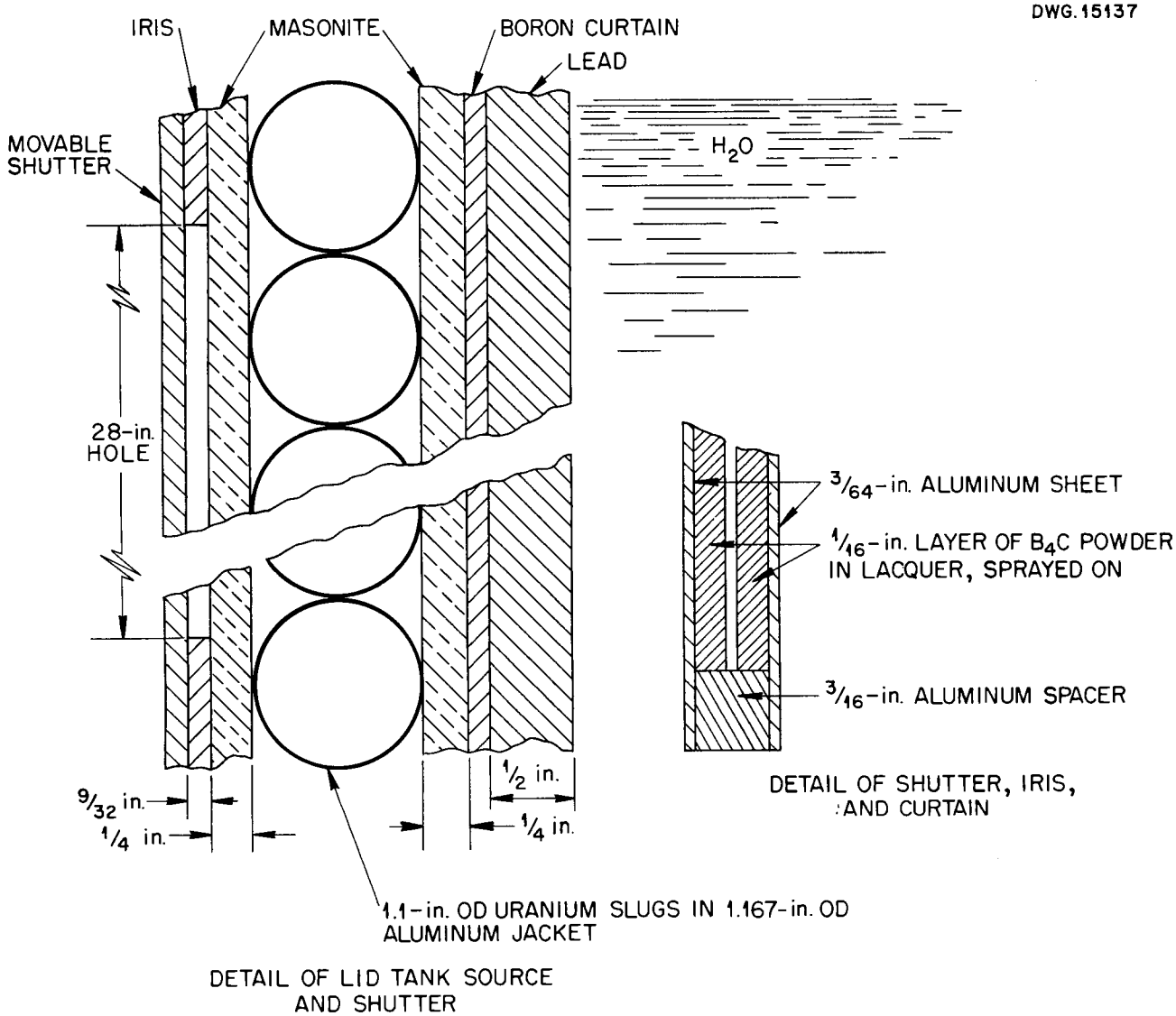

Fig. 2. Geometry of Lid Tank Source and Shutter.

UNCLASSIFIED
ORNL-LR-DWG 13591

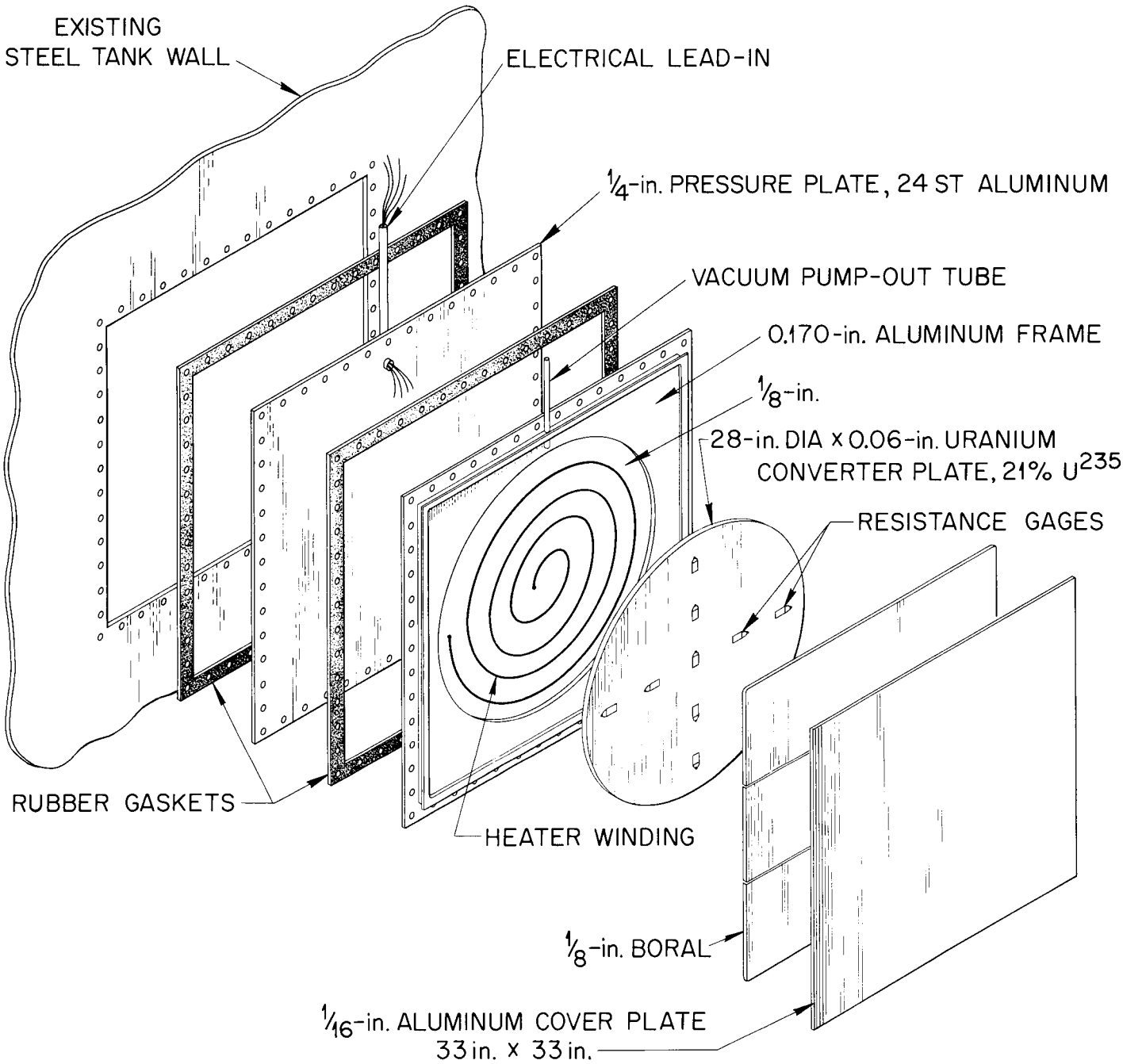

Fig.3. Lid Tank Source Plate Assembly.

times. The vacuum insures the removal of any gaseous fission products from the chamber, through the pump-out line and into the outgoing coolant gases of the Graphite Reactor. The vacuum also collapses the walls of the compartment against the source plate to form a friction hold that keeps the plate in position. For calibration purposes a heating coil was imbedded in the wall of the aluminum frame adjacent to the converter plate, and resistance gauges were attached to the source plate to measure the temperature response of the plate. The electrical leads to the heating coil and resistance gauges were passed through the wall of the aluminum frame into the void and out through the air line used to pressurize the void.

METHODS OF CALIBRATION

Thermal Flux and Utilization Measurements:

In order to determine how well the new source plate utilizes neutrons an experiment was performed with a mockup of the source plate assembly. Small sections (2-1/2" x 2-1/2") of the source plate assembly materials were laminated in the same order in which they occur in the final assembly. The section representing the source plate was fabricated from the same uranium sheet from which the source plate was taken. Gold foils were placed on both the incident and exit flux sides of the source plate section, in such a manner as to prevent one foil from casting a radiation shadow upon the other. The mockup assembly was exposed to the neutron beam from the Graphite Reactor for a short time, then removed and disassembled. The apparent neutron utilization was calculated from the difference in the gold foil activations.

A surface integration of the neutron flux over the hole in the Graphite Reactor shield was determined from the activation of gold wires. The wires were exposed in a mockup of the source plate assembly and at the position corresponding to that occupied by the uranium. Both the foil and wire measurements required corrections for neutron temperature, resonance absorption, and self-shielding in order to obtain a corrected integrated flux, and flux utilization in the converter plate. The plate power was calculated from the integrated flux incident upon the plate and from the fraction of neutrons utilized by the plate.

SUMMATION OF NEUTRONS EMITTED FROM THE SOURCE PLATE

A second calculation of the source plate power was made on the basis of the integrated neutron flux emitted by the source plate. Maps of thermal neutron flux were made over planes parallel to the face of the source plate and extending up to eighty centimeters from the center of the plate. After summing up all the neutrons emitted into the Lid Tank an estimate of the power of the plate was made based upon 2.5 neutrons per fission.

COMPARISON OF TEMPERATURE RESPONSE FOR ELECTRIC HEATING AND FISSION HEATING

The temperature response of the plate was obtained by putting a known amount of electrical power into the heating coils imbedded in the aluminum spiral groove plate adjacent to the source plate and recording the change in resistance of the several resistance gauges as a function of heating time. Several constant electrical power runs were made over a range of power inputs, from 3.7 to 16.4 watts, as shown in Fig. 4. The maximum temperature rise represented in Fig. 4 was about 4°F.

Electrical power runs were followed by fission power runs in which the change in resistance was plotted as a function of heating time. The heat transfer mechanisms were not necessarily the same for the electrical power runs as for the fission power runs. Evidence of the difference in mechanism was the crossing of the curves (Fig. 4) of the fission power runs with those of the electrical power runs after approximately thirty minutes heating time. A different mechanism would not be surprising in view of the fact that the heat source was external to the source plate for electrical power runs while it was internal for the fission power runs. In addition, the shutter was open for the fission power runs while it remained closed during the electrical power runs. When closed the shutter could have had a slight insulating effect between the Graphite Reactor and the converter plate.

A cross plot of the resistance change versus heating time curves was made at heating times of 0.5, 1.0, 1.5, 2.0, 2.5 and 3.0 hours to obtain a plot of resistance change versus power input, as shown in Fig. 5. A first estimate of the source plate power was obtained by taking the resistance change of the fission power runs and fitting it to the resistance change versus power input curves of the electrical power runs, at the appropriate heating time. The power estimates obtained by this method showed some scatter and in general the estimated power became larger when made on the basis of longer heating periods. The spread in estimated power seemed to verify the hypothesis that the heat transfer mechanism was not the same for fission and electrical runs. The difference and a revised power estimate will be given in the following paper.

SUMMARY

Gamma ray measurements showed that the gamma field from the Graphite Reactor was so great that there was very little difference in gamma detector response between shutter open and shutter closed. In order to make the source plate radiations a larger fraction of the total gamma radiation field, a one-inch lead slab was inserted between the converter plate and the Graphite Reactor. The effect of the lead slab was a large reduction in the gamma field from the reactor but only a modest reduction in the neutron beam intensity. All data taken without the lead gamma suppressor was normalized by taking the ratio of the thermal neutron flux with the

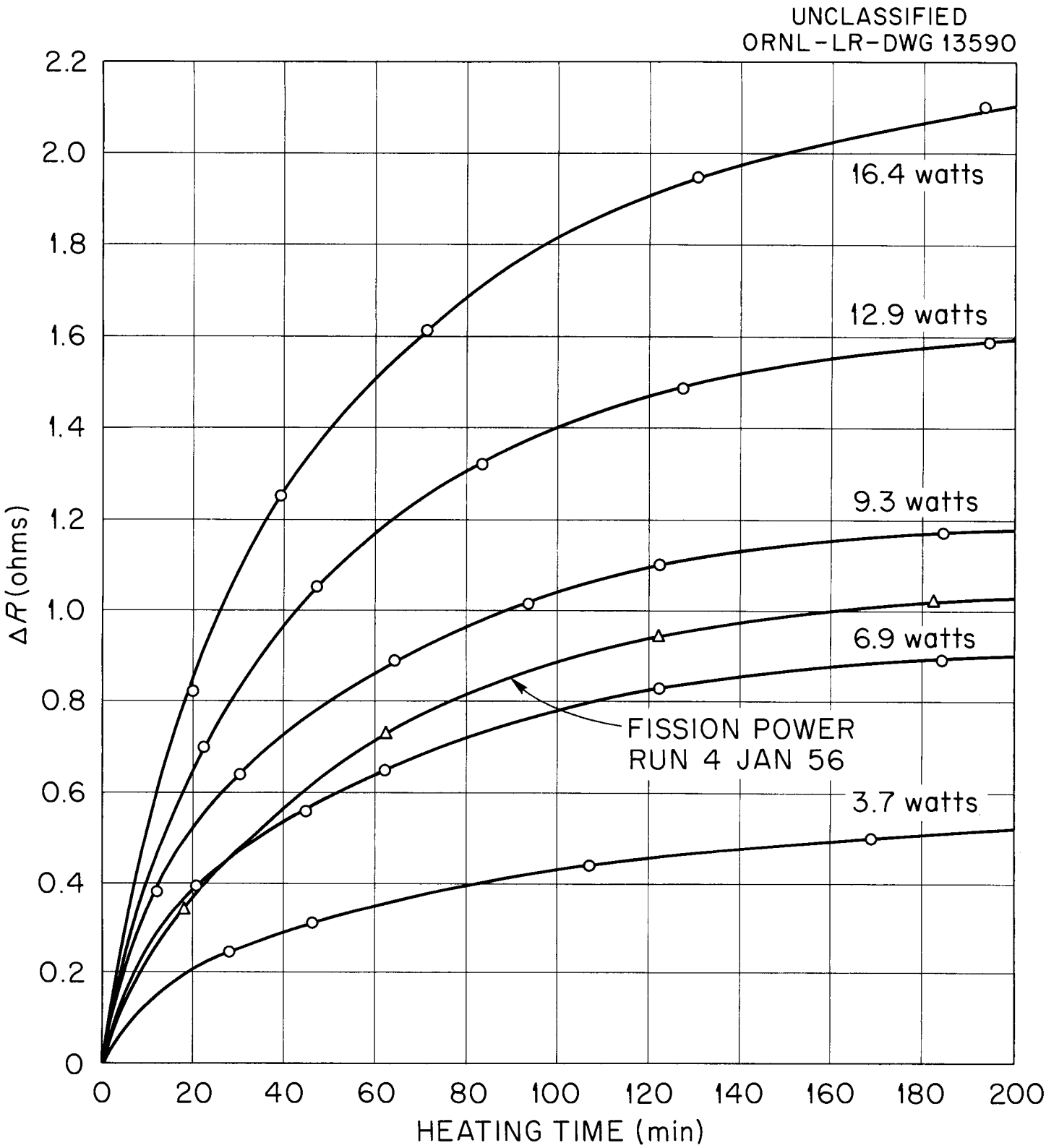

Fig. 4. Lid Tank Source Plate Power Calibration. Temperature response as a function of time for different power inputs (Resistance gage number 7)

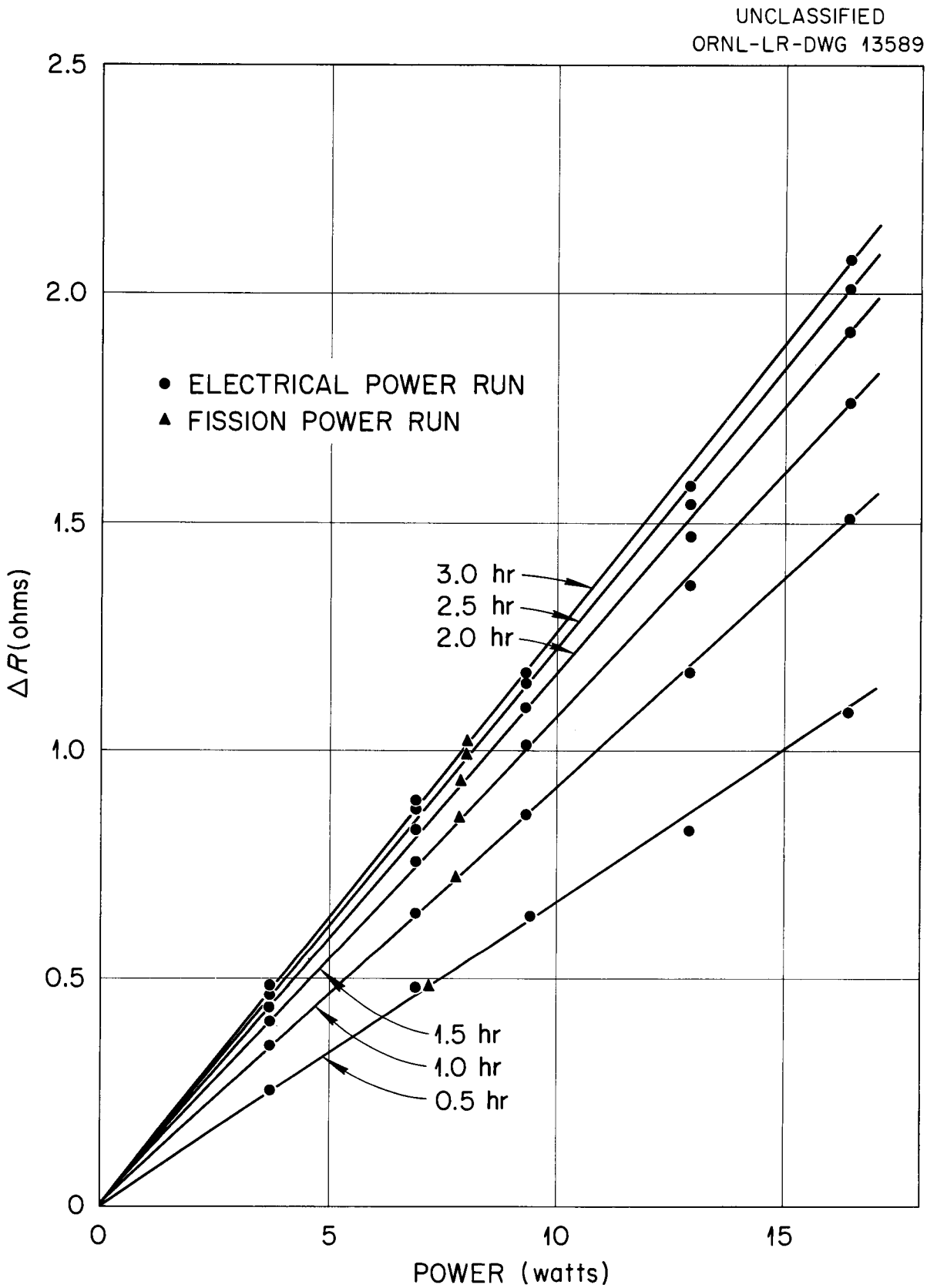

Fig. 5. Lid Tank Source Plate Power Calibration. Temperature Response as a Function of Power Input for Different Heating Times (Resistance Gage Number 7).

lead suppressor to the flux without the suppressor. Most data taken in the future will utilize the one-inch lead gamma suppressor.

Errors were estimated for the three methods of calibration, and a weighted average of the source plate power made.

ACKNOWLEDGEMENTS

The author would like to recognize the engineering and technical staffs at the Lid Tank Shielding Facility for their efforts during the power calibration of the Lid Tank source plate. The engineering staff is composed of R. W. Peelle, J. M. Miller, D. R. Otis*, J. R. Smolen**, and W. R. Burrus,*** The technical staff is made up of E. B. Beckham, J. R. Taylor, B. M. Millican, H. R. Hendrix and H. J. Jarvis. The duties of the technical staff were the manipulations of the instruments involved and the accumulation of data, while the engineering staff duties were largely supervision of the above operation and analysis of the data.

* Loan employee from Convair, San Diego, California.
**Loan employee from Pratt and Whitney Aircraft Company, E. Hartford, Conn.
***Loan employee from Wright-Patterson Air Force Base, Dayton, Ohio

Paper I-H

ANALYSIS OF LTSF SOURCE PLATE CALIBRATION DATA

D. R. Otis*

Oak Ridge National Laboratory
Oak Ridge, Tennessee

*Loan employee from Convair, San Diego, California

ANALYSIS OF LTSF SOURCE PLATE CALIBRATION DATA

by

D. R. Otis*

Oak Ridge National Laboratory
Oak Ridge, Tennessee

The power of the new source plate of the Lid Tank Shielding Facility has been estimated using three independent methods. The three methods are discussed briefly and the results of the several calculations are tabulated in Table I. The new source plate power has been estimated to be 5.5 ± 0.5 watts.

INTRODUCTION

This paper is a complement to the previous paper presented by W. J. McCool and gives the best estimate of the source plate power available at this time. This work should be of general interest for at least two reasons: (1) the accuracy of future Lid Tank data can be no more accurate than the estimated power, and (2) the new source plate calibration will enable a more accurate prediction of the old source plate power thereby decreasing the uncertainty of the old data.

The previous paper has described both the old and new source plates, the experiments performed for calibrating the new source plate, and preliminary analysis of the data. Each of the three independent methods in the previous paper for estimating the source plate power will be discussed in turn.

THERMAL FLUX AND UTILIZATION MEASUREMENTS

If the thermal flux incident upon the source plate and the attenuation of the thermal flux in passing through the source plate are both known, then one can estimate the power using the following equation:

$$P = K e f I A$$

where

P = estimated power, watts

K = 0.323×10^{-10} watt sec/fission

e = fraction of neutron captures resulting in fissions

f = fraction of incident neutrons captured in source plate (utilization)

---

* Loan employee from Convair, San Diego, California

I = average incident thermal neutron current, neutrons/cm^2 sec.

A = source plate area, 3976 cm^2.

The fraction of neutron captures resulting in fissions was calculated from the known thermal neutron absorption and fission cross sections and the source plate composition (21% U^{235}, 79% U^{238}). The utilization factor was obtained using the mockup of the source plate assembly discussed in the previous paper. The incident thermal neutron flux was measured using gold wires mounted in an aluminum frame which was placed in the space between the Lid Tank and the Graphite Reactor. From the activation of gold wires the thermal neutron flux distribution in the core hole was calculated. This flux was not uniform but varied about $\pm$ 10% from the mean.

The estimated power based on the thermal neutron flux and the neutron utilization was 5.9 watts.

SUMMATION OF NEUTRONS EMITTED FROM THE SOURCE PLATE

Since the number of neutrons released per fission is well known, the power can be estimated knowing the rate of neutron emission from the source plate. If the Lid Tank were symmetric with respect to the source plate, then the number of neutrons emitted to either side of the source plate would be equal. This condition is not satisfied but it can be assumed that one half of the fission neutrons enter the Lid Tank so long as the measured flux is corrected for the effects of asymmetry.

Almost all of the fast neutrons entering the Lid Tank become thermalized and captured, and to a first approximation the total number of fast neutrons entering the Lid Tank is given by

$$\Sigma_a \int \phi_{thermal}\, dV$$

where the integral is taken over the tank volume. Measurements of thermal flux were taken throughout the Lid Tank in order to evaluate this integral. However, in the immediate vicinity of the source plate the thermal flux was depressed due to the combined effects of the strong absorption of thermal neutrons by the boral and uranium in the source plate assembly, and the scattering of fast neutrons out of the Lid Tank before thermalization. The curves were redrawn to eliminate this flux depression, and the correction was based on the theoretical solution for an infinite plane source of fast neutrons in an infinite homogeneous medium. Figure 1 shows an example of how the thermal flux traverses were corrected for the flux depression at the source plate.

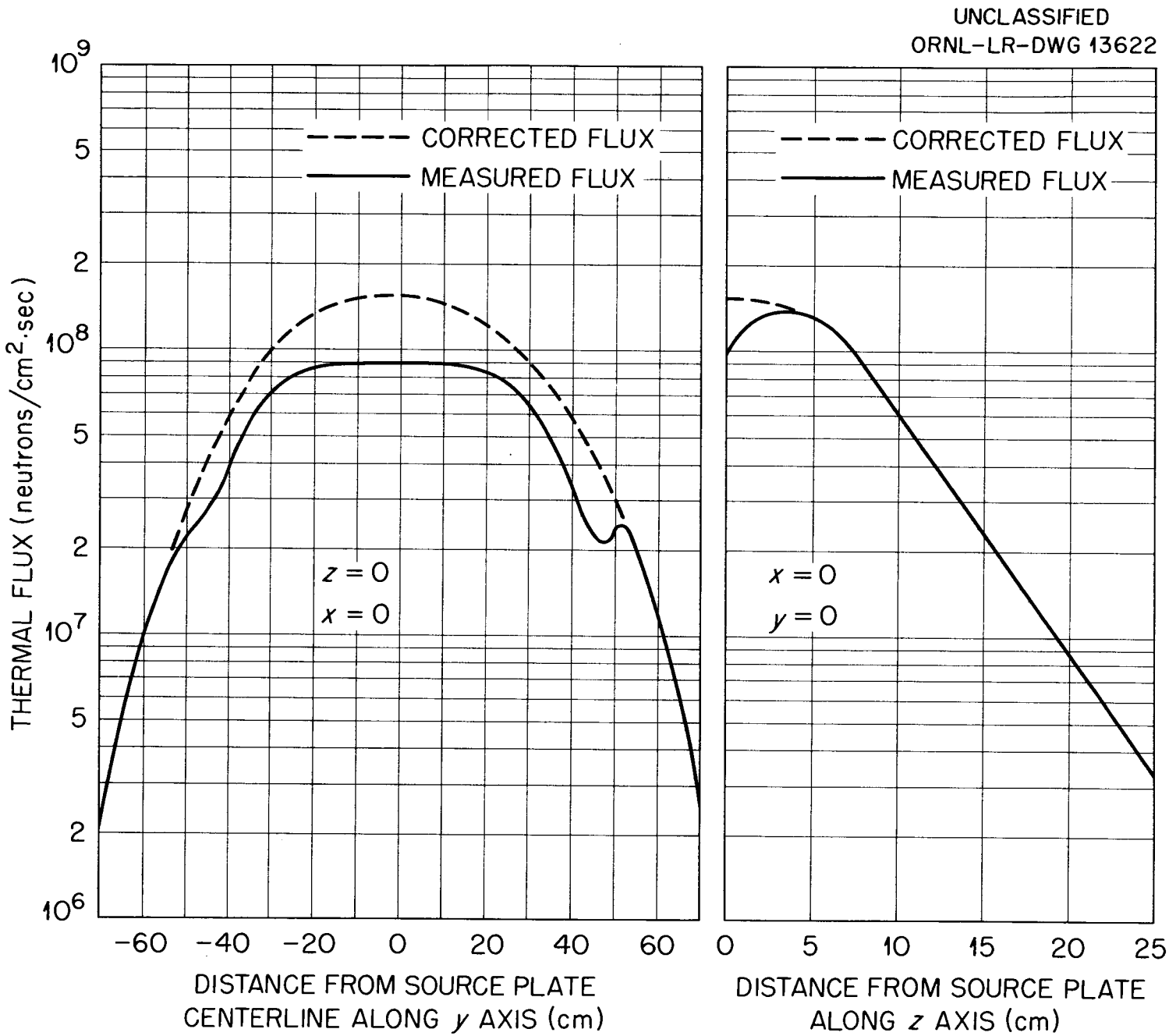

Fig. 1

Typical Thermal Flux y and z Traverses.

The power was estimated using the following equation:

$$P = \frac{2 \Sigma_a \int \phi_{thermal}\, dV}{(3.1 \times 10^{10} \text{ fissions/watt sec.})\ (2.46 \text{ neutrons/fission})}$$

where $\phi_{thermal}$ is the corrected thermal flux (neutrons/cm^2•sec). The factor of two accounts for the fact that only one half of the fission neutrons enter the Lid Tank. The power estimated using this method was 4.5 watts.

COMPARISON OF SOURCE PLATE TEMPERATURE RESPONSE FOR ELECTRIC HEATING AND FISSION HEATING

The power of the source plate was also estimated by comparing the temperature histories under conditions of fission heating and electric heating. It was evident from the data that the estimated power varied in a consistent manner with the time of heating, and this indicated that the heat loss characteristics were different for fission heating and electric heating. At the suggestion of Mr. Ross Burrus, of the Wright-Patterson Air Force Base, a simple analysis was made to predict the shape of the estimated power versus time of heating curve. In this analysis it was assumed that the heat loss was entirely by convection and that the heat transfer coefficients for the two conditions of heating were different. The shape of the predicted curve was similar to the observed behavior, and it was indicated that the effect of differences in heat transfer coefficients could be eliminated by extrapolation to zero time of heating.

Figure 2 shows the relationship between the estimated power and the time of heating based upon one resistance gage for five fission heating runs. The curves have been extrapolated to zero heating time for the reason mentioned above. It is of interest to note that the runs made with either lead or styrofoam between the source plate and shutter resulted in power estimates that were less dependent upon the time of heating. This indicated that the heat loss characteristics were more nearly the same for fission and electric heating when the shutter was isolated from the source plate. This is quite possible since the shutter was open for fission runs and closed for electric heating runs, and this could account for the differences in heat loss characteristics for the two methods of heating. The power estimation based on the temperature response data is summarized in Table I.

CONCLUSIONS

All estimated powers shown in Table I are normalized for a standard energy absorption of 200 Mev. per fission. The Lid Tank source plate actually absorbs only about 175 Mev. per fission since

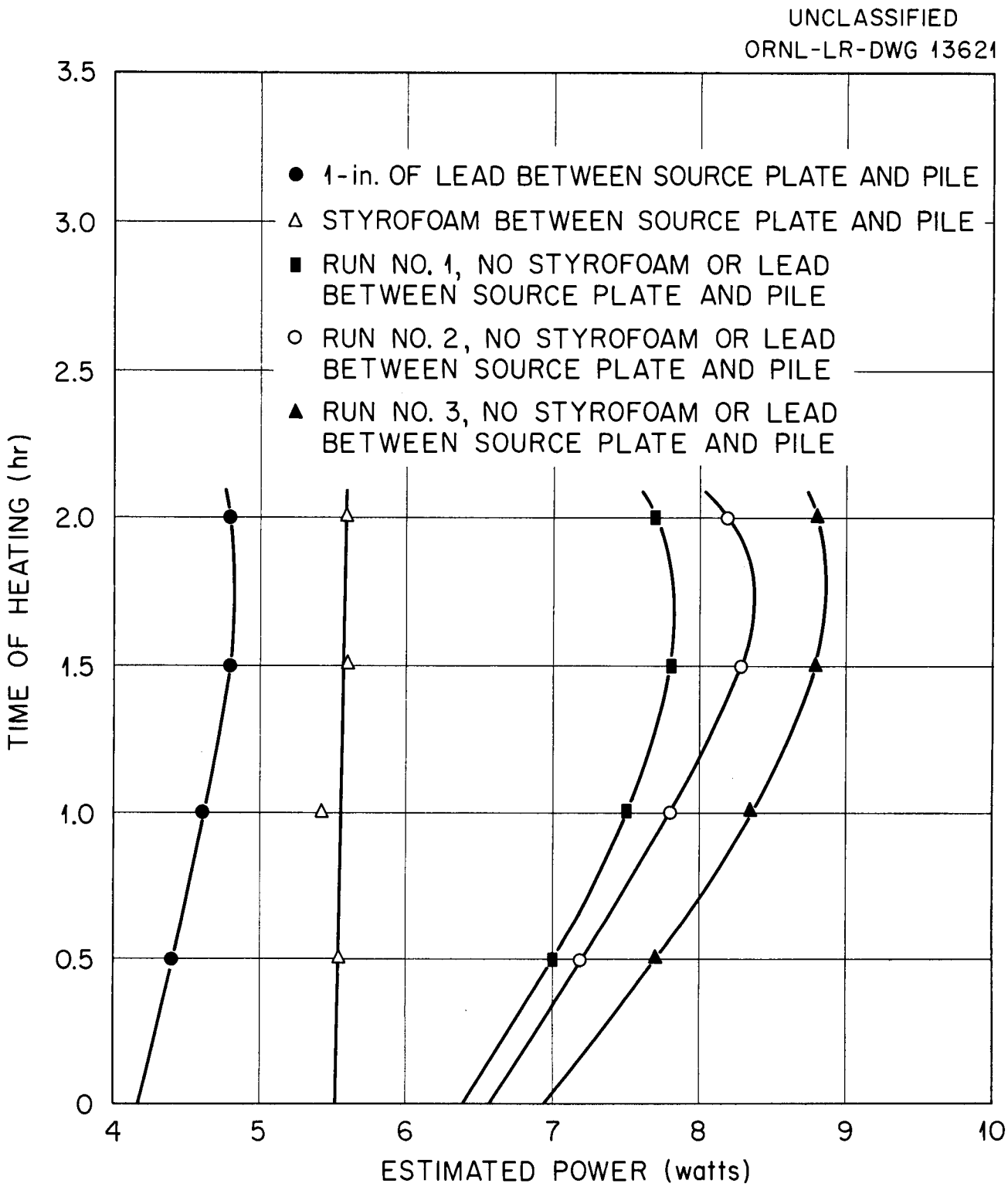

Estimated Power as a Function of Time of Heating.

Fig. 2

only the kinetic energy of the fission products and beta particles are absorbed. Therefore, all power estimates based on the temperature response data were increased by the factor 200/175.

The effective power of the old source plate can now be determined using the new source plate estimate by comparing the thermal neutron traverse data for the two source plates. This results in a power for the old source plate of 2.0 ± 0.2 watts.

ACKNOWLEDGMENTS

Most of the experimental work and preliminary analysis were directed by Mr. W. J. McCool. Mr. John Miller was responsible for the gold wire measurements used to determine the thermal flux field in the core hole. Mr. Ross Burrus, Wright-Patterson Air Force Base, did a great deal of study on the interpretation of the gold foil and gold wire measurements. Mr. R. W. Peelle, as supervisor of the LMSF, certainly had much to do with the planning, execution, and interpretation of the experiments. The efforts of the entire LMSF staff are represented in this work.

TABLE I. SOURCE PLATE POWER ESTIMATE

1. Thermal Flux and Utilization Measurements:		5.9 ± 0.7 watts
2. Summation of Neutrons Emitted from the Source Plate:		4.5 ± 0.8 watts
3. Temperature Response Comparison:		
a. No styrofoam or lead between source plate and pile:		
Run No. 1	5.77 watts	
Run No. 2	5.97 watts	
Run No. 3	5.82 watts	
b. One inch of lead between source plate and pile:		
Run No. 4	5.06 watts	
c. Styrofoam between source plate and pile:		
Run No. 5	5.54 watts	
Average of Runs 1 to 5		5.6 ± 0.6 watts
Source Plate Power (weighted average of 1, 2, and 3		5.5 ± 0.5 watts

Note: All estimated powers have been normalized for one inch of lead between the source plate and pile and for an energy dissipation of 200 Mev. per fission.

[redacted]

Paper I-I

ANALYSIS OF THE DYNAMIC SOURCE TESTS ON MOCKUPS OF THE REFLECTOR-MODERATED REACTOR AND SHIELD

H. C. Woodsum*
Oak Ridge National Laboratory

*Loan employee from Pratt and Whitney Aircraft Company

[redacted]

RESTRICTED DATA
"This document contains restricted data as defined in the Atomic Energy Act of 1954. Its transmittal or the disclosure of its contents in any manner to an unauthorized person is prohibited."

[redacted]

ANALYSIS OF THE DYNAMIC SOURCE TESTS ON MOCKUPS OF THE REFLECTOR-MODERATED REACTOR AND SHIELD

by

H. C. Woodsum*
Oak Ridge National Laboratory
Oak Ridge, Tennessee

Analysis of the dynamic source tests on mockups of a circulating-fuel reflector-moderated reactor and shield (RMR-shield) has been completed. The circulating-fuel reactor was mocked up by means of a belt containing fuel plates which was rotated between the ORNL Graphite Reactor core hole and the heat exchanger mockup. In the analysis of the experimental dose rate resulting from fission-product gamma rays emitted in the heat exchanger mockup was separated out and compared with two different calculated dose rates. In one calculation it was assumed that all the fission-product gamma rays were of a single energy (2.7 Mev/photon). The other calculation was based on the spectrum of gamma rays from the fuel belt previously measured at the LTSF. The two calculated values agreed, but differed by about 30% from the measured value. It was found that this could be attributed to the fact that the dose buildup factor for water was used in the calculation (i.e., the buildup factor was chosen as if the lead were an equivalent thickness, in mean free paths, of water). Substitution of a new buildup factor for the total mean free paths (lead and water), based on Monte Carlo studies of laminated shields, resulted in agreement between the measured and calculated dose rates.

Analysis of the dynamic source tests in the second series of experiments with mockups of a circulating-fuel reflector-moderated reactor and shield (RMR-shield) was completed. The analysis is based on an effective neutron power of 2.1 watts for the old LTSF source plate (since removed). It had previously been assumed that the power of the old source plate was 3.6 watts, but a tentative calibration of the new source plate has indicated the 2.1-watt value.

One of the main purposes of the dynamic source tests in the RMR experiments was to measure the dose rate resulting from fission product gamma rays emitted in the heat exchanger mockup. In order to mock up the sources of radiation in the heat exchanger, a belt of MTR-type fuel plates[1] was rotated from the ORNL Graphite Reactor core hole (with the LTSF source plate removed) where the thermal neutrons induce fissions, to a slot between two heat exchanger mockup tanks, where the fission product gamma rays comprise the source to be studied. Neutron and gamma-ray dose rate measurements were made in the water beyond the mockups.

---

*Loan employee from Pratt and Whitney Aircraft Company.

[redacted]

[redacted]

The basic mockup (Configuration 17) included a 3-in.-thick lead gamma-ray shield (Fig. 1). (The dimensions of all the components in the mockup are given in Table I.) Only two changes in this basic configuration were made throughout these tests: (1) 1-1/2-in. of the lead was removed (Configuration 17A), and (2) 1/2 in. of the boral next to the beryllium was replaced with 1 in. of polyethylene (Configuration 17F).

The cycle time, or time for the fuel belt to make one complete revolution, was varied as follows: infinite time (belt not rotating), and 2, 1.5, and 1.25 sec. Shorter cycle times were precluded by the danger of damage to the rig. The rotation speed was set by means of a stroboscope, and the rig was checked for constancy by means of a tachometer.

The results of the experiment were compared with calculations of the dose rate, one based on the assumption that all the fission product gamma rays were of a single energy and another based on the spectrum of gamma rays from the fuel belt previously measured at the LTSF.[1] The two calculated values agreed, but differed by about 30% from the measured value. It was found that this could be attributed to the fact that the dose buildup factor for water was used in the calculation (i.e., the buildup factor was chosen as if the lead were an equivalent thickness, in mean free paths, of water). Substitution of a new buildup factor for the total mean free paths (lead and water), based on Monte Carlo studies of laminated shields, resulted in agreement between the measured and calculated dose rates.

CALCULATED DOSE RATE FROM FISSION PRODUCT GAMMA RAYS FROM THE HEAT EXCHANGER, ASSUMING 2.7 MEV/PHOTON

The first calculation of the dose rate behind the lead-water shield was based on a single gamma-ray energy and an average number of gamma rays per fission. As a first step in arriving at the proper values for the energy and average number of gamma rays, the dose rate from an infinite plane, isotropic, surface source with a spectrum expressed as N(E) was calculated as follows:

$$D_s = \int_{E=0}^{\infty} \frac{n}{2} \frac{N(E)}{C(E)} E_1(\Sigma \mu_i t_i) B_r(\Sigma \mu_i t_i) \, dE$$

where

n = number of fissions per second per watt = 3.1×10^{10},

$N(E)$ = number of gamma rays of energy E emitted per fission per Mev,

$C(E)$ = flux-to-dose conversion factor for gamma rays of energy E,

[redacted]

[redacted]

2-01-057-66-258

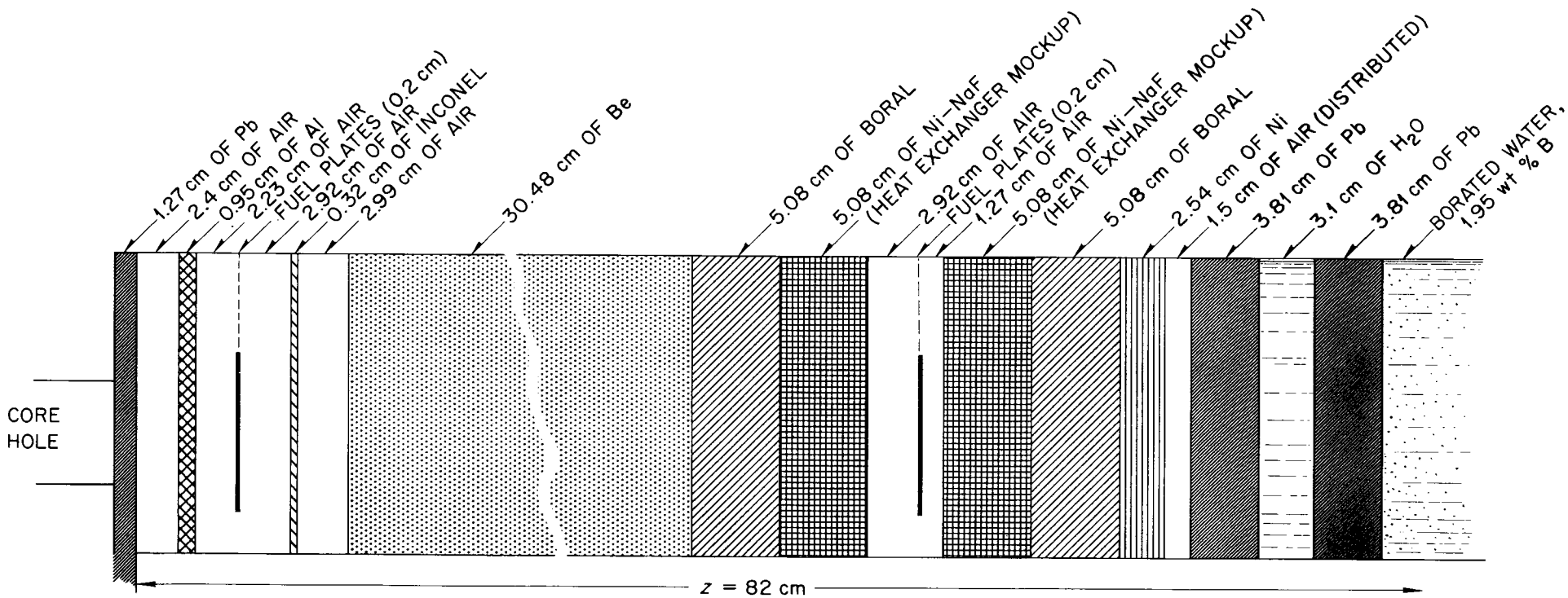

Fig. 1. RMR-Shield Mockup with Dynamic Scource (Configuration 17).

[redacted]

Table I. Basic RMR-Shield Mockup (Configuration 17)[a] Used in Dynamic Source Tests

Component	Thickness (cm)
Air	2.40
Aluminum window	0.95
Air	2.23
Fuel plates	0.20
Air	2.92
Inconel	0.32
Air	2.99
Beryllium	30.48
Boral	5.08
Ni-NaF tank	5.08
Air	2.92
Fuel plates	0.20
Air	1.27
Ni-NaF tank	5.08
Boral	5.08
Nickel	2.54
Air (distributed)	1.50
Lead	3.81
Water	3.10
Lead	3.81
Total	81.96

a. Configurations 17B through 17E had infinite, 2.5-, 1.5-, and 1.25-sec transit times, respectively. In Configuration 17A (infinite transit time) the last 3.81 cm of lead was removed. In Configuration 17F (infinite transit time) the 5.08 cm of Boral adjacent to the beryllium was replaced with 3.81 cm of polyethylene.

[redacted]

[redacted]

$E_1(\Sigma\mu_i t_i)$ = exponential integral for $\Sigma\mu_i t_i$ mean free paths in the experiment* [tabulated previously[2] as $\int_x^\infty (e^{-y}dy/y)$],

$B_r(\Sigma\mu_i t_i)$ = dose buildup factor for gamma rays of energy E in water through $\Sigma\mu_i t_i$ mean free paths.

The dose rate calculated on the basis of a single gamma-ray energy E' would then be

$$D_m = \frac{n}{2} \frac{\Gamma(E')}{C(E')} E_1(\Sigma\mu_i t_i) B_r(\Sigma\mu_i t_i)$$

where $\Gamma(E')$ is defined as the average number of "penetrating" gamma rays of energy E' per fission and all other terms apply to the single energy. Then, from setting D_m equal to D_s,

$$\Gamma(E') = \frac{\int_{E=0}^{\infty} \frac{N(E)}{C(E)} E_1(\Sigma\mu_i t_i,E) B_r(\Sigma\mu_i t_i,E)\, dE}{\frac{E_1(\Sigma\mu_i t_i,E') B_r(\Sigma\mu_i t_i,E')}{C(E')}}$$

The value of the numerator was obtained by numerical integration over E, using $N(E) = 7.0e^{-1.2E}$ gamma rays/Mev/fission.[3] For relatively thick gamma-ray shields the characteristic or average energy of the gamma rays was found to be about 2.7 Mev; hence E' = 2.7 Mev. Substituting the proper values in the equation results in $\Gamma(E') = 0.69$ for a 3-in.-thick lead gamma-ray shield.

If it is assumed that all the gamma rays emitted by a source of strength S_o are of 2.7-Mev energy, the calculated dose rate behind the lead-water shield can be obtained as follows:

$$D_{(\gamma,\text{Belt})} = \int_{\substack{\text{Area}\\ \text{of belt}}} S_o \cos\theta(y)\, dA(x,y) \frac{e^{-\Sigma\mu_i R_i(x,y,t)}}{4\pi R^2(x,y,t)} B_r\left[\Sigma\mu_i R_i(x,y,t)\right] \quad (1)$$

---

*Actually the value of t_i used in this calculation as the same as that given in Ref. (2), which is slightly different from the t_i for the present experiment.

[redacted]

[redacted]

where

$\cos\theta$ = a term to take into account the fact that the center portions of the belt were exposed for a longer period of time to the activating neutron flux than were the outer portions of the belt

$= \sqrt{1 - (y^2/a^2)}$ (see Fig. 2a),

dA = element of area on the belt (cm^2),

$e^{-\sum \mu_i R_i}$ = exponential attenuation of 2.7-Mev gamma rays from the belt in the heat exchanger through the various materials (nickel, sodium fluoride, boral, lead, and water) of slant thickness R_i with a gamma-ray absorption coefficient of μ_i at energy E,

$4\pi R^2$ = inverse square spreading for a point source from point of emission to point of detection,

$B_r(\sum \mu_i R_i)$ = dose buildup factor for 2.7-Mev gamma rays from a point isotropic source through $\sum \mu_i R_i$ mean free paths of water,

x, y, t^* = coordinates as shown in Fig. 2b.

If the length of the belt in the heat exchanger region is L, and its height is 2a (Fig. 2b), then Eq. 1 can be written in terms of x, y, and t:

$$D_{\gamma,\mathrm{Belt}} = 4 \int_{y=0}^{y=a} \int_{x=0}^{x=L/2} \frac{S_o \sqrt{1 - \left(\frac{y}{a}\right)^2}\; e^{-\left(\frac{\sum \mu_i t_i}{t}\right)\sqrt{x^2+y^2+t^2}}\; B_r\left[\left(\frac{\sum \mu_i t_i}{t}\right)\sqrt{x^2 + y^2 + t^2}\right] (dx\, dy)}{4\pi(x^2 + y^2 + t^2)} \qquad (2)$$

where t_i is the thickness of each slab of material. This integral can be separated as follows:

$$D_{\gamma,\mathrm{Belt}} = \frac{S_o}{\pi} \int_{y=0}^{a} \sqrt{1 - \left(\frac{y}{a}\right)^2}\, dy \int_{x=0}^{L/2} \frac{e^{-\left(\frac{\sum \mu_i t_i}{t}\right)\sqrt{x^2+y^2+t^2}}\, dx\; B_r\left[\left(\frac{\sum \mu_i t_i}{t}\right)\sqrt{x^2 + y^2 + t^2}\right]}{x^2 + y^2 + t^2} \qquad (3)$$

Then, since

---

* t rather than z is used to avoid confusion with the common usage of z at the LTSF representing the distance from the source plate (i.e., from the core hole). z is used as such in Figs. 1, and 3 through 5.

[redacted]

[redacted]

2-01-057-66-259

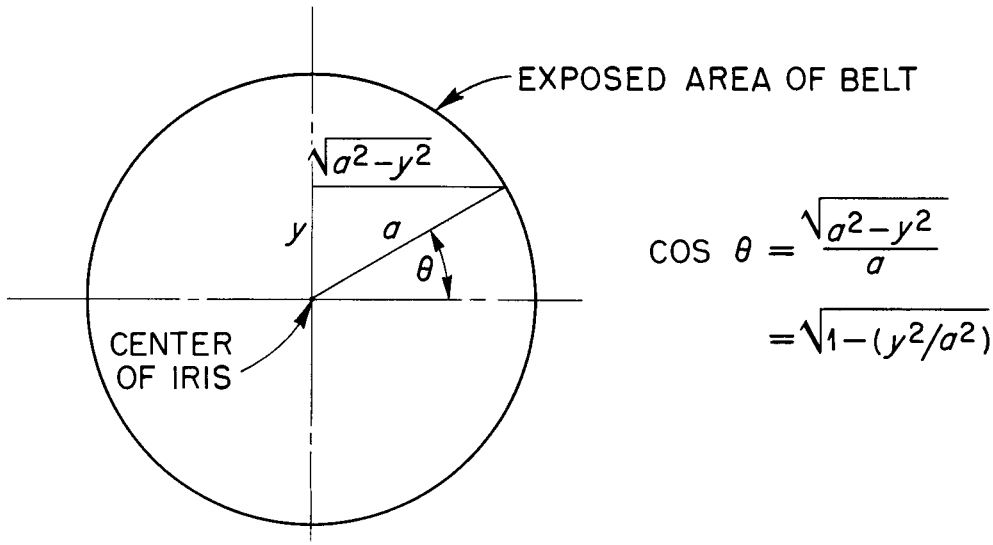

a. DERIVATION OF COS θ.

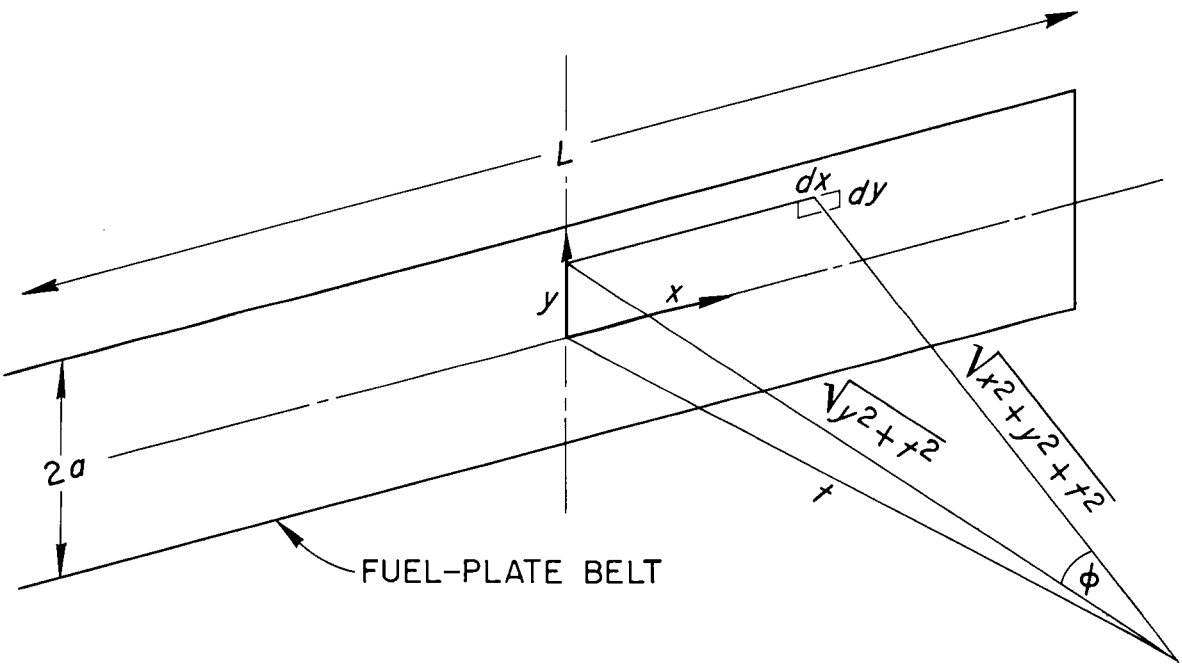

b. BELT GEOMETRY.

Fig. 2A. Geometry Used in Calculations of the Gamma-Ray Dose Rate Beyond RMR-Shield Mockups with Dynamic Source.

[redacted]

$$\frac{\sqrt{y^2 + t^2}}{\sqrt{x^2 + y^2 + t^2}} = \cos\phi \text{ (see Fig. 2b)}$$

$$d(\cos\phi) = \frac{\cancel{2}x\, dx \sqrt{y^2 + t^2}}{\cancel{2}(x^2 + y^2 + t^2)^{3/2}} = (\sin\phi)\, d\phi$$

or

$$dx = \sin\phi \frac{\sqrt{x^2 + y^2 + t^2}}{\sqrt{y^2 + t^2}} \frac{(x^2 + y^2 + t^2)}{x} d\phi$$

and since

$$\frac{x}{\sqrt{x^2 + y^2 + t^2}} = \sin\phi$$

$$dx = \frac{\sqrt{x^2 + y^2 + t^2}}{\cos\phi} d\phi = \frac{\sqrt{y^2 + t^2}}{\cos^2\phi} d\phi$$

Substituting for x in terms of ϕ, the inner integral becomes

$$\int_0^{\sin^{-1}\left[\frac{(L/2)}{\sqrt{(L/2)^2 + y^2 + t^2}}\right]} \frac{e^{-\left(\frac{\sum\mu_i t_i}{t}\right)\left(\frac{\sqrt{y^2 + t^2}}{\cos\phi}\right)}}{\sqrt{y^2 + t^2}} d\phi\, B_r\left(\frac{\mu_i t_i}{t}\sqrt{x^2 + y^2 + t^2}\right) \quad (4)$$

Now, let

$$\sqrt{y^2 + t^2}\left(\frac{\sum\mu_i t_i}{t}\right) = b$$

so that

$$\sqrt{y^2 + t^2} = b\left(\frac{t}{\sum u_i t_i}\right)$$

[redacted]

[redacted]

and let

$$\phi_o = \sin^{-1}\left(\frac{L/2}{\sqrt{(L/2)^2 + y^2 + t^2}}\right)$$

Assume that B_r is a function of y and t only (which is a slight underestimate of the buildup). Then the inner integral becomes

$$\int_0^{\phi_o} \frac{e^{-b \sec\phi}\, d\phi}{\left(\frac{bt}{\Sigma\mu_i t_i}\right)} \tag{5}$$

Since $\left(\frac{bt}{\Sigma\mu_i t_i}\right)$ is a constant for constant y and t, the integral becomes

$$\left(\frac{\Sigma\mu_i t_i}{t}\right)\left(\frac{1}{b}\right)\int_0^{\phi_o} e^{-b \sec\phi}\, d\phi \tag{6}$$

and since $\int_0^{\phi_o} e^{-b \sec\phi}\, d\phi$ has been tabulated as $F(\phi_o,b)$,[4] the total integral in terms of this function becomes

$$D_{\gamma,\text{Belt}} = \frac{S_o}{\pi}\int_0^a \frac{\sqrt{1 - \left(\frac{y}{a}\right)^2}\, B_r\left[\left(\frac{\Sigma\mu_i t_i}{t}\right)\sqrt{y^2 + t^2}\right] F\left[\phi_o\left(\frac{\Sigma\mu_i t_i}{t}\right)\sqrt{y^2 + t^2}\right] dy}{\sqrt{y^2 + t^2}} \tag{7}$$

This equation was integrated numerically using the following constants:

a = 14 in. = 35.5 cm,

t = distance between the belt in the heat exchanger and the detector

= 74.22 cm for this case (see Table II),

$\Sigma\mu_i t_i$ = 7.74 as shown in Table II,

[redacted]

[redacted]

Table II. Number of Mean Free Paths for Materials Between Fuel Plates in Heat Exchanger Mockup and Detector at t = 74.12 cm

Component	Thickness (cm)	ρ, Density (g,cm^3)	μ/ρ (2.7 Mev), Mass Absorption Coefficient (cm^2/g)	$\mu_i t_i$(2.7 Mev), No. of Mean Free Paths
NaF	3.81	1.59	0.0366	0.22
Ni	3.81	8.90	0.0382	1.29
Pb	7.62	11.3	0.0418	3.60
Boral (Al)	5.08	2.53	0.0372	0.48
H_2O	51.1	1.0	0.0420	2.15
Air	2.8	0.00293	0.04	0.000
	Σt_i = 74.22			$\Sigma \mu_i t_i$ = 7.74

[redacted]

[redacted]

$$\phi_o = \sin^{-1} \frac{L/2}{\sqrt{(L/2)^2 + y^2 + t^2}} ,$$

$L/2 = 29.5$ in. $= 75$ cm.

An upper limit of 45 deg for ϕ_o is obtained by letting $y = 0$, and a lower limit of 41 deg is obtained by letting $y = a$. For these two values of y,

$$b = \frac{\sum \mu_i t_i}{t} \sqrt{y^2 + t^2}$$

$$= 7.74 \qquad (y = 0)$$

$$= 8.58 \qquad (y = a)$$

For $\phi = 41$ to 45 deg and $b = 7.74$ to 8.58, $F\left[\phi_o, b\right]$ is essentially independent of ϕ; hence, $F\left[45 \text{ deg}, b\right]$ was used. (ϕ_o was assumed to be independent of y.)

Various values of the terms used in the numerical integration of Eq. 7 are given in Table III. The integration gave a value of

$$D_{\gamma,\text{Belt}} = 1.16 \times 10^{-4}\ S_o \text{ mr/hr}$$

MEASURED GAMMA-RAY DOSE RATES WITH AND WITHOUT ROTATION OF THE BELT

The measured gamma-ray dose rate <u>without</u> the belt rotating (which is analogous to the measured dose rate in the static source tests) includes

$$D_{\gamma,\text{WOR}} = D_P + D_C + D_{fp,\text{Core}} \tag{8}$$

where

$D_{\gamma,\text{WOR}}$ = total gamma-ray dose rate without rotation of the belt,

D_P = dose rate due to prompt gamma rays,

D_C = dose rate due to capture gamma rays produced in the mockup,

$D_{fp,\text{Core}}$ = dose rate due to fission product gamma rays from the core.

The measured gamma-ray dose rate <u>with</u> the belt rotating includes

[redacted]

[redacted]

Table III. Values of Various Terms Used in the Numerical Integration of Eq. 7

y	$\sqrt{1 - (y/a)^2}$	$\sqrt{y^2 + t^2}$	b	$F(45 \text{ deg}, b)$	$B_r(b)$ for H_2O	$\frac{\sqrt{1 - (y/a)^2}\, B_r(b)\, F(45 \text{ deg}, b)}{\sqrt{y^2 + t^2}}$
0	1.000	74.20	7.740	1.68×10^{-4}	7.38	1.671×10^{-5}
5	0.9901	74.31	7.751	1.67×10^{-4}	7.38	1.64×10^{-5}
10	0.9595	74.87	7.809	1.55×10^{-4}	7.40	1.470×10^{-5}
15	0.9063	75.71	7.897	1.40×10^{-4}	7.50	1.251×10^{-5}
20	0.8211	76.85	8.015	1.27×10^{-4}	7.55	1.025×10^{-5}
25	0.7100	78.30	8.167	1.07×10^{-4}	7.65	0.742×10^{-5}
30	0.5345	80.04	8.348	0.92×10^{-4}	7.82	0.481×10^{-5}
35.5	0	82.26	8.580	$.63 \times 10^{-4}$	8.40	0

[redacted]

[redacted]

$$D_{\gamma,WR} = D_P + D_C + D_{fp,HE} + D_{fp,Core-He} \tag{9}$$

where

$D_{\gamma,WR}$ = total gamma-ray dose rate with rotation of the belt,

$D_{fp,HE}$ = dose rate due to fission product gamma rays from the heat exchanger,

$D_{fp,Core-HE}$ = dose rate due to fission product gamma rays in the core that were not removed by the belt.

The D_P is of course the same in both Eq. 8 and Eq. 9, and it is assumed that D_C is the same since the small increase in the number of capture gamma rays due to the rotating belt is ignored. Therefore, the difference between the two measured dose rates is

$$D_{\gamma,WR} - D_{\gamma,WOR} = (D_{fp,HE} + D_{fp,Core-HE}) - D_{fp,Core}$$

Because of the fact that the belt length is much greater than the core hole diameter $D_{fp,Core-HE}$ is negligible and can be ignored; thus

$$D_{\gamma,WR} - D_{\gamma,WOR} = D_{fp,HE} - D_{fp,Core} \tag{10}$$

CALCULATED DOSE RATE FROM FISSION PRODUCT GAMMA RAYS FROM THE CORE, ASSUMING 2.7 MEV/PHOTON

Since $D_{\gamma,Belt}$ in Eq. 1 represents the calculated dose rate due to the fission product gamma rays from the heat exchanger, it can be substituted for $D_{fp,HE}$ in Eq. 10. Then if the value of $D_{fp,Core}$ is calculated, the difference between the two measured values (i.e., $D_{\gamma,WR} - D_{\gamma,WOR}$) should be equivalent to the difference between the two calculated values (i.e., $D_{\gamma,Belt} - D_{fp,Core}$).

In the mockup the core source was a 28-in.-dia disc, as defined by the boral iris in the LTSF core hole. In the calculation of $D_{fp,Core}$, the source was considered to be isotropic. Hence,

$$D_{fp,Core} = (S_1/2)\left\{E_1(\Sigma\mu_i t_i) - E_1\left[\Sigma\mu_i t_i\sqrt{1 + (a/T)^2}\right]\right\}B_r(\Sigma\mu_i t_i) \tag{11}$$

where

S_1 = equivalent isotropic source strength due to 2.7-Mev fission product gamma rays emitted from the activated portion of the belt at the core hole (mr/hr),

[redacted]

[redacted]

$E_1(x)$ = exponential integral for $\sum \mu_i t_i$ mean free paths as defined previously (see p. 5),

$\sum \mu_i t_i$ = total number of mean free paths for materials between the fuel plates at the core hole and the detector $3.14 + 7.74 = 10.88$ (see Tables II and IV),

a = radius of exposed area of the fuel plates = 35.56 cm,

T = total distance between the fuel plates at the core hole and the detector

= 49.88 cm + 74.22 cm = 124 cm (see Tables II and IV),

$B_r(\sum \mu_i t_i)$ = dose buildup factor for 2.7-Mev gamma rays in water for $\sum \mu_i t_i$ mean free paths = 10.

Self-absorption was neglected since the source was thin. Substituting in Eq. 11 and solving,

$$D_{fp,Core} = 3.05 \times 10^{-6}\ S_1\ (\text{mr/hr})$$

EVALUATION OF SOURCE STRENGTHS S_0 AND S_1

Since $D_{\gamma,Belt} - D_{fp,Core}$ can now be written as

$$(1.16 \times 10^{-4} S_0) - (3.05 \times 10^{-6} S_1)$$

the source strengths S_0 and S_1 must be evaluated in terms of the gamma-ray dose rate. S_1, the source strength of the belt at the core hole, is

$$S_1 = \frac{P_B nN}{AK} \tag{12}$$

where

P_B = power of the belt (watts),

n = number of fissions per second per watt = 3.1×10^{10},

N = number of 2.7-Mev gamma rays emitted per fission = 0.69,

A = exposed area of the belt = 3970 cm^2,

K = flux-to-dose conversion factor for gamma rays of 2.7-Mev energy = 2.45×10^2 (photons/cm^2/sec per mr/hr).

[redacted]

[redacted]

Table IV. Number of Mean Free Paths for Materials Between Fuel Plates at the Core Hole and Fuel Plates in the Heat Exchanger

Component	Thickness (cm)	ρ, Density (g/cm^3)	μ/ρ (2.7 Mev) Mass Absorption Coefficient (cm^2/g)	$\mu_i t_i$(2.7 Mev), No. of Mean Free Paths
U-235	0.01	18.7	.0442	.008
Al	0.09	2.7	.0373	.009
Ni	1.27	8.90	.0382	0.432
NaF	3.81	1.59	.0366	0.222
Boral (Al)	5.08	2.53	.0372	0.478
Be	30.48	1.85	.0334	1.885
Inconel	0.32	8.5	.0382	0.103
Air	8.83	- -	- -	- -
	$\sum t_i$ = 49.89			$\sum \mu_i t_i$ = 3.14

[redacted]

[redacted]

Substituting in Eq. 12

$$S_1 = 2.2 \times 10^4 P_B \text{ (mr/hr)}$$

S_0, the source strength for the center of the belt in the heat exchanger region, is

$$S_0 = (L_1/L_2)S_1 \tag{13}$$

where

L_1 = diameter of exposed area of belt = 71 cm,

L_2 = total length of belt = 400 cm.

Substituting in Eq. 13 and solving

$$S_0 = 3.91 \times 10^3 P_B \text{ (mr/hr)}$$

DETERMINATION OF THE POWER OF THE FUEL BELT

The power of the fuel belt P_B is determined by comparing the fast-neutron dose rate (Fig. 3), thermal-neutron flux (Fig. 4), and sodium activation curves for Configuration 17 (no rotation) with the corresponding curves for a similar configuration (3-C) in the static source tests using the old LTSF source plate.[1] The ratio of the fast-neutron dose rates is found to be 1.65, and that for the thermal-neutron flux is 1.37. These two values averaged with the ratio of the sodium activations[1,5] (1.46) give a final average of 1.49. Thus, the power of the belt is 1.49 times the previously assumed effective LTSF source power of 2.1 watts, or

$$P_B = 3.1 \text{ watts*}$$

COMPARISON OF MEASURED AND CALCULATED GAMMA-RAY DOSE RATES

From the above

$$D_{\gamma,\text{Belt}} = (1.16 \times 10^{-4})(3.91 \times 10^3)(3.1)(\text{mr/hr})$$

---

* This new power value was also determined by the LTSF staff by comparing neutron measurements taken in water.

[redacted]

[redacted]

2-01-057-66-260

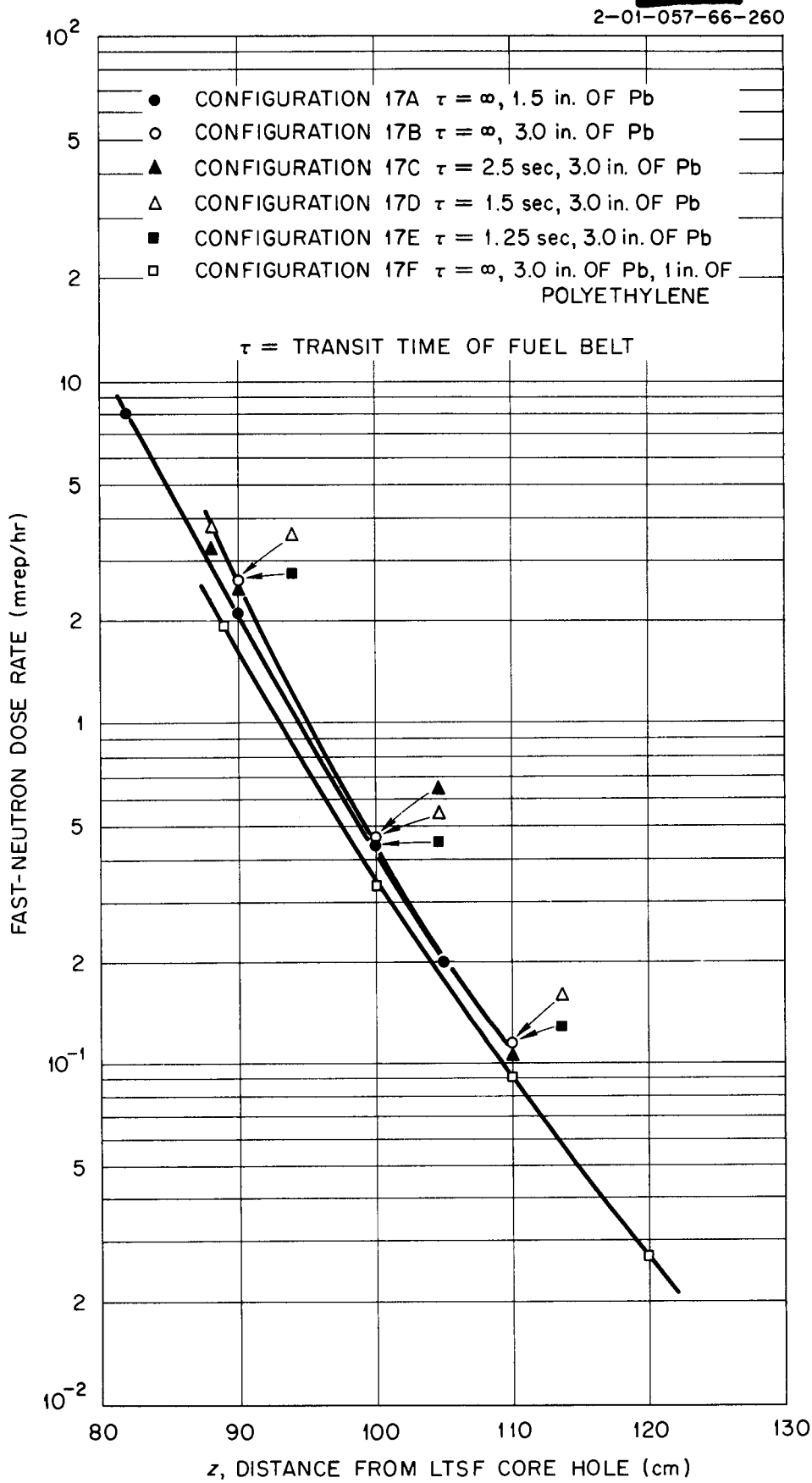

Fig. 3. Fast-Neutron Dose Rates Beyond RMR-Shield Mockups with Dynamic Source.

[redacted]

2-01-057-66-261

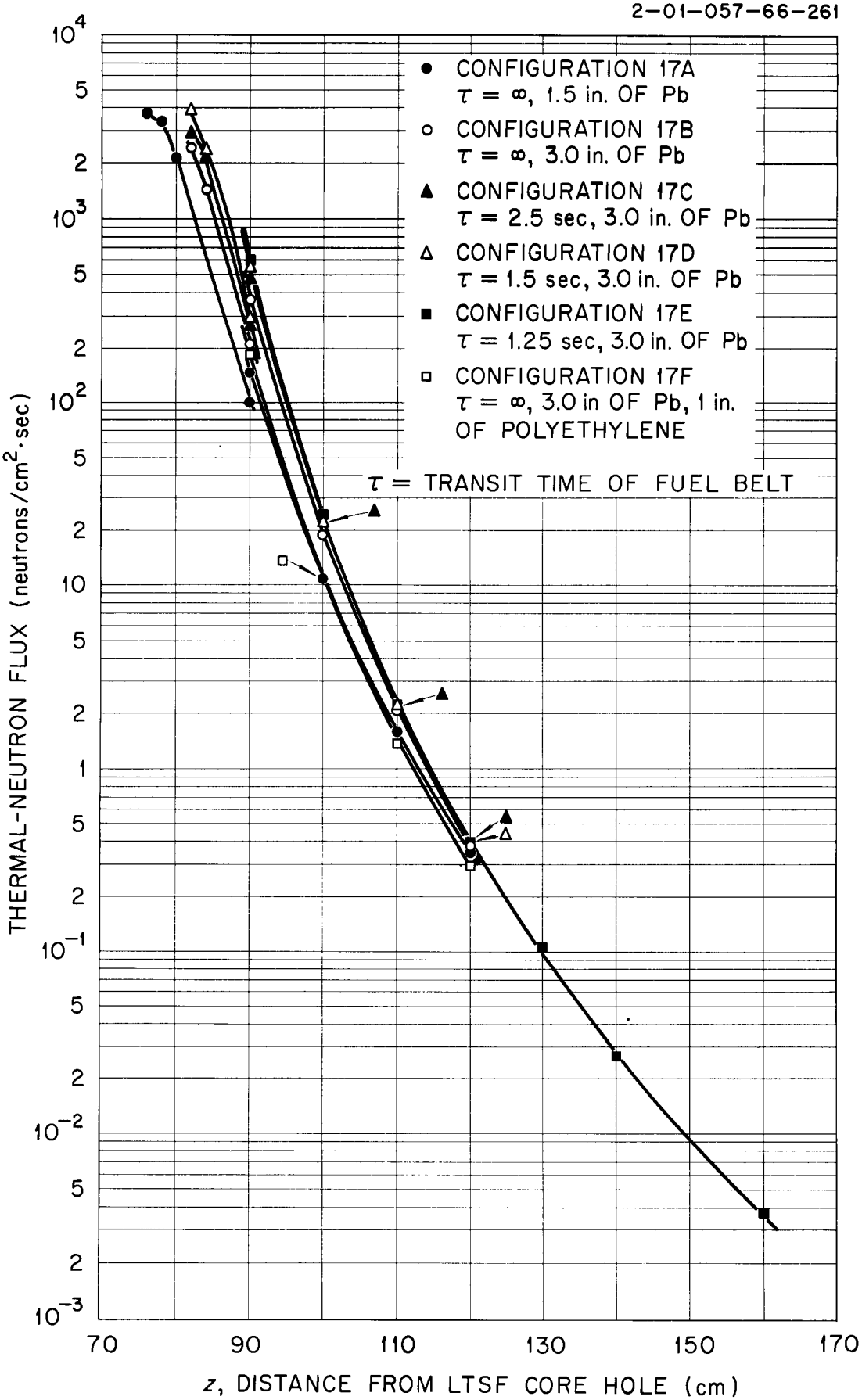

Fig. 4. Thermal-Neutron Flux Beyond RMR-Shield Mockups with Dynamic Source.

[redacted]

$$D_{fp,Core} = (3.05 \times 10^{-6})(2.2 \times 10^{4})(3.1)(mr/hr)$$

Thus the difference in the calculated values is

$$D_{\gamma,Belt} - D_{fp,Core} = 1.18 \text{ mr/hr}$$

From Fig. 5 it can be seen that the actual difference in the measured gamma-ray dose rates at z = 130 cm (z is the distance from the core hole and z = 130 cm corresponds to T = 124 cm) is

$$(4.55) - (3.65) = 0.9 \text{ mr/hr}$$

which is a factor of 1.3 less than the calculated value.

CALCULATED DOSE RATE BASED ON FISSION PRODUCT GAMMA-RAY SPECTRUM

In order to check the above calculation, a separate calculation was made using the fission product gamma-ray spectrum measured at the LTSF[1] with the same rotating fuel belt system. A numerical integration was then carried out over the spectrum from 1 to 5 Mev. The contribution to the dose rate for gamma-ray energies outside this range is negligible and by neglecting it, only a very small error should be introduced. The method of calculating the gamma-ray attenuation in this case was the same as for the 2.7-Mev gamma rays in the above case. Thus attenuations for discrete energies of 1, 2, 3, 4, and 5 Mev were calculated. If the attenuation of the gamma-ray dose rate at a distance z is represented as A(E,z) the total gamma-ray dose rate at some particular distance may be calculated as

$$D(z) = C \int_{1\ \text{Mev}}^{5\ \text{Mev}} \frac{N(E)\ A(E,z)\ dE}{K(E)}$$

where

N(E) = number of gamma rays of energy E as given by the fission product decay gamma-ray spectrum,[1]

K(E) = flux-to-dose conversion factor for gamma-ray energy E,

C = constant related to the power per unit area of the belt.

The integrals for the dose rate both from fission product gamma rays emitted in the heat exchanger region (rotating belt) and from fission product gamma rays emitted in the core region (no rotation) were evaluated by this

[redacted]

[redacted]

2-01-057-66-262

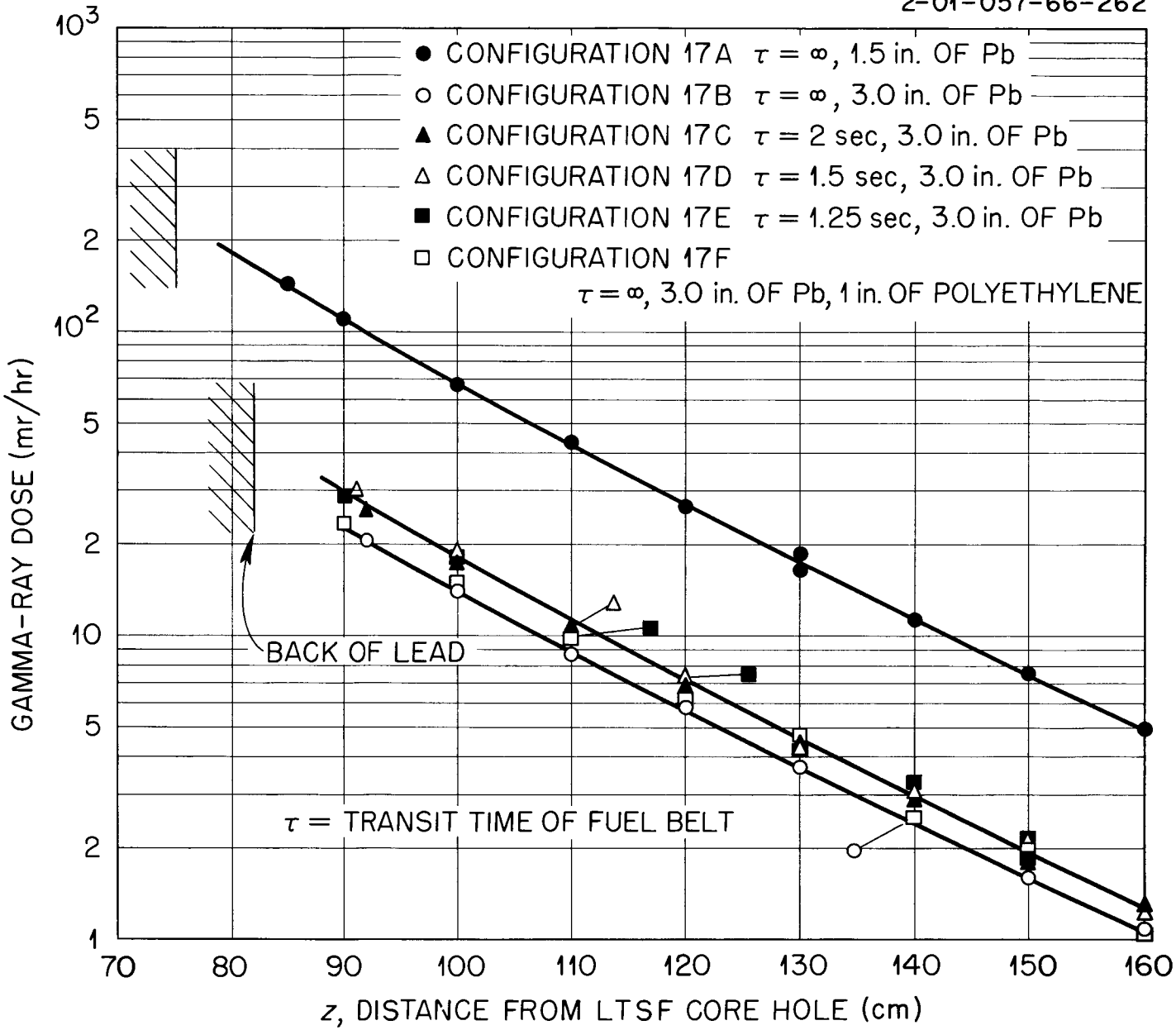

Fig. 5. Gamma-Ray Dose Rate Beyond RMR-Shield Mockups with Dynamic Source.

method, and the difference between the two should be equivalent to the difference in the experimental gamma-ray dose rate with and without the belt rotating. The difference between these more exact integrations was actually 1.17 mr/hr which was almost the same as the 1.18 mr/hr previously calculated on the basis of a single (2.7-Mev) gamma-ray energy and slightly different spectrum.

DISCUSSION

In order to resolve the 30% discrepancy between the calculated and measured dose rates, it was necessary to investigate the assumptions involved in the calculation. The most obvious uncertainty was in the choice of a buildup factor through a multiregion shield. Since the dose buildup factors in lead and water differ by a factor of 2, a considerable error could be introduced by using either one for the total number of mean free paths in the shield. The buildup factor for water for the specified number of mean free paths was used in all the calculations. It was thought that the total buildup should be more characteristic of the water since about 50 cm of water (2.15 mfp) followed the 3 in. of lead (3.6 mfp). However, some recent Monte Carlo calculations by S. Auslender* indicate that for 3 Mev gamma rays through 8 mfp of lead and water (4 mfp of lead followed by 4 mfp of water) the buildup factor is about 30% lower than the buildup factor through the same number of mean free paths of water alone. Auslender's calculations indicate that a correction should be applied to the buildup factor, reducing it to account for the presence of the lead. Such a correction would bring calculations and experiment into closer agreement. Furthermore, if it were the choice of the water buildup factor alone that gave a calculated dose rate higher than the experimental dose rate, the discrepancy should decrease as more water is placed between the lead and the detector (or the point of calculation). This theory was tested with another calculation for a z distance of 160 cm, which would place about 3.4 mfp of water behind 3.6 mfp of lead. In this case the calculated gamma-ray dose rate using a buildup factor characteristic of water alone was 0.26 mr/hr which is only about 20% higher than the experimental dose rate of 0.22 mr/hr.

Thus, since the gamma-ray dose from the fission products in the heat exchanger of a design reactor is only about 30 to 40 percent of the total dose in the crew compartment, the error incurred by using the water buildup factor for the total number of mean free paths is not great for moderate lead thicknesses. Of course, as shown by these dynamic source experiments at the LTSF, it would be better to use buildup factors more characteristic of the lead and water combination in the shield.

In the experiment, the gamma-ray dose rate due to fission product gamma rays emitted in the heat exchanger region did not change (within the limits of experimental error) as the transit times was decreased from 2 to 1.25 sec (Fig. 5). This indicates that the fission product gamma-ray spectrum did not change significantly, which substantiates the conclusions reported previously.[1]

---

* Shielding Analysis Group, Pratt and Whitney at ORNL.

[redacted]

The thermal-neutron flux increased as the transit time of the belt decreased (Fig. 4). The increase was, of course, due to more of the delayed neutrons being emitted in the heat exchanger rather than in the core region. Since the average energy of the delayed neutrons is lower than the average energy of the prompt neutrons, they would essentially all have been lost in the shield if they had been emitted only in the core. However, when they were emitted in the heat exchanger they penetrated the shield and added to the measured thermal-neutron flux. The maximum increase was about 50% at the outer surface of the lead gamma-ray shield. This percentage decreased to about 10% after about 20 cm of water and to a negligible fraction after 50 cm of water.

The discontinuity in the thermal-neutron flux curves at z = 90 cm is due to a change in instruments (3 in. fission counter to 12-1/2 in. BF_3 counter) at this point. Although both instruments were normalized to the same value in plain water, the center of detection of the 12-1/2 in. BF_3 moved toward the front of the chamber (to the left in z) as the slope of the resulting thermal-neutron flux became steeper. It is believed that this shift in the center of detection completely accounts for the difference in measurement by two instruments.

The fast-neutron dose rate (Fig. 3) after 6 cm or more of water was independent of transit time and hence the delayed neutrons did not contribute significantly to the fast-neutron dose rate. The 1 in. of polyethylene plastic inserted in the reflector region (Configuration 17F) did decrease the fast-neutron dose rate by 20 or 30 percent.

[redacted]

[redacted]

REFERENCES

1. R. W. Peelle et al., ANP Quar. Prog. Rep. Dec. 10, 1955, ORNL-2012, Parts I, II, and III, p. 210.

2. Tables of Sine, Cosine and Exponential Integrals, Vol. II, National Bureau of Standards and Work Projects Administration, New York City, 1940.

3. J. B. Dee et al., ANP Quar. Prog. Rep. Sept. 10, 1955, ORNL-1947, 1955, p. 185.

4. John Moteff, Miscellaneous Data for Shielding Calculations, APEX-176 (Dec. 1, 1954).

5. G. T. Chapman et al., ANP Quar. Prog. Rep. Sept. 10, 1955, ORNL-1947, p. 197.

[redacted]

[redacted]

Paper I-J

APPLICATION OF THE KAPL "MUG 2" REACTOR CODE TO THE ANALYSIS OF RMR LID TANK SHIELDING EXPERIMENTS

L. Joseph
P. S. Mittelman
M. S. Silberstein
Nuclear Development Corporation of America

[redacted]

[redacted]

[redacted]

NDA 12-17

APPLICATION OF THE KAPL "MUG 2" REACTOR CODE TO THE ANALYSIS OF RMR LID TANK SHIELDING EXPERIMENTS

by

L. Joseph, P.S. Mittelman, M.S. Silberstein

April 30, 1956

Nuclear Development Corporation of America

ABSTRACT

This report presents the results of a two-dimensional multigroup calculation of the neutron flux in the 12-inch thick beryllium slab representing the reflector in a lid tank mockup of a reflector-moderated circulating-fuel reactor. Flux distributions in the beryllium are given for the thermal group and for the energy group containing the 2940-ev sodium resonance. For each source neutron, 0.0242 neutrons are absorbed in the beryllium in this configuration. Of these, 0.0163 absorptions result in the emission of capture gammas; the remaining absorptions are accounted for by the high energy (n, α) reaction.

The theoretical results are compared with experimental values of the thermal flux and good agreement is found except near the boundaries of the reflector.

Note: This report is based largely on NDA 10-156, Two Dimensional Multigroup Calculation of Beryllium Flux in a CFR Lid Tank Mockup, L. Joseph, P.S. Mittelman and M.S. Silberstein (6/29/55). NDA 10-156 was prepared under a contract between NDA and the Pratt and Whitney Division of United Aircraft Corporation.

[redacted]

[redacted]

[redacted]

1. INTRODUCTION

A calculation of the flux distribution in the beryllium reflector of the lid tank mockup of the RMR reflector and shield should be of value in the interpretation of the current series of lid tank experiments. Such a calculation, if its results were confirmed by actual measurements on one lid tank configuration, could be used to determine the flux distribution for other configurations-e.g., a range of beryllium thicknesses contemplated in the experimental series. Such information is necessary in order to estimate correctly the contribution of the beryllium capture-gamma source to the total measured dose in and beyond the shield.

The importance of this problem had been recognized earlier, and an attempt at an analytical solution was made using Fermi age theory. The numerous approximations and uncertainties involved in this approach, due in part to the geometry of the lid tank configuration, led to the conclusion that an inordinately large amount of time would be required to develop a satisfactory analytical solution to the problem. As a consequence, it was decided to utilize the KAPL MUG-2 multigroup code on the UNIVAC digital computer. The MUG-2 code is designed to treat two-dimensional cylindrical geometry and includes the Goertzel-Selengut slowing down treatment for hydrogen.

[redacted]

[redacted]

CALCULATIONAL MODEL OF THE LID TANK CFR REFLECTOR MOCKUP

2.1 Configuration Used in Machine Calculation

The lid tank configuration for which calculations have been made has the following arrangement of materials, proceeding outward from the surface of the ORNL X-10 Graphite Reactor: a 1/8-inch boron carbide (B_4C) layer with a 28-inch diameter aperture which fits over the opening of the thermal beam hole; 1/4 inch of masonite; the source plate (1.1 inch thick); 1/4 inch of masonite; 1/8 inch of boron carbide; 1/2 inch of lead; and a 12-inch thick slab of beryllium 4 feet square (actually 3 slabs each 4 inches thick). The 12-inch sides of the beryllium slab are surrounded by water.

The configuration as idealized for machine calculation is shown in Figure 1. The slab geometry of the lid tank mockup has been changed to cylindrical geometry, inasmuch as the effective portion of the source plate is itself a cylinder. The 12-inch beryllium slab has been represented by a right cylinder with a radius of 35.56 cm and a height of 31.58 cm, corresponding roughly in thickness and volume to the slab. The 31.58 cm height includes a 1.1 cm^2 extrapolation length at the heat-exchanger end of the reflector. The beryllium cylinder is surrounded by a 10.7 cm annulus of water. The source plate, which is actually made up of cylindrical fuel elements, has been represented as a disc. The masonite, boron carbide, and lead regions have been consolidated into one homogeneous region. A comparison of the physical dimensions and those used in the machine calculation is given in Table 1, while Table 2 contains the compositions of the various regions in atoms/cc x 10^{-24}.

2.2 Source Distribution

Power production was assumed to take place only in that portion of the plate which is exposed by the shutter aperture. The power distribution in this region was taken to be radially constant, but decreasing exponentially through the thickness of the plate[a]. In the machine calculation the source strength is automatically normalized to one neutron per second per cubic centimeter of source volume.

[redacted]

[redacted]

2.3 Energy Group Structure

A preliminary calculation using the 31 energy groups previously used in one-dimensional reactor calculations made with the Medusa code[3] resulted in a smooth flux variation in the epithermal range, indicating that the finely divided Medusa epithermal group structure was not required for this problem. The group structure finally used had 16 groups (see Table 3), retaining the Medusa spacing in the fission spectrum groups but consolidating the many narrow Medusa epithermal groups into several larger ones.

2.4 Boundary Conditions

All fluxes were assumed to vanish at the outer surfaces of the configuration with the exception of the flux at the external surface of the source plate. At this surface, the ratio of the net current to the flux was set equal to 0.4695, which is equivalent to specifying an extrapolation length of $0.71\ \lambda_{tr}$ for each group.[b]

A preliminary calculation was made in which the ratio of net current to flux at the external surface of the source plate was reduced to zero, i.e., the surface was made a plane of symmetry. The "symmetry" boundary condition gives beryllium flux distributions similar in shape to those obtained using the other boundary condition, but with flux magnitudes about three times as large. The results of the "symmetry" boundary condition calculation are used in Section 4 in estimating an upper bound for beryllium fluxes and absorptions.

2.5 Cross Sections

The beryllium cross sections used are based on the latest available data. It is not known how to put the Be(n, 2n) reaction in the MUG code, and therefore the cross section for this reaction has been omitted. However, at energies above the threshold of the (n, 2n) reaction (the two highest-energy groups), the Be (n, α) reaction cross section has also been omitted in the hope that the two effects - one neutron-producing and one neutron-absorbing - would cancel each other. The (n, α) cross

[a] With a relaxation length of 1.627 cm.

[b] $$\frac{\text{Net Current}}{\text{Flux}} = \frac{-D(\nabla\phi)}{\phi} = \frac{\lambda_{tr}}{3\phi}\,\frac{(\phi-0)}{0.71\,\lambda_{tr}} = \frac{1}{3(0.71)} = 0.4695.$$

[redacted]

[redacted]

section has not been omitted except in the two highest-energy groups.

The cross-section data for natural uranium were obtained from BNL 250.[4] Estimates of the absorption cross section were made in the resonance region (5-200 ev) in such a way as to attempt to account for self-shielding. Cross sections for lead were taken from AECU 2040.[5] Cross sections previously used in calculations with the Medusa code were used for all other elements -- namely boron, carbon, oxygen, and hydrogen.

[redacted]

[redacted]

3. RESULTS

3.1 Flux Distribution

The calculated radial and axial distribution of thermal flux in n/cm^2 -sec in the beryllium region is plotted in Figures 2 and 3. Figure 2 shows axial flux traverses at three radii: 1) the center line, 2) at the radial boundary of the source region, 3) at the outer boundary of the beryllium. Figure 3 presents radial flux traverses corresponding to axial penetrations of 0, 4, 8 and 12 inches into the beryllium, corresponding to the faces of the 4-inch slabs used in the experiment.

Figures 4 and 5 present flux distributions for group 8 (lethargy limits 7.0 - 10.0, energy limits 9118 ev - 454 ev), which is of particular interest since this group includes the 2940-ev sodium resonance. The values plotted in the figures for group 8 represent the flux per unit lethargy, and should be multiplied by the group width, 3 lethargy units, if the total flux in the group is desired.

3.2 Beryllium Absorptions

For each source neutron, 0.0242 neutrons are absorbed in the beryllium in this configuration. Of these absorptions, 0.0163 absorptions result in the emission of capture gammas; the remaining absorption is accounted for by the high-energy (n, α) reaction.[c] The spatial distribution of the gamma-producing absorptions in the beryllium is shown in Figure 6, in which the entries for the various regions show the percentage of the (n, γ) reactions occuring in a particular region.

Beryllium absorptions in each lethargy group are presented in Table 4. All absorptions above group 7 have been assigned to (n, α) processes, while those in group 7 and below are of the (n, γ) type. The bulk of the (n, γ) absorptions, approximately 90%, occur in the thermal group.

---

c As discussed in Section 2.5, only the (n, α) reactions below energy group no. 2 are included.

[redacted]

[redacted]

4. DISCUSSION OF RESULTS

4.1 Effect of Boundary Condition

It has been noted above that the magnitude of the flux, but not its spatial distribution, depends on the value of the ratio of net current to flux chosen at the exterior source plate surface. Since an uncertainty exists as to the proper value to use, we have an uncertainty in the absolute magnitude of the flux and, as a consequence, in the fraction of source-plate neutrons absorbed in the beryllium region. One can, however, set an upper limit to the uncertainty by examining the effect of setting the current-to-flux ratio equal to zero. This boundary condition is physically equivalent to placing a neutron mirror at the external surface of the source plate. Preliminary calculations in which only this boundary condition was changed indicate that when the zero-current boundary condition is used, the thermal fluxes in the beryllium region are increased by a factor of about 3 as compared to the case where the current-to-flux ratio was set equal to 0.4695. The results for the zero-current condition are certainly overestimates since: a) those neutrons which would normally emerge from the rear of the source plate and have no chance to enter the beryllium are now reflected back toward the beryllium; b) those neutrons which normally leave the front surface of the source plate and are then scattered back through and out of the source plate assembly are also reflected back toward the beryllium. A lower upper limit to the flux can be obtained if one examines the contribution of (a) to the results of the flux calculation. If the source plate power distribution were uniform across the thickness of the source plate, then half the emerging neutrons would normally emerge from the rear surface of the source plate. Putting a neutron mirror at the rear surface of the source plate would then increase the number of neutrons available for capture in the beryllium region by almost a factor of two. The factor is not exactly two since the reflected neutrons must traverse the entire source plate thickness whereas the original source plate neutrons on the average must penetrate only a fraction of that thickness; in the reflected case there is therefore a higher probability for absorption within the plate. If the power distribution were higher at the rear surface than at the front surface of the source plate, then normally more than half of the emerging neutrons would emerge from the rear surface. The

[redacted]

[redacted]

neutron mirror would be even more effective for this configuration, in increasing the number of neutrons available for capture by the beryllium. Since the source plate region in this problem is less than a mean free path thick for fast neutrons, and since the power distribution from back to front of the source plate falls off by a factor of four, we conclude that (a) will lead to an overestimate by at least a factor of two. Dividing the results of the zero-current boundary condition problem by two should still yield an overestimate because of (b).

The fluxes and captures reported in the tables and plots of this report, based on the .4695 current-flux ratio, are a factor of 1.5 lower than this estimated upper limit, and hence there is no inconsistency. However, since it is not known whether the chosen boundary condition leads to the physically correct fraction of neutrons escaping from the back of the source plate, the results presented herein might be low by as much as a factor of 1.5.

4.2 Adequacy of the Multigroup Solution

The upper limit above assumes that, regardless of boundary condition, the multigroup code used gives the correct solution to the problem. An examination of the thermal flux plots in the beryllium near the B_4C-Pb-Masonite region indicates that the net current here is greater than the flux. This cannot be correct and is interpreted as a breakdown of the diffusion approximation near a strong absorber. Estimates of the error introduced by basic considerations of this nature would require further study.

[redacted]

[redacted]

5. COMPARISON WITH EXPERIMENT

The actual thermal flux distribution in the Be reflector mockup has been measured at ORNL[6] by placing gold foils at various positions in the reflector. Comparisons of the experimental and theoretical results are given in Figures 7 and 8. Figure 7 indicates the variation of the thermal flux as a function of penetration into the Be reflector for several values of the distance r from the reflector center line. Figure 8 indicates the radial variation of the thermal flux at several values of Be reflector thickness. The power of the source plate was assumed to be 3.5 watts.

It will be noted that the general shape of the theoretical curves-is in good agreement with the experimental flux curves except near the source plate region where - as noted in Section 4.2 - the diffusion approximation appears to have broken down.

Generally the calculated results agree with the experimental results to within 20% except near the source plate surface. The calculated results are usually smaller than the experimental results indicating that perhaps the source plate boundary condition was given too high a value or that the source plate power was given too low a value.

[redacted]

[redacted]

Table I

Comparison of Physical Dimensions
With Those Used in Machine Calculations

Region	Axial Dimension, cm Physical	Axial Dimension, cm Machine
Source Plate	2.193[a]	2.2557
Masonite, Boron Carbide, Lead	2.223	2.2557
Beryllium	31.58[b]	31.58[b]
Water	31.58	31.58

Region	Radial Dimension, cm Physical	Radial Dimension, cm Machine
Source plate shutter aperture radius	35.56	35.56
Source plate outer radius	78.953	81.78
Beryllium outer radius	68.793[c]	71.12
Radial thickness of water annulus		10.668

[a] Thickness of plate equivalent in volume to a 1.1-inch diameter cylinder.

[b] Includes an extrapolation distance of 1.1 cm.

[c] Radius of cylinder having the same cross-sectional area as a slab 4 ft high and 4 ft wide.

[redacted]

[redacted]

Table II

Compositions of Regions in Machine Calculation

Region	Constituent	Atoms/cc x 10^{-24}	Percent by Weight of Constituents of Region
Source Plate	U (Natural)	0.0473	100.0
Composite of boron carbide, masonite and lead slabs	Pb	0.01878	93.77
	B	0.01246	3.25
	C	0.00630	1.82
	H	0.005313	0.13
	O	0.00266	1.03
Beryllium	Be	0.12310	100.0
Water	H	0.06692	11.19
	O	0.03346	88.81

[redacted]

[redacted]

Table III

Lethargy Groups Used in Machine Calculation

Group	Lethargy Limits, u	Group Width, Δu	Energy Limits, ev
1	0 - 0.5	.5	10^7 - 6.065×10^6
2	0.5 - 1.0	.5	6.065×10^6 - 3.679×10^6
3	1.0 - 1.5	.5	3.679×10^6 - 2.231×10^6
4	1.5 - 2.0	.5	2.231×10^6 - 1.353×10^6
5	2.0 - 2.5	.5	1.353×10^6 - 0.8208×10^6
6	2.5 - 4.0	1.5	0.8208×10^6 - 0.1832×10^6
7	4.0 - 7.0	3.0	0.1832×10^6 - 9118
8	7.0 - 10.0	3.0	9118 - 454.0
9	10.0 - 11.4	1.4	454.0 - 112.0
10	11.4 - 12.6	1.2	112.0 - 33.72
11	12.6 - 13.8	1.2	33.72 - 10.16
12	13.8 - 14.6	1.2	10.16 - 4.564
13	14.6 - 16.2	1.6	4.564 - 0.9214
14	16.2 - 18.0	1.8	0.9214 - 0.1523
15	18.0 - 19.8	1.8	0.1523 - 0.02518
16	19.8 (thermal)		.02518

[redacted]

[redacted]

Table IV

Distribution of Beryllium Absorptions by Lethargy Groups

Group	Absorptions per Source Neutron		
1	0.000000		
2	0.000000		
3	0.000544	(n, α)	
4	0.004549		
5	0.002542		
6	0.000269		Total (n, α) abs. 0.007904
7	0.000036		
8	0.000012		
9	0.000014		
10	0.000028	(n, γ)	
11	0.000042		
12	0.000045		
13	0.000157		
14	0.000381		
15	0.000835		
16 (thermal)	0.014746		Total (n, γ) abs. 0.016296
			Total abs. 0.024200

[redacted]

[redacted]

LID TANK MOCKUP OF CFR REFLECTOR AS IDEALIZED FOR MACHINE CALCULATION

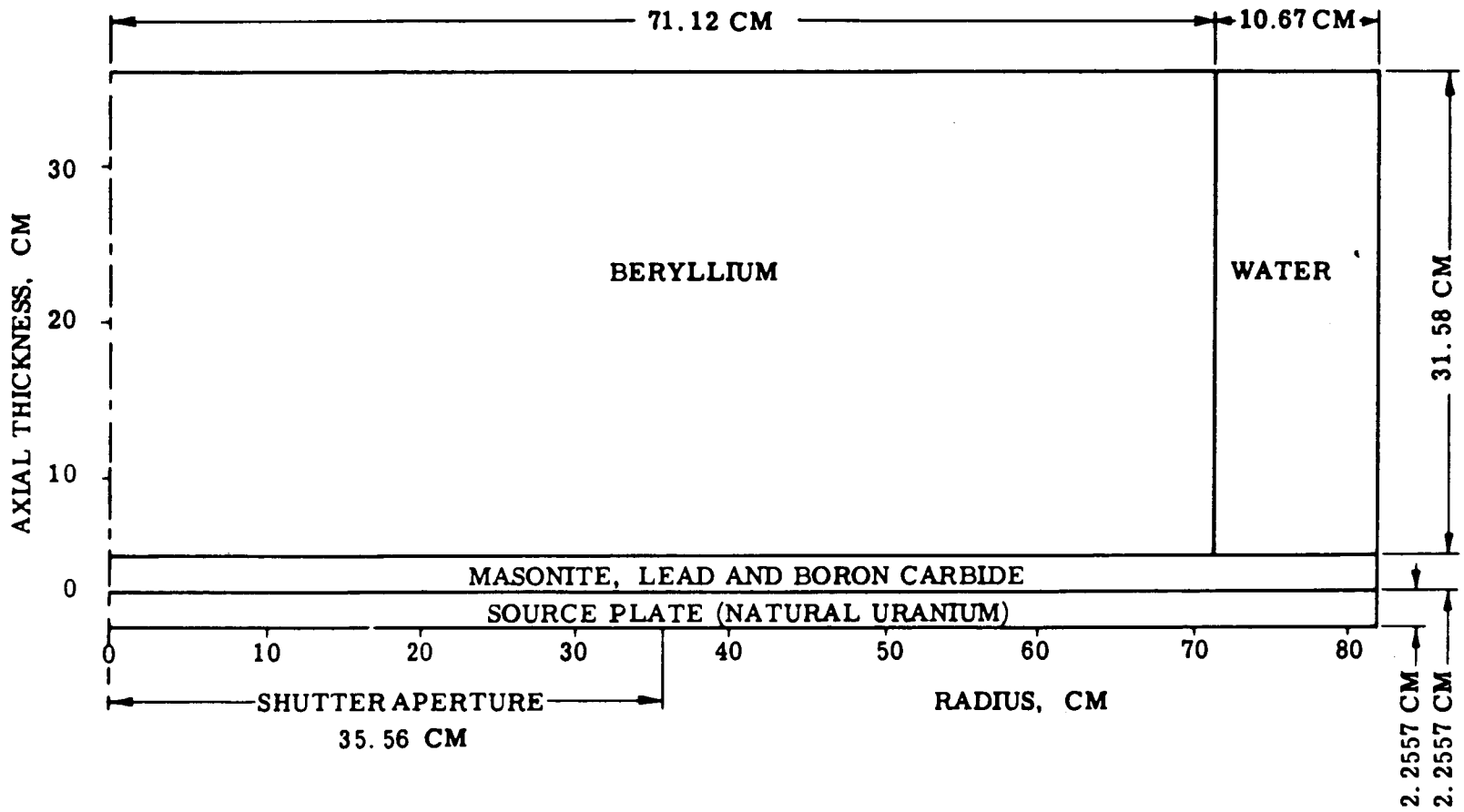

Figure 1

NDA 10-TR-365

[redacted]

[redacted]

AXIAL DISTRIBUTION OF THERMAL FLUX IN BERYLLIUM

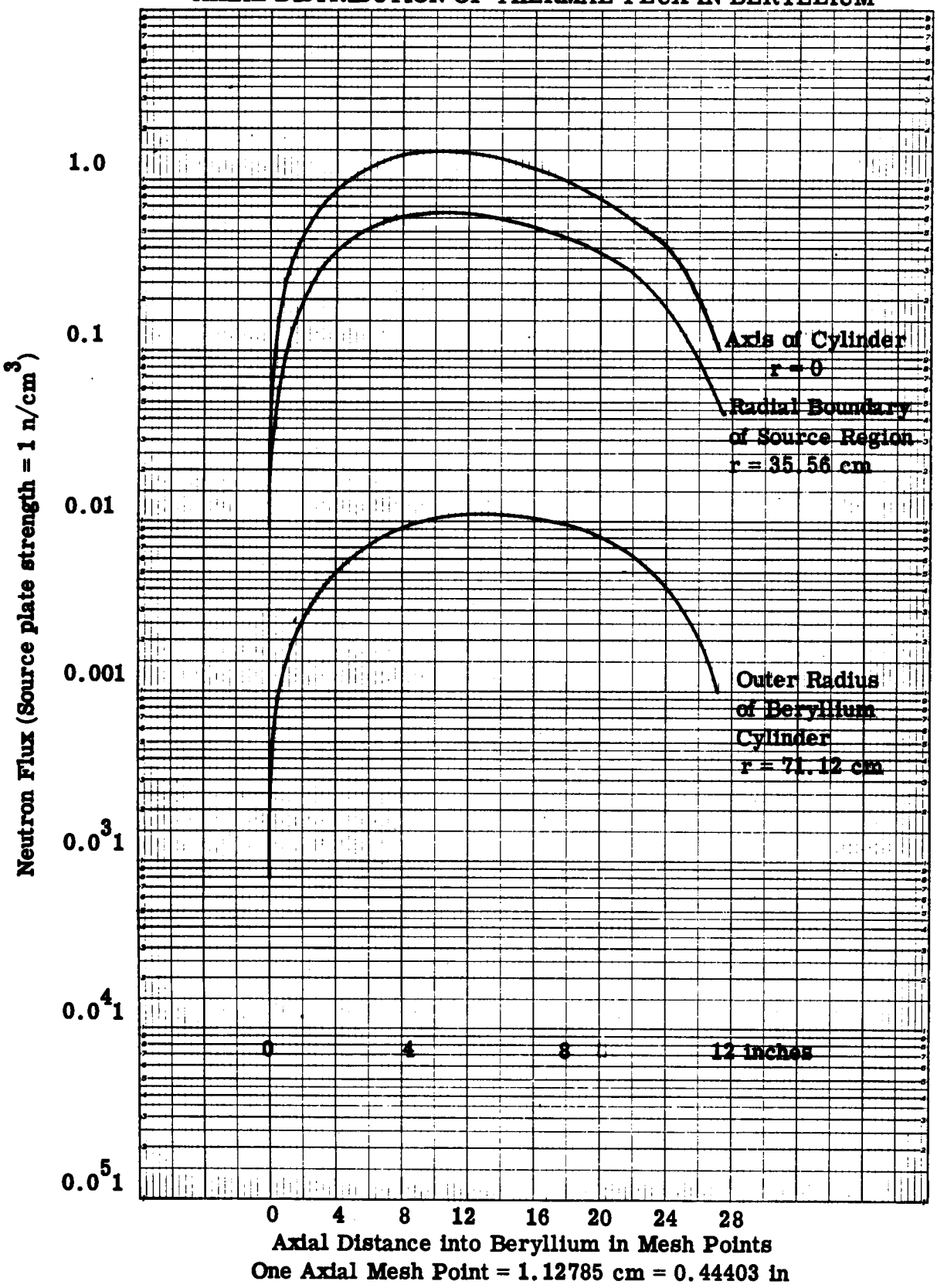

Figure 2

[redacted]

[redacted]

RADIAL DISTRIBUTION OF THERMAL FLUX IN BERYLLIUM

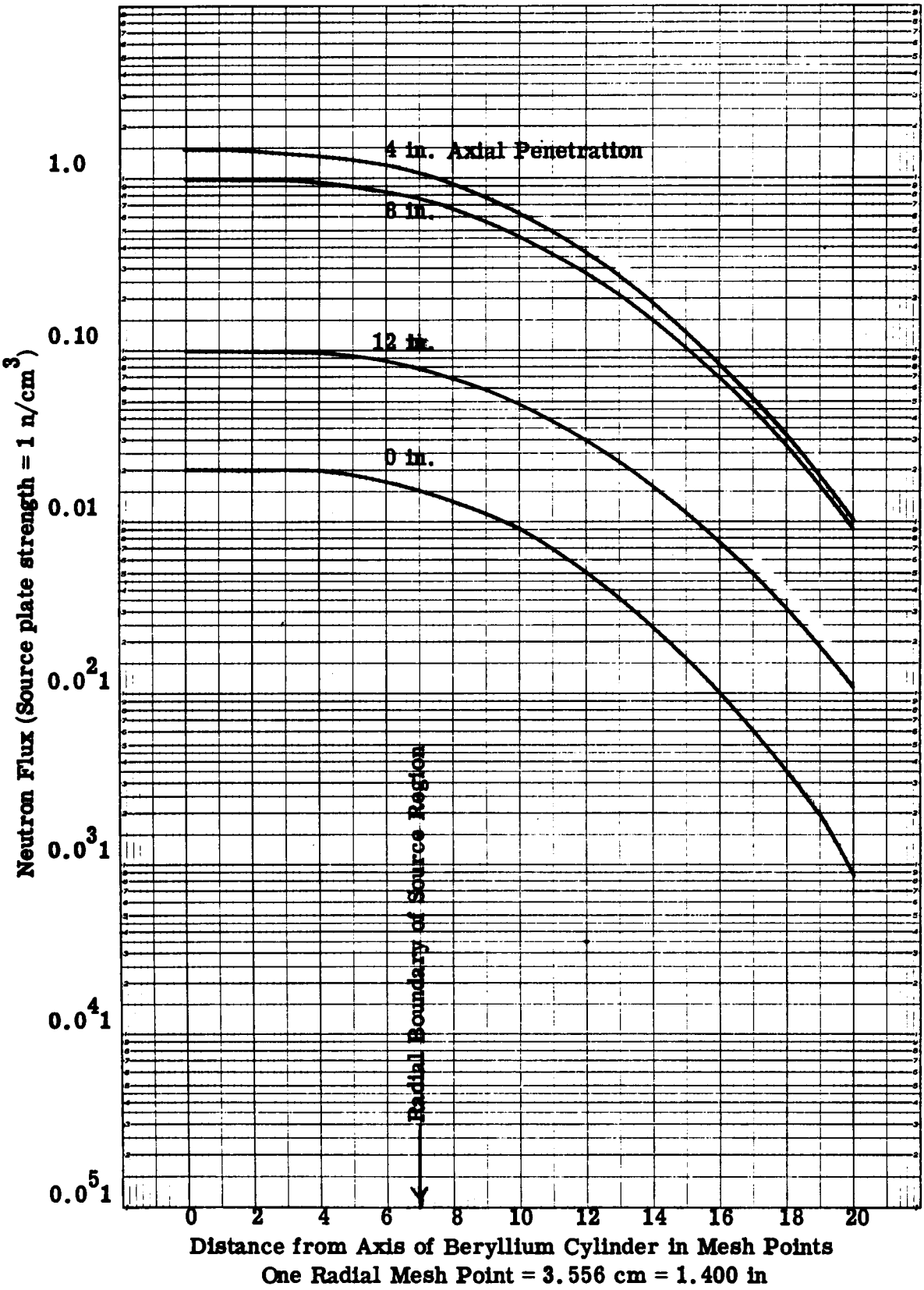

Figure 3

[redacted]

[redacted]

AXIAL DISTRIBUTION OF GROUP "8" FLUX IN BERYLLIUM

Lethargy Limits: 7.0 - 10.0 Energy Limits: 9118 ev - 454 ev

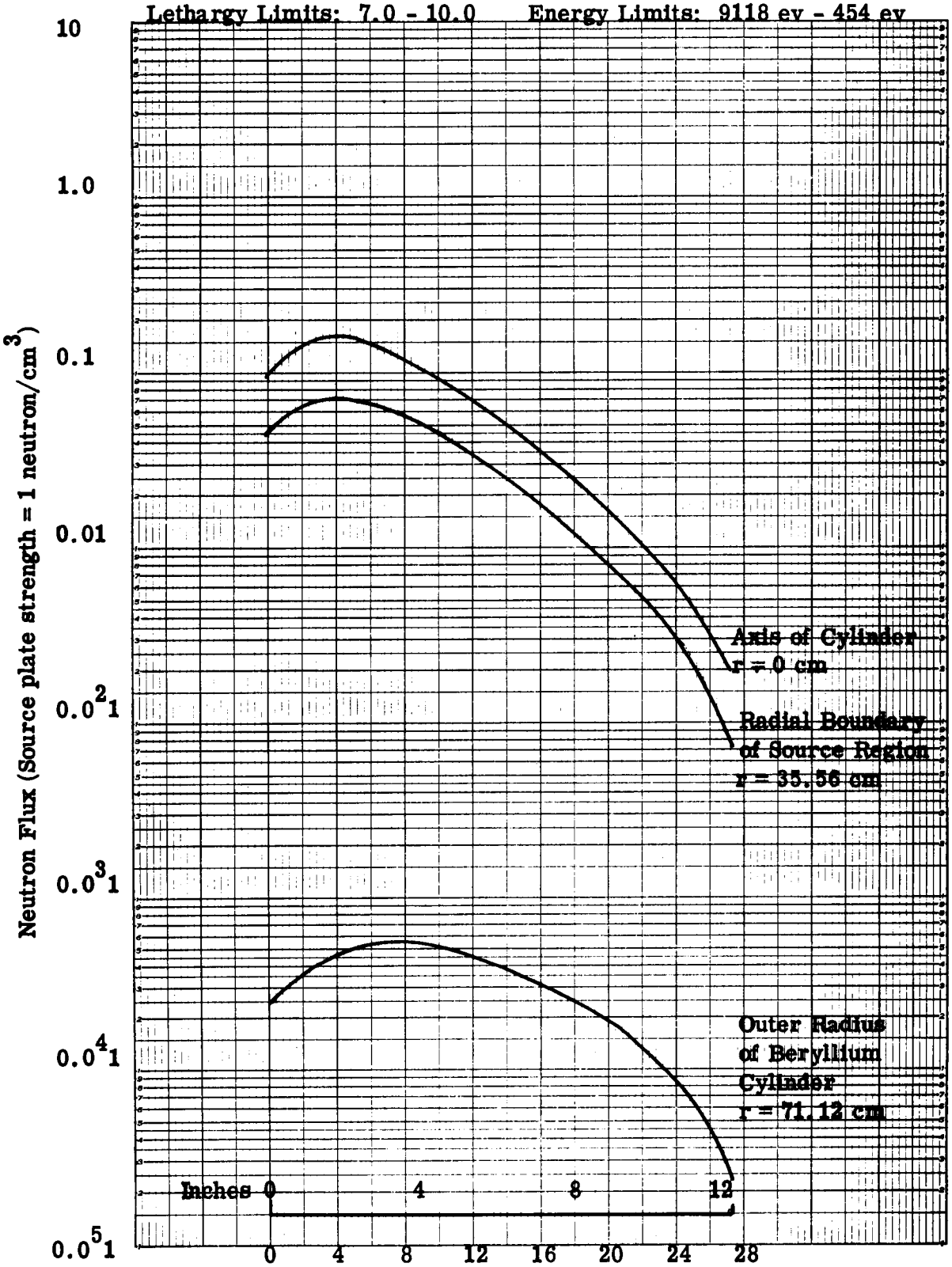

Axial Distance into Beryllium in Mesh Points

One Mesh Point = 1.12785 cm = 0.44403 in

Figure 4

[redacted]

[redacted]

RADIAL DISTRIBUTION OF GROUP "8" FLUX IN BERYLLIUM

Lethargy Limits: 7.0 - 10.0 Energy Limits: 9118 ev - 454 ev

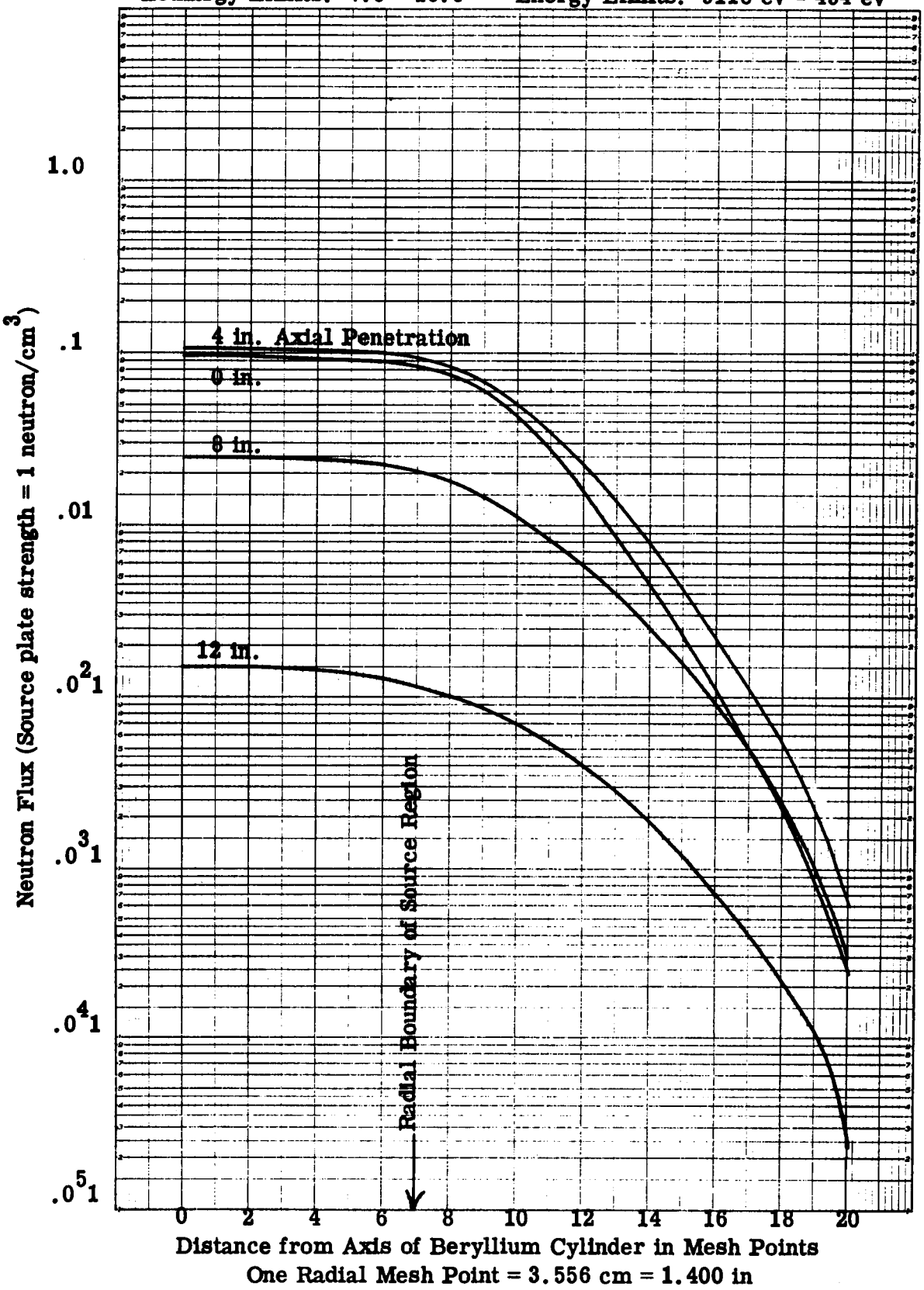

One Radial Mesh Point = 3.556 cm = 1.400 in

Figure 5

[redacted]

[redacted]

DISTRIBUTION OF GAMMA-PRODUCING ABSORPTIONS IN THE BERYLLIUM CYLINDER

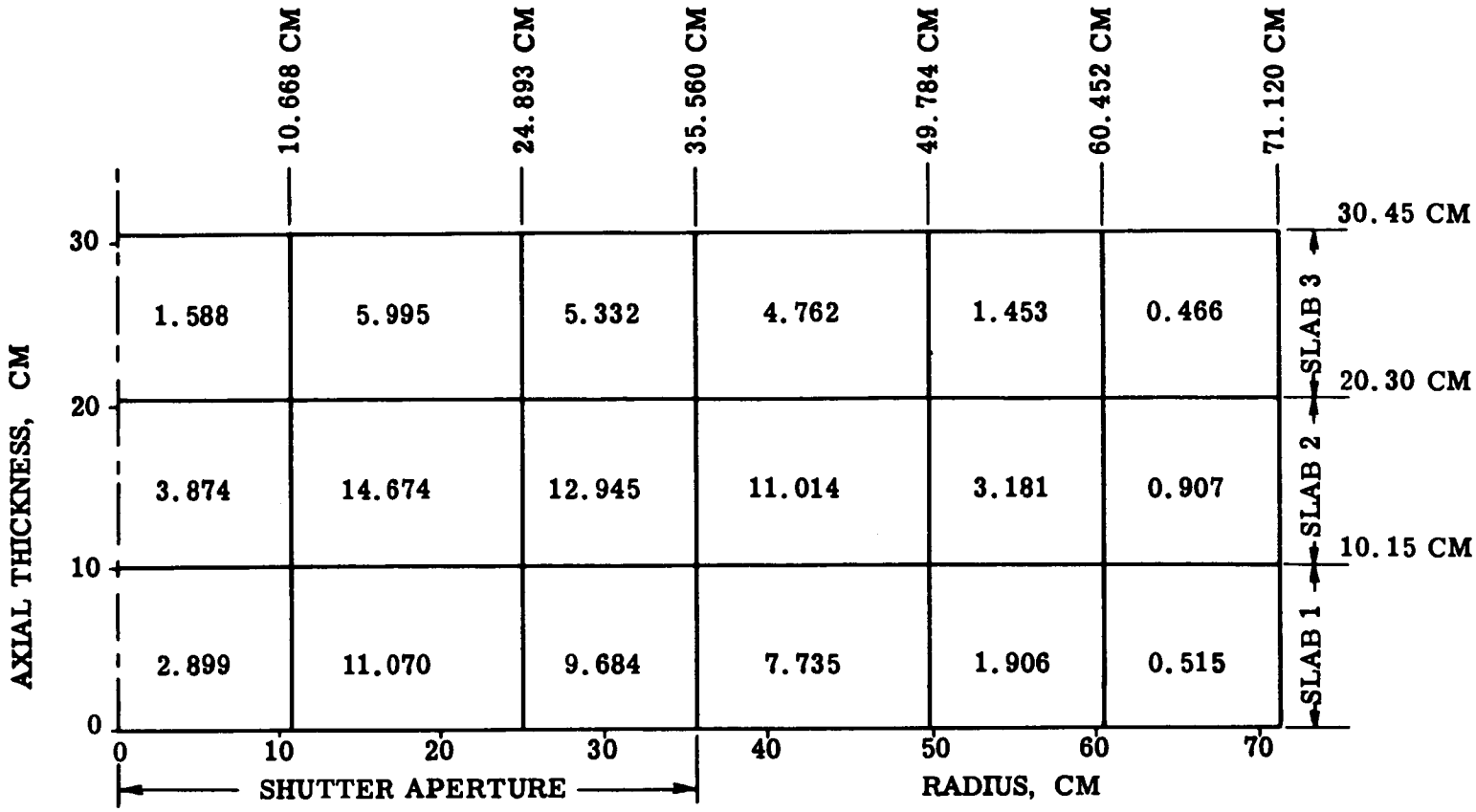

NOTE: VALUES WITHIN BOXES INDICATE PERCENTAGE OF GAMMA-PRODUCING BERYLLIUM ABSORPTIONS OCCURRING IN EACH VOLUME ELEMENT

Figure 6

NDA 10-TR-370

[redacted]

[redacted]

COMPUTED AND MEASURED THERMAL FLUX VS. BERYLLIUM THICKNESS

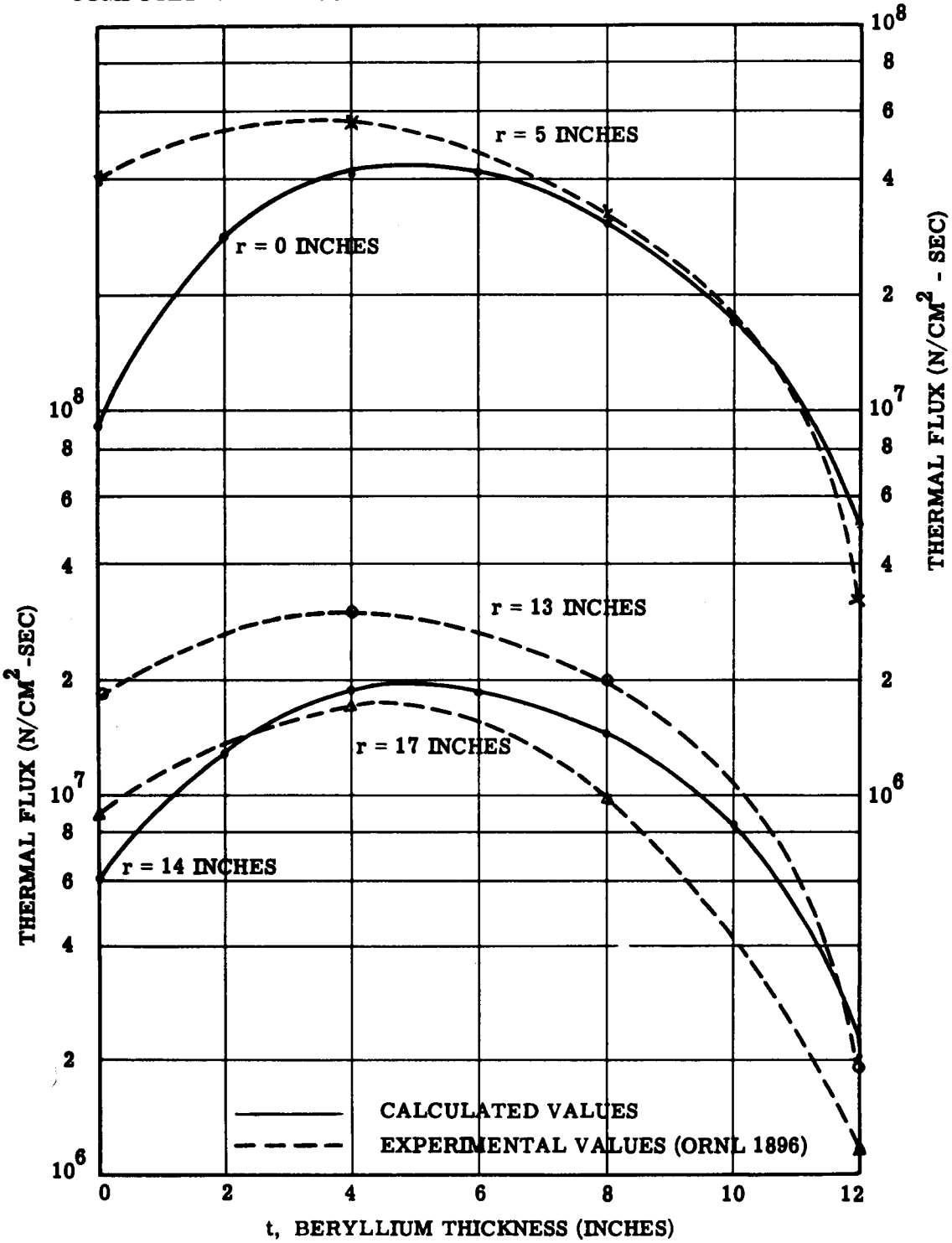

Figure 7

NDA 2012-TR-73

[redacted]

[redacted]

COMPUTED AND MEASURED THERMAL FLUX VS. RADIAL PENETRATION

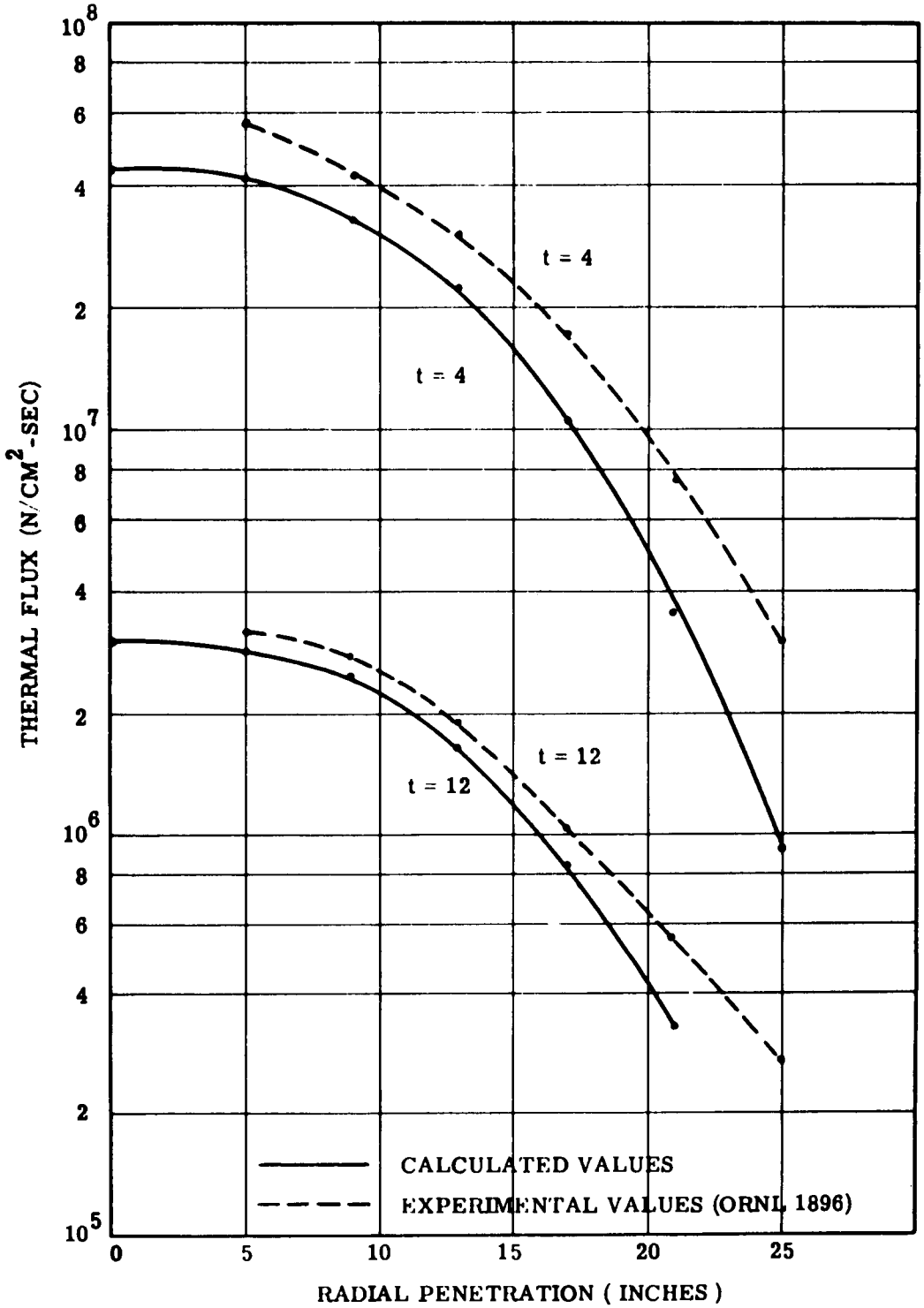

Figure 8

NDA 2012-TR-74

[redacted]

[redacted]

REFERENCES

[1] KAPL-950, Adaptation of Multigroup Methods to Cylindrical Geometries, G. M. Roe, September 27, 1954.

[2] Based on results described in NDA 10-22, CFR Studies Part I, April 8, 1954, p. 27.

[3] NDA 10-122, op. cit., p. 19.

[4] BNL-250, Classified Neutron Cross Sections, Brookhaven Cross-Section Advisory Group, 1954.

[5] AECU-2040, Neutron Cross-Sections, USAEC.

[6] ORNL-1896, ANP Project Quarterly Progress Report, G. T. Chapman, J. B. Dee, H. C. Woodsum, June 10, 1955, p. 198.

[redacted]

[redacted]

DISTRIBUTION

Series A

	Copy Number
Oak Ridge National Laboratory	
Attn: D. D. Cowan	1-150
NDA	
Library	151
Project Work File	152-155

E. I. M.

[redacted]

[redacted]

Paper I-K

TIME DEPENDENCE OF FISSION PRODUCT GAMMA RADIATION

by

W. Zobel and T. A. Love

Oak Ridge National Laboratory
Oak Ridge, Tennessee

RESTRICTED DATA
This document contains restricted data as defined in the Atomic Energy Act of 1954. Its transmittal or the disclosure of its contents in any manner to an unauthorized person is prohibited.

[redacted]

[redacted]

TIME DEPENDENCE OF FISSION PRODUCT GAMMA RADIATION

by

W. Zobel and T. A. Love

Oak Ridge National Laboratory
Oak Ridge, Tennessee

An interim report on the time behavior of fission product gamma radiation in the time range from 1.25 sec to 1600 sec after fission is presented. The need for this information for ANP shield design is discussed. Curves are included showing the time decay of six energy groups covering the energy range from 0.28 Mev to 5.0 Mev. The total number of photons per fission is given as 2.67 and the total energy per fission is 2.92 Mev. The errors on these numbers are estimated as ± 25%.

INTRODUCTION

The importance of fission product gamma radiation in the design of a reactor has been emphasized repeatedly. In any reactor this radiation gives rise to a handling problem after shutdown, for which special shielding may have to be provided. In addition, in the case of a circulating fuel reactor, such as the one under consideration for use in aircraft propulsion, the fission product gamma radiation gives rise to a secondary source of gamma rays in the heat exchanger, since the fission products are carried by the fuel into that region. As the heat exchanger is embedded in the reactor shield, this source may constitute an appreciable fraction of the total gamma ray dose appearing at the surface of the reactor shield. It has been estimated that the dose contribution from this source amounts to about 20% of the total gamma ray dose in the crew compartment.[1]

It has been proposed at this laboratory, and will be reported in another paper, that a Shield Mockup Reactor be constructed which will have a core shape similar to that of the circulating fuel aircraft reactor, but will utilize stationary fuel elements. Such a reactor has obvious advantages in the testing of shield design configurations envisaged for use with the circulating fuel reactor. After careful consideration it became clear, however, that no such reactor can

[redacted]

[redacted]

properly mockup the radiation source in the heat exchanger region; hence, the amount and type of radiation to be expected there must be determined from separate experiments. Then the dose from this source may be calculated and taken into consideration in the final shield design.

Some data on the decay characteristics of the gross fission product gamma rays have been published.[2-4] In general, these papers are concerned with the after-shutdown behavior of a reactor as a function of operating time. Furthermore, the shortest time after fission that has been reported was 10 min. It is thus seen that these data cannot be applied to the problem of the circulating fuel reactor where circulation times are of the order of seconds.

A program has been under way at this laboratory for some time, designed to furnish information on the decay characteristics of fission product gamma rays. Two methods of approach were used: The energy spectrum of the fission product gammas was measured with the Circulating Fuel Reactor Mockup at the Lid Tank Shielding Facility as a function of circulation time of the fuel belt. The other method involved the irradiation of small samples of enriched uranium in the ORNL Graphite Reactor for short periods of time, and was used for measurements of the time decay characteristics of the fission product gammas for relatively large energy groups starting at short times (about 1.25 sec) after fission, as well as the photon energy spectrum. The first method will be discussed in the succeeding paper. This report will be confined to the time decay characteristics measurements only, since data for the energy measurements taken with this method are not yet available.

EXPERIMENT

The experiment proceeded by the following steps:

1. A sample of U^{235} of known weight was introduced into the flux of the ORNL Graphite Reactor for a known length of time;

2. After irradiation, the sample was moved to the detector with reproducible geometry;

3. The gamma ray energy group to be investigated was selected;

4. The decay was followed for the desired time interval.

Equipment in the form of the fast pneumatic tube at Hole 56 of the ORNL Graphite Reactor, designed by E. C. Campbell of the Physics Division, was made available to us. This equipment, with small modifications, was used for steps 1 and 2 above.

The detection equipment used in this experiment was the multiple-crystal spectrometer of the Bulk Shielding Facility, moved to the fast pneumatic tube at Hole 56. The spectrometer and associated electronic

[redacted]

[redacted]

equipment, which remained at the Bulk Shielding Facility, is very thoroughly described in other reports,[5-7] so that no amplification should be necessary here. For convenience, a block diagram of the electronics is shown in Fig. 1. The equipment was designed to carry out steps 3 and 4 above.

The experiment proceeded in the following manner: After the electronics were lined up, the single channel analyzers set for the proper window widths, and the gain in the channels adjusted to the proper values, a time calibration was taken with a 60-cycle pulser. After recording this information, a number of samples of U^{235}, very closely alike, were irradiated and counted successively, using the same settings of the electronics throughout. The maximum number of samples used in any one run was 123. After recording the data obtained from the samples, another time calibration was taken. If the results of these time calibrations differed by more than 2%, the run was discarded.

In this manner data were taken for six energy groups (one group was taken twice, once with the pair spectrometer, and once with the Compton spectrometer) over the range 0.28 to 5.0 Mev, and for three time ranges, covering from 1.25 to 1600 sec. after fission.

The data, obtained as outlined above, were divided, channel by channel, by the time per channel as obtained from the time calibration runs. For this purpose the average of the calibrations before and after the run was used. The data were then corrected for counting losses, a correction which amounted to as much as 25%. Next the data were divided by the total weight of uranium in the samples of that run, by the energy interval used, and by the corrected bombardment time. The average efficiency of the detector over the energy range involved was calculated, using the spectrum obtained in the measurement at the Lid Tank Shielding Facility as the weighting factor. Dividing through by this average efficiency, and by the flux in the Graphite Pile, finally gave the number of photons/sec. Mev·fission. This number is plotted against time after fission in Fig. 2., where time after fission is reckoned from the center of the bombarding interval to the center of the counting interval. In all but three cases the waiting time, i.e., the time before the time-sweep is turned on, is at least as long as the bombarding time, and in the other three cases it is only half as long, so that the error introduced in this manner should be small.

It should be noted that these curves deviate from the $t^{-1.2}$ relation, particularly in the very short time region, i.e., up to about 5 sec.

The curves were integrated over the time range from 1.25 sec to 1600 sec after fission, and multiplied by the energy interval of the

[redacted]

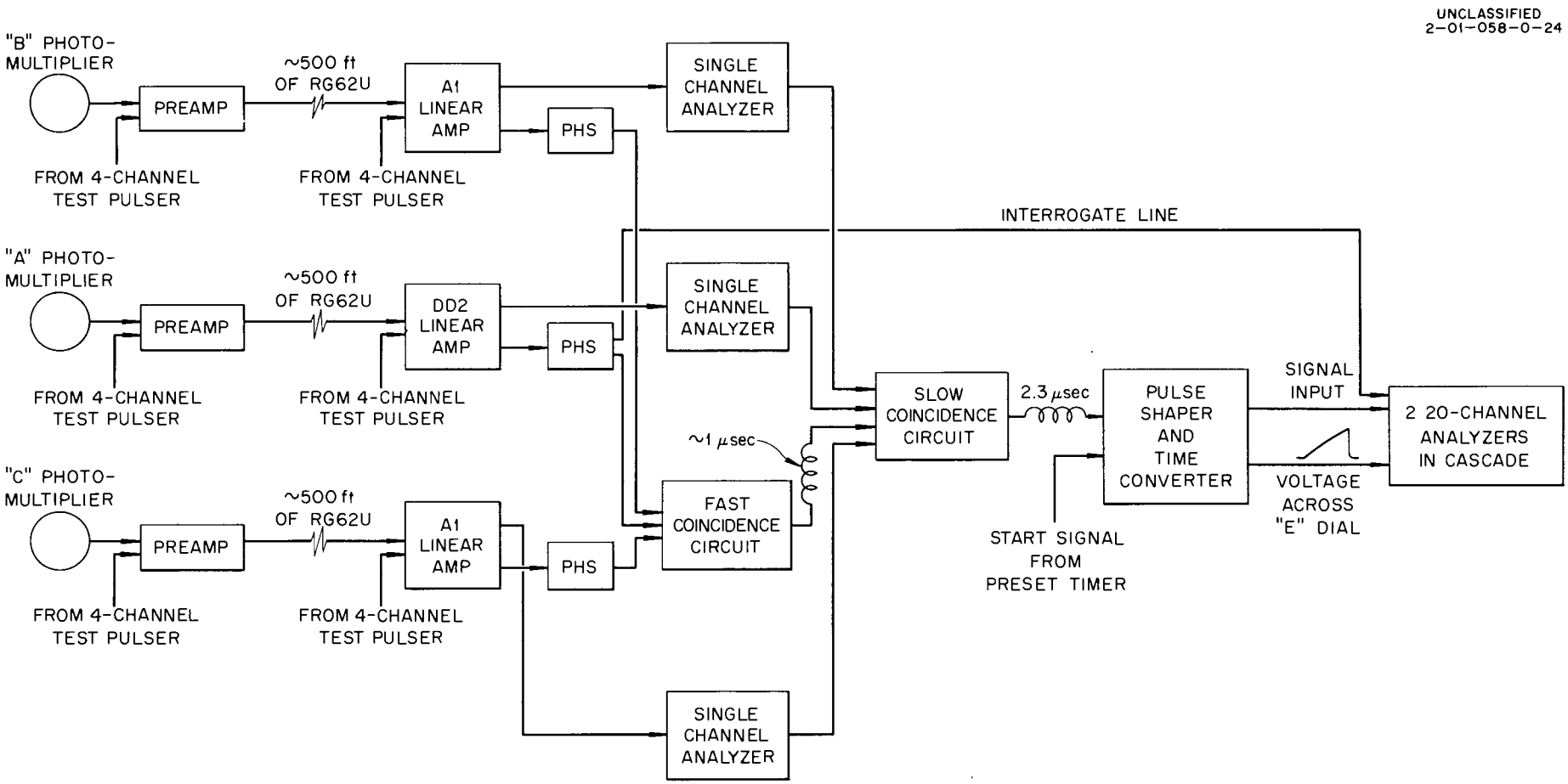

Fig. 1. Block Diagram of Electronics for Time Measurements.

UNCLASSIFIED
2-01-058-0-6

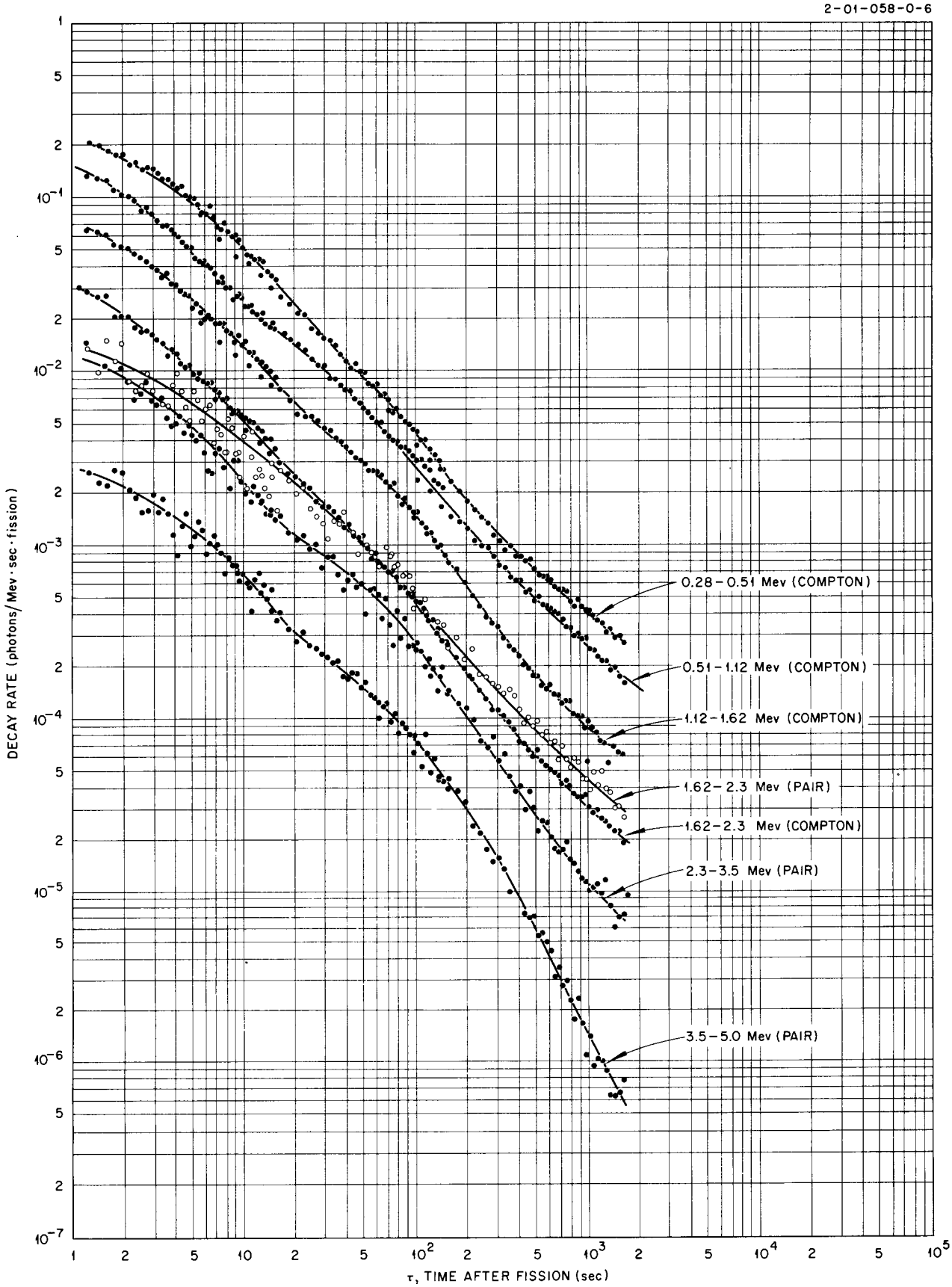

Fig. 2. Fission-Product Gamma-Ray Decay Rates as a Function of Time After Fission for Six Photon Energy Groups.

[redacted]

group. This gave a value of the number of photons per fission emitted in this energy range for the period of time considered. Multiplying this number by the average photon energy in the group gave a value for the energy released in the form of fission product gamma radiation per fission, again for the time interval and energy range in question. These data are shown in Table I.

The number of photons per fission, and the energy per fission for each energy group were then added, giving a total number of photons per fission equal to 2.67 in the time interval 1.25 to 1600 sec after fission over the energy range 0.28 to 5.0 Mev, and the total fission product gamma energy per fission over the same range of time and energy was 2.92 Mev. These numbers carry an estimated error of ± 25% as discussed in the next section.

SOURCES OF ERROR

There are many possible sources of error in this experiment. While these have not yet been completely investigated, a rough estimate may be made here.

The statistical error on the points of a curve varies from about 29% in the worst case to less than 2% in the most favorable one. In general, the statistics are much better for a Compton run than for a pair run. Even in the poorest case, though, the curve should have a much smaller error than the statistical error on a point of that curve, so that an error of 5 to 10% should not be out of line and is more probably conservative.

For the efficiency, an error of 15% has been assumed. Since the efficiency is dependent on the spectrum obtained at the Lid Tank Shielding Facility, and since this spectrum is an integral over several hours, the error has been deliberately made conservative.

Another source of error is in the value used for the flux. In the first place, only thermal fissions were considered. This will introduce an error of 1 to 2%. In addition, no error was quoted on the value of the thermal flux given us by Moteff.[8] A reasonable error appears to be about 10%.

There will also be an error in the bombardment time which we take to be about 5%. Errors in the sample weight or in the calibration of the energy range should be less than 1% each and thus be virtually negligible in comparison with the other errors mentioned.

It thus appears that, at least for the present, the results of this experiment must carry an estimated error of about 25%. It is hoped that further analysis will reduce this error considerably.

[redacted]

[redacted]

SUMMARY

The decay characteristics of fission product gamma radiation have been measured. While the evaluation of the data is not fully completed, a fairly thorough evaluation yields a total number of photons per fission of 2.67 in the energy range from 0.28 to 5.0 Mev being emitted by fission products in the time interval from 1.25 to 1600 sec. after fission, and a total amount of energy of 2.92 Mev. being emitted per fission in that time interval by fission products in the form of gamma rays with energies in that energy interval. The errors on these numbers are estimated as ± 25%. Further work to refine the evaluation is contemplated.

The experiment has been extended to measure the energy spectrum of fission product gamma rays at ten points in the time range of 2 to 1550 sec. inclusive. The results of this experiment are expected to be available in the near future.

[redacted]

[redacted]

TABLE I. MEASURED VALUES OF PHOTON INTENSITY PER FISSION AND TOTAL ENERGY RELEASE PER FISSION INTEGRATED BETWEEN 1.25 AND 1600 SEC. AFTER FISSION

Energy Range	Photons per Fission	Energy per Fission (Mev)
Compton Spectrometer		
0.28 - 0.51	0.696	0.275
0.51 - 1.12	1.103	0.894
1.12 - 1.62	0.428	0.586
1.62 - 2.30	0.210	0.412
Pair Spectrometer		
(1.62 - 2.30)	(0.197)*	(0.385)*
2.3 - 3.5	0.178	0.515
3.5 - 5.0	0.038	0.057
Total	2.67	2.92

*Not included in total.

[redacted]

[redacted]

REFERENCES

1. Keller, F. L., private communication.

2. Moteff, J., "Fission Product Decay Gamma Energy Spectrum," APEX-134.

3. Clark, F. H., "Decay of Fission Product Gammas," NDA-27-39 (Dec. 30, 1954).

4. Boyer, L. H., "Decay Gamma Energy Spectrum from Uranium Fission Products," IDO-16218 (April 13, 1955).

5. Love, T. A. ANuP Semi-Annual Progress Report for Period Ending December 31, 1955, ORNL-2081 (to be issued).

6. Love, T. A., Peelle, R. W., and Maienschein, F. C., "Electronic Instrumentation for a Multiple-Crystal Scintillation Spectrometer," ORNL-1929 (Oct. 3, 1955).

7. Maienschein, F. C., "Multiple-Crystal Gamma Ray Spectrometer," ORNL-1142 (April 14, 1952).

8. Moteff, J., private communciation.

[redacted]

[redacted]

Paper I-L

THE GROSS FISSION PRODUCT PHOTON ENERGY SPECTRUM

by

R. W. Peelle, T. A. Love, W. Zobel

Oak Ridge National Laboratory
Oak Ridge, Tennessee

[redacted]

[redacted]

[redacted]

THE GROSS FISSION PRODUCT PHOTON ENERGY SPECTRUM

by

R. W. Peelle, T. A. Love, W. Zobel

Oak Ridge National Laboratory
Oak Ridge, Tennessee

An experiment has been performed to determine the energy spectrum of the fission product photons from the heat exchanger region of a circulating fuel reactor. The measured spectrum is presented here for photon energies between 0.36 and 5.8 Mev. The total observed energy release by fission product gamma rays as measured in this experiment is 4.8 Mev/fission.

INTRODUCTION

The purpose of this paper is to discuss briefly a spectral measurement of the equilibrium fission product gamma-ray source in the heat exchanger region of a circulating fuel reactor system. The result of this measurement also may be reasonably well interpreted as the gross fission product photon energy spectrum during reactor operation. The work was performed at the Oak Ridge National Laboratory by Zobel, Love, and Peelle with the considerable cooperation of the entire LITSF staff. The scintillation spectrometer was placed in the Lid Tank, but the associated electronic equipment was retained at the Bulk Shielding Facility.

These results in the present form have already been presented in report ORNL-2012, the December 10, 1955 Aircraft Nuclear Propulsion Project Quarterly Progress Report. They are repeated here for completeness and for comparison with the more recent results of Zobel.

The fission product gamma-ray photons, as defined here, include all those photons given off from the gross fission product nuclide mixture at any time clearly later than the fission event itself. They are here contrasted with the prompt fission gamma rays given off in time coincidence with the fission event.

The present experiment was carried out to obtain a direct measurement of the photon spectrum from a circulating fuel loop. The results have already been used in an attenuation analysis of the CFR heat

[redacted]

[redacted]

exchanger gamma rays, and plans call for the continued use of this spectrum in future aircraft shield design calculations.

EXPERIMENTAL METHOD

Figure 1 shows a top view of the experimental configuration as placed in the Lid Tank. On the right is the outline of the massive shield belonging to the multiple-crystal gamma-ray spectrometer. Outside this shield was placed a wall of lithiated paraffin bricks about one foot thick to protect against neutron induced background in the spectrometer. On the left is shown the rotating belt fuel loop placed adjacent to the "core hole" on the Oak Ridge National Laboratory Graphite Reactor. This is the same fuel loop used for the Lid Tank Shielding Facility dynamic source tests. Within the circumference of the fuel belt is placed a massive shield of borated water and lead. This shield protects the spectrometer from background radiations originating in the graphite reactor, and from the prompt fission gamma rays.

Experimental spectra were obtained by opening the boral shutter at the extreme left to allow thermal neutrons to impinge on the rotating fuel loop. The scintillation spectrometer observed through its collimator a fraction of those fission product decay photons originating on the part of the fuel loop within its geometric acceptance angle. In practice, two background spectra had to be obtained to enable proper interpretation of the results. The results to be shown below neglect data taken during the first two hours after startup, so the spectrum reported here is typical of the spectrum observed about 3 hours after startup of the fuel loop. It is clear that the amount of radiation would have increased somewhat (about 5%) had the fuel loop been irradiated longer before data was taken.

RESULTS

A typical result is shown in Fig. 2. The other spectra obtained were almost indistinguishable from this. The average number of photons per Mev for one fission is plotted against photon energy. The open-circled points were obtained with the two-crystal Compton spectrometer, and the closed-circled points with the three-crystal pair spectrometer. The scatter in the points is explicable on the basis of statistical errors alone. An integration of the data plotted here gives an average of 4.8 Mev/fission for the total photon decay energy in the range between 0.36 and 5.8 Mev. An estimated error of 20% in the absolute magnitude of the above curve and in the integrated energy per fission arises largely from the estimate made of the fission rate in the fuel plates of the rotating fuel belt. Any plausible error in the shape of the spectrum is insignificant compared to the normalization error. Before application to the CFR, this data should probably be corrected for the following effects:

[redacted]

[redacted]

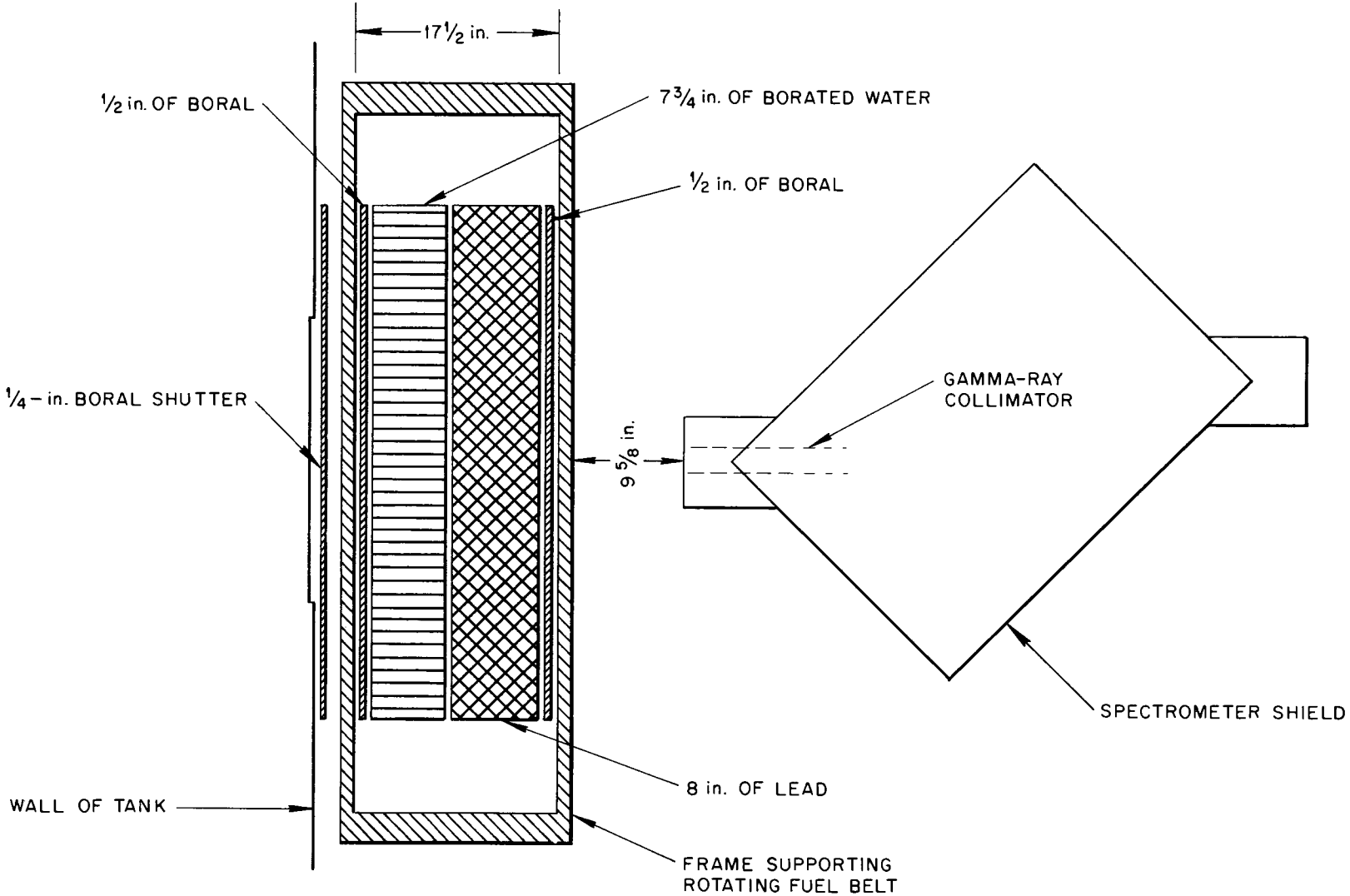

Fig. 1. Experimental Arrangement for Measurement of the Fission-Product Gamma-Ray Spectrum of the Circulating Fuel.

[redacted]

2-01-057-66-181

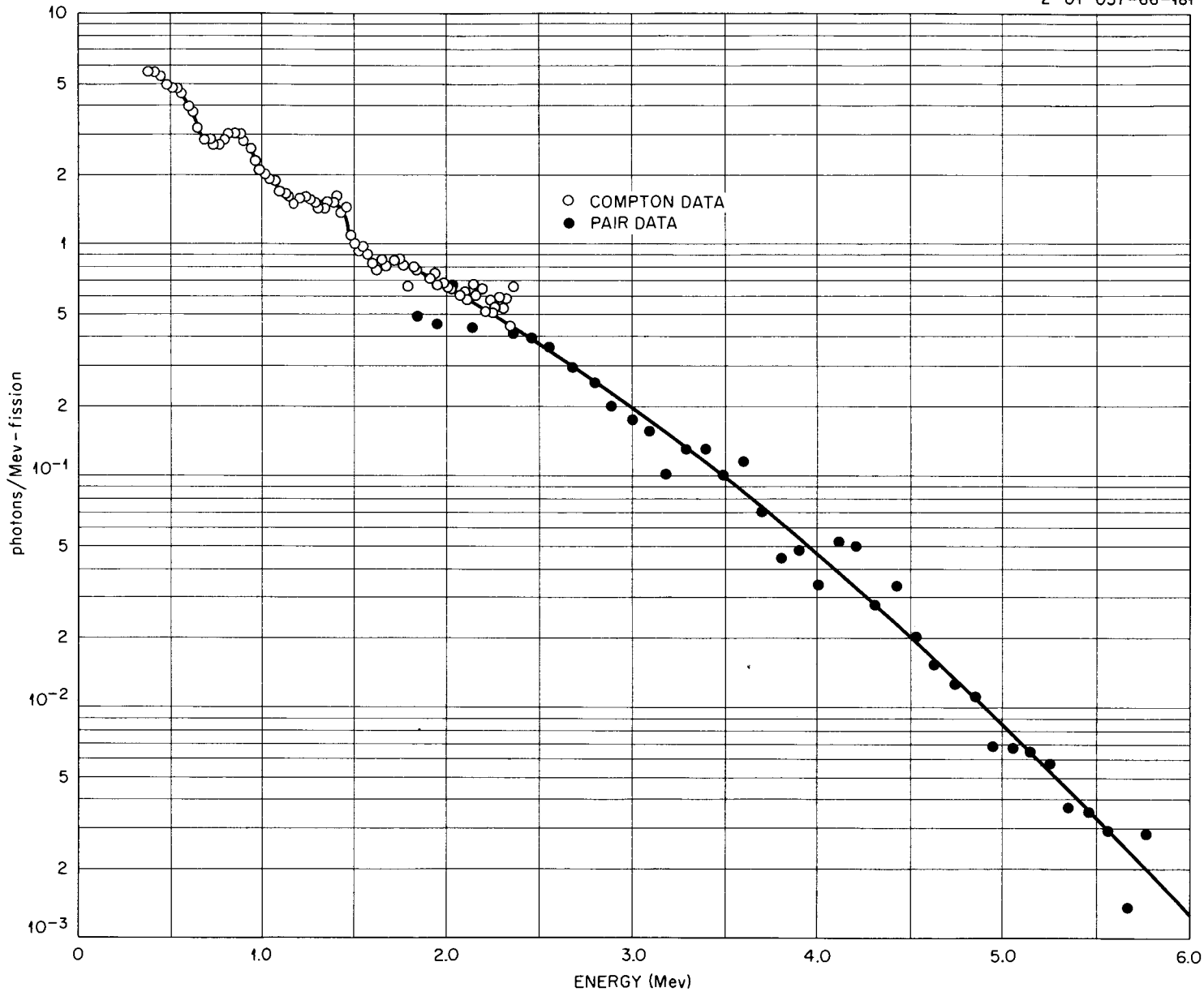

Fig. 2. Fission-Product Gamma-Ray Spectrum of the Circulating Fuel.

[redacted]

1. Escape of gaseous fission products.

2. Plating out of elements such as Ruthenium.

3. The buildup of long-lived fission product activities.

COMPARISON WITH "TIME SWEEP" RESULTS

No careful effort has been made to correlate these results with those given by Zobel.* At the present, however, there is a marked disagreement in the apparent total fission product gamma-ray energy per fission. The two experiments do, however, cover quite different ranges of the time and energy variables. Furthermore, there are systematic differences between the two analysis methods used.

Until the above discrepancies have been resolved, it is recommended that shield designers use each set of data where it naturally applies. For the steady-state fission product gamma-ray spectrum from the heat exchanger region of a circulating fuel reactor, the spectrum given here should be used.

* ANP Shielding Information Meeting, May 1956.

[redacted]